SEP 26 1956

Атомная энергия

Number 3, 1956

LIBRARY OF CONGRESS
SEP 28 1956

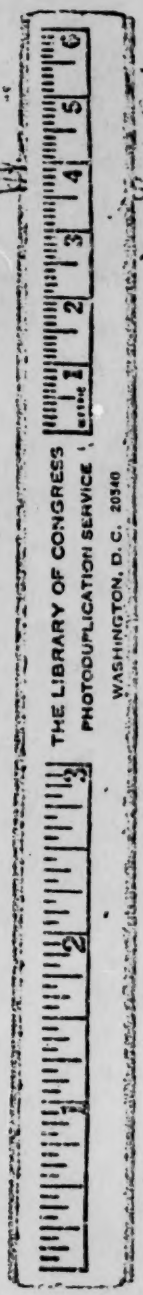

The Soviet Journal of

ATOMIC ENERGY

IN ENGLISH TRANSLATION

CONSULTANTS BUREAU, INC.

227 WEST 17TH STREET, NEW YORK 11, N. Y.

SEP 28 1956

Атомная энергия

Number 3, 1956

THE LIBRARY OF CONGRESS PHOTODUPLICATION SERVICE WASHINGTON, D. C. 20540

LIBRARY OF CONGRESS FINAL RECORD SEP 28 1956 COPY

The Soviet Journal of

ATOMIC ENERGY

IN ENGLISH TRANSLATION

CONSULTANTS BUREAU, INC.

227 WEST 17TH STREET, NEW YORK 11, N. Y.

SEP 28 1956

ATOMNAYA ENERGIYA

Academy of Sciences of the USSR

Number 3, 1956

EDITORIAL BOARD

A. I. Alikhanov, A. A. Bochvar, V. S. Fursov, V. F. Kalinin,
G. V. Kurdyumov, A. V. Lebedinsky, I. I. Novikov (Editor in Chief),
V. V. Semenov (Executive Secretary), V. I. Veksler, A. P. Vinogradov,
N. A. Vlasov (Acting Editor in Chief)

The Soviet Journal

of

ATOMIC ENERGY

IN ENGLISH TRANSLATION

Copyright, 1956

CONSULTANTS BUREAU, INC.
227 West 17th Street
New York 11, N. Y.

Printed in the United States

Annual Subscription $ 75.00
Single Issue 20.00

Note: The sale of photostatic copies of any portion of this copyright translation is expressly prohibited by the copyright owners. A complete copy of any article in the issue may be purchased from the publisher for $12.50.

SOME PROBLEMS OF ATOMIC POWER DEVELOPMENT IN THE USSR*

I.V. Kurchatov

The principal directions taken by the development of atomic power in the USSR are explained and some problems of the physics of water-moderated atomic reactors are discussed.

The power structure of the Soviet Union is very large. We possess various natural power resources. Siberia possesses extensive and easily accessible coal deposits and good conditions for the establishment of a network of very powerful hydroelectric power stations. The rich water resources there provide cheap water power and the open coal pits provide cheap electric and thermal power. In the next 15 to 20 years we plan to set up a huge power network in the Angaro-Enisei basin with a capacity of 250 to 300 billions of kilowatt hours annually.

However, the larger part of the population and industry of the USSR is at present concentrated on the plains of the European portion of the country. The cheap water power resources of this region will soon be exhausted and the mining and transportation of coal to great distances is very expensive. In addition, the rapid growth of our industry and agriculture require a greatly expanded production of electric and thermal power.

Our present resources will be sufficient for the next few decades, but in the more distant future atomic energy may prove to be the practically inexhaustible and relatively cheap source that will insure an abundance of power in the European portion of the USSR.

We shall have the problem of providing atomic power which, at least under the conditions prevailing in the European part of the Soviet Union, will be economically more advantageous than coal power. It is clear that only huge atomic electric power plants can provide atomic power economically.

Therefore we plan for the very near future atomic power plants which will each produce about 400 to 600 thousand kilowatts in order to accumulate experience in the construction and operation of such plants as well as in the large-scale production and processing of fuel elements.

The construction and operation of large plants will also enable us to determine which types of installation will be least harmful or dangerous to the surrounding population. Such data and the economic factors will determine the type of electric power plants and the scale of atomic power production during the period from 1960 to 1970.

Between 1955 and 1960 the Soviet Union plans to build five experimental atomic power plants. Construction of these plants will begin at the end of 1958; some will begin operation in 1959 and the remainder in 1960.

The reactors to be installed in two of the plants will use thermal and epithermal neutrons with a water moderator and coolant. The electric power obtained from one reactor will be 200,000 kilowatts. In conjunction with each reactor three turbines rated at 70,000 kilowatts will be operated by saturated steam at about 30 atmospheres pressure.

A second type of plant will be built with reactors similar to the reactor of the first atomic power plant of the USSR Academy of Sciences (Professor Blokhintsev reported on this plant at the Geneva Conference). The thermal neutron reactors will have a graphite moderator; heat will be transfered by water and steam. Steam at 90 atmospheres and superheated to 480-500° will feed turbines with a combined power of 200,000 kilowatts.

A third type of plant will use a heavy water moderated heterogeneous reactor. Heat will be removed by a circulating gas. At the New York national conference in October 1955 Professor Vladimirsky reported on the

*Lecture delivered April 25, 1956 at the British Atomic Research Center at Harwell.

basic characteristics of this type of reactor, which will produce steam at about 30 atmospheres pressure and at a temperature of about 400°C to feed turbines with a total output of 200,000 kilowatts.

In addition to these three types of large atomic power plants we shall construct and put into operation during 1959 and 1960 a few experimental plants each producing 50 to 70 kilowatts of electric power.

These include:

1) A thermal neutron reactor with ordinary water moderator and a turbine operating with slightly radioactive steam coming directly from the reactor;

2) A heavy water homogeneous reactor with breeding of nuclear fuel by the $Th^{232} - U^{233}$ cycle.

3) A thermal neutron reactor with graphite moderator and sodium coolant;

4) A fast neutron reactor with sodium coolant and breeding of nuclear fuel by the $U^{238} - Pu^{239}$ cycle.

Completion of this program of experimental atomic power plants will make it possible to choose the best types and to act discriminately with regard to many problems of reactor physics which have not yet been solved.

We hope that our achievements will be useful to those nations which because of the state of their natural resources require the immediate development of atomic power.

We shall now discuss some physical problems associated with reactors in which neutrons are slowed down by water. In the last few years the institute of which I am director has devoted a great deal of time to these problems. Water-moderated reactors have a high breeding ratio of atomic fuel as well as simple and compact construction. In our opinion they are likely to provide a large amount of atomic power in the very near future.

The theory of reactors operating with thermal or fast neutrons, except water-moderated reactors in which special conditions arise because of the strong influence of epithermal neutrons on physical processes, has already been comparatively well worked out. In a uranium-water lattice a comparatively large fraction of the neutrons can be absorbed to produce fission in the range from 0.1 to 3-5 ev, i.e., above the thermal energy range and below the lowest resonance levels of U^{238}. This fraction, depending on the lattice parameters and burn-up, can be as high as 80%.

The simplest theoretical study of a reactor in which the epithermal neutrons strongly affect the process of multiplication was reported by Professor Feinberg to a session of the Academy of Sciences in 1955. He based his theory on elementary slowing-down theory, neglecting chemical bonds between the protons of the moderator; this assumption yielded a qualitative determination of the fundamental properties of the reactor, principally in connection with the large resonance peak of the Pu^{239} cross section at 0.3 ev.

So long as there is no plutonium in the reactor core the rated multiplication factor k_∞ is almost independent of the absorption of epithermal neutrons. However, with large uranium burn-up resulting in the accumulation of a considerable quantity of plutonium it is important to allow for the epithermal neutrons. Despite the decrease of η of plutonium in the 0.3 ev resonance, the increase in the proportion of epithermal neutrons results in an increase of k_∞.

Let us consider, for example, two lattices with 50 mm spacing and lumps of enriched uranium and a mixture of U^{238} and Pu^{239}.

TABLE 1

Composition of lump	k_∞	
	Neglecting epithermal neutrons	Allowing for epithermal neutrons
0.9% U^{235} + 99.1% U^{238}	1.079	1.047
0.73% Pu^{239} + 99.27% U^{238}	1.079	1.272

As can be seen from Table 1 the capture of neutrons in the epithermal region is very important for the attainment of large burn-up of uranium in a water-moderated reactor.

For plutonium the value of η in the epithermal region, and especially near its lower limit, is strongly dependent on the energy; it is thus important to know the neutron spectrum and, above all, to determine to what extent the elementary theory corresponds to reality.

For an exact calculation of the neutron spectrum formation in the region which is of interest to us, it is first necessary to study the mechanism of neutron collisions with protons which are chemically bound in water molecules. Theoretical work by Drozdov and Goryunov has established the dependence of the elastic and inelastic

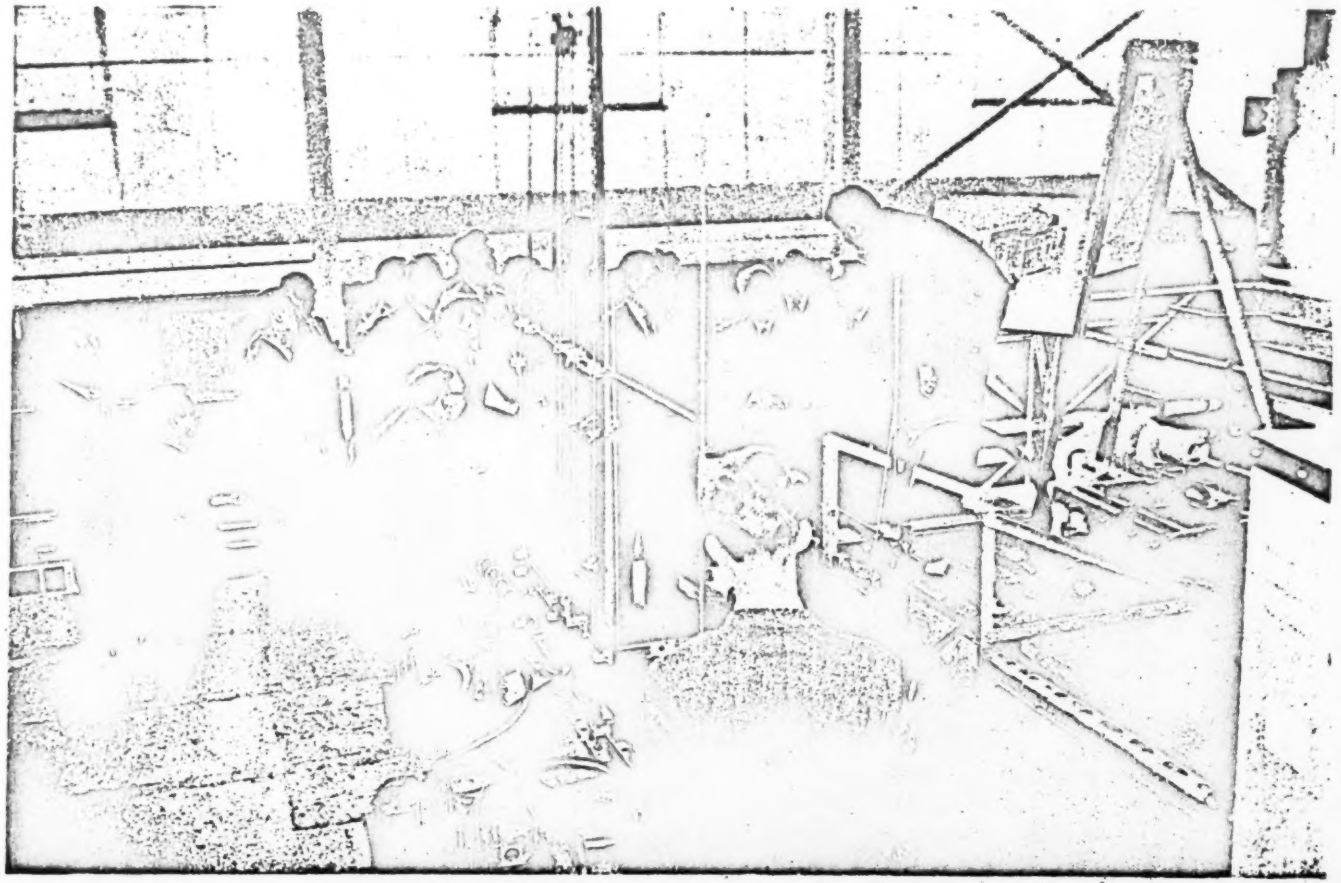

On April 21, 1956 N.A. Bulganin, N.S. Khrushchev and their party visited the Atomic Research Center at Harwell (England). The photograph shows them examining the new atomic reactor "Zeus".

neutron scattering cross sections for molecules of hydrogen and water on neutron energy below 0.5 ev. It was assumed that the neutrons are scattered by free molecules of hydrogen and water. The rotational and vibrational levels of the molecules were taken into consideration. Fig. 1 presents some of these results. The experimental curves are given for comparison.

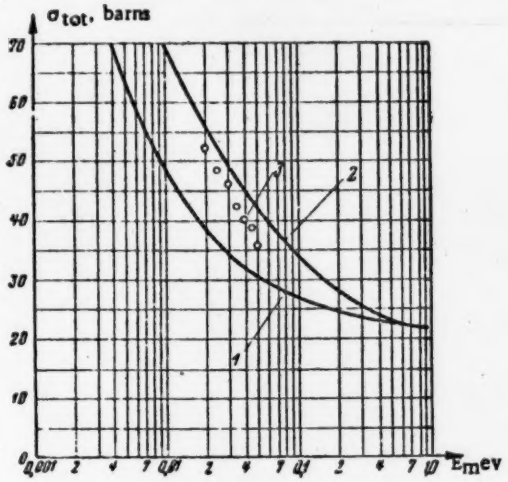

Fig. 1. Comparison of experimental and calculated values of the total neutron scattering cross section in bound hydrogen. 1) Experimental curve for molecular hydrogen; 2) experimental curve for water; 3) calculated values obtained by Goryunov.

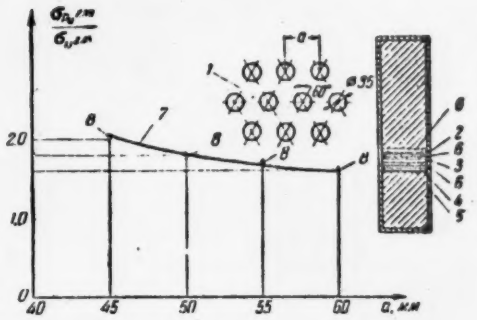

Fig. 2. Pu^{239} and U^{235} cross sections in a subcritical uranium-water lattice. 1) Triangular subcritical uranium-water lattice consisting of natural uranium lumps of 35 mm diameter with spacing a. The size of the subcritical lattice is much greater than the neutron migration length, therefore the neutron spectrum is determined at points that are distant from the boundary; 2) nickel disk with film of Pu^{239}; 3) paper disk for determining background; 4) nickel disk with film of U^{235}; 5) copper disks for shielding from fission fragments; 6) paper disks for collection of fission fragments; 7) theoretical curve; 8) experimental points obtained by Stolyarov, Nikolsky, Katkov and Antsiferov.

Another method of checking the elementary theory is the experimental determination of the most important features of the processes which occur in the epithermal region and a comparison with calculated values.

Stollyarov, Nikolsky, Katkov and Antsiferov have irradiated targets consisting of thin films of Pu^{239} and U^{235} deposited on a thin nickel backing. The targets were placed inside slots in the lumps of a subcritical uranium-water lattice (Fig. 2). From the activity of fission fragments collected on paper disks the ratio of the Pu^{239} and U^{235} cross sections was determined as a function of the hardness of the neutron spectrum in the lattice. In Fig. 2 these experimental results are compared with Feinberg's theoretical curve. Of course, these results cannot be considered to be a proof of the ability of the elementary slowing-down theory to explain the nature of the phenomenon, but they do show that this scheme can be used to estimate the burn-up of uranium in a water-moderated reactor.

Measurements performed by Barkov and Mukhin to determine the slowing-down length of neutrons from the energy of the first indium resonance down to thermal energies show that chemical binding has only a small effect on the slowing-down of neutrons.

Komissarov, Tarabanko and Katkov from the formation of U^{239} determined experimentally the breeding ratio of Pu^{239} for the initial instant of reactor operation, i.e., when there is still no Pu^{239} in the core. The experimental and calculated values of the breeding ratio as a function of the lattice spacing are shown in Fig. 3. The agreement can be considered satisfactory in this case also.

On the basis of the foregoing considerations Feinberg, Levin, Osmachkin, Novikov and Saulyev carried out a series of calculations of uranium burn-up in uranium-water lattices using the electronic calculator of Academician Lebedev. For these calculations they used the nuclear constants obtained by Mostov, Pevzner and their collaborators with a mechanical selector and by Spivak, Erozolimsky, Kutikov and others with a graphite prism.

It is very important in such calculations to allow correctly for neutron absorption in the accumulated Pu^{240}. The results of the calculations depend considerably on the values chosen for the nuclear constants and on the assumptions made regarding the spectrum of the absorbed neutrons.

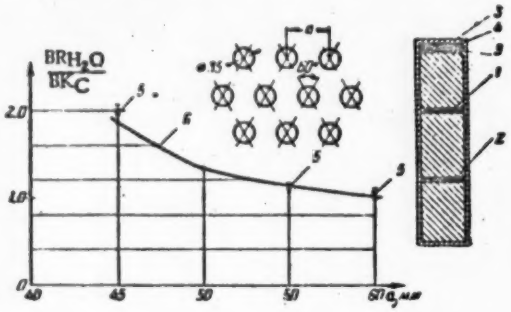

Fig. 3. Breeding ratio (BR) of nuclear fuel in a subcritical uranium-water lattice. 1) Paper disk for collection of fission fragments; 2) uranium disk for subsequent measurement of β-activity of U^{239}; 3) paper disks for shielding from fission fragments; 4) paper disk for determining background; 5) experimental points obtained by Tarabanko, Komissarov and Katkov; 6) theoretical curve.

In connection with the possibilities for U^{238} burn-up great interest attaches to the recirculation of nuclear fuel, i.e., to successive runs of burning-up in the uranium-water lattice. There is ground for believing that by the use of circulating nuclear fuel in uranium-water lattices a very high degree of utilization of U^{238} can be attained. If we keep in mind the inevitable considerable losses of nuclear fuel during the chemical and metallurgical processing we must conclude that the possibilities for a uranium-water lattice are similar to those for fast-neutron breeding reactors. More accurate values of the constants, a more detailed study of slowing-down processes and, above all, further knowledge concerning the operation of water-moderated reactors with large accumulations of Pu^{239} will make it possible to arrive at reliable conclusions regarding this important problem.

In connection with the possibility of achieving large uranium burn-up (even in one run) great practical importance attaches to the task of producing a fuel element which can operate for long periods while being irradiated.

We consider baked uranium dioxide, which is stable under irradiation and does not dissolve in hot water, to be an excellent material for use in the lumps of a uranium-water lattice. Our prolonged experimentation with the RFT reactor showed that lumps of uranium oxide even when their cladding is not hermetically sealed function satisfactorily; there is no contamination of the loop by fission products, and the small activity due to gaseous fission products disappears soon after stoppage of the reactor.

Utilization of the dioxide results in an appreciable diminution of the breeding ratio in a uranium-water lattice. Therefore we have not ceased to work towards the production of stable lumps of metallic uranium. After a number of failures a group of Soviet scientists have succeeded in working out the technology of manufacturing good uranium metal lumps. With burn-up of 3 kg per ton of uranium no change of shape is observed in these lumps; therefore it will be quite possible in the future to plan to use metallic uranium in uranium-water lattices.

In conclusion I would like to discuss the use of ordinary water in a system employing thorium as fuel.

The problem of breeding U^{233} from thorium in thermal neutron heavy-water-moderated reactors and in fast neutron reactors has frequently been discussed by Feinberg, Kunegin and Nemirovsky, who are members of the Institute; their researches showed that through the use of ordinary water as moderator in a Th^{232} - U^{233} system it is possible to achieve a breeding ratio close to 1.2 and thus attain complete burn-up of the thorium.

This type of reactor would consist of a core of laminar elements containing U^{233} and a breeding zone surrounding the core and containing lumps of Th or ThO_2. The moderator would be ordinary water at 300°C and about 100 atmospheres pressure flowing between the laminar fuel elements whose heat charge would be very high.

An estimate of the possibilities for such a system can be obtained by calculating the breeding ratio for different ratios of the quantities of water, U^{233} and construction materials. For the latter aluminum, zirconium, stainless steel etc. were considered. An important property of a thorium system is the fact that η for U^{233} is practically constant at ~2.3 in a very broad energy range.

The breeding ratio BR of nuclear fuel can be determined from the simple formula

$$BR = \eta - 1 - \delta$$

where δ is the neutron loss in water, construction materials and fission products in the breeding zone and as a result of the formation of the isotopes U^{234}, U^{236} and U^{235}.

δ Depends strongly on the neutron spectrum in the reactor as well as on the burn-up of nuclear fuel in one run.

TABLE 2

η as a Function of Neutron Energy for U^{233}.*

Neutron energy range	η	Neutron source
Thermal	2.28 ± 0.02	Spectral ranges isolated by filters
0.15 - 0.5 ev	2.28 ± 0.09	" "
0.4 - 3 ev	2.24 ± 0.05	" "
0.6 - 6 ev	2.24 ± 0.05	" "
2.5 - 25 ev	2.28 ± 0.05	" "
8 - 130 ev	2.28 ± 0.05	" "
30 kev	2.25 ± 0.07	Photoneutrons
140 kev	2.43 ± 0.12	" "
250 kev	2.45 ± 0.12	" "
900 kev	2.60 ± 0.13	" "

*Data obtained from Spivak, Erozolimsky, Dorofeev, Lavrenchik, Kutikov and Dobrynin.

TABLE 3

η as a Function of Neutron Energy for U^{235}.*

Neutron energy range	η	Neutron source
Thermal	2.06 ± 0.02	Spectral ranges isolated by filters
0.15 - 0.5 ev	2.06 ± 0.06	" "
0.4 - 3 ev	1.60 ± 0.04	" "
0.6 - 6 ev	1.50 ± 0.04	" "
2.5 - 25 ev	1.52 ± 0.04	" "
8 - 130 ev	1.48 ± 0.04	" "
300 kev	1.86 ± 0.04	Photoneutrons
140 kev	2.12 ± 0.10	" "
250 kev	2.21 ± 0.15	" "
900 kev	2.28 ± 0.08	" "

*Data obtained from Spivak, Erozolimsky, Dorofeev, Lavrenchik, Kutikov and Dobrynin.

Neutron losses in water and construction materials diminish as the amount of water and construction materials in the lattice is reduced. When a changes from 20 to 1 the neutron losses become quite small. The spectrum of neutron absorption in the core is quite hard even at a=20 (the thermal region amounts to only a few per cent of all neutrons absorbed in the lattice) and at $a = 5$ it approximates the spectrum of a fast neutron reactor (Fig. 4). For such values of a Xe^{135} poisoning is considerably smaller than in thermal neutron reactors.

A considerable contribution to the size of δ can come from the absorption of neutrons with the formation of U^{234}, U^{235} and U^{236}. For 30% burn-up the amount of U^{234} accumulated in one run is about 3%. The amount of U^{235} accumulated per run is ~0.5%. Since the resonance integral of U^{234} is probably at least 5 times smaller than the resonance integral of U^{233}, the contribution to δ from the latter does not exceed 0.005. After many successive runs for the purpose of consuming the U^{233} larger quantities of other uranium isotopes will be accumulated. If we consider a stationary state of the system attained after a considerable period of time and take η= 1.5 (Table 3) for U^{235} in the epicadmium neutron spectrum, δ does not exceed 0.2. It can be reduced by separating

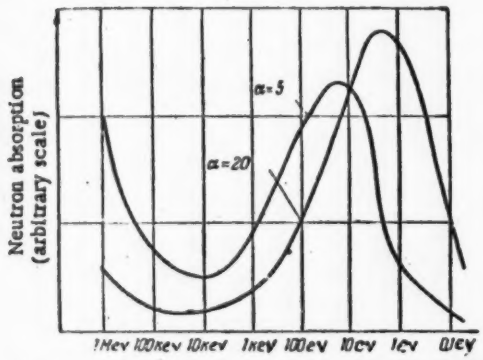

Fig. 4. Neutron absorption spectrum in Th^{232} - U^{233} system as a function of relative concentrations of hydrogen and uranium atoms. α) Relative concentration of hydrogen and U^{233} atoms.

U^{233} from the mixture of uranium isotopes. This method is technologically and economically advantageous for the additional reason that the quantity of reprocessable uranium obtained by isotope separation is comparatively small.

Thus the breeding ratio for the U^{233} - Th^{232} cycle in a reactor using a considerable fraction of epithermal neutrons can reach values from 1.10 to 1.20 with 30% burn-up in one run.

For economically profitable nuclear power we require in addition to a high breeding ratio a high specific thermal capacity (per unit weight of nuclear fuel). By the use of an ordinary water moderator it is possible to achieve a volumetric heat release rate in the core of from 1000 to 2000 kw/liter while the heat release rate of the nuclear fuel is 2000 - 5000 kw/kg.

These heat release rates are also characteristic of fast neutron reactor cores, but one advantage can be pointed out for the type of reactor which we have considered. The nuclear fuel in it can be "diluted" with a considerable quantity of construction materials such as aluminum with practically no reduction of the breeding ratio; this simplifies the task of constructing long-lasting fuel elements. It must also be mentioned that thorium behaves much better in the reactor than does uranium. Even when a large amount of U^{233} was accumulated in thorium we observed no instance in which thorium lumps went out of order nor any of the changes which are well-known in the case of uranium.

In England you are proceeding very cautiously with respect to water systems; partially for this reason our research in this area seems to be painted in brighter colors than experimental caution would require. As a supplement to this report I have the pleasure of submitting more detailed data* and I await your comments.

*Editor's Note: The author refers to articles in this issue, except for articles by D.I. Blokhintsev and V.V. Vladimirsky, which appeared in Issue No. 1.

ON THE NUMBER OF NEUTRONS EMITTED BY Pu^{239} ON FISSION BY THERMAL AND SUPERTHERMAL NEUTRONS*

V.I. Kalashnikova, V.I. Lebedev, L.A. Mikaelian, and M.I. Pevzner

The average number of neutrons emitted on fission of Pu^{239} by thermal and superthermal neutrons (E_w from 0.15 to 0.5 ev) is measured.

The fast neutrons that arise on the fission of heavy nuclei are emitted, as is well known, from the fission fragments, and therefore the average number of neutrons, ν, emitted in one event should be determined both by the excitation energy of the fragments and their mass distribution. The excitation energy of the fragments is to some extent dependent on the excitation energy of the nucleus that undergoes fission, although it is clear that small variations of the latter (of the order of the separation of the energy levels) should not lead to variations in the magnitude of ν. Neighboring energy levels of the intermediate nucleus may, however, have different spins, and possible different mass distributions for the decay products. This situation could lead to a new distribution of excitation energy for the fragments, and thus cause a variation in ν [1]. In connection with this, it is interesting to compare the values of the quantities ν for various levels of the splitting nucleus.

Indirect data as to the behavior of ν in the resonance region can be obtained by comparing the results of experiments on the capture cross section, the cross section for splitting, and the average number of neutrons emitted in one capture event, $-\nu_{eff}$. Such a comparison, carried out for U^{233}, U^{235} and Pu^{239} on the basis of several works [2-4], does not contradict the usually accepted assumption of the constancy of the quantity ν in the region of low energy for the neutrons causing the fission. In reference [5], however, a discrepancy was found between the calculated value of ν_{eff} for Pu^{239} and the directly measured value of ν_{eff}.

Recently there have appeared several communications in the literature referring to works whose goal was direct observation of the change in ν on fission of U^{235} [6] and Pu^{239} [6-8] by neutrons with energies from 0.01 to 0.5 ev.

As for U^{235}, in the region in which the experiments were performed, no variation in ν was observed. The measurements made on Pu^{239} gave contradictory results. In references [6] and [7], no variation in ν was observed, but in reference [8], it was found that on going from thermal neutrons to neutrons with energies of 0.3 ev, ν decreases by 12%.

In connection with this, we consider it worthwhile to publish the data that we have obtained on this question.

We performed a relative measurement of the value of ν for fission of Pu^{239} by thermal neutrons and neutrons with energies in the interval from 0.15 to 0.5 ev. There is a strong resonance level in Pu^{239} at 0.3 ev, and the cross section in the thermal region is to a large extent determined by a resonance level for negative energy values.

The work was carried out on the neutron beam leaving the reflector of the reactor RFT. The energy intervals were separated with the aid of gadolinium and cadmium filters. The thickness of the filters was chosen

*The results of this work were presented in discussions at the Geneva Conference on the Peaceful Uses of Atomic Energy in August, 1955.

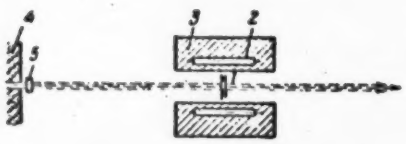

Figure – 1) Chamber; 2) BF_3 counters; 3) paraffin; 4) reactor shielding; 5) filter.

so that the lowest effective energy limits of the neutrons should be, respectively, 0.15 and 0.5 ev. Thus the resonance level at 0.3 ev was essentially included between these two limiting absorbing filters.

A fission chamber with a thin layer of Pu^{239} was inserted into the neutron beam. The neutron detector was composed of BF_3 proportional counters surrounded by paraffin. A schematic diagram of the set-up is shown in the figure.

The pulses from the neutron detector were connected in coincidence with the fission chamber pulses. The ratio of the number of coincidences of fast neutrons with fission fragments to the number of fission events is given by the quantity $\nu\omega\eta$, where $\omega\eta$ is a coefficient determined by the apparatus (η is the effectiveness of the neutron detector, and ω is the solid angle). A more detailed description of the method and the apparatus used is presented in reference [9].

The measurement of the quantity $\nu\omega\eta$ was performed in the free neutron beam and in the beam after it had passed through the gadolinium or the cadmium filter. It turned out that the quantity $\nu\omega\eta$ remains constant to within 1%.

The results of the measurements are presented in the table.

TABLE

Filter	Effective neutron energy interval, in ev	Number of fission fragments	Number of coincidences	$\nu\omega\eta$
–	0.025	331584	46132	0.1391 ± 0.0008
Gd (0.08 g /cm^2)	> 0.15	335616	46828	0.1395 ± 0.0009
Cd (0.86 g /cm^2)	> 0.5	80320	11272	0.140 ± 0.002

On the basis of these results we may conclude that the quantity ν is the same for the two resonance levels of Pu^{239} (at 0.3 ev and in the negative energy region). In order to evaluate the accuracy of this assertion, however, we must take account of the fact that in the whole region of energy investigated the fission is caused by both resonance levels (we may neglect the effect of the 7.4 ev resonance level). If we assume that there is no interference between the levels, then the final result may be evaluated as good to within 2%.

LITERATURE CITED

[1] A. Bohr, "Collective motion in atomic nuclei" (Report No. 911 presented by Denmark at the International Conference on the Peaceful Uses of Atomic Energy, 1955).

[2] S.Ya. Nikitin, S.I. Sukhoruchkin, K.G. Ignatyev and N.D. Galanina, Session of the Acad. Sci. USSR on the Peaceful Uses of Atomic Energy, July 1-5, 1955 (Div. Phys.-Math. Sci.), p. 87.

[3] B.G. Erozolimsky, P.E. Spivak, G.A. Dorofeev, and V.N. Lavrenchik, Session of the Acad. Sci. USSR on the Peaceful Uses of Atomic Energy, July 1-5, 1955 (Div. Phys.-Math.Sci.), p. 397.

[4] V.F. Gerasimov, V.S. Zenkevich, and V.I. Mostovoi, Session of the Acad. Sci. USSR on the Peaceful Uses of Atomic Energy, July 1-5, 1955 (data presented by V.S. Fursov).

[5] H. Palevsky et al., "Measurement of capture to fission ratio of U^{235}, U^{233} and Pu^{239} by a new method" (Report No. 587 presented by the USA at the International Conference on the Peaceful Uses of Atomic Energy, 1955).

[6] B.R. Leonard, Jr., E.J. Seppi and W.J. Friessen, Bull. of Am. Phys. Soc., 1,1,A2 (1956).

[7] J-M. Anclair, H.H. Landon and M. Jacob, Compt. rend. 241, 1935 (1955).

[8] R.L. Zimmerman, H. Palevsky and D.J. Hughes, Bull. Am. Phys. Soc. 1, 1, A1 (1956).

[9] V.I. Kalashnikova, V.P. Zakharova, A.V. Krasnushkin, V.I. Lebedev, and M.I. Pevzner, Session of the Acad. Sci. USSR on the Peaceful Uses of Atomic Energy, July 1-5, 1955 (Div. Phys.-Math. Sci.), p. 161.

DETERMINATION OF THE AVERAGE NUMBER OF NEUTRONS ν_{eff} EMITTED IN A SINGLE CAPTURE EVENT BY THE ISOTOPES U^{233}, U^{235} AND Pu^{239} IN THE SUPERTHERMAL REGION OF NEUTRON ENERGIES

P.E. Spivak, B.G. Erozolimsky, G.A. Dorofeev, V.N. Lavrenchik, I.E. Kutikov and Yu.P. Dobrynin

The variation of ν_{eff} for the isotopes U^{233}, U^{235} and Pu^{239} is measured in the superthermal region of neutron energies. For U^{233} ν_{eff} remains constant up to an energy of the order of 100 ev. For Pu^{239} ν_{eff} drops by 12% on going from the thermal spectrum to the spectrum of energies from 0.15 to 0.5 ev, and then remains constant. For U^{235} ν_{eff} remains constant on going from the thermal spectrum to the spectrum of energies from 0.15 to 0.5 ev, and then drops by 18% on going to the spectrum of energies from 8 to 130 ev.

INTRODUCTION

One of the basic parameters of a nuclear chain reaction which is of use in reactor calculations is the average number of secondary neutrons that are emitted by the splitting nucleus in one capture event, $\nu_{eff} = \nu \frac{\sigma_f}{\sigma_a}$, where ν is the average number of secondary neutrons emitted per fission event, and σ_f and σ_a are the effective cross sections for fission and absorption, respectively.

The values of ν_{eff} that have been obtained for the isotopes U^{233}, U^{235} and Pu^{239} in several experiments [1-3] indicate that a chain reaction is possible in any one of these three isotopes.

For extensive breeding of "nuclear fuel" the value of ν_{eff} must be greater than two. In the thermal neutron region this condition is realized for the thorium cycle (for the isotope U^{233}: $\nu_{eff} - 2 = 0.28$). For the plutonium cycle the difference $\nu_{eff} - 2$ is close to zero.

In order to solve the problem of extensive breeding, it is imperative to know the values of ν_{eff} for fissionable isotopes in other neutron energy regions.

In the present article we give a description of the measurement of the variation of ν_{eff} for the isotopes U^{233}, U^{235} and Pu^{239} for intermediate neutron energies from the thermal region to 100 ev. The various results of these investigations were stated briefly by the authors in references [4] and [5].

Here we give a complete account of the data concerning the measurement of ν_{eff} in the superthermal region of neutron energies which was performed on the reactor RFT [6] by P.E. Spivak, B.G. Erozolimsky, G.A. Dorofeev, and V.N. Lavrenchik, and of the additions to this work on the measurement of ν_{eff} in the neutron energy region from 0.15 to 0.5 ev which were performed by B.G. Erozolimsky, I.E. Kutikov, and Yu.P. Dobrynin on the reactor VVR [7] (water-water reactor).

The measurement method

A diagram of the measuring apparatus is presented in Fig. 1. The neutron beam from the reactor passes through a filter of gadolinium, cadmium, or boron, which establishes the neutron spectrum, then through an inlet collimator, and enters the cavity of a graphite prism. Outside the cavity and evenly spaced throughout the volume of the prism, are located boron neutron counters, which comprise the indicating system.

In the center of the prism is a sample of the fissionable isotope. In this set-up the number of neutrons recorded varies both because of absorption of neutrons by the sample and because of neutrons resulting from fission. This variation in the indicating system can be expressed in the following way:

$$\Delta N_1 = -F\Sigma_{av}k_1 + F\Sigma_{av}k_2\nu_{eff}. \qquad (1)$$

where F is the total neutron flux passing through the sample, Σ_{av} is the macroscopic cross section for neutron absorption per square centimeter of the sample, averaged over the whole spectrum of the neutron beam, k_1 is the indicator efficiency for the primary spectrum of the neutron beam, and k_2 is the indicator efficiency for the fission neutron spectrum.

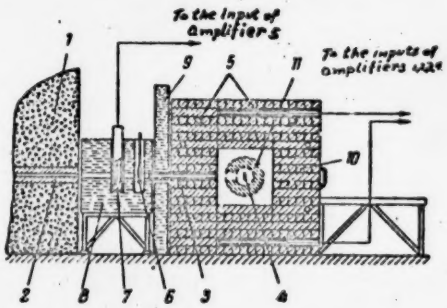

Fig. 1. Schematic cross section of the measuring apparatus. 1) Shielding of the pile; 2) first collimator; 3) second collimator; 4) the sample being studied in the center of the cavity; 5) proportional counters (BF_3); 6) filter and adapter; 7) monitoring fission chamber with a layer of U^{235}; 8) shielding (parafin with boron); 9) shielding for the front wall of the prism (parafin with boron); 10) insert, retractable for changing the sample; 11) boron-parafin filter, inserted for the second measurement.

In order to eliminate the determination of the absolute values of the neutron flux F and the total cross section Σ_{av} from the measurements, a second measurement was performed with the same sample surrounded with a spherical boron-paraffin filter. The dimensions of the filter are chosen so that the primary neutron spectrum is completely absorbed. In this case variation in the counting rate of the indicator ΔN_2 will be caused only by the neutrons resulting from fission

$$\Delta N_2 = F\Sigma_{av}k_3\nu_{eff}. \qquad (2)$$

where F and Σ_{av} have the same meaning as in Equation (1), and k_3 is the indicator efficiency for the fission neutron spectrum in the presence of the boron-paraffin filter.

Comparing expressions (1) and (2), we obtain

$$\nu_{eff} = \frac{k_1}{k_2}\,\frac{1}{1-\frac{k_1}{k_2}X}. \qquad (3)$$

where X is the ratio of ΔN_1 to ΔN_2.

As will be shown below, the ratio of the coefficients k_1 and k_2 is easy to determine with sufficient accuracy with the aid of simple measurements. It is not difficult to see that the direct determination of the ratio of the coefficients k_1 and k_2 would necessitate measuring the magnitudes of the neutron flux for the primary spectrum and the fission spectrum.

We may limit ourselves to the relative variation of the coefficient k_1 and thus obtain the relative variation of ν_{eff}. In order to obtain the absolute value of ν_{eff}, we can normalize the variation to a known value of ν_{eff} measured for thermal neutrons. The ratio of ν_{eff} for the observed spectrum to ν_{eff} for thermal neutrons will be of the form

$$\frac{\nu_{eff}}{\nu^0_{eff}} = \frac{k_1}{k_1^0}\,\frac{1-\frac{k_2}{k_2}X_0}{1-\frac{k_2}{k_2}X}, \qquad (4)$$

where quantities with the index 0 are the values obtained from measurements on thermal neutrons.

It should be noted that in the derivation of expression (4) it is assumed that there are no effects from the

scattering of neutrons by the sample, that the magnitude of the flux F incident on the sample remains the same in measurements with the boron-paraffin filter ΔN_2 and without it ΔN_1, and that the primary neutron spectrum is entirely absorbed in the measurements with the boron-paraffin filter.

Relation (4) will be valid, and the value of ν_{eff} measured by this method will contain no systematic errors, only if the above conditions are strictly satisfied. Since the measurements of the effects ΔN_1 and ΔN_2 are performed on the same sample, the necessity of knowing the value of Σ_{av} is avoided, and it becomes possible to use samples thick enough for practical measurement, since the effect of self-absorption by the sample cancels out of the expression for $X = \frac{\Delta N_1}{\Delta N_2}$. In this it is assumed that the primary neutron spectrum is not significantly altered by blocking of the neutrons at resonance energies.

Thus the problem of measuring ν_{eff} reduces simply to the measurement of the relative values $\frac{\Delta N_1}{\Delta N_2}$, $\frac{k_2}{k_2}$ and $\frac{k_1}{k_1^0}$.

Apparatus and control experiments.

1. The graphite prism was 190 x 190 x 190 cm^3, and its cavity was 50 x 50 x 50 cm^3. The group of boron counters that are located at distances from 50 to 60 cm from the boundary of the cavity comprise the indicator system, whose efficiency depends little on the neutron energy. As will be shown later, this property of the sensitivity of the indicating system makes for the best conditions for obtaining accurate results of measurement for ν_{eff}. The large dimensions of the cavity were chosen so as to minimize the effect of interaction of the sample with the neutrons moving in the opposite direction, which arise as a result of slowing down the neutrons of the initial spectrum in the graphite.

In order to reduce the effect of these return neutrons, in all the measurements in the superthermal regions the specimens on which the measurements were being performed were surrounded by a cadmium jacket.

The magnitude of the return effect was determined by a special control experiment. Instead of the sample, an ionization chamber with a U^{235} layer covered with cadmium was placed in the cavity. The insert at the rear wall of the prism was then removed, allowing the beam to pass freely through the prism. It was shown that the fission fragment count for the hardest spectrum changed within the limits of $\pm$ 1% when the insert was removed and replaced.

The indicating system made up of the counters equally distributed in the graphite prism was insensitive to the effects of neutron scattering by the sample. The independence of the indicator sensitivity from the direction of motion of the neutrons in the cavity was verified with the aid of a thick graphite sample with a large scattering cross section (1.5 g /cm^2 of graphite). It was shown that the effect of neutron scattering by such a sample is no greater than 0.1%.

The boron-paraffin filter was in the form of a sphere of 26 cm diameter, filled with paraffin and boron, with an internal cavity diameter of 6 cm for mounting the sample and an opening for admitting the neutron beam.

As was shown by experiment, the wall thickness of the spherical filter (10 cm) was sufficient for practically complete absorption of the neutrons passing through the opening into the spherical cavity of the filter. In order to verify this, a thick sample of boron (1.5 g /cm^2 of boron), whose absorption coefficient is known to be several times that of any of the samples of uranium and plutonium used, was placed into the spherical filter. Careful measurement showed that insertion of this sample into the cavity of the filter in the path of the beam leads to no changes in the counting rate of the indicator system greater than $\pm$ 0.05%.

2. The dimensions and shape of the neutron beam in the prism cavity were established by the following collimating procedure: a boron carbide plug 25 cm long with a central opening of diameter 25 mm was placed in the exit channel of the reactor; further along the axis of the beam in the front wall of the prism was placed an entry collimator, made of a boron carbide cylinder whose diameter was 10 cm and whose length was 60 cm and having a central channel of 8 mm diameter.

The dimensions of the beam in the center of the cavity depend to some extent on the neutron energy, since the effective length of the entry collimator differs for different neutron energies. For thermal neutrons

the collimating set-up creates a beam diameter no larger than 15 mm at the center of the cavity. For faster neutrons the collimation is somewhat poorer. Up to energies of the order of 100 ev, however, the beam diameter is no larger than 18-20 mm.

The small beam cross section and, correspondingly, those of the samples were chosen so as to secure sufficiently great values for the $\Delta N/N$ effect for a limited amount of matter. In addition, reduction of the area of the sample and the cross section of the beam leads to decrease both in the return effect, and in the leakage of neutrons through the opening in the boron-paraffin filter and the collimator. The beam cross section, however, may not be too small, since then the hard to avoid external background and the background due to neutrons scattered in the entry channel significantly reduce the relative effect $\Delta N/N$.

As has already been demonstrated, it is very important that the neutron flux F be the same for the measurements both with and without the boron-paraffin filter. For this reason the diameter of the samples and the entry channel of the boron-paraffin filter were chosen somewhat larger than the dimensions of the beam (22 mm).

That the flux remained the same was verified by two control experiments.

An aluminum sample of 22 mm diameter was placed in the position of the fissionable sample and was activated with and without the boron-paraffin filter by thermal neutrons and by neutrons that have passed through cadmium, in which the neutron fluxes were sufficient for activation.

As a result of these measurements, it was established that the activities were the same in both cases within the limits of $\pm$ 1%.

The second experiment was performed with the aid of a group of boron counters surrounded by boron-paraffin shielding. These counters recorded only the fission neutron spectrum, and were not sensitive to the superthermal neutrons. The counters were placed in a corner of the cavity. Then the relative effects from a fissionable sample were measured with and without the filter and with various filters forming the neutron spectrum. In this the ratio of the counts in both measurements remained constant within the limits of $\pm$ 1%.

3. The isotopes were investigated in the form of powdered oxides which were poured into aluminum boxes and compressed into small 22mm diameter tablets. A large amount of oxygen in the samples causes the neutrons to be slowed down, which can alter the results of measurement of ν_{eff} due to the capture of slow neutrons by the cadmium jacket. In order to determine the possible error, the fissionable sample was replaced by a graphite one, whose thickness was 1.6 g /cm^2, and measurements were taken with and without the cadmium jacket. A correction was introduced on the basis of the results of this experiment for the slowing down of the neutrons by the oxygen, and this correction was no larger than 1% of the total effect.

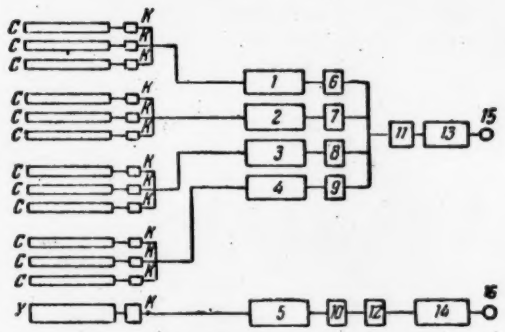

Fig. 2. Block diagram of the counting circuit. C) Boron counters; K) cathode repeaters; Y) fission chamber with a layer of U^{235}; 1,2,3, 4, and 5) amplification channels; 6,7,8,9, and 10) diode discriminators; 11,12) Schmidt cascade circuits; 13,14) scalers; 15,16) electromechanical counters (1:16,000).

The choice of thickness for the samples is established by the magnitude of the relative effect $\Delta N/N$ that can be measured with sufficient accuracy. Even for samples of considerable thickness (2 g /cm^2), however, the relative effect $\Delta N/N$ for measurements in the fast neutron spectrum was merely 5%.

4. In order to measure ΔN with an error of $\pm$ 2%, it is necessary that the neutron count recorded by indicating system be taken with an error no greater than $\pm$ 0.1%.

The magnitude of the neutron flux incident on the sample was 5×10^6 cm^{-2} sec^{-1} for the hardest spectrum.

For an indicating system efficiency of about 2% the necessary statistical accuracy of measurement was achieved in a relatively short time as a result of a few series of measurements.

Stability of the counting circuit was achieved by the use of negative feed-back in the amplifiers

and by supplying it from stabilized sources. In order to account for the instability of the reactor power, and correspondingly of the neutron flux, an ionization chamber with a layer of U^{235} placed in the beam was used as a monitor.

A block diagram of the counting circuit is presented in Fig. 2. Pulses from twelve cathode repeaters connected directly to the boron counters entered four amplification channels. Each of the amplification channels had an amplification factor of 10^5 with quadruple negative feed-back, embracing all three cascades. After cut-off by diode discriminators that follow the amplifiers, the pulses entered a common shaping cascade circuit, after which they entered a scaling circuit with a resolving time of 0.2 μsec. The total scaling factor was 16,000. The total resolving time of the whole counting circuit was 1 μsec; this made it possible to count up to 10^4 pulses per second without noticeable omissions.

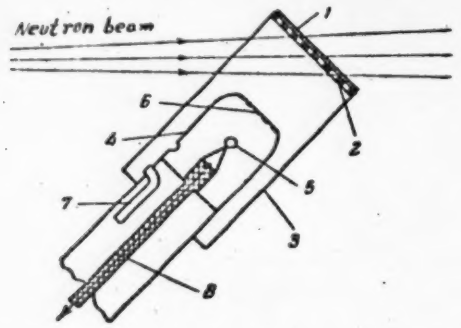

Fig. 3. Construction of the proportional counter and its position relative to the neutron beam. 1) Target; 2) aluminum cover with openings covered with mica (1.2 mg/cm²); 3) casing of the counter; 4) cathode of the counter; 5) anode of the counter (a sphere of diameter 0.16 cm); 6) grid covered by a thin collodion film; 7) copper tube for connection to a gas ballast volume (90% argon and 10% methylal at a pressure of 30 mm Hg); 8) insulation.

Measurement of the constants of the apparatus.

1. In order to determine the ratio of the sensitivity k_1 of the indicating system for neutrons of a given spectrum to the value of this same constant for thermal neutrons k_1^0, a proportional counter with a thin mica window was placed into the cavity of the prism; on this counter was placed a target covered by a thin layer of lithium fluoride (98% Li^6) in such a way that it was in the same place as is ordinarily occupied by the fissionable sample. First the number of Li^6 (N_{Li}) fission events induced by the neutrons of the given spectrum was measured. Then a boron or lithium absorber was placed at the same point, and the decrease in the count ΔN was measured. The ratio of the effects was of the form

$$\frac{\Delta N}{N_{Li}} = \frac{1}{\beta} \frac{\Sigma_{absorber}}{\Sigma_{layer}} k_1,$$

where k_1 is the coefficient that we are looking for.

Since β (the counting efficiency of the proportional counter) does not depend on the neutron energy, and the absorption cross section for the thin lithium layer (Σ layer) and for the absorber (Σ absorber) depend in the same way on the neutron energy, we can find the variation of k_1 by measuring the ratio $\Delta N/N_{Li}$ in various spectra.

In determining the variation of k_1 by the above method, it was necessary, in order to secure measurable effects, to use thick absorbers. Therefore the effect of self-absorption in the thick absorber, which varies with the energy, leads to an error in measuring the variation of k_1.

In order to determine the correction in the variation of k_1 due to the effect of self-absorption, it became necessary to measure the dependence of ΔN on the target thickness for each spectrum. The weight of the target was chosen so that the effect of self-absorption should be approximately 15%, and the change in this effect on going over from one spectrum to another should be no greater than 2-3%.

In order to exclude possible errors due to the presence in the samples of impurities whose cross section differs from the 1/v law (rare earths, cadmium), measurements of ΔN were performed both on boron and lithium. The results of these measurements turned out to be the same.

It should be noted that the coefficient k_1, which enters into expression (4), characterizes the sensitivity of the indicating system to the absorption of neutrons by the fissionable samples, for which the dependence of the absorption cross section does not coincide with the corresponding variation for boron and lithium. It is therefore very important that the dependence of the indicator sensitivity k_1 on neutron energy not vary too sharply. In this case the correction to the value of k_1 measured for boron and lithium is insignificant.

Measurements showed that the value of k_1 increased by 1% on going from thermal neutrons to those that have passed through cadmium, and by 2% for those that passed through a 1 g /cm² thick boron filter; i.e., in this neutron energy interval, it is nearly constant.

2. It turned out to be impossible, however, to measure ν_{eff} with sufficient accuracy in this prism throughout the whole neutron energy interval, because on going to harder spectra the background ratio became worse and the counting rate of the indicating system decreased.

Therefore the measurement of the variation of ν_{eff} from the thermal neutron spectrum to the spectrum of neutrons that have passed through the cadmium was performed with the aid of the prism described above, but the measurement of the rest of the variation of ν_{eff} into the more energetic spectrum, was performed with the aid of a smaller prism of dimensions 90 x 90 x 90 cm³ with a cavity 30 x 30 x 30 cm³. The variation of k_1 measured with this prism is characterized by a sharp drop (Table 1) on going from thermal neutrons (0.025 ev) to those that have passed through cadmium (>0.4 ev), whereas the change in k_1 on going from these latter neutrons to those that have passed through a 4 g /cm² boron filter is only 14%, that is, depends weakly on the energy.

TABLE 1

The Results of Measurements on the Variation of k_1 in the Small Prism

Free beam	1 g /cm² Cd filter (1.2 mm)	B_4C filters		
		0.5 g /cm² B	1 g /cm² B	4 g /cm² B
1	0.866 ± 0.009	0.82 ± 0.01	0.79 ± 0.01	0.72 ± 0.01

In this case the correction to the coefficient k_1 that accounts for the difference in the variation of the absorption cross section of the isotopes being investigated and the variation of the absorption cross section for boron and lithium is about 2% on going from the spectrum of neutrons passing through the cadmium to the spectrum of those passing through the 4 g /cm² boron filter. All the control experiments that were performed with the large prism were repeated with the small one.

3. The decrease in the sensitivity of the indicating system to fission neutrons when the boron-paraffin filter is placed in the cavity (k_3/k_2) was measured with the aid of a thermal neutron converter – a fissionable sample placed in the cavity and enclosed by a cadmium hood. The ratio of counts in the indicating system with the boron-paraffinfilter to the counts without it, that is, k_3/k_2, turned out to be 0.31 ± 0.01 for the large prism and 0.40 ± 0.01 for the small one.

The results of measurement.

In measuring the effects ΔN_1, ΔN_2, the role of impurities due to other isotopes in the samples being investigated were accounted for. The Pu^{239} samples contained about 1.5% of the isotope Pu^{240}, which has a strong absorption resonance at 1.06 ev, and the U^{235} samples contained about 15% of the isotope U^{238}. In this connection, when the effects ΔN_1 and ΔN_2 were measured for Pu^{239}, in addition to the filter that shapes the neutron spectrum, a filter made of a similar mixture of plutonium isotopes was used to block the resonance neutrons at 1.06 ev. Similarly, for the U^{235} samples, an additional filter of U^{238} was used. The corrections corresponding to this were from 1 to 4%.

The results of measurement of ν_{eff} with all the above corrections taken into account are presented in Table 2. The first column indicates the material and thickness of the filters, the second gives the effective neutron energy interval derived by calculation, and the rest give the relative and absolute values of ν_{eff} for the isotopes U^{233}, U^{235} and Pu^{239}. The absolute values of ν_{eff} are normalized according to the value of ν_{eff} for thermal neutrons [1].

From the data presented it follows that ν_{eff} for the isotopes U^{233} and U^{235} in the energy region of 0.1-0.5 ev is the same as ν_{eff} for thermal neutrons, and for the isotope Pu^{239} it is 12% lower than the thermal value. In the intermediate neutron energy region (behind the cadmium filters) the value of ν_{eff} for Pu^{239} does not vary. The decrease of ν_{eff} for Pu^{239} in the energy region of 0.1-0.5 ev seems to be connected with the relation between the radiation and fission widths of the 0.3 ev energy level. For the isotope U^{235} a sharp drop in ν_{eff} is observed for the neutrons that have passed through the cadmium filters, which is probably caused by the properties

of the set of resonances lying in the region from 1 to 100 ev. For the isotope U^{233}, the value of ν_{eff} remains constant throughout the investigated interval.

TABLE 2

Results of Measurement of ν_{eff} in the Superthermal Region of Neutron Energies.

Conditions of measurement	Effective neutron energy interval in ev	Isotope			Remarks
		U^{233}	U^{235}	Pu^{239}	
Thermal neutron beam	0.025	1 2.28 ± 0.02	1 2.06 ± 0.02	1 2.08 ± 0.02	Relative value Absolute value
Difference of the effects obtained with a 1 g /cm² thick cadmium filter and a 0.08 g /cm² thick gadolinium filter	0.15-0.5	1.00 ± 0.04 2.28 ± 0.09	1.00 ± 0.03 2.06 ± 0.06	0.88 ± 0.03 1.79 ± 0.07	Relative value Absolute value
Cadmium filter 1 g /cm² thick	0.4-3	0.98 ± 0.02 2.24 ± 0.05	0.78 ± 0.02 1.60 ± 0.04	0.88 ± 0.02 1.79 ± 0.04	Relative value Absolute value
Cadmium and boron carbide filter 0.5 g /cm² thick	0.6-6	0.98 ± 0.02 2.24 ± 0.05	0.73 ± 0.02 1.50 ± 0.04	0.89 ± 0.02 1.81 ± 0.04	Relative value Absolute value
Cadmium and boron carbide filter 1 g /cm² thick	2.5-25	1.00 ± 0.025 2.28 ± 0.05	0.70 ± 0.02 1.52 ± 0.04	0.88 ± 0.02 1.79 ± 0.04	Relative value Absolute value
Cadmium and boron carbide filter 2 g /cm² thick	8-130	1.00 ± 0.025 2.28 ± 0.05	0.72 ± 0.02 1.48 ± 0.04	– –	Relative value Absolute value

The results presented are in good agreement with the work of S.Ya. Nikitin et al. [8], who measured the variation of ν_{eff} in this neutron energy region by other methods.

The basic results of the present paper were reported at the Session of the Academy of Sciences USSR on the Peaceful Uses of Atomic Energy in July of 1955 [5]. In August of the same year American and English investigators published some new data on ν_{eff} at the Geneva Conference on the Peaceful Uses of Atomic Energy.

Our values for ν_{eff} for U^{235} and Pu^{239} agree with the results of the work of Kanne et al. [9]. In Kanne's work, the dependence on energy of the ratio of the cross section for radiative capture to fission cross section: $\alpha = \sigma_r/\sigma_f$ is measured. These results make it possible to calculate corresponding values of $\nu_{eff} = \nu \frac{1}{1+\alpha}$.

For the isotope U^{235} the value of α for a neutron spectrum with an average energy of 100 ev is, according to Kanne's data, 0.52 ± 0.10, which corresponds to $\nu_{eff} = 1.64 \pm 0.10$. According to the direct measurement of ν_{eff} in our work, $\nu_{eff} = 1.48 \pm 0.04$ for an analogous spectrum. For the isotope Pu^{239}, according to the American data for a neutron spectrum with a lower bound of 5 ev, $\nu_{eff} = 1.82$, and according to our results for a similar spectrum, $\nu_{eff} = 1.79 \pm 0.04$.

We should also mention the results of measurements by two groups in the Brookhaven and Hanford laboratories [10], in which the variation of ν_{eff} is measured on a mechanical selector for the isotopes U^{233} and Pu^{239}

in the neutron energy region of 0.1 ev and for the isotope U^{235} in the region of 0.5 ev. The drop of ν_{eff} which we discovered for Pu^{239} behind the gadolinium filter, and the constancy of ν_{eff} for U^{233} are entirely confirmed by this work. The average values of ν_{eff} for U^{233} in the energy interval of 0.1-0.5 ev are in satisfactory agreement with our data for that part of the spectrum from 0.15 to 0.5 ev.

Values of ν_{eff} for the isotopes U^{233} and U^{235} have been obtained by a group of English scientists [11], which also agree well with our data.

Further investigations of the dependence of ν_{eff} on neutron energy in the region of several hundred kiloelectron volts is of some practical interest for construction of fast neutron reactors. The authors have carried out work on measurements of ν_{eff} for the isotopes U^{233}, U^{235} and Pu^{239} in the neutron energy interval from 30 kev to 1 mev, the results of which will be presented in the following article.

LITERATURE CITED

[1] P.E. Spivak, B.G. Erozolimsky, "Physical investigations", (Reports of the Soviet Delegation at the International Conference on the Peaceful Uses of Atomic Energy) Acad. Sci. USSR Press, 1955, p. 184.

[2] A.I. Alikhanov, V.V. Vladimirsky, and S.Ya. Nikitin, loc. cit., p. 199.

[3] D.J. Hughes and J.A. Harvey, Neutron Cross Sections, McGraw-Hill Book Company, New York (1955).

[4] P.E. Spivak, B.G. Erozolimsky, G.A. Dorofeev and V.N. Lavrenchik, "Physical investigations", (Reports of the Soviet Delegation at the International Conference on the Peaceful Uses of Atomic Energy) Acad. Sci. USSR Press, 1955, p. 213.

[5] B.G. Erozolimsky, Session of the Academy of Sciences USSR on the Peaceful Uses of Atomic Energy, July 1-5, 1955 (Div. Phys.-Math. Sci.), Acad. Sci. USSR Press, 1955, p. 369.

[6] "Reactor construction and reactor theory", (Reports of the Soviet Delegation at the International Conference on the Peaceful Uses of Atomic Energy) Acad. Sci. USSR Press, 1955, p. 49.

[7] Ibid., p. 91.

[8] S.Ya. Nikitin, S.I. Sukhoruchkin, K.G. Ignatyev, N.D. Galanina, P.A. Krupchitsky and V.F. Belkin, Session of the Academy of Sciences USSR on the Peaceful Uses of Atomic Energy, July 1-5, 1955 (Div. Phys.-Math. Sci.), Acad. Sci. USSR Press, 1955, p. 87.

[9] W.R. Kanne, H.B. Stewart and F.A. White, "Capture-to-fission ratio of Pu^{239} and U^{235} for intermediate energy neutrons," (Report No. 595 presented by the USA at the International Conference on the Peaceful Uses of Atomic Energy, 1955).

[10] H. Palevsky et al., "Measurement of capture to fission ratio of U^{235}, U^{233} and Pu^{239} by a new method," (Report No. 587 presented by the USA at the International Conference on the Peaceful Uses of Atomic Energy, 1955).

[11] P.A. Egelstaff, J.E. Sanders, "Neutron yields from fissile nuclei," (Report No. 425 presented by England at the International Conference on the Peaceful Uses of Atomic Energy, 1955).

THE AVERAGE NUMBER OF NEUTRONS ν_{eff} EMITTED BY THE ISOTOPES U^{233}, U^{235} AND Pu^{239} ON CAPTURE OF NEUTRONS WITH ENERGIES FROM 30 TO 900 kev*

P. E. Spivak, E. G. Erozolimsky, G. A. Dorofeev, V. N. Lavrenchik, I. E. Kutikov, Yu. P. Dobrynin

Measurements are taken on ν_{eff} for the isotopes U^{233}, U^{235} and Pu^{239} for neutrons with energies from 30 to 900 kev. It is discovered that in this energy region ν_{eff} increases substantially as the neutron energy increases.

Recently several articles [1-10] devoted to the measurement of the number ν_{eff} of secondary fission neutrons per absorbed neutron have appeared in print.

In these works, the values of ν_{eff} are measured for the isotopes U^{233}, U^{235} and Pu^{239} for slow neutrons in the energy region from the thermal spectrum to a few kev.

In the present article we describe measurements of ν_{eff} for the same isotopes for neutrons in the energy interval from 30 to 900 kev.

The determination of ν_{eff} is of great interest for calculations of reactors without a moderator.

Measurement of the absolute values of ν_{eff} for neutron energies of 30, 140, and 250 kev

1. Method of measurement

A method for the direct measurement of the quantity ν_{eff} for fissionable isotopes and thermal and superthermal neutrons with the aid of a graphite prism was developed in our laboratory and described previously [1], [4], [10].

Further extension of this method to two indicating systems, whose efficiencies depend differently on the neutron energies, made possible its application to the measurements described below, which were carried out with the aid of photoneutron sources.

The indicating systems consisted of two groups of BF_3-counters located in the graphite prism, with a central cavity into which could be placed the spherical samples and neutron sources (Fig. 1).

The group of counters that were located in the cavity had a higher sensitivity to neutrons from the source than to neutrons of the fission spectrum, whereas the group of counters located at distances of about 50 cm from the cavity boundaries had a higher sensitivity to the fission neutrons. The difference in the sensitivities of the two groups of counters was made greater by the introduction of cadmium rods into the prism.

* Part of the results of this work have been communicated at discussions at the Geneva Conference on the Peaceful Uses of Atomic Energy in August, 1955.

The measuring procedure consisted of introducing a photoneutron source into the cavity and of recording the number of pulses in both groups of counters simultaneously. The source was then surrounded by a spherical sample of the isotope being investigated, and the measurement was repeated.

The indications of each counter group ($\Delta N'$ and $\Delta N''$ respectively) which are caused by absorption of primary neutrons by the sample and the creation of fission neutrons, can be written in the following way:

$$\Delta N' = -Fk_1'\Sigma_c + Fk_2'\nu_{eff}\,\Sigma_{av} \qquad (1)$$

$$\Delta N'' = -Fk_1''\Sigma_c + Fk_2''\nu_{eff}\,\Sigma_{av} \qquad (2)$$

where k_1' and k_1'' are the indicator system efficiencies to the primary neutrons, k_2' and k_2'' are the same efficiencies to the fission neutrons, F is the total primary neutron flux passing through the sample, and Σ_{av} is the average absorption cross section of the sample for the primary neutrons.

From Expressions (1) and (2) it follows that

$$\nu_{eff} = \gamma\,\frac{1-\alpha X}{1-\beta X}, \qquad (3)$$

where

$$X = \frac{\Delta N'}{\Delta N''};\quad \alpha = \frac{k_1''}{k_1'};\quad \beta = \frac{k_2''}{k_1'};\quad \gamma = \frac{k_1'}{k_2'}.$$

Thus, except for the ratio $\frac{\Delta N'}{\Delta N''} = X$, only the constants for the apparatus α, β, and γ, which characterize the relative efficiencies of the two indicators to primary and fission neutrons enter Expression (3).

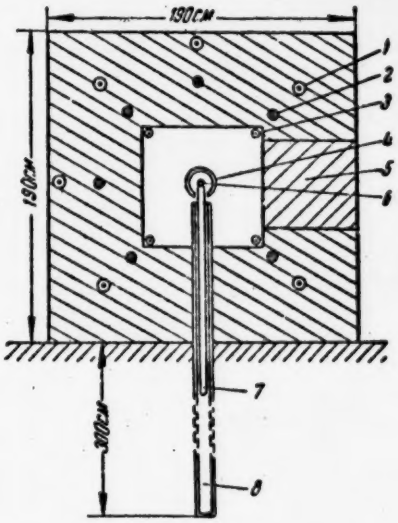

Fig. 1. Schematic cross section of the measuring apparatus.
1) BF_3-counters of the "outer" system; 2) cadmium rods; 3) BF_3-counters of the "inner" system; 4) sample; 5) graphite insert; 6) photoneutron source; 7) tube of the mechanism for inserting the source; 8) pocket for holding the source.

2. Neutron sources

In the measurements, photoneutron sources composed of Sb^{124} + Be, Ga^{72} + D_2O, and Na^{24} + D_2O were used; data regarding these is presented in Table 1.

Gamma emitters were obtained by the activation of the corresponding isotopes in the center of the RFT reactor. The high activity of the sources made it necessary to take serious precautionary measures in carrying out the experiments.

TABLE 1

Source	Half-life	Neutron energy in kev	Neutron yield in number of neutrons per second
Sb^{124} + Be	60 Days	30	$3 \cdot 10^7$
Ga^{72} + D_2O	14.3 Hours	140	$0.8\ 10^7$
Na^{24} + D_2O	14.8 Hours	250	$2 \cdot 10^7$

3. Measurement of the effects $\Delta N'$ and $\Delta N''$

The relative change of the counting rate $\frac{\Delta N}{N}$ caused by the hollow spherical sample weighing about 200 g was only a few percent.

Therefore in order to obtain the value of X with sufficient accuracy, it was necessary to achieve the possibility of measuring the indicating system counting rate accurately to within some hundredths of a percent.

The stability of the counting system was achieved by the use of feedback in the amplifiers and by stabilized power sources. In order to obtain numerical values for the magnitude of the effects ($\Delta N'$ and $\Delta N''$) due to the sample being investigated, the indicating system counting rate before the sample was placed in the cavity was averaged with the counting rate after it had been removed, and then this arithmetic average was subtracted from the counting rate with the sample in position.

Each of these three successive measurements was taken for 12 minutes, with 3 minute intervals for inserting or removing the sample. For this method of measurement, the correction for radioactive decay of the source was no greater than 0.25% of the value of X.

The fact that $\Delta N'$ and $\Delta N''$ were measured simultaneously made it easier to use rapidly decaying sources.

4. Measurement of the constants of the apparatus

In order to determine the constant of the apparatus α, a photoneutron source was placed into the center of the cavity and the counting rate in both indicating systems was measured. The ratio of these quantities gives the value of the constant $\alpha = \frac{k_1''}{k_1'}$.

The constant $\beta = \frac{k_2''}{k_2'}$ was determined in a similar way. For this, the graphite prism was placed close to the reactor in such a way that one of its beams entered through a collimator into the cavity. In the center of the cavity and in the beam was placed a convertor (sample of U^{235}) used as a fission neutron source. The convertor was covered with a cadmium sphere with an opening for admitting the thermal neutron beam. The magnitude of the constant γ was determined as the ratio of the counting rates of the inner indicating system taken first with the corresponding photoneutron source and then with the fission neutron source. The ratio of the output of these sources was determined in the graphite prism by a method developed earlier in our laboratory [11].

TABLE 2

		30 Kev	140 Kev	250 Kev
α		0.192±0.0005	0.131±0.0005	0.134±0.0005
β		0.254±0.001	0.181±0.001	0.175±0.001
γ		1.19 ±0.01	1.26 ±0.01	1.22 ±0.01
X	U^{233}	3.22 ±0.017	4.42 ±0.04	4.78 ±0.05
	U^{235}	2.815±0.015	4.06 ±0.05	4.55 ±0.06
	Pu^{239}	3.06 ±0.014	4.40 ±0.05	4.85 ±0.06

In Table 2 we present the values of the constants α, β, γ as well as X, for various neutron energies. On going from one neutron energy to another, the distribution of the counters in the measuring apparatus was somewhat changed in order to secure sufficient difference in the values of α and β.

5. Control experiments and corrections

a) The scattering of neutrons within the samples may cause additional effects which were not accounted for in the derivation of Expression (3). Errors in measurement related to elastic scattering of neutrons were determined in the following way. A graphite diffusor ($n\sigma \approx 2$) was placed into the center of the cavity next to the source. The counting rates of the indicating systems did not change by more than 0.5% in the process. If we take into account the geometry of the experiment and the thickness of the samples used, it turns out that the experimental error due to elastic scattering of neutrons is no greater than 0.1-0.2%

Inelastic scattering of neutrons in the sample may introduce errors in the results of the measurement by changing the neutron spectrum and therefore the efficiency with which the neutrons are recorded by the indicating system. The influence of inelastic scattering on the accuracy of the measurement was studied with the aid of a sample of the isotope U^{238}, whose inelastic scattering cross section, as is well known, is much greater than that for the isotopes U^{233}, U^{235} and Pu^{239}. The relative effects $\frac{\Delta N}{N}$ coming from a spherical sample of U^{238}, measured with a source made of $Na^{24} + D_2O(E_n = 250$ kev), turned out to be the same in both the outer and inner indicating systems within the experimental accuracy, which indicates the absence of effects from inelastic scattering.

b) The neutrons from the source that is placed into the cavity, in slowing down in the graphite, create a field of slowed-down neutrons in the cavity. In order to decrease the effects of interaction of the sample with these neutrons, all the samples were located inside a cadmium hood, and the dimensions of the cavity were chosen sufficiently large in comparison with the dimensions of the samples.

In addition, for the measurements "without the sample" the sample being investigated was moved a distance of about 25 cm away from the source, but remained in the cavity. In this case the direct interaction of the neutrons from the source with the sample was negligibly small, and the sample interacted only with the slowed-down neutrons, whose field was practically uniform within the prism cavity. Thus the effect of the interaction with the slowed-down neutrons, which was no greater than 4% of the basic effect, was automatically excluded in the measurement of $\Delta N'$ and $\Delta N''$.

c) The fission neutrons created within the sample pass through some distance within the sample itself, giving rise, in turn, to other fission neutrons. In a thick sample this multiplicative effect leads to a significant contribution, which makes it necessary to introduce a corresponding correction. The neutron multiplication factor is determined experimentally. To do this, a spherical source which reproduces the fission neutron spectrum is placed in the center of the cavity, and the counting rate N_0 in the indicating system is recorded. Then the source is surrounded by a fissionable sample and the measurement is repeated.

The relative effect $\frac{\Delta N}{N_0}$ due to the sample is a measure of the fission neutron multiplication. This effect, measured for the central geometry, was converted to a distribution of primary fission neutrons throughout the volume of the sample. The problem reduced to finding the ratio $\frac{L}{\delta}$, where L is the mean free path in the sample of the neutrons created in the sample, and δ is the mean free path in the sample of the neutrons emitted by the source located in the center of the sample. For the samples and sources used, the conversion factor turned out to be 1.92.

As a result of measurement, the following neutron multiplication factors $\mu = 1.92\left(\frac{\Delta N}{N_0}\right) + 1$ were found for the samples studied:

$$U^{238} - 1.10 \pm 0.01,$$
$$U^{235} - 1.05 \pm 0.01,$$
$$Pu^{239} - 1.10 \pm 0.10.$$

In calculating ν_{eff}, the value obtained by Formula (3) must be divided by the corresponding value of μ. The results of measurements of ν_{eff} at neutron energies of 30, 140, and 250 kev are presented in Table 3.

Measurement of the absolute values of ν_{eff} for neutron energies of 250 and 900 kev

1. It is impossible, with the above apparatus, to carry out measurements of ν_{eff} for higher primary neutron energies, since as the energy increases, the difference in the efficiency of the indicating system to the primary neutrons and the fission neutrons decreases, causing the accuracy to drop sharply.

In addition, and this is even more important, inelastic scattering of neutrons by the sample begins to have effect. Therefore, in order to determine ν_{eff} for energies of 900 kev, it is necessary to use a different pair of indicating systems which could avoid the above mentioned complications.

In this variation, a threshold ionization chamber with a layer of U^{238} placed in the center of the prism cavity was used (Fig. 2). The other indicator was a group of BF_3-counters located at a distance of about 50 cm from the boundaries of the cavity. The efficiency of this system was therefore practically independent of the neutron energy; this was verified with the aid of calibrated sources. Thus in this case both indicating systems were shown to be insensitive to the effects of inelastic scattering of the primary neutrons.

TABLE 3

The dependence of ν_{eff} on neutron energy for the isotopes U^{233}, U^{235} and Pu^{239} in the neutron energy interval from thermal energies to 900 kev.

Neutron energy interval	U^{233}	U^{235}	Pu^{239}
Thermal neutron beam	2.28±0.02	2.06±0.02	2.03±0,02 [1]
0,15—0.5ev	2.28±0.09	2.06±0.06	1.79±0.07 [10]
0.4—3 »	2,24±0.05	1.6 ±0.04	1.79±0.04 [10]
0.6—6 »	2.24±0.05	1.50±0.04	1.81±0.04 [10]
2.5—25 »	2.28±0.05	1.52±0.04	1.79±0.04 [10]
8—130 »	2.28±0.05	1.48±0.04	— [10]
Data from the present article			
a) Method of two groups of counters			
30 kev	2,25±0,07	1,86±0,04	2,01±0,05 *)
140 »	2,43±0,12	2,12±0,10	2,35±0,12
250 »	2,45±0,12	2,21±0,15	2,60±0,18
b) Threshold chamber method			
250kev	2,46±0,10	2,00±0,10	2,50±0,11
900 »	2,60±0,13	2,28±0,08	2,57±0,12

* G. N. Flerov and S. M. Polikanov [12], for Pu^{239} and 30 kev, obtained $\nu_{eff} = 2.22 \pm 0.16$.

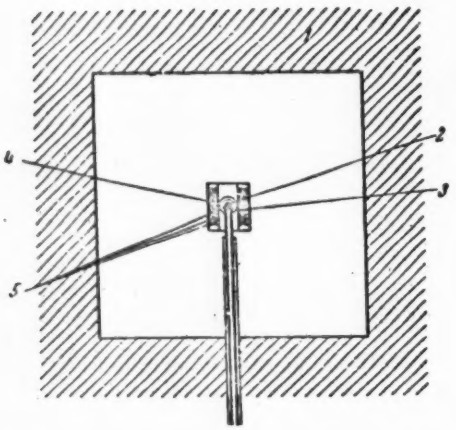

Fig. 2. The location of the threshold chamber, the source, and the sample in the prism cavity.
1) Graphite prism; 2) photoneutron source; 3) fissionable isotope sample; 4) threshold ionization chamber; 5) cylindrical electrodes with layers of U^{238}.

The measurement of ν_{eff}, as in the previous variation, consisted of determining the change in the counting rate of the indicators when the source was surrounded by a sample of fissionable isotope.

It follows from the above mentioned properties of the indicating systems, that in this case in Equations (1) and (2) $k_2' = k_1'$ (the efficiency of the group of counters in the prism does not depend on the energy) and $k_1'' = 0$ (the ionization chamber is insensitive to neutrons with energies lower than the fission threshold of U^{238}). Thus the constant $\alpha = 0$, the constant $\gamma = 1$, and Expression (3) for ν_{eff} takes on the simpler form

$$\nu_{eff} = \frac{1}{1-\beta X}. \qquad (4)$$

2. Measurement of $X = \frac{\Delta N'}{\Delta N''}$ was carried out for neutron energies of 30, 250, and 900 kev (Na^{24} + Be).

By using the value of ν_{eff} obtained from the previous measurements for 30 kev neutrons, and the value of X measured by the threshold chamber method for the same energy, we may calculate the value of the

constant of the apparatus β and thereby obtain the absolute value of ν_{eff} for 250 and 900 kev neutrons. The values of ν_{eff} for 250 kev obtained by the threshold chamber method, proved to be in agreement, within the limits of error, with the results of the previous measurements.

In the measurements, the same control experiments were performed for the evaluation of the corrections as were performed in the previous variation. In addition, at neutron energies of 900 kev, a correction was introduced (no larger than 1.5 -2%) related to the fact that a small fraction of the neutrons from the source was recorded by the threshold chamber.

Results of measurement

The present work completes a series of studies of ν_{eff} undertaken by our laboratory in the wide energy interval from thermal energies to 900 kev.

Table 3 presents the data on ν_{eff} for the whole neutron energy range investigated.

The results of the last work indicate that the values of ν_{eff} for the isotopes U^{238}, U^{235} and Pu^{239} increase materially in the fast neutron energy region. This is in agreement with the qualitative results of statistical theory, according to which the ratio of the radiative capture cross section to the fission cross section decreases as the energy increases in this energy region.

If we know the variation of the fission cross section [3, 13, 14] in this neutron energy region, we can make some conclusions as to the variation of the radiative capture cross section. It turns out that the radiative capture cross section for U^{233}, U^{235} and Pu^{239} follows the 1/V law in the neutron energy region from 30 to 900 kev. The substantial increase of ν_{eff} of the fissionable isotopes establishes conditions favorable for the operation of fast neutron reactors with extensive breeding of nuclear fuel.

The authors take this opportunity to express their gratitude to Academician I. V. Kurchatov, under whose initiative the experiments devoted to the study of the dependence of ν_{eff} on neutron energy were conducted.

LITERATURE CITED

[1] P. E. Spivak, B. G. Erozolimsky, Physical Investigations (Reports of the Soviet Delegation to the International Conference on the Peaceful Uses of Atomic Energy), Acad. Sci. USSR Press, 1955, p. 184.

[2] A. I. Alikhanov, V. V. Vladimirsky, S Ya. Nikitin, Physical Investigations (Reports of the Soviet Delegation to the International Conference on the Peaceful Uses of Atomic Energy), Acad. Sci. USSR Press, 1955, p. 199.

[3] D. Hughes, and A. Harvey, Neutron Cross Section, U. S. Atomic Energy Commission, July, 1955.

[4] P. E. Spivak, B. G. Erozolimsky, G. A Dorofeev, V. N. Lavrenchik, Physical Investigations (Reports of the Soviet Delegation to the International Conference on the Peaceful Uses of Atomic Energy,) Acad. Sci. USSR Press, 1955, p. 213.

[5] B. G. Erozolimsky, Session of the Academy of Sciences USSR on the Peaceful Uses of Atomic Energy, July 1-5, 1955 (Div. Phys.-Math. Sci.), Acad. Sci. USSR Press, p. 369.

[6] S. Ya. Nikitin, S. I. Sukhoruchkin, K. G. Ignatyev, N. D. Galanina, P. A. Krupchitsky, B. F. Belkin, Session of the Academy of Sciences USSR on the Peaceful Uses of Atomic Energy, July 1-5, 1955 (Div. Phys.-Math. Sci.), Acad. Sci. USSR Press, p. 87.

[7] W. R. Kanne, H. B. Stewart, F. A. White, Capture-to-Fission Ratios of Pu^{239} and U^{235} for Intermediate Energy Neutrons (Report No. 595 Presented by the USA at the International Conference on the Peaceful Uses of Atomic Energy, 1955).

[8] H. Palevsky, Measurement of Capture-to-Fission Ratio of U^{235} and Pu^{239} by a New Method. (Report No. 587 Presented by the USA at the International Conference on the Peaceful Uses of Atomic Energy, 1955).

[9] P. A Egelstaff, J. E. Sanders, Neutron Yields from Fissile Nuclei (Report No. 425 Presented by England at the International Conference on the Peaceful Uses of Atomic Energy, 1955).

[10] P. E. Spivak, B. G. Erozolimsky, G. A. Dorefeev, V. N. Lavrenchik, I. E. Kutikov, Yu. P. Dobrynin, Atomic Energy 1956. No. 3, 13 (T. p. 295)*.

[11] P E Spivak, B. G. Erozolimsky (to be published).

[12] G. N. Flerov and C. M. Potkanov, Report Acad. Sci. USSR, 1954.

[13] G. A. Dorofeev and Yu. P. Dobrynin (to be published).

[14] V. I. Shigin, Dissertation, Inst. Phys. Prob. Acad. Sci. USSR, 1954.

* T. p. = Consultants Bureau Translation pagination.

MEASUREMENT OF THE AVERAGE NUMBER ν_{eff} OF NEUTRONS EMITTED PER SINGLE CAPTURE EVENT FOR SAMPLES OF Pu^{239} WITH IMPURITIES OF THE ISOTOPE Pu^{240} AND THE EFFECTIVE RESONANCE CAPTURE INTEGRAL OF Pu^{240}

B. G. Erozolimsky, I. E. Kutikov, Yu. P. Dobrynin, M. I. Pevzner
L. S. Danelian, S. S. Moskalev

In this article we present the results of measurement of ν_{eff} in Fermi spectra with lower bounds of 0.15 ev (gadolinium filter) and 0.4 ev (cadmium filter) for samples of Pu^{239} with various concentrations of impurities of the isotope Pu^{240} (0%, 1.6%, 2.5%, 6.5%, 16%) and the effective resonance absorption integral of Pu^{240}.

Introduction

In using an atomic reactor as an energy source, it is economically profitable to make use of long lasting fuel cycles, that is to operate at conditions of thorough "burning" of the fissionable isotopes. For these conditions, the neutron balance in a plutonium reactor will depend not only on the properties of Pu^{239}, but also on the properties of the isotope Pu^{240} that accumulates in the reactor.

A very convenient gauge of the influence of the isotope Pu^{240} on the neutron balance in a reactor is the quantity ν_{eff} for samples with impurities of one or another concentration of Pu^{240}, which characterizes the duration of operation of Pu^{239}.

When this data is obtained, it makes possible the determination of the effective resonance capture integral of Pu^{240}.

In the present paper we present the results of measurement of ν_{eff} in the Fermi spectra with lower bounds 0.15 ev (gadolinium filter) and 0.4 ev (cadmium filter) for two sets of samples with impurity concentrations of the isotope Pu^{240} of 0%; 1.5%, 2.5%, 6.5%; 16%; also the effective resonance capture integrals are evaluated.

Analysis of the Pu^{239} samples for impurity concentrations of the isotope Pu^{240}

In the operation of a uranium reactor, as a result of successive neutron capture, several plutonium isotopes are created (Pu^{239}, Pu^{240}, Pu^{241}, Pu^{242}, etc.).

The half-life for α-decay of Pu^{240} (6500 years) is less than the half-life for α-decay of Pu^{239} (24,000 years). Therefore the amount of Pu^{240} in the sample can be found by determining the specific α-activity of the sample. But this method gives sufficient accuracy only for the case when the α-activity of Pu^{240} is a noticeable part of the total α-activity, and it is therefore not applicable to samples with small concentrations of Pu^{240}.

An analysis by amplitude of the α-particle spectrum of plutonium samples is made extremely difficult by the fact that the basic α-particle energies of Pu^{239} and Pu^{240} differ only by 12 kev.

The spontaneous fission half-lives of Pu^{239} and Pu^{240} differ in a more substantial way, being equal to $1.25 \cdot 10^{11}$ years for Pu^{240} and $5 \cdot 10^{15}$ years for Pu^{239}. Clearly the number of spontaneous fission events in a plutonium sample is proportional to the concentration of Pu^{240}, the part due to Pu^{239} being negligibly small. Only Pu^{242} can give a noticeable additional contribution to the number of spontaneous fission events ($T_{1/2} = 7.25 \cdot 10^{10}$ years). The amount of Pu^{242} in our samples is, however, extremely negligible.

The analysis of the isotope composition of plutonium samples by measuring the number of spontaneous fission events in an ionization chamber is promising, but involves much work. Therefore, this method was used to find the percent concentration of Pu^{240} only in one sample. Determination of Pu^{240} concentrations in the other samples was carried out relative to this standard sample. The presence of a strong isolated resonance in Pu^{240} at 1.06 ev energy, and the absence of resonances at this energy in the other plutonium isotopes, makes it possible to determine the relative concentration of Pu^{240} in samples from the areas of the dips in the transmission curves obtained on a mechanical neutron neutron chopper.

Determination of the Pu^{240} concentration in the standard sample. The fragments from spontaneous fission of Pu^{240} were recorded in a multi-layer ionization chamber. The substance being studied was deposited on a thin nylon film, which made it possible to record the pulses from both fission fragments simultaneously and therefore to work at a discrimination level that excluded the pulses contributed by α-particles. The construction of the ionization chamber and the method of preparing the layers on the nylon films is described in reference [1].

The amount of substance deposited onto the film was determined by comparing the total α-activity of the layer on the film with the α-activity of a layer of the same substance whose weight was known, which was electrolytically deposited on a platinum target. The concentration of Pu^{240} in the sample which was chosen as the standard was $6.4 \pm 0.25\%$.

TABLE 1

Concentration of Pu^{240} in the samples

	Sample			
	No. 2	No. 3	No. 4	No. 5
Concentration of Pu^{240} in %	1.56 ± 0.12	2.5 ± 0.2	6.4 ± 0.25	15.8 ± 1.3

A control experiment on the determination of the absolute number of α-particles emitted by the layer on the platinum target gave a value of $6.7 \pm 0.4\%$ which is in good agreement with the previous result.

Determination of the concentration of Pu^{240} in the samples by the transmission curves. As was mentioned, the presence of a strong neutron resonance in the isotope Pu^{240} at 1.06 ev energy makes it possible to determine the concentration of Pu^{240} in the rest of the samples relative to the standard one by the area of the dips in the transmission curves. For thin samples, the area of the dip is proportional to the number of Pu^{240} atoms in the sample. In order that the transmission curves for samples with various percent concentrations of Pu^{240} not be measurably different in the resonance region, samples with about the same number of Pu^{240} atoms per cm^2 were prepared. In this, previous data from isotope analysis with a mass spectrographwere used. The area of the dip was determined by the usual method, with corrections for the area under the wings of the transmission curve [2].

Since, in actuality, the samples studied did not satisfy the conditions for a thin sample ($n\sigma_0 \ll 1$), a correction was also introduced for the thickness of the sample [3].

The final values for the number of Pu^{240} atoms in the sample were made more accurate by successive approximations.

In order to verify the reliability of the measurement, we determined the ratio of the areas of dips in the transmission curves for two samples with the same percent concentration of Pu^{240}, but with different numbers of Pu^{240} atoms per cm^2. The ratio of the areas proved to be equal to the known ratio of Pu^{240} atoms in these samples within the limits of 5%.

The results of the measurements on the Pu^{240} concentrations in the samples are presented in Table 1.

Method of measuring ν_{eff} for fissionable isotopes

The method of measuring ν_{eff} which was developed by P. E. Spivak and co-workers [4] is based on the direct measurement of the effects of capture and emission of neutrons in the excited neutron field caused by the sample being studied. The apparatus was a graphite prism with a central cavity. The sample was placed in the center of the cavity and in the path of a collimated neutron beam from a reactor. The necessary neutron spectrum was formed by using the proper filter. The neutrons were recorded by proportional counters (BF_3), uniformly distributed throughout the whole volume of the prism.

The measurement of the total number of pulses in the counters per unit time that were recorded when the sample being studied was introduced into the cavity is related to the change in the number of neutrons in the cavity that results from the absorption or emission of neutrons in the sample.

When the sample of fissionable matter is brought into the cavity, the change in the number of pulses per unit time ΔN_1 in the indicating system can be written in the following way:

$$\Delta N_1 = K_1 Q + K_2 Q \nu_{eff} \tag{1}$$

where Q is the number of neutrons of the primary spectrum that are absorbed by the sample, K_1 is the indicating system efficiency for neutrons of the primary spectrum, and K_2 is the indicating system efficiency for the secondary fission neutrons.

In order to determine ν_{eff}, one other measurement was taken, for which the sample was enclosed by a boron-paraffin sphere with an opening for admitting the neutron beam. In this case the change in the counting rate of the same indicating system as a result of the introduction of the sample is of the form

$$\Delta N_2 = K_3 Q \cdot \nu_{eff} \tag{2}$$

where K_3 is the indicating system efficiency for secondary fission neutrons.

Writing $\frac{\Delta N_1}{\Delta N_2} = X$; $\frac{K_1}{K_2} = \alpha$; $\frac{K_2}{K_3} = \beta$, and solving the system of Equations (1) and (2), we get

$$\nu_{eff} = \alpha \frac{1}{1 - \beta X}. \tag{3}$$

Performing the measurements on X for samples of Pu^{239} without and with Pu^{240} impurities (X' and X'', respectively), we find that

$$\frac{\nu''_{eff}}{\nu'_{eff}} = \frac{1 - \beta X'}{1 - \beta X''}.$$

The constant of the apparatus $\beta = \frac{K_2}{K_3}$ was measured with the aid of a fast neutron convertor, and turned out to be 0.314 ± 0.003. A detailed account of the method of measurement is presented in reference [4].

Results of measurement

The measurements were performed on samples prepared in the form of 22 mm diameter discs of uniform mixtures of the substance being investigated and fine graphite powder compressed in a small aluminum box. The results for two sets of samples of different weights are presented in Tables 2 and 3.

TABLE 2

Measurement of $\frac{\nu''_{eff}}{\nu'_{eff}}$ in the Fermi Spectrum Formed by a Gadolinium Filter ($E_{bound} \sim 0.15$ ev)

	Sample									
	№ 1	№ 2	№ 3		№ 4		№ 5			
Percent Pu^{240}	0	1.6	2.5		6.5		16			
Weight of sample (g)	8	0.55	0.39	1.00	0.51	1.02	0.52	0.99		
X	1.43±0.01	1.37±0.02	1.35±0.03	1.35±0.03	1.13±0,02	1.17±0.02	0.90±0.02	1.03±0.02		
$\frac{\nu''_{eff}}{\nu'_{eff}}$	1.00	0.97±0,01	0.96±0.01	0.96±0.01	0.86±0.01	0.87±0.01	0.77±0.01	0.83±0.01		

TABLE 3

Determination of $\frac{\nu''_{eff}}{\nu'_{eff}}$ in the Fermi Spectrum Formed by a Cadmium Filter ($E_{bound} \sim 0.4$ ev)

	Sample					
	№ 1	№ 2	№ 3		№ 5	
Percent Pu^{240}	0	1.6	2,5		16	
Weight of sample (g)	8	0.55	0.39	1.00	0.52	0.99
X	1.43±0.01	1.07±0.05	1.00±0,08	1.17±0.03	−0.42±0.01	−0.02±0,07
$\frac{\nu''_{eff}}{\nu'_{eff}}$	1,00	0.84±0.02	0,81±0.03	0.87±0,02	0.49±0.02	0.55±0,02

TABLE 4

Amount of Pu^{240} in g/cm^2	$2.32 \cdot 10^{-3}$	$2.57 \cdot 10^{-3}$	$6.58 \cdot 10^{-3}$	$21.9 \cdot 10^{-3}$	$41.6 \cdot 10^{-3}$
Amount of Pu^{239} in g/cm^2	$142 \cdot 10^{-3}$	$100 \cdot 10^{-3}$	$256 \cdot 10^{-3}$	$115 \cdot 10^{-3}$	$219 \cdot 10^{-3}$
p	$1.6 \cdot 10^{-3}$	$2.57 \cdot 10^{-3}$	$2.57 \cdot 10^{-3}$	$19 \cdot 10^{-3}$	$19 \cdot 10^{-3}$
$\frac{\Sigma_{49}}{\Sigma_{39}}$	11.9±2	9.0±1,5	5.9±1,5	5.4±0,1	4.3±0,2
Σ_{40} eff	$5450 \cdot 10^{-24}$ cm^2	$4150 \cdot 10^{-24}$ cm^2	$2700 \cdot 10^{-24}$ cm^2	$2500 \cdot 10^{-24}$ cm^2	$2000 \cdot 10^{-24}$ cm^2
Experimental error	±20%	±20%	±20%	±4%	±4%

The lowest concentration of the isotope Pu^{240} in the samples was about 1.5%. Therefore, in measuring ν_{eff} for pure Pu^{239} (sample No. 1 in Tables 2 and 3), in addition to the filter forming the neutron spectrum, a Pu^{240} filter was used to block the 1.06 ev resonance neutrons. It follows from the definition of ν_{eff} that the ratio

$$\frac{\nu^{\circ}_{eff}}{\nu^{\circ}} = 1 + p\frac{\Sigma_{40}}{\Sigma_{39}}$$

where Σ_{39} and Σ_{40} are the resonance capture integrals of Pu^{239} and Pu^{240} and p is the ratio of the weights of Pu^{240} and Pu^{239} in the sample.

According to measurements performed by G. A Dorofeev [5], the absorption integral for Pu^{239} for the neutron spectrum formed by the cadmium is

$$\Sigma_{39} = (460 \pm 23) \cdot 10^{-24}\ cm^2.$$

By using the data of Table 4 it is possible to calculate the values of the effective resonance absorption integrals for Pu^{240} as a function of the amount of Pu^{240} per cm^2.

Extrapolating the value of Σ_{40} to zero Pu^{240} density, we can obtain the true value of the resonance absorption integral:

$$\Sigma_{40} = (9000 \pm 3000) \cdot 10^{-24}\ cm^2.$$

The present work was carried out on the suggestion of Academician I. V. Kurchatov. The authors take this opportunity again to express their gratitude to him for his constant interest in the work.

We also express our indebtedness to P. E. Spivak for directing the work.

LITERATURE CITED

[1] Yu. V. Adamchuk, V. I. Mostovoi, M. I. Pevzner, A. P. Tsitovich, and others, Physical Investigations (Reports of the Soviet Delegation to the International Conference on the Peaceful Uses of Atomic Energy), Acad. Sci. USSR Press, 1955, p. 86.

[2] F. G. P. Seidl, D. J. Hughes, H. Palevsky, J. S. Levin, W. Y. Kato, and N. G. Sjöstrand, Phys. Rev.. 95, 976 (1954). E. Melkonian, Analysis of Low Energy Neutron Resonances (Report No. 583 Presented by the USA at the International Conference on the Peaceful Uses of Atomic Energy, 1955).

[3] Havens and Taylor, Nucleonics 6, No. 2, 66 (1950).

[4] P. E. Spivak, B. G. Erozolimsky, G. A. Dorofeev, V. N. Lavrenchik, I. E. Kutikov, Yu. P. Dobrynin, Atomic Energy 1956, No. 3, 13, (T. p. 295)*.

[5] G. A. Dorofeev, Report Acad. Sci. USSR, 1953.

* T. p. = Consultants Bureau Translation pagination.

SLOWING DOWN OF FISSION NEUTRONS BY WATER

L. M. Barkov, K. N. Mukhin

In this article we describe the method and results of measurement of τ for U^{235} fission neutrons slowed down by water to energies of 1.46 ev. The value obtained for $\tau_{1.46\ ev} = 29.4 \pm 1.5\ cm^2$.

A large class of reactors use water as the moderator, and it is therefore of great interest to investigate the slowing down of fission neutrons by water.

In the present work, carried out on the RFT reactor with the aid of an indium detector, the density distribution of neutrons with energy E = 1.46 ev, that occur as a result of slowing down U^{235} fission neutrons by water, is measured.

The neutron source was a target-convertor made of uranoso-uranic oxide U^{235} which transforms thermal neutrons of the beam to fast fission neutrons. Two targets were used: one of 22 mm diameter and 5 mm thickness (4.15 g U^{235}) for measurements at large distances from the source, and the other of 8 mm diameter and 2.5 mm thickness (0.21 g U^{235}) for measurements close to the source.

The measurements were performed in a large aluminum tank 140 cm long, 100 cm wide, and 105 cm high, into which the thermal neutron beam was introduced with the aid of a 50 cm long steel tube which was sealed at one end. The target was attached to the sealed end of the tube and was covered, together with the tube, by a cadmium case.

The distance from the convertor to the walls of the tank or the surface of the water was 50 cm, and in the direction of measurement the distance was 90 cm.

The construction described makes measurements possible to distances of about 70 cm with practically no edge effects and a weak background. The fast neutron background passing through the walls of the tank and the background due to neutrons scattered by the target was measured with the aid of additional experiments, in which, in place of the convertor, a scatterer made of tungsten oxide was used.

The measurement of the density of slowed down neutrons $\rho(r)$ was carried out with the aid of indium foils of optimal thickness (100 mg/cm^2) placed in cadmium holders. The foils were calibrated as to thicknesses, area, and weight. Their activity was measured in both directions on a β-apparatus with low background.

A special verification of the reliability of the method was performed with the aid of a control experiment with a thicker indium foil in which the self-shielding of neutrons of the basic resonance was observed. This verification showed that the indium foil of optimal thickness registers mainly neutrons with energy corresponding to the basic resonance (1.46 ev).

In order to avoid over-irradiation of the foils located close to the convertor, the irradiation with the large convertor was performed in two series: the foils were irradiated at small distances from the convertor ($r < 30$ cm) and at large ones ($15\ cm < r < 60\ cm$).

In each series several foils (as many as 8 in a series) were irradiated simultaneously. In order to increase the statistical accuracy for $r > 40$ cm, measurements for each point were carried out with two or three foils irradiated at different locations, but at equal distances from the convertor. The activity of these foils was measured on a β-counter simultaneously. Both series were repeated 6 to 8 times, and the results of each series were joined at two or three points that were common to all the series. In the measurements, good reproducibility was obtained for the results of series of the same type, as well as for the common points for different series.

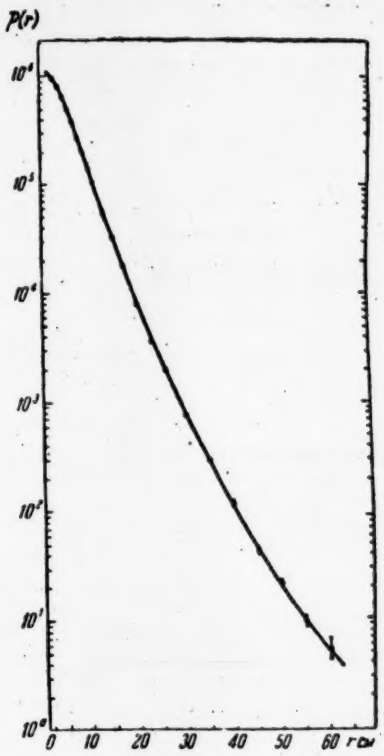

Distribution density of neutrons with energy E = 1.46 ev that occurs as a result of slowing down of U^{235} fission neutrons by water.

Measurement of density $\rho(r)$ of the fission neutrons slowed down by water was carried out both with the large and the small convertor in the ranges, respectively, of $5 \text{ cm} \leq r \leq 60$ cm and $3 \text{ cm} \leq r \leq 15$ cm. Both curves coincided at the point $r = 15$ cm, and were identical in the interval $10 \text{ cm} \leq r \leq 15$ cm. For $r < 10$ cm, the curve from the small convertor is higher than that for the large one, and the divergence at the point $r = 5$ cm is 15%.

The final curve (see the Figure) was taken as the combination of the curve from the small convertor for $3 \text{ cm} \leq r \leq 15$ cm, and the curve from the large one for $15 \text{ cm} \leq r \leq 60$ cm, since the curve at large distances depends little on the dimensions of the convertor. From this curve the quantities

$$\tau_{1.46\,ev}(R) = \frac{\bar{r}^2_{exp}}{6} = \frac{1}{6}\frac{\int_0^R r^4 \rho(r)\,dr}{\int_0^R r^2 \rho(r)\,dr}$$

were calculated for various intervals of measurement $0 \leq r \leq R$ ($R = 30$, 40, 50 and 60 cm), and from this it was possible to extrapolate the value

$$\tau_{1.46\,ev} = \frac{\int_0^\infty r^4 \rho(r)\,dr}{6\int_0^\infty r^2 \rho(r)\,dr} = 29.4 \pm 1.5 \text{ см}^2.$$

The experimental uncertainty is composed of errors in measuring $\rho(r)$, which, as is shown by calculation, can give an uncertainty in τ no greater than 2-3%, errors in extrapolation, which are taken to be equal to the difference between the extrapolated value and the last experimental value for R = 60 cm (0.3 cm^2), and errors related to the fact that the small convertor is not a "point" source (0.5 cm^2). The error caused by the fact that the convertor is not a point source was found by comparing the results of measurement with the small convertor (29.4 cm^2) and the large one (30.5 cm^2).

Taking into account the additional slowing down in the interval from 1.46 to 0.025 ev, which is about 1 cm^2, the value we have found for τ agrees within the experimental error with the value $\tau_{0.025\,ev} = 33$ cm^2 given in the book by Glasstone and Edlund [1].

In conclusion, the authors express their sincere gratitude to I. I. Gurevich and D. V. Timoshuk for reviewing the results, to A. P. Venediktov for help in the work, and to G. R. Golbek for lending the β-apparatus with low background.

LITERATURE CITED

[1] S. Glasstone and M. Edlund, The Elements of Nuclear Reactor Theory, Foreign Lit. Press, Moscow, 1954.

MEASUREMENT OF SLOWING DOWN OF NEUTRONS BY WATER IN THE ENERGY INTERVAL FROM 1.46 to 0.025 ev

L. M. Barkov, V. K. Makaryin, K. N. Mukhin

With the aid of an indium detector the spatial distribution of resonance (E_r = 1.46 ev) and thermal neutrons that arise as a result of the slowing down in water of the photoneutrons emitted by an Sb + Be source is measured. The age of the neutrons $\tau_{1.46\ ev}$, the thermal neutron diffusion length in water, and the square of the slowing-down length $\Delta\tau$ from neutron energies of 1.46 ev to thermal energies (0.025 ev) are determined.

Use of the resonance detector method makes it possible to determine the square of the slowing-down length for neutrons slowed down to some energy E_r higher than thermal energies, for instance to the energy E_r = 1.46 ev if indium is used as the detector [1, 2].

Slowing down from the energy E_r = 1.46 ev to the energy E = 0.025 ev is usually calculated theoretically. Such evaluations are made also when the slowing-down medium is water, and they give the value $\Delta\tau \approx 1\text{-}2\ cm^2$. Because of the chemical bonds of the hydrogen atoms in the water molecules, however, the calculations of energy loss by collisions with protons becomes unreliable, and therefore the evaluation of the distance through which the neutrons pass in the process of slowing down from E_r = 1.46 ev to E = 0.025 ev is also inexact. Thus an experimental evaluation of this quantity is necessary.

Such an evaluation can be made by comparing two experimental determined curves of the spatial distributions for resonance $\rho_{E_r = 1.46\ ev}(r)$ and thermal $\rho_t(r)$ neutrons.

The value of $\overline{r^2}/6$ calculated from the first curve gives the value of the square of the slowing-down length $\tau_{1.46\ ev}$, to the resonance energy E_r = 1.46 ev, and the value of $\overline{r^2}/6$, calculated from the second curve gives the value of the migration area

$$M^2 = \tau_{0.025\ ev} + L^2.$$

Here $\tau_{0.025\ ev}$ is the square of the slowing-down length to E = 0.025 ev; and L is the diffusion length for thermal neutrons. Thus the slowing down of neutrons from the energy E_r = 1.46 ev to the thermal energy E = 0.025 ev is characterized by the quantity

$$\Delta\tau = \tau_{0.25\ ev} - \tau_{1.46\ ev} = M^2 - L^2 - \tau_{1.46\ ev}.$$

The quantity $\Delta\tau$ contains the difference of the experimentally determined quantities M^2 and $\tau_{1.46\ ev}$, which depends on the initial energy E_0 of the neutrons that are being slowed down. Therefore, in order to obtain $\Delta\tau$ with the greatest possible accuracy, the energy E_0 should be as small as possible.

In the present work the indium detector method is used to determine the experimental values of $\tau_{1.46\ ev}$, M^2 and L, which characterize the slowing down and diffusion of photoneutrons from an SB + Be source (E_0 = 30 kev) in water, and the quantity $\Delta\tau_{(1.46\ ev - 0.025\ ev)}$ is found.

The measurement of the density distribution of thermal and resonance neutrons was performed in a large tank 80 cm in diameter and 100 cm high placed over a shaft for holding the source and filled with water (Fig. 1). From the shaft SH the source S was lifted along the maintaining rails MR with the aid of the electromagnet E which was automatically turned off when the source reached the operating position. The presence of the source in the operating position was indicated by a sensitive γ-ray indicator, and the time at which it arrives there, by the flashing of a lamp included in the electromagnet circuit. The source was let down again by pulling out a special pin P which holds the source in the operating position.

In measuring τ for the neutrons with low initial energy (30 kev) and therefore low slowing-down length, it is important to measure the distance between the source and detector with accuracy. Placing the detector at the necessary distance was carried out with the aid of three horizontal rules R with slots milled into them, which were placed one over the other. The rules were attached to the maintaining rails of the source, so that any possible tilt of the maintaining rails would not change the distance between the source and the indium foil. The adapter A with the foil was hung on the top rule as is shown in Fig. 1.

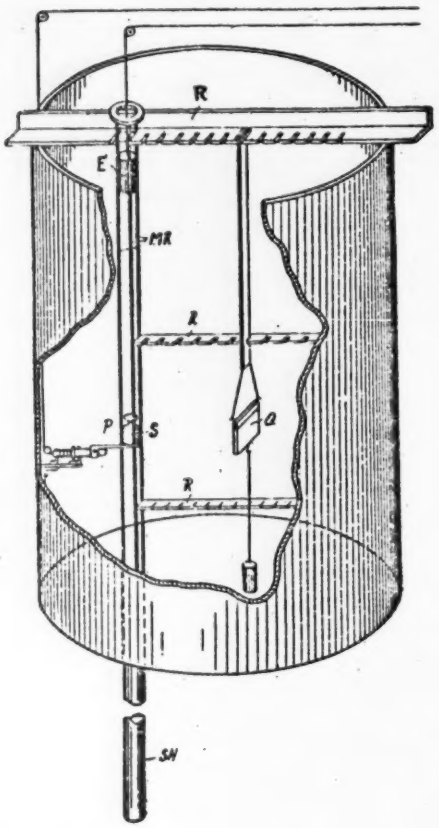

Fig. 1. General view of the apparatus.

In order to irradiate several foils simultaneously at large distances, the apparatus had three systems of rules located at different radii. In order not to alter the slowing-down properties of the medium being investigated, the maintaining rails, the rules, and other details of the apparatus were made of plexiglass, which has slowing-down properties similar to those of water.

The measurement of the density of resonance neutrons $\rho_{In+Cd}(r)$ was performed with adapters made of sheet cadmium 0.6 mm thick, and that of the thermal neutrons with adapters made of 0.2 mm thick stainless steel.

Depending on the distance from the source, the measurements were performed with foils of various sizes: 30 x 25 mm, 15 x 25 mm and 7.5 x 12.5 mm, and the results were reduced to foils whose dimensions were 15x 25 mm. The transformation factors were found by comparing the activities of foils of various dimensions which were irradiated under the same conditions. For irradiation with resonance neutrons, these factors proved to be proportional to the target areas, and for irradiation with thermal neutrons the value of the coefficients agrees with calculations made according to Bothe's formula [3, 4], which takes into account the fact that the thermal neutron field is altered by the detector. For the largest irradiation distances, three foils 30 x x 25 mm were irradiated, and their activity was measured simultaneously on the counter.

An apparatus with a reduced background was used to measure the β-activity. The activity of the foils was measured on both sides. In all cases foils of optimal thickness were used (100 mg/cm^2). In the measurements two sources were used: a large cylindrical source (diameter Be = 18 mm, h = 22 mm; diameter Sb = 8 mm, h = 17 mm) with a neutron yield of $\sim 10^6$ neutrons per second, and a small source (diameter Be = 10 mm, h = 20 mm; diameter Sb = 6 mm, h = 20 mm) with a yield of $\sim 10^5$ neutrons per second.

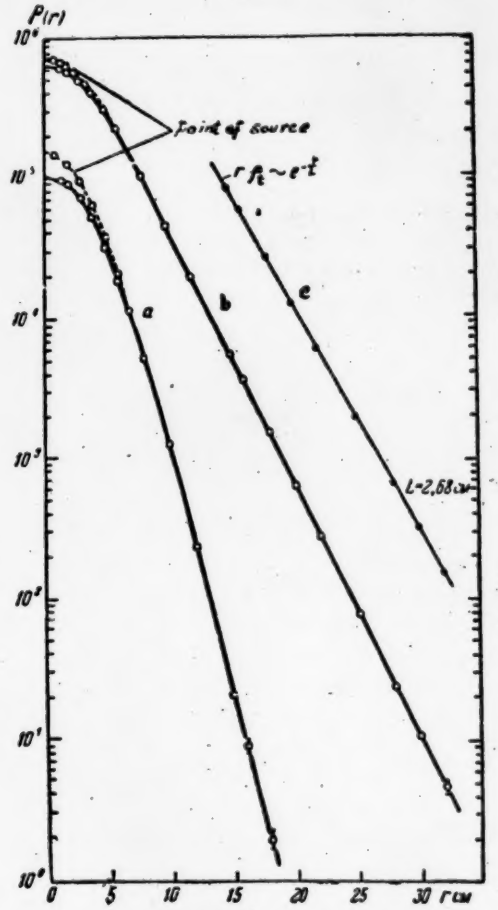

Fig. 2. Density distribution curves for (a) resonance and (b) thermal neutrons, and (c) the function $\rho_t(r)$.

The resonance neutron density $\rho_{In+Cd}(r)$ was measured from 1.5 to 18 cm for the large source, and from 1.0 to 10.5 cm for the small one. The value of τ for the large source proved to be

$$\tau = \frac{1}{6}\frac{\int_0^{18} r^4 \rho(r)\,dr}{\int_0^{18} r^2 \rho(r)\,dr} = 5{,}65 \text{ см}^2.$$

Additional measurements made with the small source led to some changes in the curve of $\rho_{In+Cd}(r)$ in the region of small distances (dotted curve on Fig. 2). The value of τ determined from the corrected curve is $\tau = 5.27 \pm 0.04$ cm^2. By considering the increase of τ in the last few centimeters, we were able to find the extrapolated value

$$\tau = \frac{1}{6}\frac{\int_0^{\infty} r^4 \rho(r)\,dr}{\int_0^{\infty} r^2 \rho(r)\,dr},$$

which, for the large and small source, respectively, is 5.66 ± 0.04 cm^2 and 5.28 ± 0.04 cm^2.

It is known that in addition to the principal resonance at E = 1.46 ev indium has two other relatively strong resonances at E = 3.9 ev and E = 9.1 ev, which will have a stronger effect as the thickness of the foil used increases. A calculation performed on the assumption that the neutron flux incident on the detector is isotropic and that the Fermi law $\Phi \sim 1/E$ holds, showed that for the foils and cadmium used, the contribution from the second resonance to the activity is about 10% and that of the third, about 4%. In addition some contribution to the activity is caused by neutrons of energy E > 10 ev. All this should lead to too low a value for the experimentally determined value of τ, since it corresponds to the slowing of neutrons to an energy E > 1.46 ev.

The correction to τ_{exp} was calculated with the aid of the relation

$$\tau = \tau_{1.46\text{ ev}} - \tau_{(3.9\text{-}1.46\text{ ev})}\frac{N_{3.9\text{ ev}}}{N} - \tau_{(9.1\text{-}1.46\text{ ev})}\frac{N_{9.1\text{ ev}}}{N} - \int_{10\text{ ev}}^{30\text{ kev}} \tau_{(E\text{-}1.46\text{ ev})}\frac{c\,dE}{E\sqrt{E}}.$$

Here N is the total number of neutrons absorbed by the indium foil, N_i is the contribution of the particular resonance to the foil's activity, $\tau_{(E-1.46\text{ ev})} = \frac{\lambda_t \lambda_s}{3} \ln\frac{E\text{ ev}}{1.46\text{ ev}} = 0.42 \ln\frac{E\text{ ev}}{1.46}$; c is a constant determined by the activation cross section in the energy region E > 10 ev, where we took the cross section to have the dependence $\sigma = \frac{20}{\sqrt{E}} 10^{-24}$ cm^2. The magnitude of the correction proved to be 0.2 ± 0.1 cm^2.

The large value for the uncertainty ± 0.1 cm² is related to the possibly inaccurate determination of $\tau(E=1.46\ ev)$ by age theory and to the uncertainty in the variation of the activation cross section in the energy region E > 10 ev. Thus the following values are obtained for the square of the slowing-down length to an energy of 1.46 ev:

$$\tau_{1.46\ ev} = 5.86 \pm 0.15\ cm^2 \text{ for the large source, and}$$

$$\tau_{1.46\ ev} = 5.48 \pm 0.15\ cm^2 \text{ for the small source.}$$

In principle it is possible for the indium foil to be activated by the γ-rays of the photosource according to the reaction $In^{115}(\gamma, \gamma')In^{115m}$. In order to verify the absence of an error due to this effect, $\rho_{In+Cd}(r)$ was measured at distances greater than 18 cm. The absence of activation as a result of the γ-rays at a distance of 20 cm proves that it is also absent at small distances, since water absorbs γ-rays weakly, whereas the neutron density decreases rapidly with distance.

In order to determine the thermal neutron density $\rho_t(r)$, a measurement of the dependence of the indium foil activation (in the steel adapters) on distance from the source was performed. In this case, as opposed to the measurements of $\rho_{In+Cd}(r)$ in the cadmium adapters, the indium foil is activated not only by resonance neutrons, but also by thermal neutrons and neutrons of "intermediate" energies from 0.025 to 0.5 ev, which are blocked out by the cadmium in the measurements of $\rho_{In+Cd}(r)$. Therefore in order to get the correct value of M^2, the activity caused by the resonance and intermediate neutrons must be excluded from the total activity of the indium. The activation by the intermediate neutrons can be evaluated by calculation. In fact the neutron flux activating the foil is proportional to $1/\xi\Sigma_s E$. It follows, then, that we may compare the activity of the foil caused by the intermediate neutrons with the activity caused by the resonance neutrons. The latter is known from the measurements of $\rho_{In+Cd}(r)$. The results of the calculation must be normalized to $\rho_{In+Cd}(r)$.

Such a calculation, however, cannot give an accurate result, because of the fact that in the energy region E < 1 ev scattering by water molecules begins simultaneously with scattering by free protons. It is possible to give only two evaluations, above and below the magnitude of the contribution to the activity caused by the intermediate neutrons. In getting the low value, it was assumed that from E = 0.5 ev up to thermal energies, the scattering is by free protons only ($\xi = 1$, $\sigma_s = 20 \cdot 10^{-24}\ cm^2$). In getting the high value, it was assumed that in the energy interval from 0.5 to 0.1 ev the scattering is by free protons, but that from the energy E = 0.1 ev on down, it is by water molecules ($\xi = \frac{2}{A + 2/3} = 0.107$, $\sigma_s = 80 \cdot 10^{-24}\ cm^2$). The results are, respectively

$$\rho_{inter}^{(1)} = 0.77\ \rho_{In+Cd}(r),$$

$$\rho_{inter}^{(2)} = 1.43\ \rho_{In+Cd}(r).$$

Thus M^2 should be calculated from the curve

$$\rho_t^{(1)}(r) = \rho_{In}(r) - 1{,}77\,\rho_{In+Cd}(r)$$

in one case, and from the curve

$$\rho_t^{(2)}(r) = \rho_{In}(r) - 2{,}43\,\rho_{In+Cd}(r)$$

in the other. The corresponding values for M^2 are $M^2_{(1)} = 13.92 \pm 0.05\ cm^2$ and $M^2_{(2)} = 14.35 \pm 0.05\ cm^2$. Since the correct value of M^2 is contained between $M^2_{(1)}$ and $M^2_{(2)}$, it was taken as $M^2 = \frac{M^2_{(1)} + M^2_{(2)}}{2}$ with an uncertainty equal to half the difference of the values, $\frac{M^2_{(2)} - M^2_{(1)}}{2} = 0.22\ cm^2$, $M^2 = 14.13 \pm 0.25\ cm^2$.

Additional measurements made with a "point" source indicate a small change in the curve for $\rho_{In}(r)$ at small distances (dotted line on curve b in Fig. 2). The value of M^2 determined from the curve for the "small source" is $M^2 = 13.64 \pm 0.25$ cm^2.

Together with $\tau_{1.46\ ev}$ and M^2, the diffusion length L for thermal neutrons in water was also determined in this experiment (t = 19°C). The necessity for measuring L arises from the fact that the experimental values for the diffusion length that appear in the literature do not agree with each other (see the Table).

For an Sb + Be source the distribution of resonance electrons in water falls so rapidly that from a distance $r \approx 15$ cm on, only thermal diffused neutrons exist. Thus for $r > 15$ cm we may write a diffusion equation without a source

$$\nabla^2 \rho - \frac{1}{L^2} \rho = 0,$$

where ρ is the neutron flux density.

In our concrete case of a spherically symmetric distribution in a system of coordinates centered at the source, the solution is of the form

$$\rho(r) \sim \frac{e^{-r/L}}{r}.$$

Then L can be found from the slope of the straight line $\rho r \sim e^{-r/L}$ drawn on semi-log paper.

TABLE

Diffusion Length of Neutrons in Water

L, (cm)	Method	Reference
3±0.3	Direct measurement	[5]
2.77±0.04	» »	[6]
2.76±0.03	» »	[7]
3.25±0.13	» »	[8]
2.67±0.02	» »	[9]
2.72±0.04	Pulse method	[10]
2.69±0.08	» »	[11]
2.85±0.05	» »	[12]

The function $\rho_1(r)$ is drawn on Fig. 2 (curve c). From the slope of the line it follows that L = 2.68 ± ± 0.02 cm. Additional measurements made in distilled water gave L = 2.69 ± 0.02 cm. The relatively high accuracy of the result is due to the large interval for the measured curve (15-35 cm).

Comparing the experimental data obtained for the large source,

$$\tau_{1.46\ ev} = 5.86 \pm 0.15\ cm^2,$$
$$M^2 = 14.13 \pm 0.25\ cm^2,$$
$$L^2 = 7.18 \pm 0.11\ cm^2$$

gives, for the quantity $\Delta\tau = M^2 - \tau_{1.46\ ev} - L^2$, the value

$$\Delta\tau_{(1.46-0.025\ ev)} = 1.1 \pm 0.5\ cm^2.$$

Comparing the experimentsl results obtained for the small source,

$$\tau_{1.46\ ev} = 5.48 \pm 0.15\ cm^2,$$
$$M^2 = 13.64 \pm 0.25\ cm^2$$

gives, for $\Delta\tau$, the value

$$\Delta\tau_{(1.46-0.025\ ev)} = 1.0 \pm 0.5\ cm^2.$$

It should be noted that a large part of the uncertainty in $\Delta\tau$ comes from the large total correction in working over the results of the measurements with the large and small sources.

The near agreement of the values of $\Delta\tau$ obtained from the large and small source is to be expected. Indeed, in the slowing down of neutrons from an energy of 1.46 ev to 0.025 ev, the resonance neutrons serve as a distributed neutron source; they rapidly slow down to 0.025 ev energy, and then diffuse. In so doing, the diffused neutrons seldom come to the point where the source is located, and therefore its influence is rather weak.

In slowing down from 30 kev to 1.46 ev, the place from which the neutrons come is the source itself, and therefore its dimensions influence the value of τ quite strongly. Comparing the values of τ obtained with the large source ($\tau = 5.86 \pm 0.15$ cm^2) and the small one ($\tau = 5.48 \pm 0.15$ cm^2), we see that the difference between them is as large as 0.4 cm^2 and that the value of τ corresponding to a point source must therefore be less than 5.48 cm^2. Calculation of τ by Marshak's formula [13] for neutrons slowed down from 30 kev to 1.46 ev gives the value $\tau_{theor} = 4.9$ cm^2, which is 0.6 cm^2 lower than the experimental value for the small source. It is possible that the fact that the source used is not a point source is one of the reasons for the difference between τ_{exp} and τ_{theor}. A second reason for this difference may be the presence of neutrons of about 300 kev in the Sb + Be source.

An additional verification of the reliability of the measured density of resonance and thermal neutrons can be obtained from their mutual agreement. If the curve of the spatial distribution of resonance neutrons is considered as a distributed neutron source, then we may find the distribution of thermal neutrons by calculation. With this purpose, the spatial distribution curve of the resonance neutrons $\rho_{In+Cd}(r)$ was approximated by the sum of three Gaussian curves $\rho_{In+Cd}(r) = \sum_{i}^{3} a_i e^{-r^2/4\beta_i}$.

The curve for neutrons slowed down to E = 0.025 ev was found by the formulas

$$\rho^{(1)}_{0.025\,ev}(r) = \int \rho_{In+Cd}(r') \frac{e^{-\frac{|r'-r|}{L'}}}{|r'-r|} dr' \sim \sum_i (4\beta_i)^{3/2} e^{\beta_i/L'^2} \frac{a_i}{r} [e^{-r/L'} \Phi(x_{1i}) - e^{r/L'} \Phi(x_{2i})],$$

$$\rho^{(2)}_{0.025\,ev}(r) = \int \rho_{In+Cd}(r') e^{-\frac{|r'-r|^2}{4\Delta\tau}} dr' \sum_i a_i \left(\frac{4\beta_i 4\Delta\tau}{4\beta_i + 4\Delta\tau}\right)^{3/2} e^{-\frac{r^2}{4\beta_i + 4\Delta\tau}},$$

where

$$\Phi(x) = \frac{1}{\sqrt{2\pi}} \int_x^\infty e^{-t^2/2} dt; \quad x_{1i} = \left(\frac{2\beta_i}{L'} - r\right)/\sqrt{2\beta_i}; \quad x_{2i} = \left(\frac{2\beta_i}{L'} + r\right)/\sqrt{2\beta_i};$$

$$L' = \sqrt{1.2}\ см; \quad \Delta\tau = 1{,}2\ см^2 *).$$

* $\Delta\tau = 1.2$ cm^2, not 1 cm^2, because the experimental curve of spatial distribution of resonance neutrons is being used, and the contribution of 0.2 cm^2, which is related to the activation of the indium foil by neutrons of energy $E > E_T$, should not be excluded.

In the first case it is assumed that the spatial distribution of neutrons slowed down from the resonance energy to the thermal energy is determined by diffusion theory; in the second case, by age theory. Since $\Delta\tau$ and L^2 are small, the difference between the curves of $\rho^{(1)}_{0.025\ ev}$ and $\rho^{(2)}_{0.025\ ev}$ is also small, and either of the curves of $\rho_{0.025\ ev}$ may be used to obtain the thermal neutron distribution due to diffusion in water:

$$\rho_t(r) = \int \rho_{0.025\ ev}(r') \frac{e^{-\frac{|r'-r|}{L}}}{|r'-r|} dr',$$

where L = 2.68 cm is the diffusion length of thermal neutrons in water. As can be seen from Fig. 3, the calculated curve agrees well with the experimentally measured one. In obtaining M^2, it was assumed that the neutrons are not thermal until their energy becomes 0.025 ev, and in order to obtain the distribution of purely thermal neutrons from $\rho_{In}(r)$, together with the activation from resonance neutrons, we subtracted out the activation caused by neutrons with energies $E_{0.025\ ev} < E < E_T$. Since the number of neutrons with energy E > 0.025 ev in the Maxwell distribution is large, the question as to the meaningfulness of this procedure arises. It was possible to pick a nominal limiting energy below which the neutrons would be considered thermal. For instance, we could have taken 4 × 0.025 ev = 0.1 ev for this energy. In this case we would have to subtract only the resonance neutrons from $\rho_{In}(r)$ and the quantity $\Delta\tau_{(1.46\ ev-0.1 ev)}$ would be 0.6 ± 0.3 cm² instead of 1.0 ± 0.5 cm² for $\Delta\tau_{(1.46\ ev-0.025\ ev)}$. Both of the experimental values can be compared with the calculation according to Marshak's formula (or according to age theory), made under the assumption that the slowing down of neutrons is achieved by the free hydrogen and oxygen nuclei

$$\Delta\tau_{theor\ (1.46\ ev-0.025\ ev)} = 1.7\ cm^2,$$

and

$$\Delta\tau_{theor\ (1.46\ ev-0.1\ ev)} = 1.1\ cm^2.$$

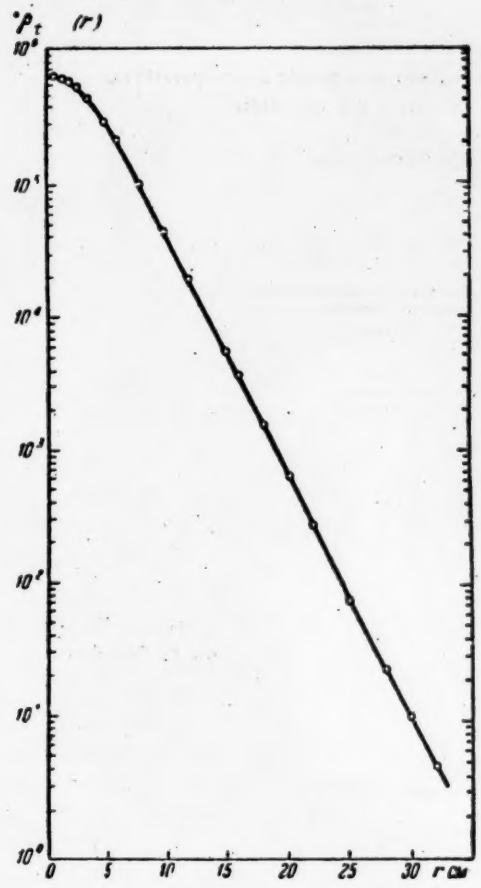

Fig. 3. Comparison of the calculated curve for $\rho_t(r)$ (solid line) with the experimental data (points on the curve).

In both cases the experimental values of $\Delta\tau$ are somewhat smaller than the calculated ones. The interpretation of the results obtained is complex, since in slowing down neutrons from 1.46 ev to 0.025 ev the effect of the chemical bond is felt in several factors acting in opposite ways: 1) the increased scattering cross section due to the fact that the proton is bound to the water molecule; 2) the increase in the symmetry of the scattering, as a result of which λ_t decreases significantly; 3) decreased energy loss in each elastic scattering event; 4) the excitation of vibrational and rotational molecular levels during scattering.

The square of the slowing-down length $\Delta\tau$ from E = 1.46 ev to E = 0.025 ev does not depend on the initial energy of the neutrons from the source being used. Therefore if we know $\tau_{1.46\ ev}$ for any neutron source, we can find the square of the slowing-down length for neutrons of this source $\tau_{0.025\ ev} = \tau_{1.46\ ev} + \Delta\tau$ to E = 0.025 ev. For instance, $\tau_{0.025\ ev}$ for fission neutrons slowed down by water is

$$\tau_{0.025\ ev} = \tau_{1.46\ ev} + \Delta\tau = 30.4 \pm 2\ cm^2,$$

since [1]:

$$\tau_{1.46\ ev} = 29.4 \pm 1.5\ cm^2.$$

In conclusion the authors express their sincere appreciation to Professor I. I. Gurevich for valuable discussions of the results of the work, to A. P. Venediktov and B. V. Sokolov, who took part in the preparation of the apparatus and in the measurements, and to A. V. Telnov, who helped in preparing the apparatus.

LITERATURE CITED

[1] L. M. Barkov, K. N. Mukhin, Atomic Energy 1956, No. 3, 317*.

[2] L. M. Barkov, A. P. Venediktov, K. N. Mukhin, Atomic Energy 1956, No. 3, 329*.

[3] W. Bothe, Z. Physik B120, 437 (1943).

[4] C. W. Tittle, Nucleonics 8, No. 6, 5 (1951).

[5] G. R. Gamertsfelder, M. Goldhaber, Phys. Rev., 62, 556 (1942).

[6] A. Berthelot, R. Cohen, H. Reel, Comptes rend., 225, 406 (1947).

[7] C. W. Tittle, Phys. Rev., 80, 756 (1950).

[8] K. E. Larsson, Arkiv Fysik 2, 47 (1950).

[9] F. J. Sisk, E. C. Campbell, Bull. Am. Phys. Soc., 26, No. 1, 58 A (1951).

[10] G. E. Dardel, N. G. Sjöstrand, Phys. Rev., 96, 1245 (1954).

[11] A. V. Antonov, A. I. Isakov, I. D. Murin, B. A. Neupokoev, I. M. Frank, F. L. Shapiro, I. V. Shtranikh, Physical Investigations (Reports of the Soviet Delegation to the International Conference on the Peaceful Uses of Atomic Energy), Acad. Sci. USSR Press, 1955, p. 158.

[12] F. R. Scott, D. B. Thomson and W. Wright, Phys. Rev., 95, 583 (1954).

[13] R. E. Marshak, Revs. Mod. Phys., 19, 185 (1947).

* C. B. Translation pagination.

SLOWING DOWN OF FISSION NEUTRONS BY URANIUM – WATER MEDIA

L. M. Barkov, A. P. Venediktov, K. N. Mukhin

The spatial distribution of resonance neutrons (E = 1.46 ev) which results from the slowing down of U^{235} fission neutrons emitted by a "point" source is measured for three variations of a uranium-water lattice made of thick slugs (35 mm) of natural uranium enclosed in cadmium tubes. The absence of anisotropies in the distribution of slowed-down neutrons is demonstrated, and the values of τ determined.

It is of considerable interest to carry out an experimental investigation of the slowing down of fission neutrons by uranium-water media whose characteristics are similar to those of projected reactors.

In the present work* we measure the spatial density distribution of 1.46 ev neutrons, which results from the slowing down of fission neutrons emitted by a "point" source in uranium-water lattices, with the aid of an indium detector. The lattice was constructed of 35 mm diameter blocks of natural uranium enclosed in aluminum jackets and placed in a tank 140 cm long, 100 cm wide, and 105 cm high. The fission neutron source was a target-convertor made of uranoso-uranic oxide U^{235} (4.15 g of uranium). A thermal neutron beam was directed at the convertor with the aid of a 50 cm long steel tube which was covered with a cadmium jacket together with the convertor. The distance from the convertor to the tank walls and the water surface was no less than 50 cm, and the distance in the direction of the measurement was 90 cm. This made it possible to perform the measurements up to distances of about 70 cm. In the experiment we used the method of measurement that is described in a previous article [1]. In order to prevent thermal neutron multiplication, the uranium slugs were enclosed in tubes made of sheet cadmium 0.6 mm thick. The tubes with the slugs in them were assembled into equilateral triangular lattices with various spacings of 4.3, 5.0, and 6.0 cm, which provided a variation of the ratio of the water volume to the uranium volume in the interval from 0.4 to 2.0. The tubes were fixed in position by the use of three plates with holes drilled through them for the tubes. The upper and lower plates, located at the ends of the tubes, were made of 6 mm thick Duralumin; the center one, located 20 cm below the convertor, was made of 8 mm thick plexiglass. The material of the center plate was chosen on the basis of the great similarity between its slowing-down properties and those of water. The three plates were attached to each other by a rigid Duralumin framework. A large window was cut into the top plate to admit the cadmium adapters with the indium foils into the lattice. In order to maintain the proper spacing between the tops of the tubes that were located within the window, small sections of the cut-out Duralumin plate were inserted between them.

Figure 1 is a photograph of the lattice, showing the distribution of the tubes (A), and tube (B) through which the beam enters, the convertor (C), the adapters with the foils (D), the three plates (E_1, E_2, and E_3), and a few sections (F) for holding the upper ends of the tubes. The tank was loaded with the tubes by use of a winch and cable with an automatic chuck (G).

In order to verify some questions as to the method used, preliminary measurements were made with a source that reproduced the fission neutron spectrum. These experiments showed the following:

* The work was performed on the RFT reactor. Preliminary results were presented at the International Conference on the Peaceful Uses of Atomic Energy in Geneva in 1955.

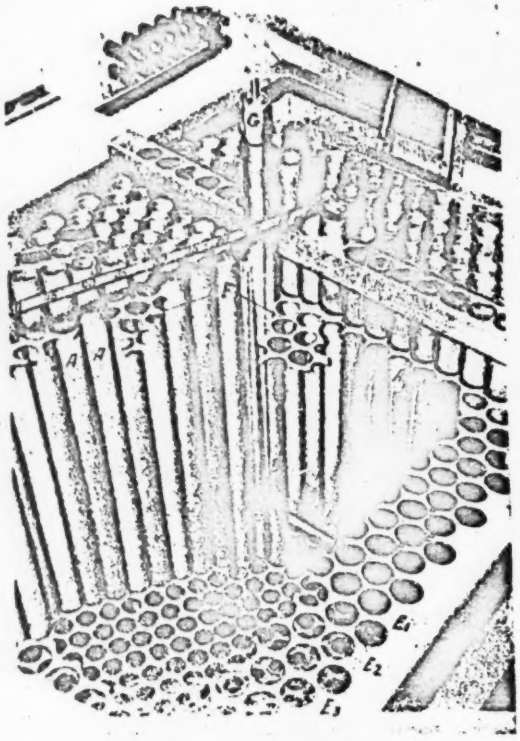

Fig. 1. General view of the apparatus.

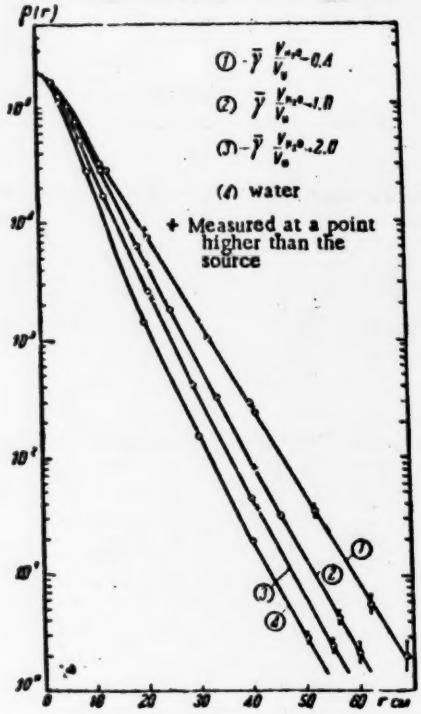

Fig. 2. Results of measurement of the resonance neutron distribution density for uranium-water lattices and for water.

1) In the horizontal plane passing through the source, the density distribution $\rho(r)$ of slowed down neutrons is isotropic with respect to the direction from the source.

2) The distribution $\rho(r)$ in the horizontal plane does not change when a cadmium tube filled with air (simulating the conditions created by the thermal neutron beam) is placed vertically over the source.

3) The influence of edge effects is not felt as close as 5-10 cm from the boundary, both in the vertical and in the horizontal directions.

Fundamental measurements were made with the convertor for three different lattices corresponding to the following values for the ratio of the water volume to the uranium volume: 0.4, 1.0, and 2.0 (spacings of 4.3, 5.0, and 6.0 cm). The results of the measurements are presented in Fig. 2. The statistical errors for the experimental points are shown only for the greatest distances $r > 45$ cm. For distances $r < 45$ cm, the statistical errors are no larger than 2%.

Separate measurements were made for $\rho(r)$ in the vertical direction, and they showed that within the experimental accuracy there is no anisotropy in the distribution $\rho(r)$ in any of the variations of the lattice. Thus the quantity τ_{exp} can be calculated by the usual formula

$$\tau = \frac{\bar{r}^2}{6} = \frac{\int_0^\infty r^4 \rho(r)\, dr}{6\int_0^\infty r^2 \rho(r)\, dr}.$$

The results of the calculation are presented in Table 1.

TABLE 1

Experimental Values of τ for Various Magnitudes of the Ratio of the Water Volume to the Uranium Volume

Spacing l (cm)	4.3	5.0	6.0	Water without uranium
$\gamma = V_{H_2O}/V_{tot}$	0.23	0.43	0.61	1
$\bar{\gamma} = V_{H_2O}/V_U$	0.4	1.0	2.0	–
τ_{exp} (cm^2)	65±3	47±2	37±2	29.4 ± 1.5

The values of τ_{exp} presented are somewhat too high because of the fact that multiplication of the neutrons incident on the cadmium is not entirely suppressed.

Values of τ corresponding to the absence of multiplication of these neutrons in the system can be derived in the following manner.

Let $\rho(r)$ be the resonance neutron density (for instance, with E = 1.46 ev) in an arbitrary system that has neutron multiplication, let $\rho_0(r)$ be the resonance neutron density in this system when the multiplication is suppressed, and let k_∞ be the multiplication factor for this system. Then neutron multiplication leads to the following relation connecting $\rho(r)$, $\rho_0(r)$, and k_∞.

$$\left.\begin{aligned} &\rho(r) = \rho_0(r) + k_\infty \rho_1(r) + k_\infty^2 \rho_2(r) + \dots, \\ &\text{where} \\ &\rho_1(r) = \int \rho_0(|\bar{r} + \bar{r}_1|)\, \rho_0(r_1)\, d\bar{r}_1, \\ &\rho_2(r) = \int \rho_1(|\bar{r} + \bar{r}_1|)\, \rho_0(r_1)\, d\bar{r}_1, \\ &\dots\dots\dots\dots\dots\dots\dots\dots \\ &\rho_n(r) = \int \rho_{n-1}(|\bar{r} + \bar{r}_1|)\, \rho_0(r_1)\, d\bar{r}_1. \end{aligned}\right\} \quad (1)$$

Here $\int \rho_0(r)\, dr = 1$ and $\int \rho_1(r)\, dr, \dots \int \rho_n(r)\, dr$ are also normalized to unity. In Expression (1), $k_\infty \rho_1(r)$, $k_\infty^2 \rho_2(r)$ . . . represent the distributions of neutrons of the second and third generations, etc.

If two of the quantities $\rho_0(r)$, $\rho(r)$ and k_∞ are known, then Equation (1) makes it possible to find the third. For instance, if $\rho_0(r)$ is known from experiment, then by calculating $\rho_1(r)$, $\rho_2(r)$ . . ., for a known k_∞, we may determine $\rho(r)$, or

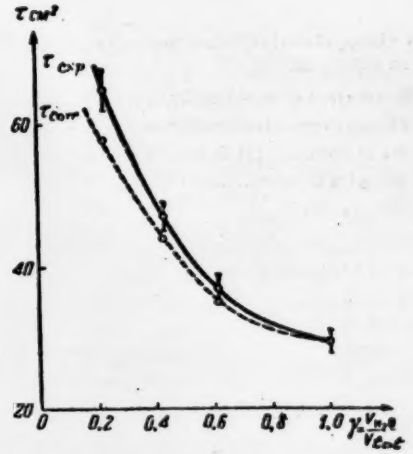

Fig. 3. The dependence of τ on the relative amount of water in the lattice $\gamma = V_{H_2O}/V_{tot}$. The solid line is the experimental value of τ; the dotted line is the value of τ corrected for neutron multiplication in the lattice.

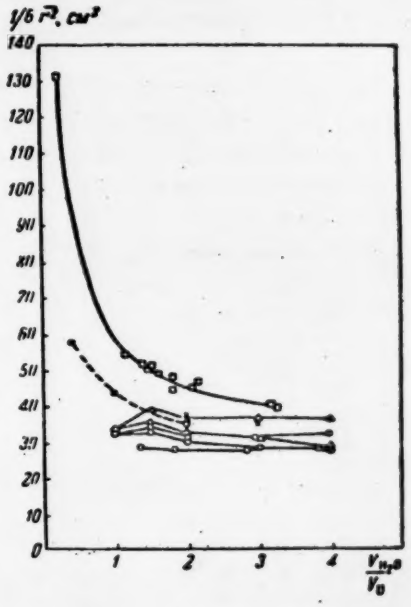

Fig. 4. Comparison of the data of various works on the slowing down of neutrons by uranium-water lattices. □) Direct Oak Ridge experiments ($\tau_{0.625\ ev}$) [3]; Δ) Brookhaven experiments; method of artificial "poisoning" and "enriching"; analysis by the one-group theory (M^2) [3]; ○) Brookhaven experiments; method of "poisoning" and "enriching"; analysis by age theory (M^2) [3]; ×) Westinghouse experiments. Critical experiments. Analysis by the one-group theory (M^2) [5]; ●) results of the present work ($\tau_{1.46\ ev}$).

conversely, from the experimental values of $\rho(r)$ and $\rho_0(r)$ we can find k_∞. In practice this problem can be solved by approximating the experimental curve for $\rho_0(r)$ by a system of functions that is convenient for integration, e.g. by a sum of Gaussian functions $\sum_i \alpha_i e^{-\frac{r^2}{4\beta_i}}$, where α_i and β_i are empirically chosen constants. In this case the integration is completely carried out, and the resulting functions $\rho_1(r)$, $\rho_2(r)$ are also obtained in the form of sums of Gaussians with coefficients expressed simply in terms of α_i and β_i. It is clear that the necessary number of terms in Formula (1) is determined by the magnitude of k_∞. Thus if $k_\infty = 0.1$-0.2, then the experimental curve for $\rho(r)$ is sufficiently well reproduced by a formula with only two terms.

$$\rho(r) \simeq \rho_0(r) + k_\infty \rho_1(r). \tag{2}$$

The relation between $\rho_0(r)$, $\rho(r)$, and k_∞ also makes it possible to evaluate the differences in the corresponding values of τ if $\rho(r)$ and k_∞ are known, and therefore also $\rho_0(r)$ from (2). Indeed, if $\rho_0(r)$ is given in the form of a sum of Gaussians $\sum_i \alpha_i e^{-\frac{r^2}{4\beta_i}}$, then integration gives

$$\begin{aligned}\tau &= \frac{1}{6}\frac{\int r^4 \rho(r)\,dr}{\int r^2 \rho(r)\,dr} = \\ &= \frac{1}{1+k_\infty}\Big[\sum_i \beta_i \alpha_i (4\pi\beta_i)^{3/2} + \\ &+ k_\infty \sum_{i,k} (\beta_k + \beta_i)\alpha_k (4\pi\beta_k)^{3/2}\alpha_i (4\pi\beta_i)^{3/2}\Big] = \frac{\tau_0}{1+k_\infty} + \\ &+ \frac{k_\infty}{1+k_\infty}\sum_{i,k}(\beta_k+\beta_i)\,\alpha_k (4\pi\beta_k)^{3/2}\alpha_i (4\pi\beta_i)^{3/2}.\end{aligned} \tag{3}$$

In the present work the above method was used to evaluate τ_0 for the system in the case for which there is no multiplication– neither of thermal neutrons, nor of those that are incident on the cadmium.

In evaluating τ_0 [by Formula (3)] the calculated multiplication factor k_∞ for the neutrons incident on the cadmium was used, and the value of $\rho_0(r)$ found according to (2) was expressed in the form of a sum of three Gaussian functions.

The evaluation of the multiplication factor of the system was made according to the formula $k = \nu\varphi\theta'\epsilon$, where ν is the number of neutrons per fission event, φ is the probability that resonance capture does not occur, ϵ is the multiplication factor for fast neutrons, and θ' is the probability of fission by the neutrons incident on the cadmium in the process of their slowing down to capture in the cadmium. The value of ν was taken from a note published in Nucleonics [2], that of ϵ from the work of Kouts et al. [3], and that of φ from the results of measurements by M. B. Egiazorov (private communication).

The value of θ' was calculated according to a formula given by Gurevich and Pomeranchuk [4], which the authors derived for the evaluation of φ and modified for the evaluation of the probability of fission by the neutrons incident on the cadmium in the process of slowing down. For this the following changes were made in the formula: the concentration of U^{238} nuclei was replaced by the concentration of U^{235} nuclei, the capture cross section of U^{238} was replaced by the fission cross section of U^{235}, the term accounting for the contribution from the strongly blocked resonances was dropped, and a coefficient that accounts for the absorption of neutrons in cadmium was introduced.

Table 2 presents the values of the multiplication factors k_∞ found in this way for the neutrons incident on the cadmium. The accuracy of the constants and formulas used allows us to suppose that the error in the multiplication factor is no greater than 50%. On the same table we present the values of τ for systems in which no multiplication takes place for the neutrons incident on the cadmium. The values of τ were derived from the values of τ_{exp} and k_∞ by the method described above.

TABLE 2

The Multiplication Factor for Neutrons Incident on the Cadmium, and τ for the System in the Absence of Multiplication of Thermal Neutrons and Those Incident on the Cadmium

Spacing $\underline{1}$ (cm)	4.3	5.0	6.0	Water without uranium
$\gamma = V_{H_2O}/V_{tot}$	0.23	0.43	0.61	1
$\gamma = V_{H_2O}/V_U$	0.4	1.0	2.0	—
k_∞	0.15	0.11	0.067	0
$\tau_{1.46\ ev}$ (cm^2)	58 ± 5	44 ± 3	35 ± 2	29.4 ± 1.5

Figure 3 presents the dependence of τ_{exp} and τ on the fraction of the lattice volume that is taken up by the water $\gamma = V_{H_2O}/V_{tot}$. It should be noted that the values of τ found include the effect of slowing down of the neutrons that arise in the slugs as a result of U^{238} fission by fast neutrons.

Figure 4 presents experimental results of various works on the measurement of $\tau_{1.46\ ev}$, $\tau_{0.025\ ev}$, and the migration area M^2.

In making comparisons it should be noted that M^2 is greater than $\tau_{0.025}$: $M^2 = \tau_{0.025\ ev} + L^2$ (L is the diffusion length). For uranium-water lattices, however, L^2 is much less than $L^2_{H_2O}$, being equal to $L^2 \approx L^2_{H_2O}(1-\theta) \sim 1\text{-}2$ cm^2.

In addition, in making comparisons we must bear in mind the fact that the value of $\tau_{1.46\ ev}$ obtained in the present work is about 1 - 2 cm^2 lower than $\tau_{0.025\ ev}$. By comparing the values of $\tau_{1.46\ ev}$, $\tau_{0.025\ ev}$, and M^2 it can be seen that the results of the measurements do not agree well among themselves. Direct measurements of τ performed at Oak Ridge by a method similar to ours give substantially higher values for τ.

Since the details of the experiment are not described, it is difficult to explain the reason for such a divergence. In these experiments no account is taken of the multiplication of the neutrons incident on the cadmium. As our evaluation has shown, however, this effect is not large. The difference between our results and the determination of M^2 published by Kouts et al. [3] can be partly explained by the fact that in comparable lattices different amounts of materials that do not slow down neutrons effectively are used.

There is some doubt as to the possibility of determining M^2 from critical experiments and from experiments on the artificial "poisoning" and "enriching" of reactors. In the analysis of these experiments either the one-group theory, or age theory is used. The validity of these theories in the case of water is doubtful, and the analysis of the same experimental results leads to different values of M^2.

In conclusion the authors express their gratitude to Professor I. I. Gurevich for discussions of the results of this work, and to V. K. Makaryin A. I. Maleev, V. I. Baranov, and B. V. Sokolov, who helped in performing the measurements.

LITERATURE CITED

[1] L. M. Barkov, K. N. Mukhin, Atomic Energy, 1956, No. 3, 31 (T. p. 317)*.

[2] Nucleonics 8, No. 1, 78 (1951).

[3] H. Kouts, G. Price, K. Downes, R. Sher, and Walsh, Experimental Reactors and the Physics of Reactors (Reports of Foreign Scientists at the International Conference on the Peaceful Uses of Atomic Energy), State Tech. Press, 1955, p. 417.

[4] I. I. Gurevich, I. Ya. Pomeranchuk, Construction and Theory of Reactors (Reports of the Soviet Delegation at the International Conference on the Peaceful Uses of Atomic Energy), Acad. Sci. USSR Press, 1955, p. 220.

[5] S. Krasik, and A. Radkowsky, Atomic Power (Reports of Foreign Scientists at the International Conference on the Peaceful Uses of Atomic Energy), State Energy Press, 1956, p. 375.

* T. p. = Consultants Bureau Translation pagination.

SCATTERING OF SLOW NEUTRONS BY WATER MOLECULES

A. F. Goryunov

Perturbation theory methods are used to calculate the cross section for scattering of slow neutrons (E_n < 0.19 ev) by water molecules.

The cross section for scattering of neutrons by water has been experimentally determined by Jones and Meliconian [1, 2]. The aim of the present article is the calculation of the total elastic and inelastic cross section for scattering of slow neutrons by water at room temperature. The scattering cross section is calculated on the assumption that the molecules do not interact with each other. For this condition, the inelastic part of the cross section arises from energy changes within the separate molecules. In order to clarify the contribution of the different states to the scattering, we shall compare the vibrational [3] and the rotational [4] spectra of the water molecules. The energy of the first vibrational level is $E_1 = 0.19$ ev ($\nu = 1595$ cm^{-1}), and the rotational energy reaches this value for $j = 8$ (j is the rotational quantum number). Therefore at room temperature the molecule is in the vibrational ground state; almost no excitation of vibrational levels occurs, since $E_1 \gg kT$. The rotational levels at room temperature will obviously have low values of j. In the following we shall consider only the scattering of neutrons with energies $E \ll E_1$. Since for these neutron energies the vibrational levels are not excited, the water molecules may be considered rigid rotators.

In order to calculate the cross section we shall make use of the methods of perturbation theory. In this case the interaction of the neutrons with the nuclei of the molecule are described by a Fermi pseudopotential. The differential cross section for scattering $d\sigma$ into an element of solid angle $d\Omega$ in the center-of-mass system of the neutron and molecule is then written in the form

$$d\sigma = \frac{p}{p_0}\left(\frac{mM}{m+M}\right)^2\left(\frac{V}{2\pi\hbar^2}\right)^2 |(\Psi_f^*, U\Psi_i)|^2\, d\Omega \qquad (1)$$

where Ψ_i and Ψ_f are the wave functions of the initial and final states of the system composed of the molecule and the neutron, p_0 is the neutron momentum before scattering, p is its momentum after scattering, M is the mass of the molecule, and m is the neutron mass.

The interaction energy of the neutron and molecule depends on the orientation of their spins ($1/2\sigma_n$ and S, respectively), and can be written in the form [5]

$$U = -\frac{\pi\hbar^2}{2m^*(2S+1)}\left[(S+1)\,a_{S+1/2} + S a_{S-1/2} + (a_{S+1/2} - a_{S-1/2})\,\sigma_n S\right]\delta(\mathbf{r}-\mathbf{r}_n), \qquad (2)$$

where $a_{S+1/2}$ and $a_{S-1/2}$ are the scattering amplitudes and m^* is the reduced mass of the neutron. Let us denote the scattered amplitudes of the neutron from the proton in the singlet and triplet states, respectively, by a_0 and a_1, and from the oxygen nucleus, whose spin is 0, by a. Making use of (2), let us write the interaction energy of the neutron and the molecule:

$$U = -\frac{\pi\hbar^2}{m}\left[(3a_1+a_0)+(a_1-a_0)\,\sigma_1\sigma_n\right]\delta(\mathbf{r}_n-\mathbf{r}_1) - \frac{\pi\hbar^2}{m}\left[(3a_1+a_0)+(a_1-a_0)\,\sigma_2\sigma_n\right]\delta(\mathbf{r}_n-\mathbf{r}_2) - \frac{2\pi\hbar^2}{m\mu}(\mu+m)\,a\,\delta(\mathbf{r}_n-\mathbf{r}_3), \qquad (3)$$

* Here and in what follows $\hbar$ stands for Planck's constant divided by 2π.

where μ is the mass of the oxygen atom, and $\frac{1}{2}\vec{\sigma}_1$ and $\frac{1}{2}\vec{\sigma}_2$ are the proton spins.

Let us represent the interaction energy in the form of a sum $U = U_s + U_a$, where U_s is the symmetric part, and U_a is the antisymmetric part with respect to interchange of the proton spins. The symmetric part leads to scattering without change of the molecular spin, and the antisymmetric part leads to scattering with a spin change. It is easy to see that

$$U_c = -\frac{\pi\hbar^2}{m}[(3a_1 + a_0) + (a_1 - a_0)\sigma_n S] \times \\ \times [\delta(\mathbf{r}_n - \mathbf{r}_1) + \delta(\mathbf{r}_n - \mathbf{r}_2)] - \\ -\frac{2\pi\hbar^2}{m\mu}(\mu + m)a\delta(\mathbf{r}_n - \mathbf{r}_a), \tag{4a}$$

$$U_a = -\frac{\pi\hbar^2}{2m}(a_1 - a_0)\sigma_n(\sigma_1 - \sigma_2) \times \\ \times [\delta(\mathbf{r}_n - \mathbf{r}_1) - \delta(\mathbf{r}_n - \mathbf{r}_2)], \tag{4b}$$

where $S = \frac{\vec{\sigma}_1 + \vec{\sigma}_2}{2}$ is the molecular spin.

The initial state wave function in the center-of-mass system of the molecule and neutron can be written in the form

$$\Psi_i = \frac{1}{V} e^{\frac{i(\mathbf{p}_0 \cdot \mathbf{r}_c - \mathbf{r}_n)}{\hbar}} \Psi^j_{em} \chi_{m_n} \chi_{sm_s}), \tag{5a}$$

where the motion of the neutron and the center of mass of the molecule are described by plane waves, Ψ^j_{em} is the wave function of the molecule about its center of mass, with e the energy quantum number, j the angular momentum, m the projection of j on the stationary axis, and χm_n and χsm_s are the spin functions of the neutron and the molecule, respectively. For the function Ψ_f, a similar expression holds:

$$\Psi_f = \frac{1}{V} e^{\frac{i(\mathbf{p}, \mathbf{r}_c - \mathbf{r}_n)}{\hbar}} \Psi^J_{EM} \chi_{M_n} \chi_{SM_S}. \tag{5b}$$

The water molecule is an asymmetric rotator. The wave functions Ψ^j_{em} of the stationary states of an asymmetric rotator can be expressed as a linear combination of wave functions Φ^j_{mk}, which describe the states of a gyroscope with definite j, m, and k, where k is the projection of the angular momentum on the moving axis. The functions Φ^j_{mk} are identical with the known functions for a symmetric rotator. Thus

$$\Psi^j_{em} = \sum_k B^j_{ek} \Phi^j_{mk}. \tag{6}$$

The coefficients B^j_{ek} are found from a secular equation [6]. In the series expansion (6), as is well known, only functions Φ^j_{mk} with either even k or with odd k enter. In the present case, the numbers e are chosen so that states with wave functions symmetric in k are characterized by even e, and even values of e/2 corresponds to even values of k, whereas states with wave functions antisymmetric in k are those with odd e, and even values of (e + 1)/2 correspond to even values of k.

The wave function must be antisymmetric with respect to the operation of interchanging the protons. Let us take the z'-axis perpendicular to the plane of the molecule, and the y'-axis through the oxygen atom; then on interchanging the protons, the angular part is multiplied [7] by $(-1)^{j+e}$, and the spin part, by $(-1)^{s+1}$, where s is the total spin of the molecule. Then the requirement of antisymmetry is satisfied by those states for which when s = 0, j + e is even, and when s = 1, j + e is odd.

* Indices referring to the initial state are denoted by lower case letters; the corresponding capital letters refer to the final state.

Averaging the cross section (1) over the initial quantum numbers m, m_n, m_s and summing over the final M, M_n, M_S, which is done similarly as in reference [8], we are led to the following expressions for the cross sections without change of spin, and with it, respectively:

$$d\sigma_0 = d\Omega \frac{P}{p_0}\left(\frac{M}{m+M}\right)^2 \frac{1}{2j+1} \times$$
$$\times \sum_{m,M}\left[\frac{(3a_1+a_0)^2+2s(a_1-a_0)^2}{4}|I_1|^2+\right.$$
$$+\left(\frac{m+\mu}{\mu}\right)^2 a^2|I_2|^2+ \tag{7a}$$
$$\left.+\frac{a(3a_1+a_0)}{2}\frac{m+\mu}{\mu}(I_1^*I_2+I_1I_2^*)\right],$$

$$d\sigma_2 = d\Omega \frac{P}{p_0}\left(\frac{M}{m+M}\right)^2 \frac{1}{2j+1}\times$$
$$\times \sum_{m,M}\frac{(a_1-a_0)^2(3-2s)}{4}|I_2|^2. \tag{7b}$$

Here we have used the notation

$$I_{1,2} = \int \Psi_{EM}^{J*}\Psi_{em}^{j}\left(e^{iq\rho_1} \pm e^{iq\rho_2}\right)dO, \tag{8a}$$

$$I_2 = \int \Psi_{EM}^{J*}\Psi_{em}^{j}e^{iq\rho_2}dO, \tag{8b}$$

where the ρ_i are the distances of the nuclei from the center of mass of the molecule, and $dO = \sin\alpha\, d\alpha\, d\beta\, d\gamma$, here the angles α, β, γ are related to the Euler angles by the expressions $\alpha = \frac{\pi}{2} + \psi$, $\beta = \frac{\pi}{2} - \varphi$, $\gamma = \theta$ and are chosen so that for $\psi = 0$ or $\varphi = 0$, we get the usual spherical coordinate system. The rest of the problem reduces to the evaluation of the integrals entering into the expressions for the cross sections. Let us first consider the cross section $d\sigma_2$. The scalar products $q\rho_1$ and $q\rho_2$ in the moving coordinate system can be written in the form

$$q\rho_1 = -q\rho_0 \sin\gamma \sin(\beta+\varphi_0),$$
$$q\rho_2 = q\rho_0 \sin\gamma \sin(\beta-\varphi_0),$$

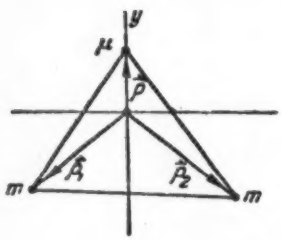

where $|\rho_1| = |\rho_2| = \rho_0$; $\operatorname{tg}\varphi_0 = x_0/y_0$, $x_0 = -|\rho_{1x}| = |\rho_{2x}|$, $y_0 = -|\rho_{1y}| = -\rho_{2y}$. Let us expand the difference of exponentials in (8a) in a series of associated functions:

$$e^{iq\rho_1} - e^{iq\rho_2} = -2i\times \tag{9}$$
$$\times \sum_{n,l} g_n(q\rho_0)Y_{nl}^*(\gamma,\beta)Y_{nl}(\pi/2, -\pi/2)\sin l\varphi_0,$$

where

$$g_n(q\rho_0) = i^n(2\pi)^{3/2}\frac{J_{n+1/2}(q\rho_0)}{\sqrt{q\rho_0}},$$

and $J_{n+1/2}(q\rho_0)$ is a Bessel function.

Making use of (8a), (8b), (6), and (9), and expanding the product of the functions

in a Clebsch-Gordan series [9], we obtain the following expression for I_s:

$$I_s = \sqrt{\frac{(2J+1)(2j+1)}{\pi}} \sum_{\varkappa, k, K} (-1)^{\varkappa+K} B^J_{EK} \times \tag{10}$$
$$\times B^j_{ek} C^{\varkappa\nu}_{J-Mjm} C^{\varkappa\nu}_{J-Kjk} Y_{\varkappa\nu}(\pi/2, -\pi/2) \sin \nu\varphi_0 \times \frac{g_\varkappa(qp_0)}{\sqrt{2\varkappa+1}},$$

where $C^{c\nu}_{a\alpha b\beta}$ is a Clebsch-Gordon coefficient. The summation over m and M is easily performed by making use of the orthogonality properties of the Clebsch-Gordon coefficients [9]. After a simple calculation, we obtain

$$\frac{1}{2J+1} \sum_{m, M} |I_s|^2 = \frac{2J+1}{\pi^2} \sum_{\varkappa} |g_\varkappa(qp_0) F^{Jj}_{E\varkappa}(\sin\varphi_0)|^2 \tag{11}$$

where

$$F^{Jj}_{E\varkappa}\begin{pmatrix}\cos\varphi_0\\ \sin\varphi_0\end{pmatrix} = \sum_{k, K} (-1)^{\nu/2} B^J_{EK} B^j_{ek} C^{\varkappa\nu}_{J-Kjk} \times$$
$$\times \Theta^\nu_\varkappa \begin{pmatrix}\cos\nu\varphi_0\\ \sin\nu\varphi_0\end{pmatrix} \quad (k = -j, \ldots, j;\ k = 0, \ldots J),$$
$$\Theta^\nu_\varkappa = \sqrt{\frac{(\varkappa-\nu)!}{(\varkappa+\nu)!}} P^\nu_\varkappa(0) \qquad (\nu = k-K); \tag{12}$$

$P^\nu_\varkappa$ is the associated Legendre polynomial.

Similar calculations lead to the following expression for the cross section:

$$d\sigma^{JEs}_{jes} = d\Omega \frac{p_1}{p_0} \left(\frac{M}{m+M}\right)^2 \frac{2J+1}{\pi^2} \times$$
$$\times \left[\frac{(3a_1+a_0)^2 + 2s(a_1-a_0)^2}{4} \sum_{\varkappa} |g_\varkappa(qp_0) \times F^{Jj}_{E\varkappa}(\cos\varphi_0)|^2 + \left(\frac{m+\mu}{\mu}\right)^2 \frac{a^2}{4} \times\right.$$
$$\left. \times \sum_{\varkappa} |g_\varkappa(qp) F^{Jj}_{E\varkappa}(\cos 0)|^2 + \frac{a(3a_1+a_0)}{2} \frac{m+\mu}{\mu} \times \sum_{\varkappa} g^*_\varkappa(qp_0) g_\varkappa(qp) F^{Jj}_{E\varkappa}(\cos\varphi_0) F^{Jj}_{E\varkappa}(\cos 0)\right] \tag{13a}$$

$$d\sigma^{JEl-s}_{jes} = d\Omega \frac{p}{p_0} \left(\frac{M}{m+M}\right)^2 \frac{2J+1}{\pi^2} \times$$
$$\times \frac{(a_1-a_0)^2(3-2s)}{4} \sum_{\varkappa} |g_\varkappa(qp_0) F^{Jj}_{E\varkappa}(\sin\varphi_0)|^2. \tag{13b}$$

For transitions of the molecule from the state (j, e, s) to the state (J, E, S), the following selection rules hold:

$$\Delta e + (-1)^e \left[(-1)^{\Delta j} \Delta s + \frac{1-(-1)^{\Delta j}}{2} \right] = 4k, \quad (k = 0, \pm 1, \ldots), \tag{14}$$

where $\Delta e = E - e$, $\Delta j = J - j$, $\Delta s = S - s$.

The total cross section is found by integrating Expressions (13a) and (13b) over the angles. Let us take the z-axis along $\mathbf{q}$, and let us introduce the new variable $x = \rho_0 / h \sqrt{(p - p_0)^2}$, ; then the integrated cross section will be expressed in the following way:

$$\sigma_{jes}^{JEs} = \frac{1}{p_0^2} \left(\frac{4\pi h M}{\rho_0 (m+M)} \right)^2 (2J+1) \times \left[\frac{(3a_1 + a_0)^2 + 2s(a_1 - a_0)^2}{4} \sum_x |I_x^{(1)} F_{Eex}^{Jj}(\cos\varphi_0)|^2 + \right. \tag{14a}$$

$$\left. + \left(\frac{m+\mu}{2\mu a} \right)^2 a^2 \sum_x |I_x^{(2)} F_{Eex}^{Jj}(\cos 0)|^2 + \frac{m+\mu}{2\mu \sqrt{a}} a (3a_1 + a_0) \sum_x I_x^{(3)} \times F_{Eex}^{Jj}(\cos\varphi_0) F_{Eex}^{Jj}(\cos 0) \right],$$

$$\sigma_{jes}^{JE1-s} = \frac{1}{p_0^2} \left(\frac{4\pi h M}{\rho_0 (m+M)} \right)^2 (2J+1) \times \frac{(a_1 - a_0)^2 (3-2s)}{4} \sum_x |I_x^{(1)} F_{Eex}^{Jj}(\sin\varphi_0)|^2, \tag{14b}$$

where we use the notation

$$I_x^{(1)} = \int_{x_1}^{x_2} J_{x+1/2}^2(x)\, dx, \tag{15a}$$

$$I_x^{(2)} = \int_{x_1}^{x_2} J_{x+1/2}^2(ax)\, dx, \tag{15b}$$

$$I_x^{(3)} = \int_{x_1}^{x_2} J_{x+1/2}(ax) J_{x+1/2}(x)\, dx, \tag{15c}$$

and we have

$$a = p/p_0 = 0{,}0685, \quad x_{1,2} = \frac{\rho_0}{h} |p_0 \pm p|,$$

$$p^2 = p_0^2 + \frac{2mM}{m+M} \Delta E, \quad \Delta E = E_j^r - E .$$

Let us sum the expression for the cross section over the final states:

$$\sigma_{jes} = \sum_{J,E} \sigma_{jes}^{JES}, \tag{16}$$

and average over the initial states:

$$\sigma = A \sum_{jes} \sigma_{jes} e^{-\frac{E_j^e}{kT}} (2s+1)\ (2j+1); \tag{17}$$

$$A = \sum_{jes} e^{-\frac{E_j^e}{kT}} (2s+1)(2j+1).$$

In order to clarify the role of the initial rotational states, we must find the values of the quantities

$$B(j) = (2j+1)\sum_s e^{-\frac{E_j^e}{kT}}(2s+1)$$

for various j. Making use of the values of E_j^e [4], it is easy to see that B (j) is a maximum at j = 3.

Below we give the results of numerical calculations of the cross sections as functions of the neutron energy E taking into account the states for which $j \leq 3$. For comparison, we present the experimental data on the scattering of neutrons by water [1]; the energy E is given in electron volts, and the cross section in barns.

E	0.05	0.045	0.04	0.035	0.03	0.025	0.02
σ	74.4	81.2	83.6	88.0	96.0	100.4	107.6
$\sigma_{elastic}$	45.6	44.6	52.8	55.6	59.6	62.4	64.0
σ_{exp}	84		92		104		118

For the amplitudes we take the values $a_0 = 2.34 \times 10^{-12}$ cm, $a_1 = -0.52 \cdot 10^{-12}$ cm [8], $4\pi a^2 = 4 \cdot 10^{-24}$ cm^2 [10].

The calculated cross section is smaller than the experimental one by about 10%. This is probably related to the fact that the molecular states with $j \geq 4$ are not taken into account, and the interaction of the molecules is ignored.

In conclusion, the author thanks B. T. Geilikman for discussions of the work, and for valuable comments.

LITERATURE CITED

[1] N. B. Jones, Jr., Phys. Rev. 74, 364 (1948).

[2] E. Meliconian, Phys. Rev. 76, 1750 (1949).

[3] G. Hertsberg, Vibrational and Rotational Spectra of Polyatomic Molecules, Foreign Lit. Press, 1949, pp. 179, 304.

[4] H. M. Randall, D. M. Denisson, N. Ginsburg and L. R. Weler, Phys. Rev. 52, 160 (1937).

[5] M. Hamermesh, J. Schwinger, Phys. Rev. 69, 145 (1946).

[6] L. Landau and E. Lifshits, Quantum Mechanics, Part 1, State Tech. Press, 1948.

[7] Wan Winter, Physica 20, 274 (1954).

[8] J. Schwinger, E. Teller, Phys. Rev. 52, 286 (1937).

[9] K. Adler, Helvetica Physica Acta 25, 235 (1952).

[10] Neutron Cross Sections, Foreign Lit. Press, 1951.

SCATTERING OF NEUTRONS BY PARA- AND ORTHO-HYDROGEN

S. I. Drozdov

The differential and total cross sections for elastic and inelastic scattering processes of neutrons by para- and ortho-hydrogen molecules are calculated in this article. In addition to the rotational degrees of freedom of the molecule, we take into account the vibrations of the nuclei in the harmonic approximation. The average neutron energy loss to excitation of the molecular levels is determined.

I

In reference [1], the authors treated neutron scattering from para- and ortho-hydrogen, proceeding from the assumption that the molecular vibrational levels are not excited. The hydrogen molecule was thus considered a rigid rotator. In the present article, the results of reference [1] are generalized to the case of neutron energies high enough to excite vibrational levels. For this we assume that the molecular vibrations may be considered harmonic. Then the molecular wave function is of the form

$$\Phi_{nlm}(\mathbf{r}) = Y_{lm}(\vartheta, \varphi)\left(\frac{b}{n!\,2^n\sqrt{\pi}}\right)^{\frac{1}{2}}\frac{H_n(bx)}{r}e^{-\frac{1}{2}(bx)^2}. \tag{1}$$

Here $Y_{lm}(\vartheta, \varphi) = \Theta_{lm}(\cos\vartheta)\frac{e^{im\varphi}}{\sqrt{2\pi}}$ are the spherical harmonics, the angles ϑ, φ determine the orientation of the molecule; l, m are the angular momentum quantum numbers, $r = R + x$ is the distance between the nuclei in the molecule (R is its equilibrium value), $H_n(bx)$ is a Hermite polynomial, n is the vibrational quantum number, $b = \sqrt{\frac{M\omega}{2\hbar}}$, M is the proton mass, and ω is the natural frequency of the vibrations. The molecular state is determined by four numbers nlmS, where S is the molecular spin, and is either zero or one. According to the Pauli principle, for a given S only those l are possible for which $(-)^S = (-)^l$.

II

Let the molecule be in its vibrational ground state prior to scattering. Then according to [1], the differential cross section for scattering of the neutron through an angle θ, with the molecule undergoing the transition $(0|^1S) \rightarrow (nl\ {}^{S}_{1-S})$ with or without spin change, can be written, in the center-of-mass coordinate system (of the neutron and the molecule), in the form

$$\sigma_{0l'S,\,nl\,1-S}^{S}(\theta)=\frac{4}{9}\frac{k_{nll'}}{k}c_{\,S\,1-S}\frac{1}{2l'+1}\times\sum_{mm'}\left|\int dr\,\Phi^{*}_{nlm}(r)\,\Phi_{0l'm'}(r)\begin{matrix}\cos\\ \sin\end{matrix}\frac{rq_{nll'}}{2}\right|^{2};\qquad(2)$$

$$c_S=(3a_1+a_0)^2+S(S+1)(a_1-a_0)^2;\ c_{1-S}=(3-2S)(a_1-a_0)^2.$$

Here a_1, a_0 are the scattered amplitudes of the neutron by a proton in the triplet and singlet states, respectively. In Formula (2) the upper part, that is, c_S and the cosine, refer to scattering without molecular spin change ($S\to S$), and the lower part, that is c_{1-S} and the sine, to scattering with a spin change ($S\to 1-S$). The wave numbers of the incident and the scattered neutrons are denoted by $\underline{k}$ and $k_{nll'}$; respectively; $|q_{nll'}|=\left|\underline{k}-\underline{k}_{nll'}\right|$.

Inserting (1) into (2), we get

$$\sigma_{0l'S,\,nl\,1-S}^{S}(\theta)=\frac{4}{9}\frac{k_{nll'}}{k}c_{\,S\,1-S}f_{\,S\,1-S}(\theta);$$

$$f_{\,S\,1-S}(\theta)=\frac{1}{\pi(2l'+1)}\frac{1}{nl\,2^n}\sum_{m}\left|\int_{-1}^{1}\int_{-\infty}^{\infty}dz\,dv\,e^{-v^2}\times H_n(v)\,\Theta_{lm}(z)\,\Theta_{l'm}(z)\begin{matrix}\cos\\ \sin\end{matrix}\left[\left(R+\frac{v}{b}\right)\frac{zq_{nll'}}{2}\right]\right|^{2}.\qquad(3)$$

The scattering cross section $\sigma_{0l'S,\,nl\,1-S}^{S}$ is also conveniently represented in another form. For this, let us insert (1) into (2) and use the rules for combination of the angular momenta l, l'. Summing over m, m', we find

$$\sigma_{0l'S,\,nl\,1-S}^{S}(\theta)=\frac{4}{9}\frac{k_{nll'}}{k}c_{\,S\,1-S}\frac{2l+1}{nl\,2^n\pi}\times$$

$$\times\sum_{L}\left|C^{L0}_{l'010}\int_{-\infty}^{\infty}\int_{0}^{1}dv\,dz\,e^{-v^2}H_n(v)\,P_L(z)\times\begin{matrix}\cos\\ \sin\end{matrix}\left[\left(R+\frac{v}{b}\right)\frac{zq_{nll'}}{2}\right]\right|^{2},\qquad(4)$$

where $C^{L0}_{l'010}$ are the Clebsch-Gordan coefficients. Since $C^{L0}_{l'010}\neq 0$ only if the sum $L+l'+1$ is even, when there is no spin change in the scattering process, L is even; similarly, when there is a spin change, L is odd. Therefore

$$\left|\int_{0}^{1}dz\,P_L(z)\begin{matrix}\cos\\ \sin\end{matrix}xz\right|=|j_L(x)|,\qquad(5)$$

where

$$j_L(x)=\sqrt{\frac{\pi}{2x}}J_{L+\frac{1}{2}}(x)=\frac{(-)^L}{i}\left(e^{ix}Q_L^{+}(x)-e^{-ix}Q_L^{-}(x)\right).\qquad(6)$$

Let us also introduce the function

$$j_{-L}(x)=\sqrt{\frac{\pi}{2x}}J_{-L-\frac{1}{2}}(x)=e^{ix}Q_L^+(x)-e^{-ix}Q_L^-(x), \tag{7}$$

where $J_{\pm L\pm\frac{1}{2}}(x)$ is the Bessel function of the first kind of half-integral order, $Q_L^{\pm}(x)$ is a polynomial of inverse powers of $x = x_0 + uv$; $x_0=\frac{Rq_{nll'}}{2}$; $u=\frac{q_{n\,ll'}}{2b}$. Since the vibrations of the nuclei in the molecule are small, $bR \gg 1$, that is $x_0 \gg uv$, and therefore

$$j_L(x)\approx\frac{(-)^L}{i}\left(e^{ix}Q_L^+(x_0)-e^{-ix}Q_L^-(x_0)\right). \tag{8}$$

Inserting (5) and (8) into (4), we arrive at the integral

$$\int_{-\infty}^{\infty}dv\,e^{-v^2}H_n(v)\,e^{\pm ivu}=(\pm)^n\sqrt{\pi}(iu)^n e^{-\left(\frac{u}{2}\right)^2}$$

and get

$$\sigma_{0l'S,\,nl\,1-S}(\theta)=\frac{4}{9}\frac{k_{nll'}}{k}c_{\,S\,1-S}\frac{2l+1}{nl}e^{-\left(\frac{q_{nll'}}{b\sqrt{8}}\right)^2}\times\left(\frac{q_{nll'}}{b\sqrt{8}}\right)^{2n}\sum_L\left[C^{L0}_{l'010}j_{(-)^nL}\left(\frac{Rq_{nll'}}{2}\right)\right]^2, \tag{9}$$

where the function $j_{(-)^nL}(x)$ is determined by Formulas (6) and (7). It would seem that the formula derived is applicable only for $n \le 2$, since for higher n the vibrations of the nuclei in the molecule can no longer be considered harmonic.

For $E \ll \hbar\omega$, the vibrational levels are not excited. In this case, we may neglect the zero-point oscillations of the nuclei and consider the molecule as a rigid rotator. The formula for the scattering cross section of neutrons on a rigid molecule is obtained from (9) for $b \to \infty$ [1]:

$$\sigma_{0l'S,\,nl\,1-S}(\theta)=\delta_{n0}\frac{4}{9}\frac{k_{ll'}}{k}c_{\,S\,1-S}(2l+1)\times\sum_L\left[C^{L0}_{l'010}j_L\left(\frac{Rq_{ll'}}{2}\right)\right]^2. \tag{10}$$

With $l = l'$, $n = 0$ (9) becomes the differential cross section for elastic scattering, which always takes place without molecular spin change:

$$\sigma_{0l'S,\,0l'S}(\theta)=\frac{4}{9}c_S(2l'+1)e^{-\left(\frac{q}{b\sqrt{8}}\right)^2}\times\sum_L\left[C^{L0}_{l'0l'0}j_L\left(\frac{qR}{2}\right)\right]^2, \tag{11}$$

where $q = 2k\sin\frac{\theta}{2}$. From Formula (11) it follows that the probability of elastic scattering through large angles $\frac{q}{b\sqrt{8}}>1\left(\theta>\sqrt{\frac{\hbar\omega}{E}}\right)$ is exponentially small; for elastic collisions, the neutrons are scattered mostly in the forward direction:

$$\sigma_{0l'S,\,0l'S}(\theta) \approx \frac{4}{9} c_S (2l'+1) \times \sum_L \left[C^{L0}_{l'0l'0} j_L\left(\frac{qR}{2}\right)\right]^2; \quad \theta < \sqrt{\frac{\hbar\omega}{E}}. \qquad (11')$$

On the other hand, for inelastic collisions, large angle scattering is very probable. Indeed, if we put $l' \neq 1$ or $n = 0$ in (9), the function $q_{nll'}(\theta)$ does not vanish and changes slower than the function $q(\theta)$ in (11). Therefore, as can be seen by comparing Formulas (9) and (11), the probability of inelastic scattering through large angles is relatively high. This is understandable, as in this case the neutron transfers more momentum on the average to the molecule than in the elastic case.

III

The total cross section for scattering with transition of the molecule from the state (0 1'S) to the state $\begin{pmatrix} n1 & S \\ 1 & -S \end{pmatrix}$ is derived by integrating (9) over all scattering angles. Changing the variable of integration as follows,

$$q^2_{nll'} = k^2 + k^2_{nll'} - 2kk_{nll'}\cos\theta;$$
$$q_{nll'}\, dq_{nll'} = kk_{nll'}\sin\theta\, d\theta,$$

we obtain

$$\sigma_{0l'S,\,nl\,{}^{S}_{1-S}} = \frac{8\pi}{9} \frac{2l+1}{(kR)^2} \frac{c_{\,{}^{S}_{1-S}}}{n!\,(bR\sqrt{8})^{2n}} \times$$

$$\times \sum_L (C^{L0}_{l'010})^2 \int_{|k-k_{nll'}|R}^{(k+k_{nll'})R} x^{2n+1} j^2_L(-)^n L\left(\frac{x}{2}\right) \times e^{-\left(\frac{x}{bR\sqrt{8}}\right)^2} dx. \qquad (12)$$

In particular, the total elastic scattering cross section is of the form

$$\sigma_{0l'S,\,0l'S} = \frac{8\pi}{9} \frac{2l'+1}{(kR)^2} c_S \sum_L (C^{L0}_{l'0l'0})^2 \times \int_0^{2kR} x j^2_L\left(\frac{x}{2}\right) e^{-\left(\frac{x}{bR\sqrt{8}}\right)^2} dx \qquad (13)$$

from which it is not difficult to obtain the approximate formula ($E > \hbar\omega$).

$$\sigma_{0l'S,\,0l'S} \approx \frac{16\pi}{9} (2l'+1)\, c_S \frac{0{,}577 + \ln 2bR}{(kR)^2}. \qquad (13')$$

Thus the elastic scattering cross section is inversely proportional to the neutron energy.

For scattering of slow neutrons ($E \ll \hbar\omega$), the molecule can be considered rigid. In this case the total scattering cross section is of the form

$$\sigma_{0l'S,\,nl_{1-S}^{S}} = \delta_{n0}\,\frac{8\pi}{9}\,\frac{2l+1}{(kl)^2}\,c_{1-S}^{S}\sum_{L}(C_{l'010}^{L0})^2 \times \int_{|k-k_{ll'}|R}^{(k+k_{ll'})R} xj_L^2\left(\frac{x}{2}\right)dx. \tag{14}$$

The integrals entering into (14) are evaluated with the aid of a formula from reference [4]

$$\left.\begin{aligned} 2\int_0^x xj_L^2(x)\,dx &= 0{,}5772 + \ln 2x - Ci2x - \\ &- x^2\Big[j_0^2(x) + \sum_{n=1}^{L-1}\frac{2n+1}{n(n+1)}j_n^2(x) + \\ &+ \frac{1}{L}j_L^2(x)\Big]; \\ Cix &= -\int_x^\infty \frac{\cos t}{t}\,dt; \end{aligned}\right\} \tag{15}$$

IV

The rotational level spacing is substantially lower than the vibrational quantum $\left(\frac{\hbar^2}{MR^2} = 0.00736\ \text{ev},\ \hbar\omega = 0.546\ \text{ev}\ [2]\right)$. Therefore if the neutron energy E is greater than the vibrational level spacing $\hbar\omega$, we may neglect the effect of the rotational states on the scattered neutron energy: $k_{nll'} \approx k_n$; $q_{nll'} \approx q_n = |k - k_n|$. In this case, it is interesting to find the cross section for excitation by scattering of the n-th vibrational level for an arbitrary rotational state:

$$\sigma_{0l'S,\,n_{1-S}^{S}}(\theta) = \sum_{l}\sigma_{0l'S,\,nl_{1-S}^{S}}(\theta).$$

Let us insert Formula (3) into the right side of this equation. In so doing, we represent the square of the integral in (3) in the form of a product of two integrals, after which we carry out a sum over l, m, under the integral sign, making use of the relation

$$\sum_{lm}\Theta_{lm}(z)\Theta_{lm}(y)\Theta_{l'm}(z)\Theta_{l'm}(y) = \delta(y-z)\,\frac{2l'+1}{2}.$$

The integrals containing $\delta(y-z)$ and the Hermite polynomial are simple to evaluate [3]. As a result we find that the cross section for excitation of the n-th vibrational molecular level for arbitrary final rotational state does not depend on the original rotational state l', and is of the form (suppressing the index l')

$$\sigma_{0S,\,n_{1-S}^{S}}(\theta) = \frac{2}{9}\,\frac{k_n}{k}\,c_{1-S}^{S}\,\frac{1}{n!}\int_0^1 dz \times \left(\frac{q_n z}{b\sqrt{8}}\right)^{2n}\left(1 \pm (-)^n \cos q_n R z\right) e^{-\left(\frac{q_n z}{b\sqrt{8}}\right)^2}. \tag{16}$$

In this formula, the upper sign refers to scattering without, and the lower sign to scattering with a molecular spin change. Making use of the condition that the vibrations of the nuclei in the molecule are small (bR >> 1), the differential cross section for inelastic scattering (16) can be approximately expressed both in the regions of small and large scattering angles θ, in the form

$$\sigma_{0S,\,n_{1-S}^{S}}(\theta) = \frac{2}{9}\,\frac{k_n}{k}\,c_{1-S}^{S}\,\frac{1}{n!(2n+1)}\left(\frac{k\theta}{b\sqrt{8}}\right)^{2n};\quad \theta < \frac{b\sqrt{8}}{k} \sim \sqrt{\frac{\hbar\omega}{E}}; \tag{17}$$

$$\sigma_{0S,\,n_{1-S}^{S}}(\theta)=\frac{2}{9}\frac{k_n}{k}c_{1-S}^{S}\frac{\sqrt{2\pi}\,(2n-1)!!}{(2n)!!}\frac{b}{2k\sin\frac{\theta}{2}};\quad \theta>\frac{b\sqrt{8}}{k}. \tag{18}$$

From these formulas it follows that the inelastic scattering with excitation of vibrational levels is related to scattering through large angles $\theta>\sqrt{\frac{\hbar\omega}{E}}$, as opposed to elastic scattering, which takes place mainly for small angles [compare (9) and (11)]. The total inelastic scattering cross section with excitation of the n-th molecular vibrational level is obtained by integrating (16) over all scattering angles. An approximate expression can be found, however, by integrating Formula (18) over all angles, since the small angle region does not give a significant contribution for $E \gg \hbar\omega$. We obtain

$$\sigma_{0S,\,n_{1-S}^{S}}=\frac{8\pi}{9}\frac{k_n}{k}c_{1-S}^{S}\frac{\sqrt{2\pi}\,(2n-1)!!}{(2n)!!}\frac{b}{k}, \tag{19}$$

from which it follows that the probability of excitation of a vibrational level decreases with its energy.

V

For the case when the neutron energy is substantially greater than the vibrational level spacing, we may derive a fairly simple expression for the average energy lost by the neutron scattered through an angle θ (in the common center-of-mass system of the neutron and molecule):

$$\Delta\overline{E}(\theta)=\frac{\sum_{nl}(E_{nl}-E_{0l'})\,(\sigma_{0l'S,\,nlS}(\theta)+\sigma_{0l'S,\,nl1-S}(\theta))}{\sum_{nl}(\sigma_{0l'S,\,nlS}(\theta)+\sigma_{0l'S,\,nl1-S}(\theta))} \tag{20}$$

where $E_{nl}=n\hbar\omega+\frac{\hbar^2}{MR^2}l\,(l+1)$ are the molecular levels, and the sum is carried out over all the levels. Inserting Formula (3) into Expression (20), setting $k_{nll'}\approx k$, $q_{nll'}\approx q$, we obtain

$$\Delta\overline{E}(\theta)=\frac{\hbar\omega\,(c_S\sum_{nl}nf_S(\theta)+c_{1-S}\sum_{nl}nf_{1-S}(\theta))}{c_S\sum_{nl}f_S(\theta)+c_{1-S}\sum_{nl}f_{1-S}(\theta)}+$$

$$+\frac{\frac{\hbar^2}{MR^2}(c_S\sum_{nl}l\,(l+1)f_S(\theta)+c_{1-S}\sum_{nl}l\,(l+1)f_{1-S}(\theta))}{c_S\sum_{nl}f_S(\theta)+c_{1-S}\sum_{nl}f_{1-S}(\theta)}-E_{0l'}. \tag{20'}$$

The sums in the denominator of this formula and in the first bracket in the numerator are evaluated by a method indicated in reference [3]:

$$\sum_{nl}f_{1-S}^{S}(\theta)=\frac{1}{2}\int_0^1 dz\left(1\pm e^{-\left(\frac{qz}{2b}\right)^2}\cos qRz\right); \tag{21}$$

$$\sum_{nl} nf_{\frac{s}{1-s}}(\theta) \doteq \frac{1}{4}\left(\frac{q}{2b}\right)^2 \int_0^1 dz \cdot z^3 \left(1 \mp e^{-\left(\frac{qz}{2b}\right)^2} \cos qRz\right). \tag{22}$$

With the aid of the relation

$$\int_{-1}^{1} dy \sum_{lm} l(l+1)\Theta_{lm}(z)\Theta_{lm}(y)\Theta_{l'm}(z)\Theta_{l'm}(y)F(y) =$$
$$= \frac{2l'+1}{2}\left[l'(l'+1) - \frac{d}{dz}(1-z^2)\frac{d}{dz}\right]F(z)$$

we may perform the sum

$$\sum_{nl} l(l+1) f_{\frac{s}{1-s}}(\theta) = \frac{1}{2}\left(\frac{qR}{2}\right)^2 \int_0^1 dz (1-z^2) \times$$

$$\times \left(1 \mp \cos qRz \cdot e^{-\left(\frac{qz}{2b}\right)^2}\right) + \frac{1}{2} l'(l'+1) \times \int_0^1 dz \left(1 \pm e^{-\left(\frac{qz}{2b}\right)^2} \cos qRz\right). \tag{23}$$

Inserting Relations (21)-(23) into (20'), we find that the average energy loss depends on the original molecular rotational state, and is of the form (in the common center-of-mass system)

$$\Delta\overline{E}_{\cdot}(\theta) = \frac{(\hbar k)^2}{2M} \times \frac{(1-\cos\theta)\left[c_s(1-I_{\cdot}(\theta)) + c_{1-s}(1+I(\theta))\right]}{c_s(1+I(\theta)) + c_{1-s}(1-I(\theta))}; \tag{24}$$

$$I(\theta) = \int_0^1 dz\, e^{-\left(\frac{qz}{2b}\right)^2} \cos qRz \approx e^{-\left(\frac{q}{2b}\right)^2} j_0(qR).$$

As was to be expected, the average energy loss vanishes for $\theta \to 0$, since in the small angle region mainly elastic collisions take place. The average energy loss is maximum for large angle scattering, which corresponds to the angular distributions (17) and (18) for the inelastically scattered neutrons.

The average neutron energy loss (in the common center-of-mass system) for scattering through an arbitrary angle is obtained by integrating the numerator and denominator of Formula (24) over all scattering angles. In this, the small angle region $\theta < \sqrt{\frac{\hbar\omega}{E}}$ gives no significant contribution, so that

$$\Delta\overline{E} = \frac{(\hbar k)^2}{2M}. \tag{25}$$

Thus in the limit of high energy, the average energy loss to excitation of molecular levels is proportional to the energy of the incident neutron. This means that for such a high energy, the nuclei of the molecule may be considered free. In this case, the average loss $\Delta\overline{E}$ represents the kinetic energy acquired by the nuclei of the molecule after scattering the neutron (in the center-of-mass system of the neutron and the molecule).

If the neutron energy is not large, so that in scattering only a small number n_0 of the vibrational levels are excited, then the summation over n in Formula (20) should be performed numerically. Summing over all l in this formula, we obtain

$$\Delta\overline{E}(\theta)=\frac{\hbar\omega\sum\limits_{n=0}^{n_0} n\,(\sigma_{0S,\,nS}(\theta)+\sigma_{0S,\,n1-S}(\theta))}{\sum\limits_{n=0}^{n_0}(\sigma_{0S,\,nS}(\theta)+\sigma_{0S,\,n1-S}(\theta))}+$$

$$+\frac{\frac{\hbar^2}{MR^2}\sum\limits_{n=0}^{n_0}(\bar{\sigma}_{0S,\,nS}(\theta)+\bar{\sigma}_{0S,\,n1-S}(\theta))}{\sum\limits_{n=0}^{n_0}(\sigma_{0S,\,nS}(\theta)+\sigma_{0S,\,n1-S}(\theta))},$$

where $\bar{\sigma}_{0S,\,n\frac{S}{1-S}}(\theta)$ is of the form (for $l' = 0$):

$$\sigma_{0S,\,n\frac{S}{1-S}}(\theta)=\sum_l l(l+1)\sigma_{0l'S,\,nl\frac{S}{1-S}}(\theta)=\frac{1}{18}\frac{k_n}{k}\frac{1}{n!}c_{\frac{S}{1-S}}(q_nR)^2\int_0^1 dz(1-z^2)\times$$

$$\times(1\mp(-)^n\cos qRz)\left(\frac{qz}{b\sqrt{8}}\right)^{2n}e^{-\left(\frac{qz}{b\sqrt{8}}\right)^2}. \qquad (26)$$

A simple expression for this quantity in the region of small and large angles θ, as well as the integral of it over the angles, is not difficult to derive by comparing Formulas (26) and (16)-(19).

The author expresses his gratitude to B. T. Geilikman, N. M. Polievktov-Nikoladze, and A. I. Akheizer for discussions of the results of the work.

LITERATURE CITED

[1] J. Schwinger and E. Teller, Phys. Rev., 52, 4, 286 (1937).

[2] A. M. L. Messiah, Phys. Rev., 84, 2, 204 (1951).

[3] P. Morse, Phys. Rev., 90, 1, 51 (1953).

[4] M. Hamermesh, J. Schwinger, Phys. Rev., 69, 5, 145 (1946).

RELATIVE Pu^{239} BREEDING RATIO IN NATURAL URANIUM-ORDINARY WATER LATTICES

L. V. Komissarov and V. A. Tarabanko

Measurements were performed of the quotient of breeding ratios in uranium-water lattices and a uranium-graphite lattice at the start of conversion. The plutonium breeding ratio in uranium-water lattices for certain lattice spacings is larger than in a uranium-graphite lattice.

Introduction

An important index of the operation of a nuclear reactor which breeds plutonium is the Pu^{239} breeding ratio, which is defined as the ratio of the number of Pu^{239} nuclei (N_9) produced in the reactor to the number of consumed U^{235} nuclei (N_5):

$$P = \frac{N_9}{N_5} .$$

At the present time the parameter of uranium-water lattices which are required for the computation of the breeding ratio are not sufficiently well known. It is therefore important to verify the results of a computation by experimental means.

In the present work we measured the quotient of the breeding ratios in uranium-water lattices and in a uranium-graphite reactor whose parameters have been well investigated:

$$\frac{P_{water}}{P_{graphite}} = \frac{(N_9)_{water}}{(N_9)\ graphite} \quad \frac{(N_5)_{graphite}}{(N_5)_{water}} .$$

We studied triangular lattices (with 45,55 and 60 mm spacings) composed of natural uranium and ordinary water as moderator.

The lattices were composed of avialite tubes 43 x 1.0 mm in diameter containing uranium slugs 35 mm in diameter and 100 mm long. The slugs were sheathed in 1 mm aluminum. The experiments were performed on physical uranium-water reactors with a natural uranium zone measuring about 1 m (Fig. 1).

The uranium-graphite reactor had a square lattice with 200 mm spacing. The slugs of natural metallic uranium with the same dimensions as in the uranium-water lattices were not provided with aluminum sheathing.

Experimental Method

1. Determination of $\frac{(N_9)_{water}}{(N_9)_{graphite}}$

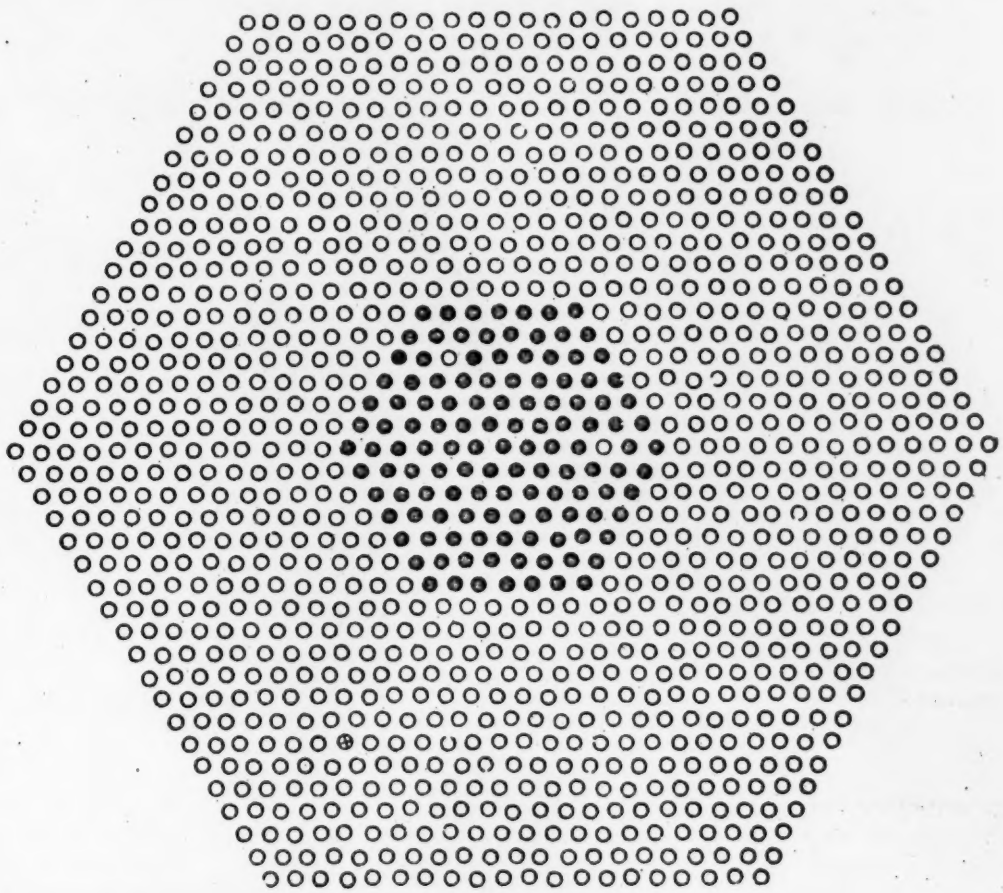

Fig. 1. Diagram of a physical uranium-water reactor. ●) channels with enriched uranium slugs; ○) channels with natural uranium slugs; ⊗) channels with experimental slug.

It is well known that the production of Pu^{239} in a reactor occurs according to the following scheme:

$$U^{238} + {}_0n^1 \rightarrow U^{239} \xrightarrow[23,5\ min]{\beta^-}$$

$$\rightarrow Np^{239} \xrightarrow[2,3\ day]{\beta^-} Pu^{239}.$$

Since the measurements are relative, the determination of the number of Pu^{239} nuclei produced in a uranium slug can be reduced to the measurement of the β-activity of U^{239}*. In order to determine the relative quantity of U^{239} we used disks of natural uranium 35 mm in diameter and 0.1 mm thick placed between the ends of separated sections of a uranium slug (Fig. 2). The experimental slug was inserted into the lattice and irradiated with a neutron beam of $\sim 10^7$ neutrons/cm^2/sec. for 30 min. The irradiation times in the uranium-water lattices and the uranium-graphite lattice were identical. After irradiation the uranium disk was chemically cleansed of fission fragments and of the products of natural radioactive decay of uranium by sodium-uranyl-acetate precipitation. The purified uranium was pressed into tablets (of ~300 mg/cm^2 density) whose β-activity was measured with constant geometry by a Geiger counter. The background of natural uranium decay products was disregarded since it amounted to only one percent of the measured effect. Measurements of the β-activity of the purified uranium for 1 to 1.5 hours showed that the half-life was 23.5 $\pm$ 0.2 min, which agrees with the

* The effect of Np^{239} consumption during the irradiation period was negligibly small.

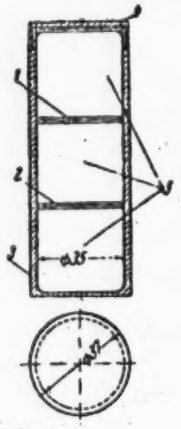

Fig. 2. Experimental uranium slug. 1) Paper disk; 2) uranium disk; 3) aluminum can; 4) background paper disk; 5) sections of uranium slug.

data of other authors [1]. This indicates that the U^{239} was sufficiently purified of decay and fission products. The ratio $\frac{(N_9)_{water}}{(N_9)_{graphite}}$ was determined as the ratio of β-activity of tablets obtained from the uranium disks which were irradiated in the uranium-water and uranium-graphite lattices.

2. Determination of $\frac{(N_5)_g}{(N_5)_w}$.

The depletion of U^{235} has two causes: nuclear fission and radiative neutron capture, so that the ratio $\frac{(N_5)_G}{(N_5)_W}$ can be given in the form

$$\frac{(N_5)_G}{(N_5)_W} = \frac{(N_5^f + N_5^\gamma)_G}{(N_5^f + N_5^\gamma)_W} = \frac{\left[N_5^f \cdot \left(1 + \frac{N_5^\gamma}{N_5^f}\right)\right]_G}{\left[N_5^f \cdot \left(1 + \frac{N_5^\gamma}{N_5^f}\right)\right]_W}$$

where N_5^f is the number of U^{235} nuclei undergoing fission and N_5^γ is the number of U^{235} nuclei involved in radiative capture.

The experimental determination of the desired ratio was rendered difficult by the fact that depletion of U^{235} through radiative capture is not equal in uranium-water and uranium-graphite lattices.

The corrections for this factor,

$$\frac{\left(1 + \frac{N_5^\gamma}{N_5^f}\right)_G}{\left(1 + \frac{N_5^\gamma}{N_5^f}\right)_W},$$

were estimated from qualitative data on the spectral composition of neutrons in uranium-water and uranium-graphite lattices as well as the known curves for fission and radiative capture cross sections in U^{235} as a function of neutron energy. An estimate of the correction indicated that it is close to unity for all the cases investigated. The direct measurement of $(N_5^f)_g / (N_5^f)_w$ is possible if pure U^{235} is used as an indicator. However, we were using natural uranium, for which reason it was necessary to make an experimental correction (N_5^f) for fission of U^{238}; consequently, in this case the quantities to be determined are

$$\frac{(N_5^f + N_5^f)_G}{(N_5^f + N_5^f)_w} \quad \text{and} \quad \frac{\left(1 + \frac{N_5^f}{N_5^f}\right)_W}{\left(1 + \frac{N_5^f}{N_5^f}\right)_G}.$$

Using these quantities the desired ratio can be obtained from the following expression:

$$\frac{(N_5^f)_G}{(N_5^f)_w} = \frac{(N_5^f + N_5^f)_G}{(N_5^f + N_5^f)_w} \cdot \frac{\left(1 + \frac{N_5^f}{N_5^f}\right)_W}{\left(1 + \frac{N_5^f}{N_5^f}\right)_G}.$$

The ratio $\frac{(N_5^f + N_8^f)_g}{(N_5^f + N_8^f)_W}$ was determined by measuring the β-activity of fission fragments on paper disks of 35 mm diameter which were inserted between sections of the experimental uranium slug (Fig. 2). The uranium disk for the measurement of $(N_9)_W/(N_9)_g$ and the paper disk were inserted into the experiment metal slug and were irradiated simultaneously in the neutron field of the lattice. After irradiation the β-activity of the fission fragments was measured with a Geiger counter. The measured activation of the paper disks was 3% of the activity of the collected fission fragments. For each experiment curves were constructed which showed the decay of the activity with time $N = f(t)$ (Fig. 3).

$$\frac{(N_f^f + N_\delta^f)_G}{(N_f^f + N_\delta^f)_W}$$

was determined from the relationship of the areas under the β-decay curves of fission fragments in the same time interval. The measured β-activity of fission fragments will be proportional to the number of fissions with the same proportionality coefficient if the fragment yields do not change with changes of the neutron spectra in the lattices. Katkov, using a fission chamber which was described in the paper of Stollarov et al. [2] found that the relationship between the number of fissions in a layer of natural uranium and the β-activity of fission fragments from natural uranium was constant for all the lattices investigated.

The quantity $\left(1+\frac{N_\delta^f}{N_f^f}\right)_W - \left(1+\frac{N_\delta^f}{N_f^f}\right)_g$, which takes into consideration the different contribution of U^{238} to the fission of natural uranium in uranium-water and uranium-graphite lattices, was determined by the method described in [2].

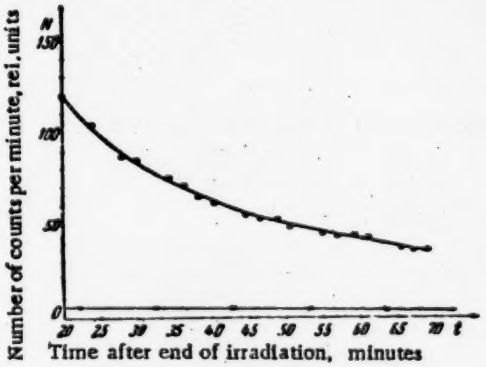

Fig. 3. Decay of β-activity of fission fragments from natural uranium.)β-activity of fission fragments collected on paper disk;) β-background of paper disk.

Thus the breeding ratio quotient can be calculated from the following relationship:

$$\frac{P_W}{P_G} = \frac{(N_\delta)_W}{(N_\delta)_G} \cdot \frac{(N_f^f + N_\delta^f)_G}{(N_f^f + N_\delta^f)_W} \times \times \frac{\left(1+\frac{N_\delta^f}{N_f^f}\right)_W}{\left(1+\frac{N_\delta^f}{N_f^f}\right)_G} \cdot \frac{\left(1+\frac{N_\delta^r}{N_f^f}\right)_G}{\left(1+\frac{N_\delta^r}{N_f^f}\right)_W}.$$

TABLE 1

Lattice spacing (cm)	$\frac{(N_\delta)\text{ water}}{(N_\delta)\text{ graphite}} \cdot \frac{(N_f^f+N_\delta^f)\text{ gra.}}{(N_f^f+N_\delta^f)\text{ water}}$	$\frac{\left(1+\frac{N_\delta^f}{N_f^f}\right)_{\text{water}}}{\left(1+\frac{N_\delta^f}{N_f^f}\right)_{\text{graphite}}}$	$\frac{\left(1+\frac{N_\delta^r}{N_f^f}\right)_{\text{graphite}}}{\left(1+\frac{N_\delta^r}{N_f^f}\right)_{\text{water}}}$	$\frac{P\text{ water}}{P\text{ graphite}}$
4,5	1,84±0,04	1,17±0,02	0,92	1,98±0,1
5,5	1,06±0,03	1,1 ±0,01	0,98	1,14±0,05
6,0	1,02±0,03	1,05±0,01	1	1,07±0,05

Measurements and Comparision with Calculations

All measurements and the calculated correction are shown in Table 1.

The errors shown in Table 1 were calculated from the mean square deviation of the separate measurements.

Kunegin and Levina obtained the following formula for the breeding ratio:

$$P = \frac{\frac{(\sigma^c\rho)_\delta}{(\sigma^c\rho)_f} + \frac{\mu(1-\varphi)\nu_\delta^s}{1-\mu\varphi p_\delta \nu_f^r} + \frac{\mu\varphi p_\delta \nu_\delta^r}{1-\mu\varphi p_\delta \nu_f^r}}{1+\frac{\mu\varphi p_\delta \nu_\delta^s}{1-\mu\varphi p_\delta \nu_f^r}},$$

where $(\sigma^c\rho)_8$ and $(\sigma^c\rho)_5$ are the macroscopic neutron absorption cross sections for U^{238} and U^{235}, respectively; μ is the fast fission factor; φ is the resonance escape probability; ν_5^c is the number of secondary fast neutrons per thermal neutron captured by U^{235}; ν_5^r is the number of secondary fast neutrons per epithermal neutron captured by U^{235}; p_5, p_8 are the probabilities that an epithermal neutron will be captured by U^{235} and U^{238}, respectively. The values of the quotient of breeding ratios calculated by this formula for the investigated uranium-water lattices are given in Table 2.

TABLE 2

Lattice spacing (cm)	4.5	5.0	5.5	6.0
P_w/P_g	1.89	1.35	1.16	1.04

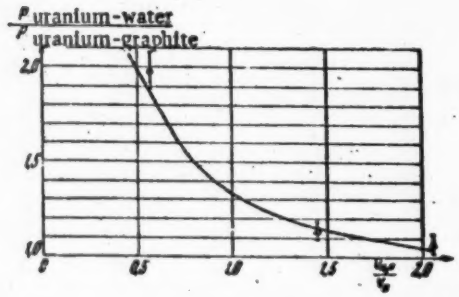

Fig. 4. Dependence of the quotient of breeding ratios for uranium-water lattices on the ratio of the volume of water and uranium Δ values of $\frac{P_{\text{uranium-water}}}{P_{\text{uranium-graphite}}}$ in a physical uranium-water reactor. The theoretical curve is solid.

A comparison of the data in Table 1 and Table 2 shows that the experimental values of the quotient of breeding ratios is in satisfactory agreement with the calculated values (Fig. 4).

The measurements show that in uranium-water reactors it is possible to obtain a higher plutonium breeding ratio than in uranium-graphite reactors.

The authors wish to thank V. I. Mostovoi, M. B. Eglazarov, V. P. Katkov and G. A. Stolyarov for their participation in a discussion of the results.

Note: No literature references were given in the original.

THE RATIO OF THE AVERAGE FISSION CROSS SECTIONS OF Pu^{239} and U^{235} IN URANIUM-WATER LATTICES

V. P. Katkov, Yu. V. Nikolsky and G. A. Stoliarov

The ratio of the average fission cross sections of Pu^{239} and U^{235} is determined for lattices consisting of natural uranium and ordinary water. For comparison the same ratio was measured for a uranium-graphite reactor. It was found that the ratio $\bar{\sigma}_{Pu}^{f}/\bar{\sigma}_{U}^{f}$ for uranium-water lattices with spacings of 45, 50, 55 and 60 mm and for a uranium-graphite reactor with 200 mm lattice spacing are 2.24, 1.99, 1.88 and 1.79, respectively.

Introduction

The important quantities which determine the physical properties of a reactor are averaged over the neutron spectrum of the fission cross section for the elements used as nuclear fuel.

In this article we describe experiments performed for the purpose of determining the ratio of the average* fission cross sections of Pu^{239} and U^{235} in uranium-water lattices and in a uranium-graphite reactor.

The experiments were performed on a physical uranium-water reactor which consisted of two zones. The central zone contained slugs of enriched uranium, while the peripheral zone contained slugs of natural uranium. The slugs (of 35 mm diameter) of both natural and enriched uranium in aluminum cladding were placed in avialite tubes. The tubes were loaded with uranium slugs to a height of 2.5 m. We studied triangular lattices with spacings of 45, 50, 55 and 60 mm. The measurements were made in the natural uranium zone.

The lattice of the uranium-graphite reactor was body-centered with 200 mm spacing; the slugs of natural uranium were of the same diameter as above.

Experimental Method

The ratios of the average fission cross sections of Pu^{239} and U^{235} can be obtained, as will be shown below, from the β-activity ratio of fission fragments ejected from the layers of plutonium and uranium in the lattice.

Films weighing ~0.5 mg were deposited electrolytically on disks of nickel foil 35 mm in diameter and 0.05 mm thick. Quite pure isotopes of plutonium and uranium were used. For safety of operation and in order to prevent mechanical damage to the films both films were covered with a lacquer thin enough to ensure the escape of a large fraction of the fission fragments. Special attention was paid to the uniformity of thickness of the films prepared in this manner.

The fission fragments were collected on disks of filter paper 35 mm in diameter and ~0.15 mm thick placed in contact with the films.

* By average fission cross sections we mean cross sections which have been averaged over the neutron spectrum and taking into consideration the changes according to the radius of the slugs.

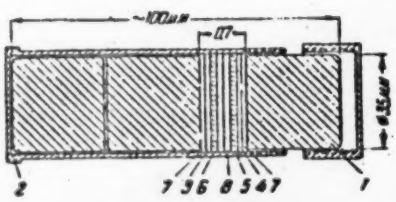

Fig. 1. Position of Pu^{239} and U^{235} films in a slug of uranium.
1) Uranium slugs; 2) sealed aluminum holder; 3) U^{235} film; 4) Pu^{239} film; 5) paper disk to collect fragments of Pu^{239}; 6) paper disk to collect fragments of U^{235}; 7) 15 μ copper foil to shield indicator from uranium fission fragments; 8) paper "background" disk.

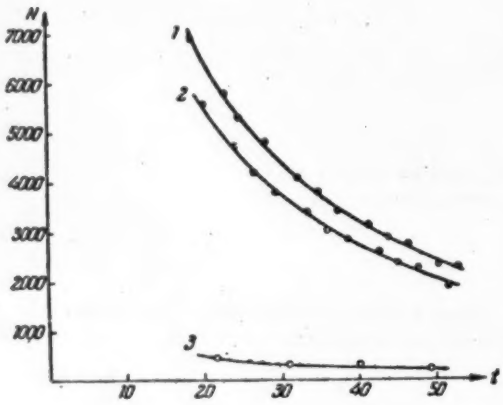

Fig. 2. Decay curves of β-activity of fission fragments from Pu^{239} and U^{235}.
N) Activity of fission fragments (pulses/min); t) time after irradiation (min.); 1) β-activity of Pu^{239} fission fragments; 2) β-activity of U^{235} fission fragments; 3) β-activity of "background" disk.

The plutonium and uranium films and three paper disks (one was a "background" disk to record the activation of the paper in the neutron field) were placed in a slot in a uranium slug (Fig. 1), and irradiated in the lattice for 15 minutes. The β-activity of the paper disks was measured successively with a Geiger-Müller counter. The measurements were begun 20 minutes after irradiation and continued for 30 minutes.

Figure 2 illustrates the decay curves of β-activity of plutonium and uranium fission fragments and of the paper "background" disk.

Treatment of the Data

The experimentally measured quantity was the ratio $\frac{A_{Pu}}{A_U}$ which was determined as the ratio of the areas under the β-activity decay curves of Pu^{239} and U^{235} fission fragments. The activity is associated with the number of fissions in the films by the following relationships:

$$\left.\begin{aligned} N_{Pu} &= \alpha_{Pu} A_{Pu}, \\ N_U &= \alpha_U A_U, \end{aligned}\right\} \qquad (1)$$

where N_{Pu} and N_U are the numbers of fissioning nuclei of plutonium and uranium in the films, which are given by

$$\left.\begin{aligned} N_{Pu} &= \int_0^\infty W_{Pu}\,\overline{n(v)}\,v\sigma'_{Pu}(v)\,dv = \\ &= W_{Pu}\bar{\sigma}'_{Pu}\int_0^\infty \overline{n(v)}\,v\,dv, \\ N_U &= \int_0^\infty W_U\,\overline{n(v)}\,v\sigma'_U(v)\,dv = \\ &= W_U\bar{\sigma}'_U\int_0^\infty \overline{n(v)}\,v\,dv. \end{aligned}\right\} \qquad (2)$$

Here W_{Pu} and W_U are the numbers of nuclei of plutonium and uranium in the films; $\overline{n(v)}$ is the average density of neutrons in the slug (with velocity v), which can be obtained from

$$n(v) = \frac{\int_0^R 2\pi r n\,dr}{\int_0^R 2\pi r\,dr};$$

R is the slug radius; α_{Pu} and α_U are the proportionality coefficients between the number of fissions in the film and the β-activity of the fission fragments.

From (2) the ratio of the average cross sections is obtained:

$$\frac{\bar{\sigma}^f_{Pu}}{\bar{\sigma}^f_U} = \frac{W_U}{W_{Pu}} \frac{N_{Pu}}{N_U}; \qquad (3)$$

Using (1) we obtain:

$$\frac{\bar{\sigma}^f_{Pu}}{\bar{\sigma}^f_U} = B \frac{A_{Pu}}{A_U},$$

where

$$B = \frac{W_U}{W_{Pu}} \frac{\alpha_{Pu}}{\alpha_U}.$$

Thus, in order to determine the cross section ratio it is necessary to know the corresponding value of B. When this coefficient is independent of the neutron spectrum it is sufficient to obtain it from some known spectrum. This can be done by using the relationship $\frac{\bar{\sigma}^f_{Pu}}{\bar{\sigma}^f_U} = B \frac{A_{Pu}}{A_U}$. The ratio $\frac{A_{Pu}}{A_U}$ is obtained experimentally and the ratio $\frac{\bar{\sigma}^f_{Pu}}{\bar{\sigma}^f_U}$ by calculation. This experiment was performed in a 150 x 150 x 250 cm graphite prism combined with the reflector of the uranium-graphite reactor. $\frac{A_{Pu}}{A_U}$ was measured at a point 130 cm from the core. The reflector had a thickness of 80 cm. The neutron spectrum in the prism was assumed to be close to the Maxwellian spectrum at neutron temperature 285°K. $\bar{\sigma}^f_{Pu}/\bar{\sigma}^f_U$ was calculated from the known curves of plutonium and uranium fission cross sections. It should be noted that for our calculation detailed knowledge of the neutron spectrum was not required, since in this energy region the plutonium and uranium cross sections follow the 1/v law approximately. We assumed σ^f_{239} = 720 barns and σ^f_{235} = 580 barns for neutrons with 2200 m/sec velocity.

The value obtained for B for the neutron spectrum in the graphite prism was 1.70 ± 0.04.

We studied experimentally the dependence of B on the neutron spectrum.

As can be seen from (3) the cross section ratio of plutonium and uranium fissions can be determined by an ionization chamber which records the number of fissions directly. For this purpose we must know the ratio of the quantities of fissionable substances in the chambers. But for the calculation of the spectral dependence of B this ratio is not required, since for this purpose it is sufficient to determine the relative change of $\frac{\bar{\sigma}_{Pu}}{\bar{\sigma}_U}$ with the lattice spacing, from values obtained by the above-described method with an ionization chamber. From the identical dependence of these quantities on the lattice spacing we can conclude that B is constant in the corresponding spectral range.

We compared* the relative changes of $\frac{\bar{\sigma}_{Pu}}{\bar{\sigma}_U}$, obtained by the methods indicated in lattices with 45 and 60 mm spacings; B is independent of the neutron spectrum in these lattices with an accuracy of 4%.

* For this purpose we used a double ionization chamber with Pu^{239} and U^{235} films. The construction of this chamber was similar to that described by Stoliarov et al. in the paper "Method of Measuring Fast Neutron Multiplication Factors in Uranium-Water Lattices" (Reports at Conference of the Academy of Sciences USSR on the Peaceful Uses of Atomic Energy, 1955).

In using experimental results for all of the lattices studied we shall hereafter assume for B the value 1.70 ± 0.04.

Measurements and Results

As indicated earlier, the quantity $\frac{A_{Pu}}{A_U}$ was measured in the natural uranium zone. When this zone is of limited size (~50-60 cm) it is important to make the measurement in a region which will not be influenced by the boundary. Then the measured value will characterize the lattice. For this purpose the measurements were made at several points along the radius of the zone. It appeared that at 20 cm the boundary effect practically disappears. This was confirmed by control experiments which increased the size of the natural uranium zone to 70-80 cm. The final results given in the table were obtained by averaging the data at three points in a region where the measurements did not change as the natural uranium zone was enlarged.

Experimental Results*

Location of measurements	Lattice spacing (mm)	$\frac{A_{Pu}}{A_U}$	$\frac{\bar{\sigma}_{Pu}}{\bar{\sigma}_U}$
Graphite prism		0,80±0,02	1,37±0,02**
Uranium-graphite	200	1,05±0,02	1,79±0,05
Uranium-water lattices	60	1,05±0,01	1,79±0,05
	55	1,11±0,01	1,88±0,06
	50	1,17±0,01	1,99±0,06
	45	1,32±0,01	2,24±0,07

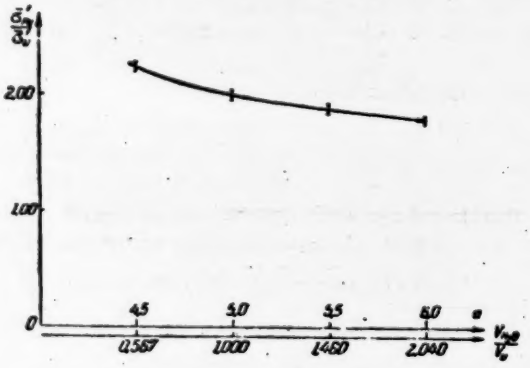

Fig. 3. Ratio of average Pu^{239} and U^{235} fission cross sections as a function of uranium-water lattice spacing. $\frac{\bar{\sigma}_{Pu}}{\bar{\sigma}_U}$ is the ratio of average plutonium and uranium cross sections; a is the lattice spacing in mm; $\frac{V_{H_2O}}{V_U}$ is the ratio of the volumes of water and uranium in a lattice cell.

* These values pertain to a reactor whose lattice does not contain Pu^{239}.

** Calculated value.

The dependence of the ratio of average fission cross sections for Pu^{239} and U^{235} on the spacing of uranium-water lattices is shown graphically in Figure 3. It follows from the curve that $\frac{\bar{\sigma}_{Pu}}{\bar{\sigma}_U}$ in a uranium-water lattice with 45 mm spacing reaches a value of 2.2, i.e., it exceeds by more than one and one half times the value of the same ratio for a Maxwellian spectrum ($T_{neutrons}$ = 285°K) and exceeds by 30% the ratio obtained for a uranium-graphite reactor. It should also be noted that the neutron spectrum in all the uranium-water lattices which we studied except that with 60 mm spacing is harder than the neutron spectrum in the uranium slugs of the uranium-graphite reactor.

Further studies will enable us to determine in greater detail the characteristics of the neutron spectrum in uranium-water lattices.

In conclusion the authors wish to thank E. S. Antsiferov for much valuable assistance.

THE POSSIBILITY OF PRODUCING THERMONUCLEAR REACTIONS IN A GASEOUS DISCHARGE*

I.V. Kurchatov

Of foremost significance among the more important problems of modern engineering science is utilization of the energy of thermonuclear reactions. Physicists the world over are attracted by the extraordinarily interesting and very difficult task of controlling thermonuclear reactions.

Investigations in this field are being carried out by Academician Artsimovich at our Institute. A leading role in the theoretical investigations has been played by Academician M.A. Leontovich**.

As is known, thermonuclear reactions can arise if the temperature of matter is sufficiently high for atomic nuclei to surmount the forces of the Coulomb barrier with appreciable probability during thermal collisions. The excitation of thermonuclear reactions in deuterium or in a mixture of deuterium and tritium is especially interesting since in this case a noticeable effect should be obtainable at relatively low temperatures.

Physics is indebted to the founder of nuclear physics, Ernest Rutherford, for information regarding the interaction of deuterons. In one of his last investigations Rutherford studied the nuclear reactions that occur when two deuterons collide. It was difficult to suspect at that time that the new facts discovered by him would help realize our hope of mastering the energy sources of the hot interior of the sun and distant stars that shine overhead.

The intensity of thermonuclear reactions in deuterium should increase rapidly with temperature up to several billion degrees.

Some idea of the conditions under which thermonuclear reactions should be experimentally observable can be obtained by considering several concrete cases. In deuterium at densities equal to that of a solid body under normal conditions a temperature of 2×10^5 °C would be required to obtain 1 neutron/sec/g of deuterium. In highly rarefied deuterium with a concentration of about 10^{13} atoms/cm^3 a temperature of about 5×10^5 °C would be required to produce the same effect in a gram of deuterium, which would occupy a volume of 30,000 m^3.

Thus, even to approach the threshold for production of thermonuclear processes the temperature of matter must be raised to a very high level. At such temperatures and under stationary conditions the deuterium should be an almost totally ionized plasma.

The amount of energy that must be concentrated in the plasma to raise its temperature to a level sufficient for the production of intense thermonuclear reactions should be comparatively small. Thus, the amount of thermal energy necessary to raise the temperature of 1 g of deuterium to 10^6 °C equals only a few kilowatt-hours. This is about the same amount of energy required to boil water in a large family samovar.

Therefore, if one were able to devise a method of heating the plasma with practically no thermal losses, even a low-power energy source could be used to induce intense thermonuclear processes. The main problem is to exclude heat losses, which rapidly increase with the temperature since the thermal conductivity of the plasma is proportional to $T^{5/2}$. If matter is heated to a temperature of only several tens of thousand degrees in the absence of thermal insulation, the losses will be so great that further increase of temperature will be practically impossible.

*Lecture given April 26, 1956 at the British Atomic Energy Research Establishment at Harwell, England.

**Some works of L.A. Artsimovich and M.A. Leontovich appear in this issue.

There is another obstacle that arises when dense substances are heated: one must overcome the enormous mechanical forces that result from increase of the pressure with temperature. On heating initially solid or liquid deuterium we find that already at $T = 10^5$ °C the pressure exceeds 10^6 atmos. Therefore, thermonuclear reactions can be induced only during a very short period of time in dense substances and such a process will always resemble an explosion (which, however, may not be dangerous) or a brief pulse.

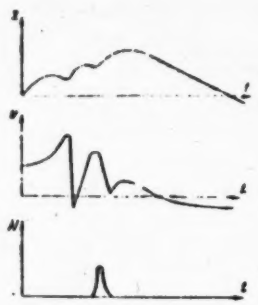

Fig. 1. The general form of the variation of the current and voltage in pulse discharges, and the neutron pulse that accompanies the discharge.

On considering the various ways of generating intense controllable thermonuclear processes one finds that there is a number of directions that can be taken in attempting to solve this problem.

On the one hand, there are the approaches that lead to stationary thermonuclear reactions, and on the other hand, those that are based on the idea of utilizing an instantaneous temperature rise in transient processes of very brief duration. However, irrespective of the way the investigation is carried out, there is one problem that is inevitably encountered; namely, the insulation of the plasma, which is heated to a high temperature, from the walls of the vessel in which it is confined. In other words, a means must be found to keep the fast particles within the plasma over a period sufficient for the particles to have a good chance to react with each other.

One of the ideas proposed in connection with this problem was that of using a magnetic field for thermal insulation of the plasma. Academicians Sakharov and Tamm were the first to point out this possibility in 1950.

In a sufficiently strong magnetic field, electrons and ions can move freely only along the lines of magnetic force. In a plane normal to these lines of force the particles will move along circles of small radius. The positions of the centers of these circles can vary only as a result of collisions, each collision displacing the center by a distance of the same order of magnitude as the radius of curvature of the particle trajectory. If the radius of curvature of the trajectory is small compared to the mean free path, diffusion of the particles and thermal conductivity of the plasma in the plane normal to the magnetic field will be greatly diminished. The theory of the processes taking place in completely ionized plasma indicates that at high field strengths H and high temperatures the transverse thermal conductivity coefficient is inversely proportional to H^2 and is many orders of magnitude less than the value found in the absence of a magnetic field. However, under these conditions radiation losses must be considered.

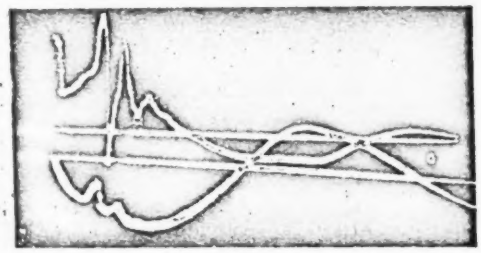

Fig. 2. Oscillogram of current and voltage in a discharge in deuterium, $V_0 = 40$ kv, $P_0 = 0.2$ mm Hg.

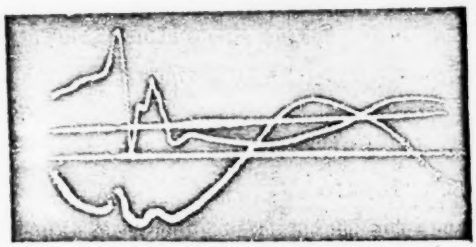

Fig. 3. Oscillogram of current and voltage in a discharge in deuterium, $P_0 = 0.2$ mm Hg, $V_0 = 40$ kv.

The magnetic field required to provide the thermal insulation can be produced by passing a sufficiently intense current through the plasma. The current will also heat the plasma as a result of Joule losses and of the work of electrodynamic forces. These considerations were the basis for carrying out theoretical and experimental studies of the physical processes that occur when intense currents pass through a plasma.

We shall first examine the principal theoretical concepts that preceded the experimental work. When a current is passed through a plasma the latter should contract under the action of electrodynamic forces (attraction of parallel currents). An increase of the plasma temperature should follow. If a contracted column of the

plasma is detached from the vessel wall as a result of electrodynamic contraction ("pinch" effect) its temperature may be estimated from the condition that the pressure of the ionized gas is balanced by the electrodynamic forces.

A simple computation shows that in such quasi-stationary contraction processes the plasma temperature should increase proportionally to the square of the current. As is known, if the electrons and ions are in thermal equilibrium the plasma temperature can be expressed by the equation:

$$T = I^2/4Nk$$

where I is the curent expressed in electromagnetic units, N is the number of particles of a given sign per centimeter length of discharge tube, and k is the Boltzmann constant. Investigation of the conditions for thermal equilibrium showed that for $N \sim 10^{17}$ the electron and ion temperature should be practically identical. At appreciably lower values of N only the electron temperature will increase.

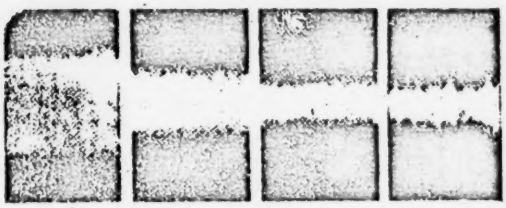

Fig. 4. Frames of a moving picture of a pulse discharge.

Fig. 5. Photograph of the development of discharge in deuterium for a pressure $P_0 = 10$ mm Hg. The electrodes are hemispheres. The interelectrode spacing is 45 mm. The scale of the photograph is 1 μsec = 18 mm. $I_{max} = 1.2 \cdot 10^6$ amps. $T/4 = 9.5$ μsec. The diameter of the chamber is 180 mm.

A contracted plasma column detached from the walls can exist only while the discharge current is building up. If the current is constant the column will disintegrate and come in contact with the walls.

It is evident that a thermonuclear reaction with a constant yield over an appreciable period of time cannot be produced by passing a current through a plasma. In principle, it should be feasible to periodically heat the plasma and induce thermonuclear reactions in phase with the peak current. Calculations of the expected thermonuclear effect led to the following result, which at first glance may seem paradoxical. It was found that during a single heating cycle the total number of elementary nuclear interactions for a given value of the peak current should be independent of the duration of this cycle. Thus, it seemed that it should be possible to excite very intense thermonuclear reactions by sending pulse discharges of very short duration through deuterium if the current was sufficiently large. Theoretical calculations indicated that even a current of 300 kiloamps should be sufficient to produce an observable emission of neutrons of thermonuclear origin. At currents of several million amperes the emission should be very intense. Such were the theoretical predictions that preceded the experimental work.

Further development of concepts regarding the nature of the processes occurring in a plasma during the passage of an intense current was profoundly influenced by the new facts discovered during experimental investigation of intense pulse discharges. These results completely altered the character of the picture created by the initial theoretical efforts.

Experimental investigation of intense pulse discharges was carried out in a broad range of the parameters characterizing the initial discharge conditions.* Discharges through hydrogen, deuterium, helium, argon, xenon, and gas mixtures (deuterium-helium, deuterium-argon, deuterium-xenon) of various relative content were studied. The measurements were carried out at initial gas pressures ranging from 0.005 mm Hg to 1 atmosphere. The basic experiments were performed with straight discharge tubes. The length of the discharge gap varied from several centimeters up to 2 m and the diameter from 5 to 60 cm. The discharge was produced by a voltage of several tens of kilovolts. The peak current varied from 100 kiloamps up to 2×10^6 amps, the rate of build-up of the current lying between 10^{10} amp/sec and 10^{12} amp/sec. The maximum instantaneous power released in the plasma in these experiments was as much as 40×10^6 kw.

*In England, pulsed discharges in gases have recently been investigated by I.D. Craggs and his collaborators, S.W. Cousins and A.A. Ware, and others.

Banks of high-voltage condensers were used to produce the discharges. The leads that carried the current from the condenser to the discharge gap were designed to keep the parasitic inductance of the electric circuit to a minimum since this factor restricted the magnitude of the current and its rate of growth. For a voltage of 50 kv and total capacity of the condenser bank of several hundred μf, the parasitic inductance of the circuit and switch was only 0.02-0.03 μh (in those cases when the current growth was maximal).

Oscillographic methods of measurement of the main parameters characterizing the state of the plasma during passage of a current were developed and these were used to study the intense pulsed discharges. Besides oscillography, ultra-high-speed moving-picture cameras (up to 2×10^6 frames/sec) were used as well as photography by aid of Kerr cells supplied with special electroexplosive types of shutters.

In addition to the discharge current and voltage, oscillograph records were also made of the intensity of separate spectral lines from the plasma, of the neutron and X-ray intensity, of the magnitude of pressure pulses measured with the aid of piezoelectric elements, and also of the instantaneous magnitude of the magnetic and electric field strengths at various points within the plasma. The magnetic and electric fields were measured with small probes in the form of miniature coils, loops, or needle electrodes of various shapes that could be placed at various points within the discharge vessel.

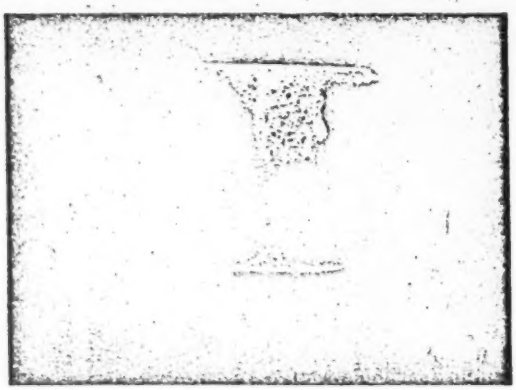

Fig. 6. The instant of contraction of the discharge column. The exposure time is 0.2 μsec. The discharge is in deuterium at a pressure $P_0 = 1$ mm Hg. The interelectrode distance is 45 mm, and the chamber diameter is 180 mm.

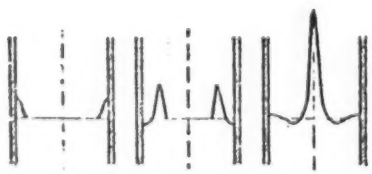

Fig. 8. Distribution of current density across the discharge tube at various times.

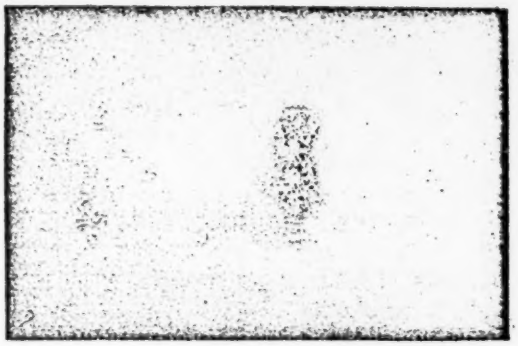

Fig. 7. Photograph of deuterium discharge made with Kerr cell 2.2 μsec after discharge began. Exposure 0.2 μsec. Initial pressure 1 mm Hg; distance between electrodes, 40 mm.

Space limitations do not permit me to give a detailed account of the numerous results obtained in this series of experiments. I will therefore report only a small part of this experimental material.

Of greatest interest is the first phase of the discharge during which the plasma current rises from zero to the peak value. In the experiments discussed here this phase lasted from 3 to 30 μsec. At the beginning of the discharge, after breakdown of the gas, a smooth increase of the current and voltage in the discharge gap takes place. After a certain period of time a sharp decrease of the voltage occurs. At the same time a more or less pronounced kink can be seen on the current oscillogram (see Fig. 1, which illustrates the general nature of time variation of the current and voltage; see also Figs. 2 and 3). After the first drop the voltage began to increase rapidly and then dropped sharply again. This second voltage decrease was paralleled by the appearance of a new kink on the current oscillogram. In some cases, three consecutive sharp changes in the otherwise smooth variation of the current and voltage were observed at the first stage of the discharge.

These characteristic features of high-current pulse discharges are especially pronounced when the discharge takes place in gases of low atomic weight (hydrogen, deuterium, helium) and at low initial pressures.

When the rate of current build-up is of the order of 10^{11} amp/sec, the interval between breakdown of the gas and appearance of the first voltage drop is several microseconds.

This time interval is a regular function of the parameters characterizing the initial conditions of the discharge. For a given discharge-tube diameter it varies approximately as the fourth root of the gas mass per centimeter length of the discharge gap.

Inductive reactance is much larger than ohmic resistance in pulsed discharges in which the current increases at a high rate. Thus, by using current and voltage oscillograms one may find the time dependence of the inductance of the plasma column and hence determine how the radius of the column changes at various stages. An analysis of this type shows that in all cases the very first stage of the process is featured by an increase of the inductance due to contraction of the plasma towards the discharge-tube axis. The speed of constriction of the plasma increases with the initial current build-up rate (that is, with the derivative dI/dt) and decreases with the gas density. At the instant when the kink on the current oscillogram appears and a sharp drop in the potential is observed, the inductance begins to decrease. This means that this time corresponds to maximum contraction of the plasma filament. This situation is followed by a rapid expansion of the plasma filament. If a few kinks are observed on the current oscillogram, it means that successive contractions and expansions of the column take place.

These conclusions, which were obtained by analyzing current and voltage oscillograms, are confirmed by data obtained by applying ultra-high-speed cinemaphotography of pulse discharges in tubes with transparent walls. On Fig. 4. are shown four successive frames of a moving picture of a pulse discharge in deuterium at a pressure of 0.1 mm Hg and peak current of about 200 kiloamp. These pictures were taken at intervals of 0.5 μsec and refer to only a very small period of development of the process, which corresponds to the time of the current and voltage break. The plasma-column minimum diameter corresponds exactly to this time (the moving picture frames were synchronized with the current and voltage oscillograms).

Figure 5 was obtained by using a moving-picture camera for continuous photography. In this method a narrow slit perpendicular to the axis of the discharge tube subtends a small segment of the discharge gap whose image is swept across the film with a high speed. As a result, a continuous picture of variation of the diameter of a small segment of the plasma column was obtained on the film. The photograph shown here was obtained for a discharge in deuterium with a peak current of about 10^6 amperes. The initial gas pressure was 10 mm Hg. The time of maximum contraction and the further development of the process are clearly visible.

Photographs of the contracting plasma column obtained with a Kerr cell are shown in Figs. 6 and 7.

Valuable data on the main physical processes occurring in intense pulse discharges can be obtained by measuring magnetic and electric field strengths in the plasma. Magnetic-field measurements permit one to draw the following picture of current distribution in the plasma: directly after breakdown, the current-conducting region is a thin cylindrical layer adjacent to the discharge-tube walls. The inner boundary of this layer moves at first slowly and then more rapidly toward the axis. After a certain interval of time the current fills the whole tube as a result of movement of the inner current boundary. The time at which the current reaches the axis practically coincides with the time of appearance of the first kink on the oscillogram. The current density near the discharge axis at this time is several dozen times greater than the mean current density over the cross section of the tube. On subsequent expansion and contractions the current density remains very high in a central region of several centimeters in diameter although fluctuations are appreciable.

The current density distribution over the cross section of the discharge tube at various times is shown schematically in Fig. 8. The current density distribution at the very first stage of the discharge is shown in the left figure. The second one refers to the time at which the current was moving towards the axis. The distribution after the first contraction of the plasma column is illustrated in the right figure. An interesting feature of this stage of the process is that in a certain zone of the discharge the current reverses its direction.

The velocity of the ionized gas is the quantity directly characterizes the dynamics of a pulse dies discharge. In a plasma of sufficiently high conductivity this velocity is determined by the ratio between the longitudinal electric field strength E and the magnetic field strength H

$$v = cE/H$$

Measurements of E and H indicate that in a pulse discharge with rapid growth of current the radial velocity of the plasma may be very high. In the experiments described here the maximal velocity during contraction and

expansion of the plasma column in rarefied gases was found to reach hundreds of kilometers per second. This signifies that the kinetic energy of the drift of the plasma ions is of the order of several hundred electron volts.

One of the most interesting effects observed in intense pulse discharge in light gases is the appearance of penetrating radiation. In 1952, soon after experiments with pulse discharges were started, it was found that at sufficiently high currents the discharge in deuterium becomes a source of neutrons.

The first experiments performed with the aim of studying this phenomenon showed that neutrons appear when the peak discharge current is 400-500 kiloamp and the initial deuterium pressure is about 0.1 mm Hg. The neutron emission was observed in a relatively narrow pressure range and its intensity rapidly increased with increase of the applied voltage, i.e., with increase of the peak current. In these first experiments the radioactivity induced in a silver target embedded in a paraffin block placed near the discharge tube served as the neutron detector. A possible explanation of this phenomenon was that the neutron emission resulted exclusively from collisions between the accelerated deuterons and deuterium adsorbed by the electrodes on tube walls; however, control experiments did not confirm this explanation.

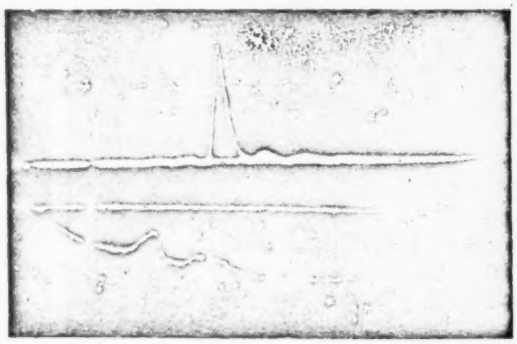

Fig. 9. Oscillograms of the current and the neutron pulse for a discharge in deuterium with $V_0 = 40$ kv and $P_0 = 5 \cdot 10^{-2}$ mm Hg.

At the early stages of investigation it was quite natural to assume that the neutrons resulted from thermonuclear reactions in the plasma heated to a high temperature. This was exactly what was expected from the beginning and the fact that the effect was detected under conditions that completely corresponded to the a priori theoretical predictions seemed to speak in favour of this viewpoint. The behavior of the neutron radiation (its dependence on pressure and current) observed in the first experiments qualitatively agreed with the assumption that the phenomenon was due to a thermonuclear mechanism. However, serious doubt concerning the correctness of this assumption soon began to appear. This happened after it was found that neutrons can be observed at comparatively small peak discharge currents, of the order of 150 kiloamp. According to the initial calculations the intensity of the thermonuclear reaction at currents of 150 kiloamp should be practically zero.

In subsequent experiments the neutrons were recorded with a scintillation counter fed to an oscillograph. It was found that the neutrons were always emitted when the second kink appeared on the current oscillogram, i.e., at the moment when the plasma was subjected to the second contraction (Fig. 9). No neutrons were produced during the first contraction.

The neutrons were always emitted as short pulses with a steep front. The rise time of the pulses was several tenths of microseconds. The chief results of the oscillographic investigations were not consistent with the initial assumption that the neutron emission is the result of quasi-stationary heating of the plasma during which the temperature increases proportionally to the square of the current.

Further investigations yielded new interesting facts pertaining to the plasma neutron radiation. In particular, it was established that in specially designed discharge tubes the neutrons could appear at fairly high deuterium densities, as much as several tens of millimeters of initial pressure. This fact signified that the neutron emission was certainly not a trivial effect.

It was found that not only neutrons but hard X-rays as well were produced in pulse discharges. Penetrating X-rays were found when large currents were passed through hydrogen, deuterium and helium. The radiation produced by discharges in deuterium always consisted of short spurts. The pulses due to the neutrons and X-ray quanta always appeared simultaneously on the oscillograms. The energy of the X-ray quanta produced in pulsed electrical processes in hydrogen and deuterium reached 300-400 kev. It is noteworthy that at the time of emission of such high-energy quanta the voltage applied to the discharge tube was only about 10 kv.

Theoretical analysis of the complex phenomena that occur in the plasma of a pulse discharge oscillating

under the action of electrodynamic forces is still at such a stage that quite a number of facts remain to be explained. However, the general picture of the process is gradually becoming clear and some of the peculiarities of the phenomenon seem to have been sufficiently elucidated.

It is now clear that contraction and expansion of the plasma are not quasi-stationary processes characterized by equilibrium between the external and internal pressures.

In the equations describing the dynamics of a pulse discharge the main term is that which accounts for momentum changes in the ionized gas due to magnetic pressure. Thus, the kinetic energy of the ordered motion should at some stages of the process greatly exceed the thermal energy concentrated in theplasma.

At the initial stage of the discharge the internal pressure in the plasma is very low; thus the electrodynamic forces produce acceleration along the radius towards the discharge-tube axis. Thus, the work of the electrodynamic forces is not expended in raising the temperature but in imparting kinetic energy to the converging plasma layer. At this stage the discharge tube operates as a peculiar type of accelerator in which the particles are driven by the magnetic field. Since charged particles will move with the same velocity irrespective of sign, the kinetic energy acquired by the ions will be quite large, whereas that of the electrons will remain effectively constant because of their small mass. From the viewpoint of gas dynamics, the contraction process should be considered as a phenomenon in which a cylindrical shock wave converging towards the axis is produced in the plasma. At first, the gas located before the inner wave front is not ionized. When the wave begins to move the gas is carried along together with the charged particles of the plasma and its atoms simultaneously become ionized. The amount of matter that begins to move therefore gradually increases and the total amount of ions and electrons in the plasma increases rapidly.

The duration of the contraction phase can be determined by calculating the velocity acquired by the contracting gas. It was found to be approximately proportional to $(M/V_0^2)^{1/4}$, where M is the mass of gas per unit length of discharge tube and V_0 is the initial voltage. This dependence is exactly what one finds experimentally for the interval between breakdown and appearance of the first kink in the current oscillogram.

The final stage of cumulative contraction sets in when the plasma accelerated by the magnetic field reaches the axis. At this instant a great part of the energy of ordered motion changes into heat and the pressure and plasma temperature sharply increases. During maximum contraction, the plasma temperature may be of the order of 10^6 °C. The nature of the processes occurring during maximum contraction is not very clear, but after maximum cumulation a diverging shock wave should appear to drive the plasma towards the walls. Inside the outgoing wave there should be a rarified zone. Under the action of elctrodynamic forces that tend to compress the current, the outgoing wave should be decelerated rapidly and a new phase of contraction should ensue. This stage differs from the first in that the density in the inner region of the discharge is small and the gas in this region is probably almost completely ionized. As a result, during the second contraction, conditions are produced that are favorable for accelerating in the longitudinal electric field a certain group of ions and electrons located near the discharge axis, i.e., in the region in which the magnetic field is small. One may note here a certain analogy with the accelerating mechanism proposed by Fermi in his theory of origin of cosmic rays. A plasma of high conductivity will move together with its magnetic field, and with respect to particles located in the inner zone it will be equivalent to a converging magnetic wall from which the enclosed electrons and ions repeatedly will be reflected, their energy increasing after each reflection. Acceleration of ions and electrons in the longitudinal electric field near the discharge axis is possibly the explanation for the appearance of neutrons and penetrating X-rays. The electric field strength during the second contraction may be very high. It can exceed the instantaneous external voltage applied to the discharge tube by a large factor.

However, it must be mentioned that not everything in this acceleration mechanism is yet clear. Under certain conditions acceleration of ions in a longitudinal electric field may also be possible outside the central zone of the discharge due to the presence of space charges. Some types of instability that are peculiar to the column may play an important role in accelerating particles in the plasma. In particular, one type of instability observed experimentally may be of importance for the acceleration of electrons. It consists of spontaneous creation of a longitudinal magnetic field in the plasma as a result of spiraling of the plasma column.

If the second contraction is followed by the few more radial oscillations of the plasma column, the acceleration of the particles may be repeated several times. Experimentally not more than three successive oscillations have been observed. A possible explanation of this,however, is that the plasma may begin to interact with the discharge-tube walls with the result that the wall material begins to evaporate and appreciable amounts of foreign gases appear in the volume.

We considered here some features of the phenomena that accompany the passage of intense pulse discharges through rarefied gases. The success of further work in this direction will greatly depend on the possibility of creating conditions under which the plasma column will experience multiple oscillations during build-up of the current without coming into contact with the walls. However, there are serious reasons to believe that this cannot be achieved.

On appraising the various approaches to the problem of obtaining intense thermonuclear reactions, we do not deem it possible to completely exclude further attempts to attain this goal by using pulse discharges. However, other possibilities must also be carefully considered. Especially interesting are those in which stationary processes may be used.

An English translation of this report was distributed at Harwell by the Soviet scientists visiting England. This translation has been verified by the Consultants Bureau Staff. and some slight modifications made.

The Kurchatov lecture, together with comments by American and British physicists and government officials, was published in Nucleonics, June, 1956.

INVESTIGATIONS OF PULSE DISCHARGES AT HIGH CURRENTS

L. A. Artsimovich, A. M. Andrianov, O. A. Bazilevskaya,
Yu. G. Prokhorov, N. V. Filippov

We present the results of an experimental investivation of intense pulse discharges with rapidly increasing current. A brief description of the experimental method used is given. The pulsation processes of the plasma column are described.

The purpose of our experiments was to study the properties of pulse discharges with intense currents. In such discharge, contraction of the plasma should take place under the influence of electrodynamic forces (attraction of parallel currents). The energy of the electromagnetic forces that compress the plasma is expended on the kinetic energy of the charged particles. As a result of this, the plasma temperature and pressure in a high current discharge can achieve extremely great values. The study of some properties of pulse discharges in rarified gases at currents from 10^2 to 10^4 amps was the subject of references [1] and [2]. We investigated pulse discharges in hydrogen, deuterium, helium, argon, and xenon at initial gas pressures from 0.005 mm to several millimeters. The maximum current strength in the various experiments was from 100 kiloamps to one million amps. The discharge voltage was from 20 to 50 kv. The voltage sources were banks of condensors with capacitance from several times ten microfarads to 400 μf. The rate at which the current increased in the initial phase of the discharge, that is, the quantity $\left(\frac{dI}{dt}\right)_0$ was $3 \cdot 10^{10}$ amp/sec to $1.5 \cdot 10^{11}$ amp/sec., and the time in which the current increased from zero to the maximum value was from 8 to 17 μ sec. The discharge tubes were porcelain cylinders from 60 to 100 cm long and from 20 to 40 cm in diameter. The electrodes were flat rings of copper or dural. Before each pulse discharge, the tube was evacuated to a very low pressure, and then filled with a fresh sample of the gas. The quantities that characterize the state of the plasma during the pulse discharge were measured by means of an oscillograph. The current was measured with a Rogovsky bridge with an RL integrating circuit. Low resistance voltage dividers connected in parallel with the discharge gap were used to measure the voltage. Oscillographic measurements of the magnetic field strength at various points of the plasma were used to clarify the current distribution in the cross section of the tube. The pressure pulses of the plasma were recorded by piezoelectric elements. Detailed accounts of the method and results of the investigations of intense pulse discharges will very soon be published in the J. Exptl.-Theoret. Phys. Here we give merely the general properties of such discharges.

For the conditions of the experiments described, the pulse discharge is a periodic process with strong damping. The investigation of the first half period of the discharge is most interesting. Figure 1 shows two oscillograms of the current and voltage on a double beam pulse oscillograph. One of these is taken for discharge in deuterium at an initial pressure of 0.03 mm Hg. The second oscillogram is for deuterium at a pressure of 0.2 mm Hg. The initial voltage in both cases is 40 kv. The maximum currents are practically identical, being 500 ka. We see that at the very beginning of the discharge, after breakdown, both the current and voltage in the discharge gap are increasing. Then at a certain instant of time a sharp drop in voltage takes place. At the same instant there appears a kink in the oscillogram of current. After the first drop the voltage begins to rise rapidly, and then decreases sharply again. At the instant of the second discontinuous voltage drop, there appears a second kink in the current oscillogram. These fluctuations from a smooth variation in the development of the discharge are

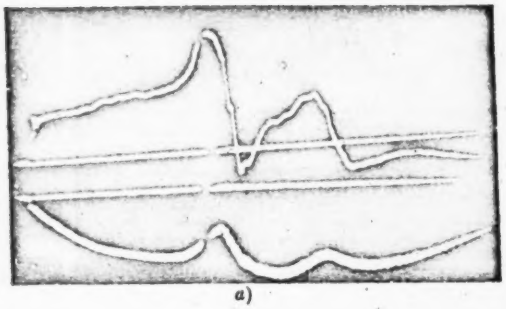

a)

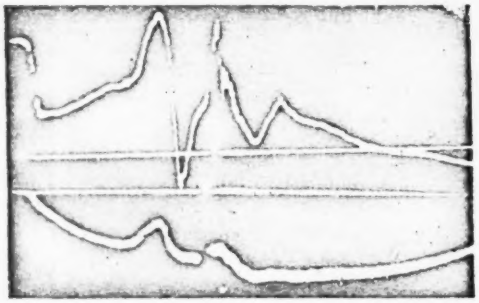

b)

Figure 1. Oscillograms of current and voltage for discharge in deuterium with $U_0 = 40$ kv.
a) $P_0 = 0.03$ mm Hg; b) $P_0 = 0.2$ mm Hg.

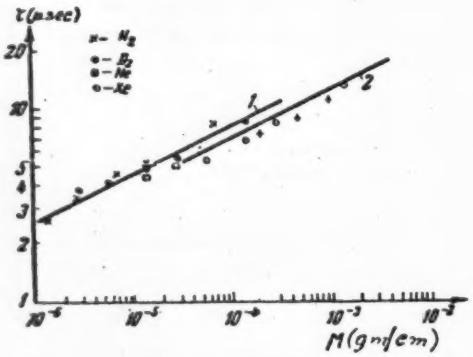

Figure 2. The dependence of τ on M for $U_0 = 30$ kv, $a_0 = 20$ cm.
1) $\frac{dI}{dt} = 6 \cdot 10^{10}$ amps/sec (for light gases);
2) $\frac{dI}{dt} = 7.5 \cdot 10^{10}$ amps/sec (for heavy gases).

a distinguishing feature of high current pulse discharges, and occur regularly. They are especially distinct in those cases in which the discharge takes place in gases with low atomic weights (hydrogen, deuterium, helium) at low initial pressures.

When the initial rate of current increase is of the order of 10^{11} amps/sec, the time interval τ from gas breakdown to the first drop in voltage is a few microseconds. The magnitude of τ is a function of parameters that characterize the initial conditions of the discharge. Figure 2 shows the dependence of τ on M, where M is the mass of the gas per unit length of the discharge tube. The values of τ are obtained from oscillograms taken for pulse discharges in hydrogen, deuterium, helium, argon, and xenon (with the same initial voltage on the tube, and the same geometric parameters). The approximate dependence is $\tau \sim \sqrt[4]{M}$. For a given value of M, the value of τ increases with increasing discharge tube radius, and decreases for increasing $\left(\frac{dI}{dt}\right)_0$.

In pulse discharges with sharply increasing currents the inductive potential drop is substantially greater than the resistive one. It is therefore possible, by making use of the oscillograms of the current and voltage, to find the dependence of the inductance of the plasma column on time, and from this data to determine the time variation in the radius of the plasma column (assuming that the column is in the form of a cylinder with a well defined boundary).

Such an analysis shows that the initial stage of the process is characterized by increasing inductance caused by the contraction of the plasma onto the discharge tube axis. The plasma contracts more rapidly when $\left(\frac{dI}{dt}\right)_0$ is greater and the gas density is smaller. At the instant when the kink occurs in the oscillogram of current, the inductance starts to drop. This means that this instant corresponds to the maximum degree of compression of the plasma column. After this, a rapid expansion of the plasma takes place, and it is followed by a second contraction phase. If a few kinks are observed on the current oscillogram, this means that successive contractions and expansions are taking place. Knowing the radius of the plasma at various instants of time, it is possible to determine the velocity with which the plasma is moving toward the axis. This velocity depends on M and $\left(\frac{dI}{dt}\right)_0$.

In our experiments, the velocity of the plasma varied between the limits of $1 \cdot 10^6$ cm/sec for discharges in gases with a high initial density, and

$1.2 \cdot 10^7$ cm/sec for discharges in hydrogen and deuterium at initial pressures of the order of 0.01 mm.

In the initial stage of the discharge, the degree of ionization of the gas is not large. Spectroscopic measurements performed by S. Yu. Lukyanov and V.I. Sinitsyn [3] show that up to the instant at which the first contraction ends, no more than 5-10% of the total number of gas atoms is ionized (for discharge in hydrogen and deuterium with a maximum current of about 200 ka, at an initial pressure of 1.0 mm Hg). After the first contraction, the degree of ionization in the central part of the discharge may be, it would seem, very high. Spectroscopic investigations show also that after the second contraction of the column, there appears in the discharge volume a large number of foreign impurities which are caused by the interaction of the plasma with the walls. Therefore, the investigation of the later stages of the discharge are not particularly interesting.

By measuring the magnetic field strength at various distances from the discharge tube axis, we may find the current density distribution in the tube cross section for any instant of time. The experimental data leads to the following picture of the current distribution in the plasma. After breakdown, the region occupied by the current is, due to the skin effect, a thin cylindrical layer close to the walls of the discharge tube. The inner boundary of this layer contracts onto the axis, at first slowly, then more rapidly. The motion of the inner boundary layer causes the current to occupy the entire tube after a short time. The instant of time at which the current reaches the axis is practically coincident with the time of the first kink in the current oscillogram. The current density in the neighborhood of the discharge axis at this instant is 25 times as great as the average current density in the tube cross section. The curve of the current distribution, however, has no sharp boundary, and the central section with a radius of a few centimeters carries less than half of the total current. In the successive compressions and expansions, the current density in the central region remains very high, although it undergoes substantial oscillations.

As an illustration of these results, we present, in Fig. 3, the current distribution in the tube cross section for discharge in deuterium at an initial pressure of 0.05 mm Hg and with an initial voltage of 40 kv. It corresponds to the second contraction of the plasma. A characteristic property of this distribution is the fact that in a region of the discharge, the current changes direction (due to the skin effect).

Measurements of the pressure pulses in the plasma with the aid of peizoelectric elements made of barium titanate show that in the first contraction stage, there is a pressure wave propagated toward the axis together with the inner current boundary. Before the instant of maximum contraction, the pressure in the neighborhood of the axis is negligibly small. At the instant at which the current reaches the axis, the pressure in the central region increases rapidly to 25-50 atmospheres (for an initial gas pressure in the tube of about 0.1 mm Hg.).

The above experimental facts lead to the following model for the mechanism of the basic processes in pulse discharge. For rapid current rise in the initial stage of the discharge, the electrodynamic forces, increasing in proportion to I^2, cannot be compensated by the internal pressure of the ionized gas. Therefore, under the influence of the electrodynamic forces, the cylindrical layer of plasma which originally is located at the walls of the discharge tube starts to accelerate toward the tube axis.

A large part of the work done by the electrodynamic forces during this stage of the process is transformed into kinetic energy of drift motion of the particles in the contracting layer of the plasma. Since particles with charges of opposite sign move with the same velocity, the ions receive a large kinetic energy, whereas the energy of the electrons, because of their small mass, remains almost constant. The process of contraction may be considered as the development of a shock wave converging on the axis. The gas located before the inner front of this wave is at first neutral. As the plasma layer moves inward, the gas is partly carried along with the charged particles of the plasma (because of the large charge exchange cross section of the ions) and becomes ionized. Therefore the mass of the gas that is set into motion increases gradually, and the total number of ions in the plasma increases rapidly. A quantitative theory of the contraction of the plasma column has been developed by M.A. Leontovich and S.M. Osovets [4]. This theory gives the following formula for the value of τ, which characterizes the time of the process (from the instant at which the plasma layer leaves the walls to the time of maximum contraction of the column):

$$\tau = 1.8 \left(\frac{M}{3}\right)^{1/4} a_0^{1/2} \left(\frac{dI}{dt}\right)_0^{-1/2}$$

[a_0 is the tube radius, and the current I is expressed in the cgs magnetic (CGSM) system].

The values of τ calculated by this formula are presented on Fig. 2 by the solid line. We may note the

good agreement between theory and experiment (in a wide interval of variation for the quantity M). The final stage of contraction occurs when the plasma accelerated by the magnetic field reaches the axis. At this instant a large portion of the kinetic energy of directed motion is transformed into heat, which causes a sharp increase in the pressure and temperature of the plasma.

According to rough calculations, in our experiments the temperature of the plasma at maximum contraction reached values of the order of 10^6 deg (for hydrogen and deuterium at initial pressures of the order of 10^{-3} to $5 \cdot 10^{-2}$ mm Hg). The evaluation of the temperature is based on the measurement of quantities that determine the energy balance of the discharge. The data taken in this way is in agreement with the results of measurements on the pressure in the central region of the discharge.

The question of the determination of the plasma temperature will be taken up in detail in the following articles. Here we shall limit ourselves to just a few remarks necessary for the clarification of this question. In order to avoid misunderstandings, we must note that in speaking of the plasma temperature we have in mind the temperature of the heavy particles, that is, the ions and the neutral atoms. We may consider, in view of the large charge exchange cross section, that the temperatures of the atoms and ions in the contracting plasma column are the same. As has already been pointed out above, in the contraction process a large part of the work expended by the electrodynamic forces goes into the kinetic energy of drift motion of the charged particles. At the same time it should be noted that as the cylindrical plasma layer contracts onto the axis, the mass that is set into motion increases gradually, and therefore part of the work must be expended on inelastic processes, that is, on raising the plasma temperature. The data on the energy balance of a pulse discharge allows us to assume that up to the time of maximum contraction the temperature of the ions and atoms reaches a few hundred thousand degrees (which corresponds to an average energy of random motion of several times ten electron volts). As opposed to this, the temperature of the electronic component of the plasma in the first contraction stage remains very low, corresponding to an average electron energy of a few electron volts. This follows from the results of spectroscopic measurements, which indicate that the plasma is not highly ionized. If the average electron energy were several times ten electron volts, then the gas would be completely ionized even before the time of maximum contraction.

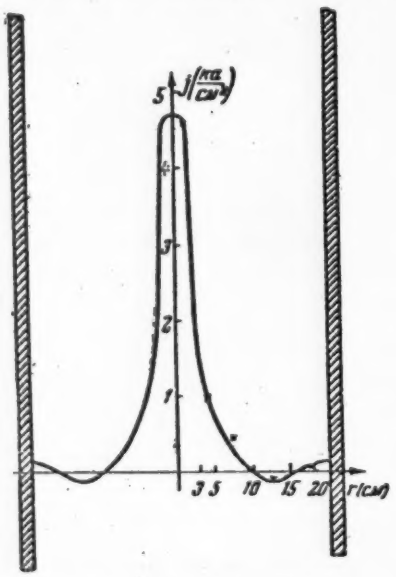

Fig. 3. The distribution of the current density through the cross section of the discharge in deuterium, for $U_0 = 40$ kv and $P_0 = 0.05$ mm Hg during the second contraction stage.

The characteristics of the processes that take place after the time of maximum contraction are not yet entirely clear. It is obvious, however, that after the maximum contraction there should be a diverging shock wave which carries the plasma in the direction of the walls. The diverging wave should be rapidly damped by the action of the electrodynamic forces tending to compress the current, as a result of which a new contraction stage arises, followed by a second expansion of the column. At this stage of the process, it would seem that various forms of instability should arise, which are characteristic of a high current plasma column, as a result of which the form of the column changes radically. The loss of stability of the plasma column and the strong interaction of the plasma with the walls lead to a substantial change in the character of the processes. At later stages of the discharge, foreign gases appear in the discharge volume, and the temperature of the plasma drops significantly.

LITERATURE CITED

[1] Cousins and Ware, Proc. Phys. Soc.(London) B 64, 159 (1951).

[2] Ware, Phil. Trans. Roy. Soc. (London) 243, 197 (1951).

[3] S.Yu. Lukyanov, V.I. Sinitsyn, Atomic Energy, 1956, No. 3, 88, 379*.

[4] M.A. Leontovich, S.M. Osovets, Atomic Energy, 1956, No. 3, 81, 371*.

* C. B. Translation pagination.

ON THE MECHANISM BY WHICH THE CURRENT CONTRACTS IN FAST AND INTENSE GAS DISCHARGE *

M.A. Leontovich and S.M. Osovets

The mechanism of the processes which take place as the current contracts under the influence of electrodynamic forces is described.

Reference [1] presents the results of experimental investigations of intense gas discharges in which the current increases at a rate of the order of 10^{10}-10^{11} amps/sec. In the course of these investigations some phenomena were discovered, and the explanation of these is the subject of this article. We shall indicate an extremely simple method by which we are able to describe very roughly the basic features of the phenomena, and to find the parameters by which they are characterized. To do this, we start from the proposition that the magnetic forces acting on the gas that is carrying the current and the mechanical inertia of the gas are of fundamental importance in these phenomena. The influence of the gas pressure on the process of contraction is felt only in the stage of its high compression; in the initial stage of the process, during the presence of a pronounced skin effect and while the center part of the gas column is only slightly heated, the gas pressure is low and plays a secondary role.

The great importance of the inertia forces in compressing the gas in the above experiments is indicated by the experimental fact that the maximum gas compression can take place after the maximum current, when the magnetic forces that contract the gas filament have already decreased.

In order to analyze the basic features of the contraction process and to examine the fundamental parameters that characterize this stage of the discharge, let us make use of the following model. We shall consider the contracting gas to be a cylinder characterized by the radius a, average pressure $\bar{p}$, and mass per unit length M.

The equation of motion of the gas can then be written in the form

$$\frac{d}{dt}\left(\frac{1}{3}M\frac{da}{dt}\right) = -\frac{I^2}{ac^2} + 2\pi a\bar{p}. \qquad (1)$$

The factor $\frac{1}{3}$ multiplying the mass is introduced in order to account approximately for the fact that the moving mass of gas is not all located at radius a, but is distributed throughout the whole cross section. This factor is obtained if one assumes that the mass is parabolically distributed. If, on the other hand, the mass is considered uniformly distributed throughout the gas column, then the factor becomes $\frac{1}{4}$, which leads to no significant difference in the results. Thus we are not considering here events that may be related to a velocity, pressure, or density distribution through the cross section of the gas. These will be considered separately. Let us note that the events that we are analyzing, which are characteristic for the rapid contraction of the gas current, are related to the action of the skin effect on the current distribution in the gas. This can be shown by comparing the outwardly directed force due to the gas pressure with the force of magnetic contraction. The gas pressure is proportional to its internal energy, which, in turn, is determined before the start of compression by the Joule heat. Such an evaluation of the ratio of these forces shows that, to within an order of magnitude, the ratio of the contracting force to the force due to pressure is determined by the ratio of the radius of the current in the gas to the thickness of the skin layer. If we therefore neglect the last term, which accounts for the gas pressure,

* This work was performed in 1953.

then the equation of motion assumes the form

$$\frac{1}{3}\frac{d}{dt}\left(M\frac{da}{dt}\right)=-\frac{I^2}{ac^2}. \qquad (2)$$

For those cases in which the dependence of the current on time is determined by the external circuit, the current increases approximately linearly in time during most of the quarter period of discharge, and we may therefore put $I = \dot{I}t$.

In so doing, $\dot{I}$ may be considered constant and given by $\dot{I}=\frac{V_0}{L}$, where V_0 is the initial potential on the condenser bank, and L is the self-inductance of the circuit and gas discharge (which, for the above condition, may be considered constant). Then the equation of motion (2) becomes

$$\frac{d}{dt}\left(M\frac{da}{dt}\right)=-\frac{3\dot{I}^2t^2}{ac^2}. \qquad (3)$$

Let us introduce the dimensionless parameters z and x, given by

$$t=t_1z;\quad a=a_0x$$

We shall naturally choose the unit of radius as its initial value, equal to the radius of the tube a_0, and the unit of time shall be chosen so as to give Equation (3) the simplest form; we therefore set

$$t_1=\frac{\left(\frac{1}{3}M\right)^{1/4}a_0^{1/2}c^{1/2}}{\dot{I}^{1/2}}.$$

Here we consider the mass constant. Then Equation (3) can be written

$$\frac{d^2x}{dz^2}=-\frac{z^2}{x},$$

and Equation (1),

$$\frac{d^2x}{dz^2}=-\frac{z^2}{x}+\frac{\bar{p}}{p_1}x, \qquad (4)$$

where p_1 is the unit of pressure, taken as

$$p_1=\frac{M}{3\cdot 2\pi t_1^2}.$$

At time t_1 the current is given by

$$I_1=\dot{I}t_1=(\dot{I}a_0c)^{1/2}\left(\frac{M}{3}\right)^{1/4},$$

and the unit of pressure p_1 is related to I_1 by the equation

$$p_1=\frac{I_1^2}{2\pi a_0^2c^2}.$$

This is the relation between the average pressure and current which corresponds to equilibrium between the pressure forces and the magnetic ones. We must, of course, bear in mind that in our case p_1 is not equal to the average pressure at time t_1 (though it is close to it). The pressure $\bar{p}$ and the current will be related by the equation $\bar{p}=\frac{I^2}{2\pi a^2c^2}$ only at that instant of time for which $\frac{d^2a}{dt^2}=0$.

In order to obtain a qualitative idea as to the variation of the contraction of the gas current filament during that time in which the temperature of the heavy particles (the ions and neutral atoms) increases, we assumed that the pressure change during the contraction is adiabatic, $\bar{p}v^\gamma=p_0v_0^\gamma$, where $\gamma=\frac{5}{3}$ (we are considering the compression of a monatomic gas); from the consideration that $\frac{v}{v_0}=\left(\frac{a}{a_0}\right)^2$, we obtain $\bar{p}=p_0\left(\frac{a_0}{a}\right)^{4/3}$. Inserting this expression for $\bar{p}$ into (4), we have

$$x\frac{d^2x}{dz^2} = -z^2 + \frac{\alpha}{x^{4/3}} \qquad (5)$$

where $\alpha = \frac{p_2}{p_1}$.

This equation was integrated by numerical methods with the initial conditions at $z = z_0$; $x = 1$, $\frac{dx}{dz} = 0$ for various times of starting the contraction z_0, and for various values of the parameter α which characterizes the initial pressure.

The figure shows a family of solutions obtained in this way. It can be seen from the figure that the time of the first maximum contraction depends only slightly on the values of z_0 and α; the values of z_{sing}, corresponding to this contraction, vary between 1.7 and 2.1. This time of the first maximum contraction is naturally identified with the time of the first "singularity" of the current, that is, its first minimum. Thus for this instant,

$$t_{sing} = z_{sing} t_{sing} \approx 1.8 t_1 \qquad (6)$$

where

$$t_1 = \left(\frac{M}{3}\right)^{1/4} \left(\frac{ac}{\dot{I}}\right)^{1/2} \qquad (7)$$

or, in practical units,

$$t_1 = 0.05 a_0 (p_0 \mu)^{1/2} \dot{I}^{-1/2}. \qquad (8)$$

Here t_1 is the time in seconds, a_0 is in centimeters, p_0 is the pressure in mm Hg, μ is the molecular weight for the cold gas, and $\dot{I}$ is in amps/sec.

It follows then, that the "singular" time is

$$t_{sing} = 0.09\, a_0 (p_0 \mu)^{1/2} \dot{I}^{1/2} \qquad (9)$$

and the "singular" current is

$$I_{sing} = 0.09\, a_0 (p_0 \mu)^{1/2} \dot{I}^{1/2} \qquad (10)$$

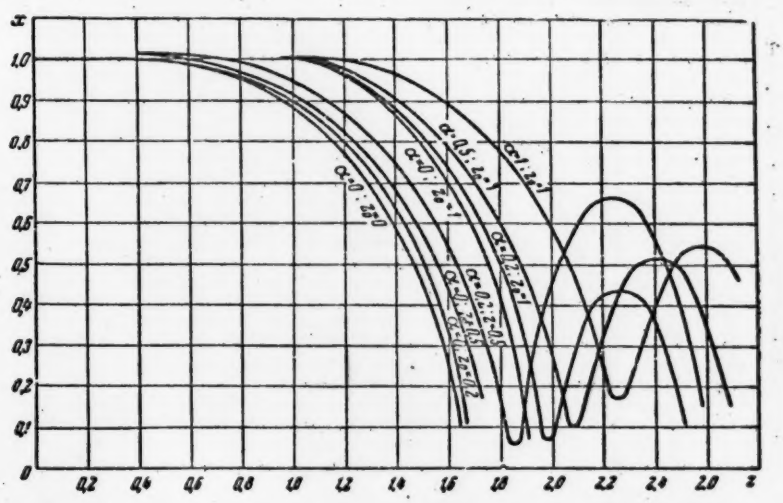

The dependence of the radius of the plasma column on time (in dimensionless coordinates).

The results of experimental measurement presented in reference [1] compare well with the expressions

obtained here. The sufficiently close agreement of the experimental results and the calculations support the suggested model for the development of the process. It should be noted that the agreement with experiment is not only qualitative, but that, in spite of the crude assumptions we have introduced, good quantitative agreement is achieved. Of course the agreement with experiment ceases when the increase of current with time is no longer linear, which can occur both for a substantial change in the self-inductance of the circuit as a result of the intense contraction of the gas filament, and for the situation in which the energy stored in the condenser bank that supplies the discharge has decreased significantly by the "singular" time.

LITERATURE CITED

[1] L.A. Artsimovich, A.M. Andrianov, O.A. Bazilevskaya, Yu.G. Prokhorov and N.V. Filippov, Atomic Energy. 1956, No. 3; 367*.

* C.-B. Translation pagination.

PENETRATING RADIATION FROM PULSE DISCHARGES

L. A. Artsimovich, A. M. Andrianov, E. I. Dobrokhotov,
S. Yu. Lukyanov, I. M. Podgornyi, V. I. Sinitsyn, N. V. Filippov

We present the results of an investigation of the neutron radiation detected in pulse discharges in deuterium, as well as some data on the penetrating X-ray radiation that arises in such discharges in light gases.

Intense current pulse discharges in light gases can, under some conditions, act as sources of penetrating radiation. In 1952 the authors discovered neutron radiation in pulse discharges in deuterium. The experiments in which this phenomenon was discovered were performed with straight discharge tubes. The tubes were porcelain cylinders (with diameters from 20 to 40 cm and 50 to 100 cm long) with copper or dural collars. They were connected to a circuit consisting of a bank of condensers and spherical dischargers. When the pulse discharge takes place, a current of several hundred kiloamps passes through the tube. The rate at which the current increased was $5 \cdot 10^{10}$-$1.5 \cdot 10^{11}$ amps/sec. In the original experiments the neutrons were recorded by the use of silver targets placed in a paraffin block located close to the tube. In later experiments, the neutrons were observed by use also of scintillation counters, and it was then possible to establish the connection between the time at which the neutrons appear and the characteristics of the pulse discharge.

Neutron emission is observed in discharge tubes with porcelain walls if the initial pressure of the deuterium is within the range of 0.01 to 0.3 mm. In tubes with metallic side walls, neutrons are emitted also for considerably higher initial pressures, up to 10 mm. The number of neutrons that are emitted while the current is passing through the tube fluctuates widely from one discharge pulse to another. In the experiments with the porcelain discharge tubes, the neutron emission reaches measurable values only if the tube has been first subjected to previous discharges in hydrogen, deuterium, or helium. For a maximum discharge current from 250 to 500 kiloamps and for an initial deuterium pressure of about 0.1 mm, the number of neutrons emitted in one discharge pulse varies between the limits of 10^7 and 10^8, sometimes reaching a value of the order of 10^9. The neutron radiation is extremely sensitive to the addition of small quantities of different gases. It is enough to add a few hundredths of a percent of hydrogen, argon, or xenon to deuterium to a pressure of 0.1 mm, for the neutron radiation to vanish entirely.

Because of the irregularities of the neutron radiation, it is difficult to establish quantitative relations that characterize the dependence of the neutron emission on such discharge parameters as the maximum current and the initial pressure. These relations are somewhat more qualitative than quantitative in character. Figure 1 shows the dependence of the neutron emission $\underline{n}$ on the maximum current in the discharge (I_{max}), obtained in experiments with a porcelain discharge tube 100 cm long and 40 cm in diameter at an initial pressure of 0.02 mm.

This data is obtained by averaging the results of a large number of separate experiments. We see that the intensity of neutron emission increases rapidly with the maximum discharge current from 200 ka to 300 ka. For further increase of I_{max} the value of $\underline{n}$ hardly changes. It should be noted that in these experiments the value of I_{max} is proportional to the initial voltage on the discharge tube. A change in I_{max} from 200 to 400 ka corresponds to an increase in the initial voltage from 20 to 40 kv. Similar curves of the dependence of $\underline{n}$ on I_{max} are obtained also at other pressures. The pressure that corresponds to the maximum neutron emission for

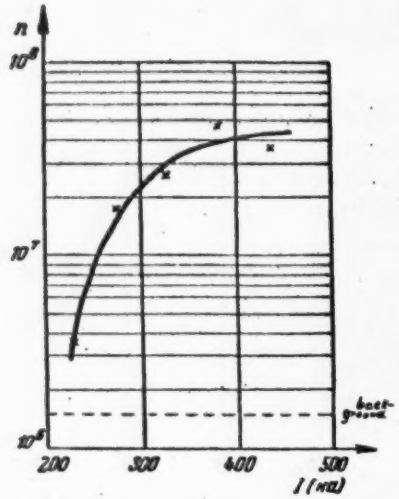

Fig. 1. The dependence of the neutron emission on the maximum discharge current.

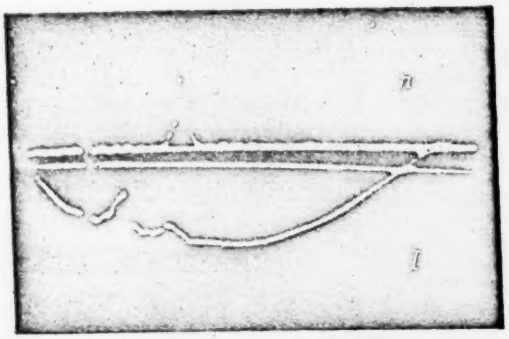

Fig. 2. Oscillogram of the current pulse and the neutron pulse accompanying discharge.

porcelain discharge tubes is about 0.05 mm. During the original phase of the investigation of neutron radiation, we were able to make the assumption that it was caused by the accelerated deuterons bombarding the deuterium absorbed by the electrodes and walls of the tube in the previous discharges. Control experiments, however, in which the preliminary discharges were performed with ordinary hydrogen, did not support this view. These experiments showed also that the emission source of the neutrons is distributed along the length of the tube, and is not located in the cathode region.

Oscillographic studies of the neutron radiation show that in all cases it occurs in the form of short pulses with very sharp fronts. The length of time it takes for the neutron radiation to grow from zero to the maximum value is 0.3-0.5 μsec. The neutron pulses appear at definite stages of the development of the discharge. In a previous communication [1], as well as in the work of M. A. Leontovich and S. M. Osovets [2], it is shown that in the first half period of the development of the pulse discharge, successive contractions and expansions of the plasma column take place. These processes are reflected in the oscillograms of the current and voltage during discharge. At that instant of time when the discharge filament passes through the stage of maximum compression, there appears a kink on the current oscillogram. The voltage at this time has reached its maximum value and starts to drop rapidly.

Figure 2 is an oscillogram of the current and neutron pulses taken with the aid of a double beam oscillograph. One of the oscillograph traces is that of the current variation, measured with the aid of a Rogovsky bridge, and the other trace is the neutron radiation intensity, recorded with the aid of a scintillation counter and a photomultiplier. As is seen from this oscillogram, (on which the neutron pulse is presented with a delay of 0.3 μsec), the neutron emission starts at a time corresponding to the second stage of maximum contraction of the plasma column. This is not a chance result, but represents a well established regularity. Analysis of an extremely large number of oscillographic measurements shows that in all cases the neutron emission starts at that part of the discharge in which the plasma column passes through the second stage of maximum contraction. In the first contraction neutrons appear. At low initial pressures in tubes of large diameter, three successive contraction and expansion stages of the discharge filament are observed. For these conditions neutrons sometimes arise both in the third, as well as the second maximum of filament contraction.

A pulse discharge with a rapid rate of current increase is also a source of penetrating X-radiation. The X-radiation always consists of short pulses whose rise time is a few tenths of a microsecond. The pulses caused by X-ray quanta and neutrons during deuterium discharge can be compared on the oscillograph. In so doing, it turns out that they arise simultaneously. The energy of the X-ray quanta that occur during discharge in hydrogen and deuterium attain values of 300-400 kev. It should be noted that at the time when quanta of such high

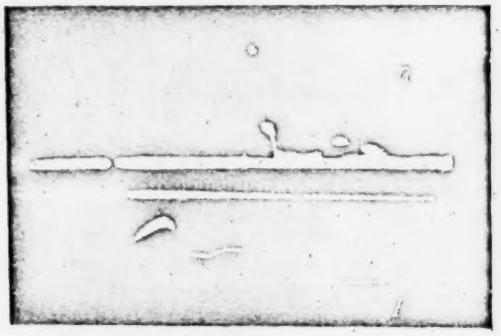

Fig. 3. Oscillogram of current pulses and neutron pulses.

energy occur, the voltage applied to the discharge tube is only 10-20 kv. A more detailed communication concerning the penetrating X-radiation that occurs during pulse discharges is presented in reference [3].

The reason for the appearance of penetrating X-radiation and neutrons in pulse discharges cannot be considered well established at the present time. One of the possible explanations is that they are caused by the acceleration of electrons and ions in the strong electric field near the center of the discharge axis, where the magnetic field strength is small. The longitudinal electric field in this region is basically inductive in origin; it is caused by the radial pulsation of the plasma column. Measurements of the longitudinal component of the electric field that were performed by A. M. Andrianov, O. A. Bazilevskaya, and Yu.G. Prokhorov show that the intensity of this field can be many times greater than the value derived from the external voltage that is applied at this instant to the discharge tube.

On the basis of the above assumption, we can also explain the time of appearance of the X-ray quanta and neutrons. In the early stages of the discharge, the contracting cylindrical plasma layer drives the neutral gas contained within it toward the axis of the discharge tube. Therefore, the gas density is high at the time of the first maximum of contraction in the region of the discharge tube axis, whereas the degree of ionization is still seemingly low. After the first expansion of the plasma column, within it there can develop a region of rarefaction in which the gas is practically entirely ionized.

As a result, in the second contraction stage, conditions are created which favor the acceleration of some of the electrons and ions in the central region by the electric field.

We do not assume, however, that the above explanation gives a complete picture of the process that accelerates charged particles in a pulse discharge. It is possible that the instability of the plasma column of intense current is an important part of the process. Indeed, we should note one of the aspects of this instability, which consists of the fact that at the time of contraction very narrow strains may develop in separate parts of the plasma column. As a result of this, instantaneous redistributions of the current and magnetic field may develop in the cross section of the column, which must lead to the appearance of very high local electric fields which will then accelerate the charged particles of the plasma. Still another aspect of the experimentally observed instability of the column may be of importance in the acceleration of the electrons. This is the spontaneous generation of a longitudinal magnetic field in the plasma due to turbulent motion of the plasma column. When the longitudinal magnetic field is generated, the vectors of the electric and magnetic field of the plasma cease being perpendicular to each other, and it therefore becomes possible for the electrons to be accelerated along the magnetic lines of the force.

LITERATURE CITED

[1] L. A Artsimovich, A. M. Andrianov, O. A. Bazilevskaya, Yu. G. Prokhorov, N. V. Filippov, Atomic Energy 1956, No. 3, 367*.

[2] M. A. Leontovich, S. M. Osovets, Atomic Energy 1956, No. 3, 371*.

[3] S. Yu. Lukyanov, I. M. Podgornyi, Atomic Energy 1956, No. 3, 389*.

* Consultants Bureau Translation pagination.

SPECTROSCOPIC STUDIES OF INTENSE PULSE DISCHARGE IN HYDROGEN

S. Yu. Lukyanov, V. I. Sinitsyn

Spectroscopic methods were used to study the properties of intense pulse discharge in a gas. It is shown that in the initial stage of the process, while the discharge is contracting onto the axis of the chamber, the velocity of the luminous front is as high as $6\text{-}8 \cdot 10^8$ cm/sec. A calculation of the number of ionized atoms is carried out. Experiments in which the luminosity of the pulse discharge plasma was investigated are described. The results of intensity measurements on the spectral lines of a hydrogen plasma are presented.

Introduction

In the present article we describe experiments devoted to spectroscopic investigations in the little known field of low pressure gas discharges at currents of several hundred thousand amperes.

Spectroscopic studies carried out for dynamic conditions make it possible for us to get some idea as to the change in the properties of the gas in which the discharge is taking place as the discharge runs its course, primarily with respect to the concentration of charged particles and the time variation of their distribution. For given conditions, it is also possible to learn something of the particle velocities in the gas discharge plasma. Let us note that when compared with other methods, the optical method of investigation has one definite advantage; this is related to the fact that the measurement process in this case takes place without any interference with the course of the effect being studied.

The large values of the current through the gas which were achieved in the experiments could have been obtained only in pulse discharge. The discharge circuit consisted of a condensor bank with a total capacitance $C = 30\ \mu f$, charged up to a voltage $U_0 = 30\text{-}40$ kv. By operating a special device, a periodically attenuated discharge was initiated in the discharge chamber. The discharge chamber was a glass cylinder with an inner diameter of 185 mm and an interelectrode distance of 450 mm. The experiments were performed at various hydrogen pressures within the interval from 0.04 to 5 mm Hg. At maximum, the current was 270-300 ka.

Measuring apparatus

An OK-17 double beam pulse oscillograph was used to record the current and voltage in the discharge process. The current was measured with the aid of a Rogovsky bridge. A low-resistance voltage divider was used to measure the potential across the electrodes. The spectroscopic investigations were performed by two methods: photographic and photoelectric. An ISP-51 spectrograph with three glass prisms was used for photographing the visible region of the spectrum. The time variation of the various lines of the spectrum were recorded with the aid of a UM-2 monochromator connected to an FEU-19M photomultiplier by a special attachment. The signal generated in the photomultiplier circuit by a separate line or part of the spectrum defined by the monochromator slit was fed through a cathode follower to a wide-band amplifier, whose output fed the oscillograph plates. Thus the optical effects could be recorded in synchronization with the current or voltage of the discharge gap.

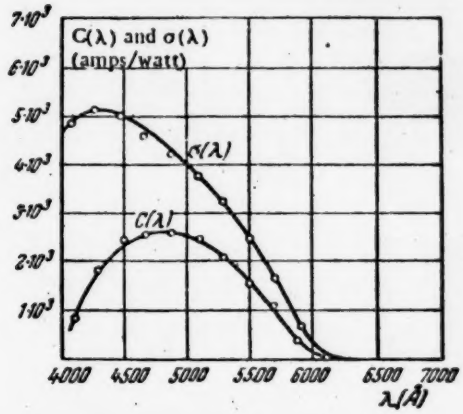

Fig. 1. $\sigma(\lambda)$ the spectral sensitivity of the FEU-19 photomultiplier; $C(\lambda)$ the spectral sensitivity of the measuring apparatus.

The apparatus at our disposal made it possible not only to study the behavior in time of the separate lines, but could also be used to obtain a quantitative evaluation of the energy radiated by the pulse discharge in the visible region of the spectrum. For the latter, however, it was necessary to know the absolute sensitivity of the measureing apparatus. The following simple method was used to calibrate it. An incandescent lamp with a tungsten filament was chosen as the light source. (W = 96 watts, U = 127 volts). The color temperature of such a lamp is 2850°K. The spectral distribution of the radiation intensity from tungsten is known in relative units for a given color temperature: in the visible region it is identical with black body radiation at the same temperature. A table of absolute values of the spectral intensity for the case of interest can be taken, for example, in the work of Forsythe [1], on the assumption that the radiation is isotropic in space. The distance from the lamp to the first slit of the monochromator was chosen large compared to the dimensions of the lamp filament. In this case the light source could be considered a point source with little error. The operating conditions of the incandescent lamp were held constant and were continuously regulated. Thus the absolute sensitivity of the measuring apparatus could be determined for any region of the visible spectrum

$$C(\lambda) = \frac{i(\lambda)}{aW(\lambda)}.$$

Here $C(\lambda)$ is the sensitivity we are looking for in amps/watt, $i(\lambda)$ is the output current of the photomultiplier in amps, $W(\lambda)$ is the power radiated by the source in the interval of wavelength from λ to $\lambda + \Delta\lambda$ into a solid angle of 4π, calculated from the tabulated data, and a is a geometric factor which determines the fraction of the source radiation that enters the spectroscopic apparatus. If, now, the incandescent lamp is replaced by any other source, its radiation for an arbitrary region of the spectrum can be easily found in absolute units, independent of the method for recording the electric signal at the photomultiplier output.

Figure 1 shows the experimentally determined curves for $C(\lambda)$ and for $\sigma(\lambda)$, the spectral sensitivity of the photomultiplier. The quantity $\sigma(\lambda) = C(\lambda)/k(\lambda)$, where $k(\lambda)$ is the transmission coefficient of the monochromator; the values of $k(\lambda)$ were determined in independent experiments.

Results of the measurements

Figure 2 shows the most characteristic spectrograms of the discharge. The spectra were photographed on panchromatic plates with a sensitivity of 45 units (All-Union State Standard 2817-50) during the course of one discharge for a spectrograph slit width of 0.002-0.003 mm.

It follows from analysis of the spectrograms that in the visible part of the spectrum, in addition to the lines of atomic hydrogen, the lines of other atoms are observed. Both the relative and the absolute intensity of the impurity lines decreases as the initial hydrogen pressure is increased, and the lines of atomic hydrogen become brighter; the intensity of the over-all background also increases with pressure. As the initial pressure is increased, the total brightness of the discharge increases rapidly. The impurity lines, whose presence indicates the strong thermal effect of the discharge on the chamber wall, occur starting with some minimum value of energy liberated by the discharge.

Figure 3 shows the intensities of the lines H_α, H_β, H_γ, Si_{II} (λ = 4128 A), synchronized with the current for an initial pressure of 0.1 mm Hg. From the oscillograms it is seen that starting at a time corresponding to

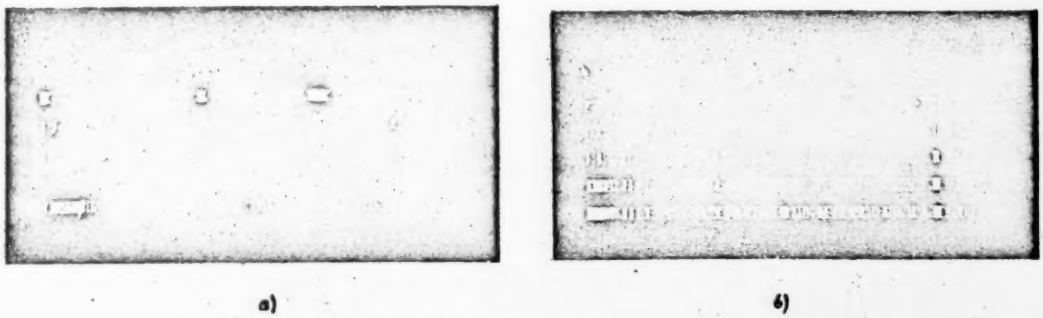

a) б)

Fig. 2. Spectra of discharges in hydrogen for various initial pressures: a) initial voltage on the condensor bank U_0 = 30 kv. Chamber pressure (from top to bottom) is 5; 0.5; 0.05; 0.025 mm Hg. At the bottom, for comparison, is the spectrum of stationary discharge in hydrogen ($i \approx 0.3$ amps); b) initial pressure in the chamber P_0 = 0.03 mm Hg; U_0 (from top to bottom) is 10; 15; 20; 30; 35 kv.

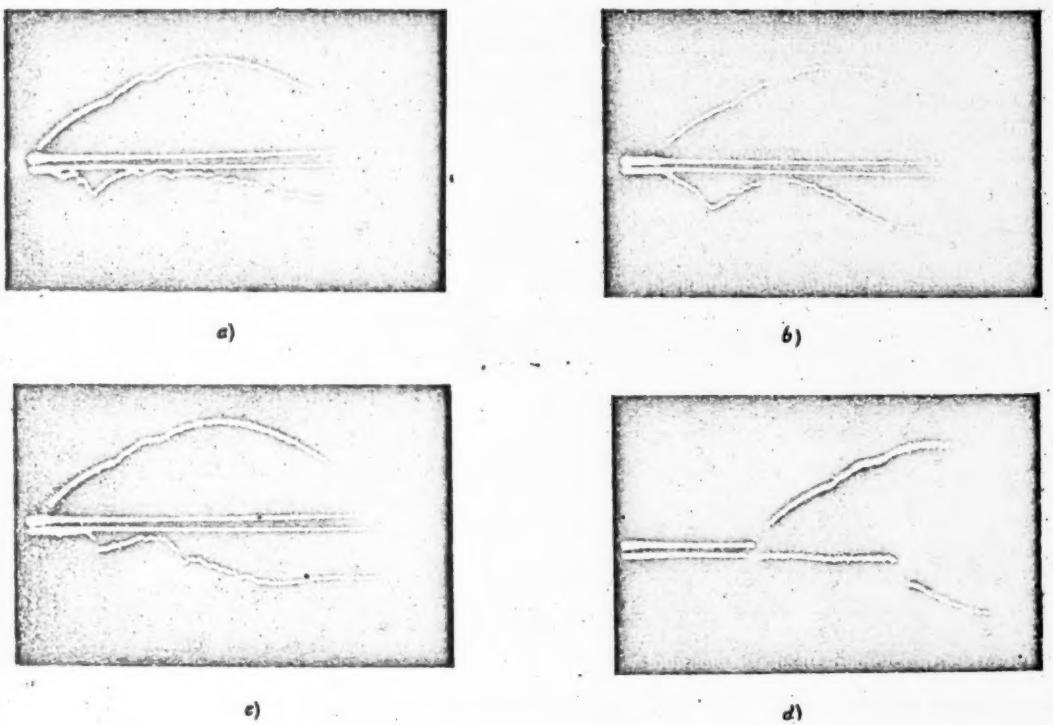

a) б)

в) г)

Fig. 3. Oscillograms of the intensity of some spectral lines (bottom lines), synchronized with the curve of the discharge current (top lines): a) H_α; b) H_β; c) $H\gamma$; d) Si_{II} (λ = 4128 A).

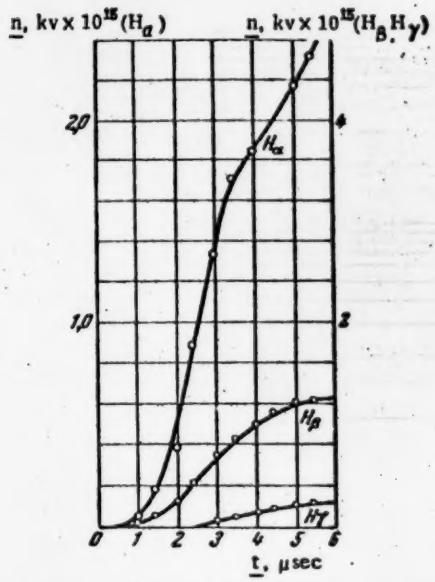

Fig. 4. The energy distribution of radiation of the lines of the Balmer series. The ordinate gives the number of quanta radiated up to the given time. The experimental data is normalized for unit length of the discharge, and account is taken of the absorption by the chamber walls, which have been clouded by previous discharges.

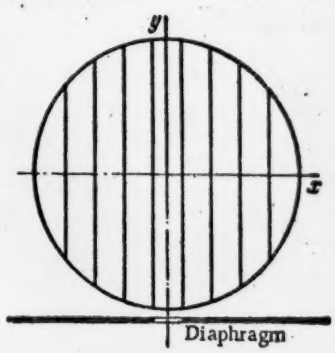

Fig. 5. Cross section of the discharge chamber divided into longitudinal zones whose radiation intensity could be recorded.

about one quarter of the period, vapors of the wall material begin to appear in the discharge volume. Thus, further variation of the photocurrent no longer refers to radiation from a hydrogen discharge under "pure conditions" and is of no great interest. Therefore, in all the oscillograms, we indicate only the beginning stage of the process.

In order to obtain a quantitative evaluation of the number of photons corresponding to the lines H_α, H_β, and H_γ, the oscillograms were analyzed according to the method described in Section 2. Figure 4 gives the time dependence of the total number of photons emitted from the starting time of the discharge for the above three lines*.

It should be noted that the energy expended on the radiation during the time from the start of the discharge to the maximum of the photocurrent (even taking into account the ultraviolet radiation, the determination of which was carried out in experiments which we shall not describe here) is merely about 0.1% of the total amount of energy liberated in this time.

The spectrograms and oscillograms describing the time variation of the intensity of the spectral lines which have been considered up to now supply us with information on properties of the discharge that are averaged over the whole cross section of the discharge gap, and do not make it possible for us to obtain information as to the internal structure of the discharge. Furthermore, experiments show that in the initial stage of development of the discharge, there takes place a rapid change in the distribution of current density within the chamber [2]. The radial change in the intensity distribution of the luminosity of the discharge which is related to the above effect, was studied with the same apparatus. For this, the monochromator with the attachment was placed at a distance of 5 meters from the discharge chamber. The whole surface of the chamber with the exception of a narrow transverse slit halfway up the cylinder was covered with an opaque material. In front of the slit was placed a diaphragm 2 cm in diameter, which could be moved perpendicular to the cylinder axis and line of sight. In this way the total cross section of the cylinder was divided into nine nonoverlapping zones (Fig. 5). The measureing apparatus recorded the time variation of the intensity of the line H_β for each of the zones. From the values

* The results illustrated in Fig. 4 are obtained for discharge in a 90 cm long cylinder with $U_0 = 40$ kv. The The half-life of the current is $T_{1/2} = 14$ μsec.

of the intensity so obtained $i_1(t)$; $i_2(t)$. . . $i_p(t)$, that is from the experimentally observed distribution i(x, t), a well known and simple calculation [3] leads to the radial distribution E(r, t).

The indicated method for going over to the radial distribution is valid only if the discharge is cylindrically symmetric and we may neglect the light absorption within the plasma. Difference from cylindrical symmetry, as will be seen from the following, is observed basically in the very beginning stages of the discharge for low gas pressures. As for the degree of transparency of the plasma to radiation of the line H_β, it was shown by a special experiment that for $P_0 = 0.1$ mm Hg and our experimental conditions the self-absorption is small and may be neglected. This experiment was performed with a mirror placed behind the discharge chamber, so that the radiant volume served simultaneously as the absorber.

The radial distribution of radiation density (H_β) for various pressures is presented on Fig. 6. Each frame corresponds to a given instant of time. At the top of the figure are the oscillograms of the current and the variation of the intensity of the line H_β on the discharge axis.

Discussion of the results

The spectroscopic data shows that, starting with a certain value of energy liberated in the discharge gap, there appears in the spectrum of a pulse discharge in hydrogen a large number of lines belonging to elements that make up the chamber walls. This critical value of the energy W_0 is attained for an initial voltage of about 15 kv in the hydrogen pressure region investigated and with the geometry of the discharge chamber that we used. Calculation shows that the value of W_0 for these conditions is sufficient to raise the temperature of the inner surface of the glass walls to the chamber by the pulse discharge to a value corresponding to the intense vaporization of the glass in the chamber. It would seem that as the current is increased, the time of appearance of the impurity vapors should be displaced closer and closer to the start of the process, since the energy liberated reaches the value W_0 in a shorter time. In other words, for an initial voltage of 35-40 kv, which is what was used in the basic part of the measurement, we should expect the impurity lines to appear in the earliest stages of the development of the discharge*. Actually, as is seen on the oscillograms, the silicon lines appear at a later time, which is related to the characteristic kinks in the current oscillograms. Such delay is direct evidence of the fact that the rate at which energy is incident on the chamber walls is slowed down, and that there exists some definite thermal insulation between the discharge and the chamber walls in the early stages of the process. This situation is in full agreement with the ideas of the magnetic constriction of the discharge in the initial stages of development of the process and with the inertial theory of pulse discharge [4].

Let us now consider the degree of ionization of the plasma. Calculations performed by V. I. Kogan [5] make it possible to evaluate the number of charged particles existing at a given time in the plasma when the absolute radiant intensity of hydrogen in the visible spectrum is known. In these calculations it is assumed that the processes of excitation and ionization of hydrogen atoms by electron collisions are concurrent and that the degree of ionization in the beginning stage is not large. No spectroscopic measurements were performed in reference [5], and the number of charged particles was evaluated on the basis of the total number of quanta emitted by the discharge in the visible spectrum, which was determined with the aid of a photo cell. The ratios of intensities of the various lines of the Balmer series, which were also necessary for the calculation, were given theoretically.

After performing the spectroscopic measurements in absolute units (see Fig. 4), we were able to change the theoretical intensity ratios of the various lines of the spectrum by amounts which were experimentally determined, and to attain greater reliability in the results obtained. Let n(t) be the total number of charged particles in the discharge cross section at the time t, and let n_0 be the number of neutral particles in the same cross section (determined by the initial pressure of the gas). Then the degree of ionization averaged over the cross section will be $\bar{\eta}(t) = n(t)/n_0$. For a pressure of 0.1 mm Hg the average degree of ionization is not large; it

* More exactly, at time t_0, when the equation

becomes valid.

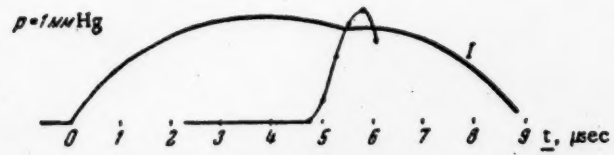

For t between 5 and 6 μsec, the vertical scale is reduced by a factor of 10.

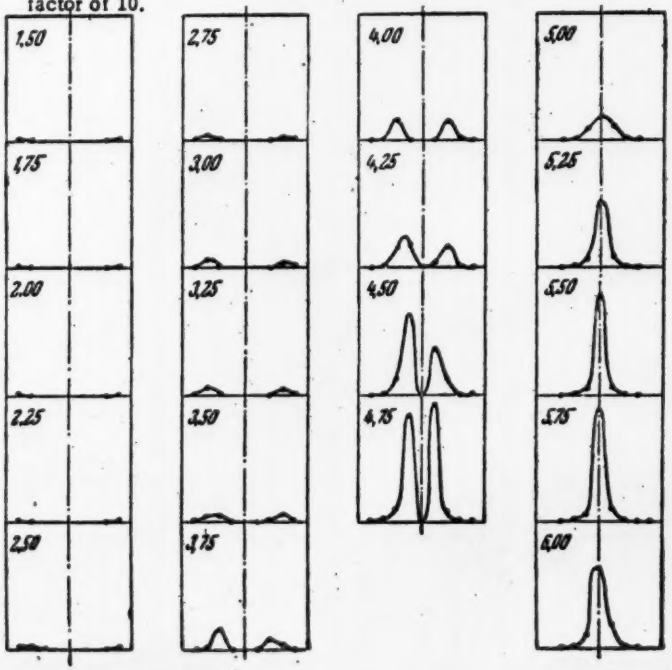

a)

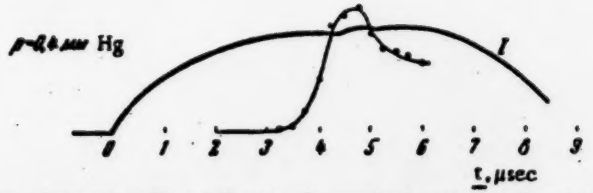

For t between 3.75 and 6 μsec, the vertical scale is reduced by a factor of 20.

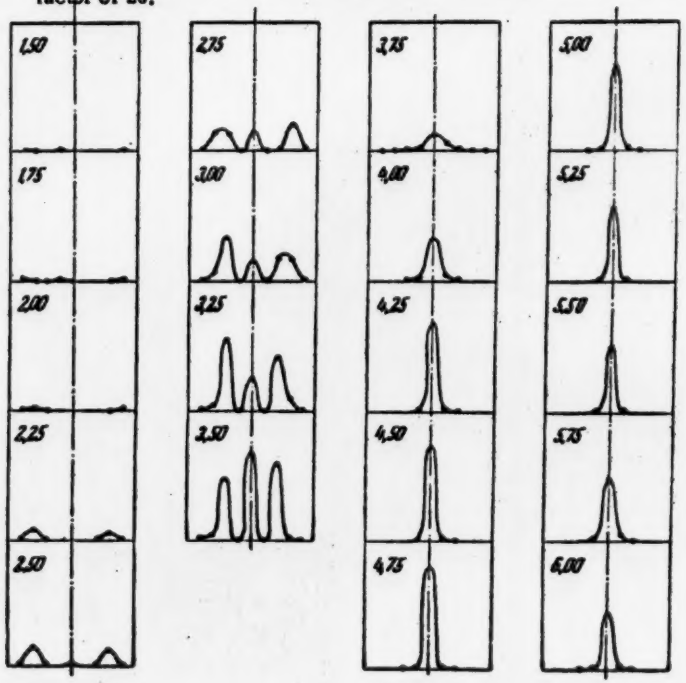

b)

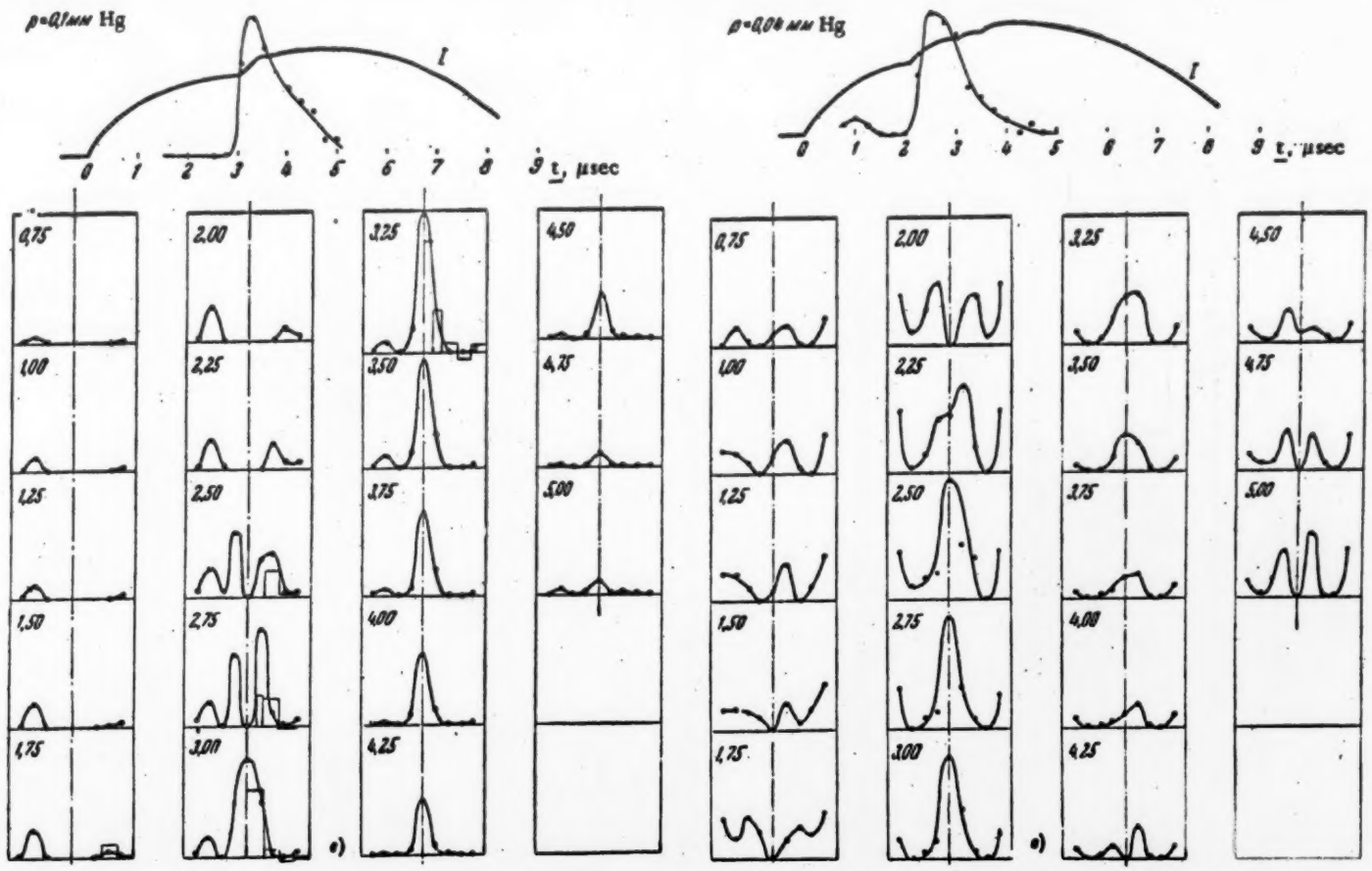

Fig. 6. Radial distribution of radiation intensity (for the line H_β) for various pressures. At the top is the oscillogram of the discharge current and the intensity of the line H_β on the discharge axis. In the upper left hand corner of each frame is the time in μsec. Since the absolute intensity of light increases rapidly with increased pressure, a different vertical scale is chosen for each pressure. To go over to a common scale, the values presented should be multiplied by the following constants 1; 1.15; 2.3; 5, respectively, for a, b, c, d, that is, for pressures 1; 0.4; 0.1; 0.04 mm Hg. Histograms which show the radial distribution of current density are drawn on some of the frames of Fig. 6b. These histograms were drawn according to the data contained in reference [2], with the corresponding change of the time and distance scales. Such a comparison shows visually the similarity of the electric and optical processes.

attains a value of merely 5% when $t \approx 3$ μsec. Obviously in later stages of the discharge the number of charged particles and the percent ionization can increase. The uncontrollable increase in the total number of particles in the discharge that occurs when foreign atoms enter the chamber as a result of vaporization of the wall material makes the corresponding calculations entirely indeterminate*.

The current density, luminosity, and concentration of charged particles do not remain constant through the cross section of the discharge, but change rapidly in time. Therefore the time dependence of the degree of ionization averaged over the cross section is only of limited value in characterizing the processes that take place. More detailed information as to the variation of the properties of the plasma can be obtained by considering the radial distribution of the luminosity. As is seen from the curves presented in Fig. 6, only the outer parts of the chamber are luminous in the beginning stage of the process. Then, a few microseconds (from 2 to 4, depending on the initial pressure) after the start of the discharge, the luminosity "breaks away" from the chamber walls, and the hollow luminous cylinder rapidly contracts on the discharge axis until a brightly glowing column arises on the axis (this time of contraction leaves a characteristic sign on the curve of the current in the discharge); the central luminous column then remains rather stable on the discharge chamber axis. The velocity of propagation of the luminous front on contraction of the discharge is about $6\text{-}8 \cdot 10^6$ cm/sec. This value for the velocity of the luminous front is in good agreement with the experimental data obtained for the velocity of propagation of the compression wave, which was measured by a piezoelectric method, and the velocity with which the current density is redistributed through the cross section [2].

For the latter, the magnetic field strength was measured directly with the aid of so-called magnetic probes.

The process of radial redistribution of the luminosity as the discharge develops is the same with respect to the general characteristics for all the pressures investigated, and has some details that are as yet difficult to explain for $P_0 = 0.4$ mm Hg. As the pressure changes, only the scales of intensity and time vary. The cylindrical asymmetry that is observed at the beginning of the process for low pressures is a manifestation of the instability of the discharge under these conditions.

Quantitative measurements make it possible to determine the fraction of the total number of quanta emitted by the central or outer part of the discharge volume at various times. After calculating the local values of the radiation density, and therefore the local values of the charged particle density, it is natural to consider not the average values $\bar{\eta}(t)$ but the values $\eta(r, t)$, which characterize the local degree of ionization at a given point at a given time. The transition from the average to the local value, however, is not simple, since the time variation of the local concentration of neutral particles is unknown. In the contraction process, in addition to the charged particles some of the neutral atoms are driven toward the discharge axis [7]. The degree to which the particles are trapped in the luminous column is, however, unknown. If we consider that all the neutral particles are concentrated in the region of the luminous central zone (about 2.5 cm in diameter), then we get the previous value for the coefficient $\eta \sim 5\%$; obviously this is hardly probable. If, on the other hand, we consider the density of the neutral gas to remain constant, then we formally obtain, for the degree of ionization in the luminous zone, the value

$$\eta = \bar{\eta}\left(\frac{D}{d}\right)^2 \sim 300\%.$$

Here D is the diameter of the discharge chamber, and d is the diameter of the luminous channel. Thus the correct values for the local degree of ionization

$$\eta(r, t) = \frac{n(r, t)}{n_0(r, t)}$$

* On the other hand, if the discharge is less intense and the spectroscopic data indicates the absence of impurity atoms in the chamber, the average percent of ionization can be determined also for later times. Thus, for instance, for a voltage of 15 kv, the percent of ionization, calculated on the basis of the broadening of the lines of the spectrum, is about 40-60% [6].

can be determined by this method after the time dependence of the distribution of neutral particles in the chamber cross section has been measured.

The authors take this opportunity to express their sincere indebtedness to L. A. Artsimovich and M. A. Leontovich for valuable discussions and for their constant interest in the work.

LITERATURE CITED

[1] B. T. Barnes, W. E. Forsythe, J. Opt. Soc. Am. 26, 314 (1936).

[2] L. A. Artsimovich, A. M. Andrianov, O. A. Bazilevskaya, Yu. G. Prokhorov, N. V. Filippov, Atomic Energy 1956, No. 3, 367*.

[3] Hörmann, Z. Physik 97, 539 (1935).

[4] M. A. Leontovich and S. M. Osovets, Atomic Energy 1956, No. 3, 371*.

[5] N. A. Borzunov, V. I. Kogan, D. V. Orlinsky (to be published).

[6] I. M. Podgornyi, Report Acad. Sci. USSR (1952).

[7] S. I. Braginsky, A. B. Migdal (to be published).

* Consultants Bureau Translation pagination.

HARD X-RADIATION ACCOMPANYING A DISCHARGE IN A GAS

S. Yu. Lukyanov and I. M. Podgornyi

In this paper it is shown that a powerful gas discharge at low pressure is accompanied by the emission of hard X-ray quanta. The radiation is observed in the discharge in various gases. The main properties of the radiation are studied, and consideration is given to a possible mechanism of origin of the effect observed.

Introduction

As is well known, the breakdown of a discharge gap in a gas can be accompanied by the appearance of X-radiation [1-3]. The X-rays arise at the anode and the walls of the discharge chamber through the stopping of fast electrons that have been accelerated by the electric field at the instant of the beginning of the discharge. The duration of this initial X-radiation is measured in tenths of a microsecond [3]. At later stages of the development of the discharge X-radiation is not observed in ordinary cases. Another picture appears in the passage of large pulses of current through a rarified gas. If the peak value of the current reaches several hundred thousand amperes, then in the discharge in hydrogen and some other gases one observes the emission of hard X-ray quanta whose origin is not connected with the inception of the discharge.

Experiments on the detection of this phenomenon and some results obtained in its study form the contents of the present paper.

Apparatus and Methods of Measurement

In this work we used a pulse generator consisting of a battery of condensers with capacity 36 mf, and a discharge chamber made of a porcelain tube; the inside diameter of the tube was 175 mm, and its length was 1000 mm. To decrease the parasitic inductance of the circuit, the discharge chamber was placed in a copper cylinder, placed coaxially with the chamber. The discharge was initiated at the proper instant by the delivery of a voltage pulse to the discharge set-up.

The strength of the current flowing through the gas was measured by a Rakowski girdle. A low-resistance voltage divider was used to measure the potential difference between the electrodes. The time characteristics of the current and voltage were obtained on the screen of a two-beam pulse oscillograph of type OK-17.

Filling the chamber with gas through a measuring volume made it possible to avoid errors in the measurement of the initial pressure caused by changes in the temperature of the walls of the chamber in the course of the experiment. The hydrogen and deuterium were given a preliminary passage through a palladium filter.

To register the soft X-radiation, which could easily be absorbed in the walls of the discharge chamber, we used measuring cartridges whose apertures were covered with thin aluminum foil. The location of the measuring cartridges is shown in Figure 1. Immediately behind the foil were placed luminescent crystals, connected by plexiglass light conveyors with the cathodes of photomultipliers. The pulses occurring on the collector of a multiplier were delivered, after amplification, to the plates of an oscillograph. The transmission band of the amplifier had width 10 megahertz. The photomultipliers were carefully screened from electromagnetic disturbances, which always accompany the operation of powerful pulse apparatus. For the

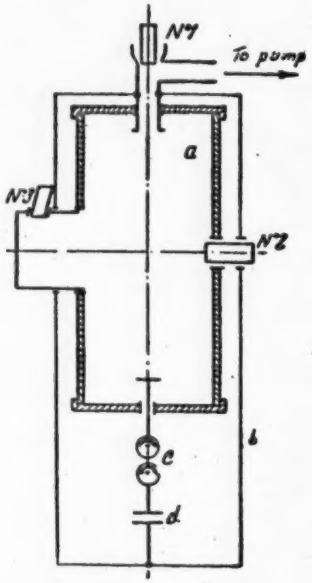

Fig. 1. Diagram of the apparatus. (Showing the locations of the measuring cartridges Nos. 1, 2, and 3, which serve to register the long-wavelength part of the spectrum of X-radiation). a) Discharge chamber; b) copper cylinder-feeder; c) discharger; d) battery of condensers.

registration of the hard part of the spectrum, for which the absorption in the walls is unimportant, the scintillation counter was placed outside the discharge chamber, at various distances from it. Besides the scintillation counter, this part of the spectrum was also studied with X-ray films provided with intensifying screens, and with thick films of electron-sensitive photographic emulsion.

Detection of the Effect

In the registration of the X-rays by the measuring cartridges, in a certain region of pressures, there are found on the oscillograms, in addition to the pulse corresponding to the beginning of the discharge, pulses of short duration occurring several microseconds after the breakdown. In Figure 2a is shown a typical oscillogram, obtained under these conditions; the second beam of the oscillograph recorded the curve of the voltage across the electrodes of the chamber. Under constant initial conditions the amplitude of the second pulse varied widely, while the time interval between the pulses remained unchanged within the limits of accuracy of the measurements. The appearance of the second pulse is always connected with breaks in the curves of voltage and current.

The unexpectedness of the observed phenomenon demanded the carrying out of a series of control experiments. On could suspect the action of electromagnetic disturbances on the electrical circuit of the detector, illumination of the photomultiplier through microscopic holes in the foil, and a number of other causes, improbable on first thought, but no completely excludable a priori.

One of the most convincing of the control experiments consisted in the removal of the luminescent crystals. When this was done both the first and the second pulses disappeared altogether. The use of various phosphors (naphthalene with anthracene, NaI, $CaWO_4$, ZnS and others) showed that the duration of the pulse changes in agreement with the decay time of the phosphor, if the decay time exceeds one microsecond.

In the course of further experiments it was established that the penetrating power of the radiation occurring in the discharge in hydrogen is relatively high. A scintillation detector, removed from the apparatus and placed in a complete metal screen, continued to detect the radiation. The radiation at the beginning of the discharge was not recorded under these conditions because of its strong absorption in the walls of the chamber (all the experiments were conducted with the initial potential difference of the condenser plates equal to 40 kv). Oscillograms obtained under such conditions are shown in Fig. 2b-e; the second beam of the oscillograph here records the voltage across the electrodes, the current through the gas, or the intensity of the spectral line H_β.

An X-ray film, placed between intensifying screens and located beside the scintillation detector, was found to be blackened after several discharges. The blackening of the X-ray film can be regarded as direct proof that the appearance of pulses at the output of the photomultiplier was caused by X-rays. In a number of cases the X-rays were detected by gas-filled counters, and also by electron-sensitive emulsions, in which the tracks of recoil electrons were observed.

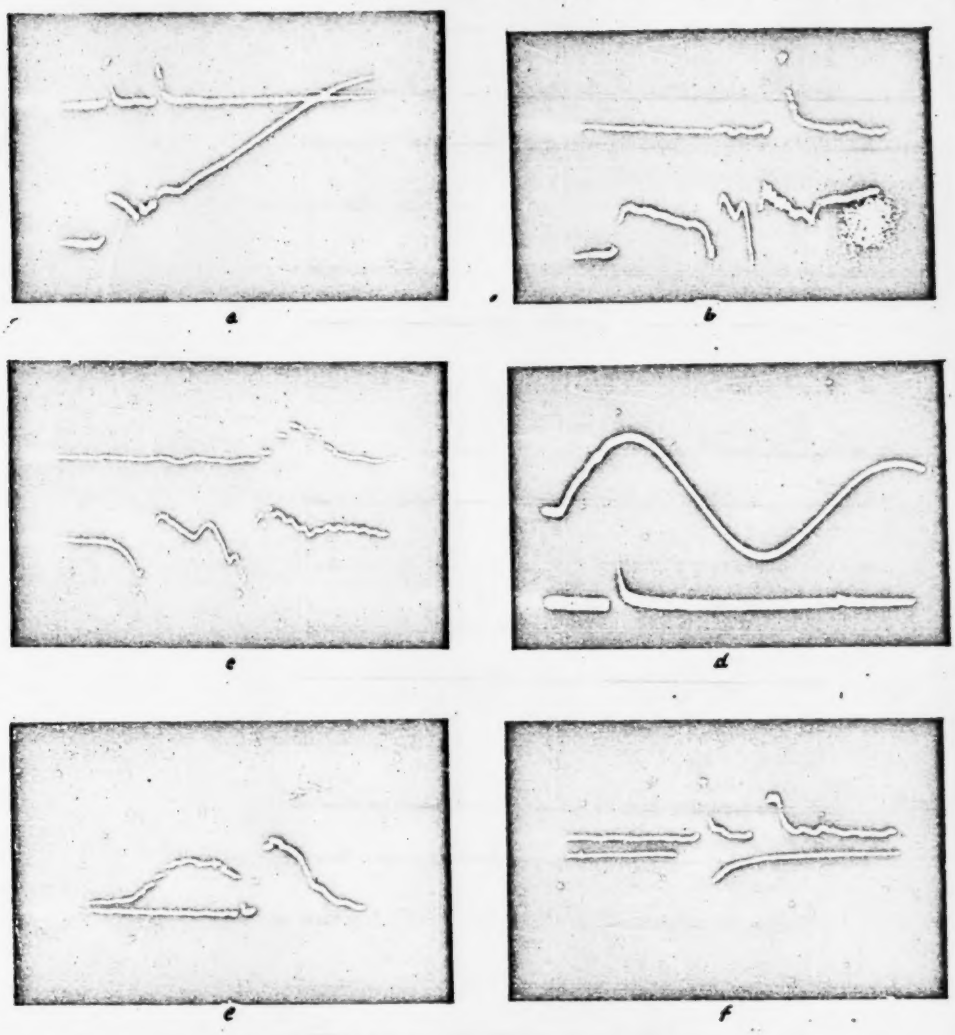

Fig. 2. Oscillograms of the pulses of X-radiation.
a, b, c) Above are the pulses of X-radiation; below is the pulse of voltage; the duration of the sweep is (a) 44, (b) 11, (c) 4.2 μsec; d) above is the pulse of current, below is the X-ray pulse, sweep time 40 μsec; e) above is the trace of intensity of the Balmer line H_β, below is the X-ray pulse, sweep time 3.7 μsec; f) above is the trace of the pulse at the output of a scintillation detector, placed at a distance of 12 m from the discharge chamber (discharge in deuterium), and below is the pulse from a γ-ray counter. The delay of the first pulse from the photomultiplier in comparison with the pulse from the counter is due to properties of the apparatus. The separation between the first and second pulses corresponds to the times of flight of neutrons produced in the reaction d – d. Duration of sweep 2.8 μsec.

Basic Properties of the X-Radiation

We now consider the results of experiments which provided evidence about the limiting energy of the radiation and its intensity. To find the energy of the radiation from a discharge in hydrogen various methods were used:

1. Filter method. The X-ray film was placed in a lead cassette with apertures which were covered with filters of various thicknesses. The materials chosen for the filters were lead and copper. Several such cassettes were exposed simultaneously so as to obtain degrees of blackening suitable for photometric measurement. To exclude action on the film of the softest part of the spectrum the cassettes were placed in a lead shield (thickness of lead 1-2 mm).

2. Method of screened scintillation counter. A scintillation counter in a lead shield was placed at a distance of several meters from the discharge chamber; the thickness of the shield amounted to several centimeters and was changed from one experiment to another. With each thickness of lead from 70 to 200 discharges were carried out, and the frequency of appearance of impulses was recorded as a function of the thickness of the shielding layer.

3. Method of measuring track lengths of recoil electrons in thick nuclear emulsions. An electron-sensitive emulsion, covered with a thin layer of lead to absorb the soft part of the spectrum, was irradiated with the X-rays. The distribution in length of the tracks in the irradiated emulsion was compared with an analogous distribution obtained by the examination of a control emulsion.

4. Method of the nuclear photoeffect. If the radiation contains quanta of energies above 1.65 Mev, then the (γ, n) reaction can be produced in nuclei of Be^9, and the neutrons produced can be detected by the artificial radioactivity produced in a silver target.

We shall consider the results obtained by each of these methods.

The use of the filter method requires a knowledge of the dependence of the blackening of an X-ray film on the intensity of the radiation producing this blackening. To obtain this dependence we used a 122 millicurie radium source. Since in each individual experiment the thickness and material of the filter were known, the absorption coefficient of the radiation accompanying the discharge could be determined by comparing the blackenings of the exposed films. The absorption coefficients obtained in the experiments with copper and lead filters gave values of the energy of the radiation that agreed with each other within the limits of accuracy of the measurements. The results of the measurements with the filter method refer to the part of the spectrum that acted most effectively on the films under the conditions of the experiment. To estimate the energy of the part of the spectrum lying near the limit, an additional lead shield was used. But the use of lead shields of thickness greater than 2 mm turned out to be unfeasible because of the excessive exposures required.

Thickness of lead shield, mm	Total number of discharges, n_0	Number of discharges accompanied by pulses, n	n/n_0 %
20	116	38	33
40	74	5	7
80	101	2	2
100	208	7	3

The average value of the energy of the radiation passing through the walls of the chamber was found to be 180 kev. The maximum energy value reliably indicated by the filter method was 230-250 kev. These data were obtained by irradiating the films with a large number of X-ray pulses, so that the blackening of the films lay on the linear part of the sensitivity curve. It is clear that these experiments give only a rough estimate of a lower limit on the maximum energy of the spectrum.

A considerably larger value for the spectral limit was obtained by the use of a scintillation counter of known efficiency. Each impulse from the output of the counter indicated the action on the crystal of one or more quanta emitted in a single discharge. The results of experiments with lead shields of various thicknesses are given in the table.

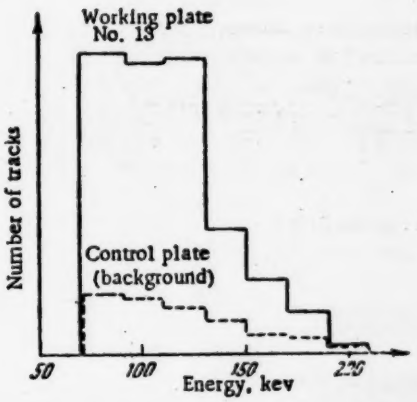

Fig. 3. Energy distribution of electrons, obtained from the examination of the tracks formed in a photographic emulsion irradiated with shielding by 2 mm of lead.

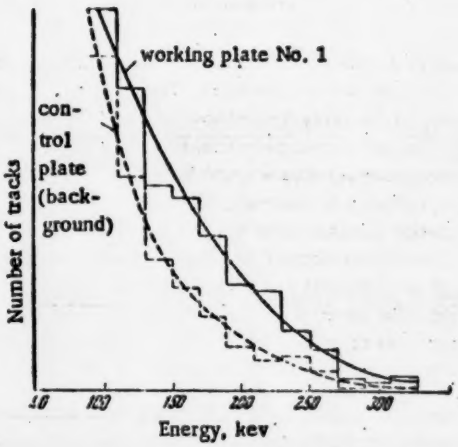

Fig. 4. Energy distribution of electrons, obtained from the examination of 1500 tracks formed in a photographic emulsion shielded by 20 mm of lead.

Besides a knowledge of the efficiency of the counter and of the geometry of the experiment, the analysis of these results requires the use of data on the intensity of the radiation. Measurements of the intensity, considered in greater detail below, showed that at each discharge an average of $5 \cdot 10^{10}$ quanta are emitted, but that individual pulses occur containing up to 10^{12} quanta. Calculations show that to explain the results of the experiments in question one must assume the presence in the spectrum of quanta with energies up to at least 800 kev. To make the data more reliable one would have to carry out a calibration of the counter using an X-ray tube operated in pulses; these experiments have not been performed.

The main difficulty arising in work with nuclear emulsions comes from the presence of extraneous tracks caused by cosmic radiation and natural radioactivity. In a number of cases the influence of this background was comparable with the effect of the radiation, and the following out of tracks of electrons with energies of several hundred kev in the presence of a large number of short tracks was a difficult and sometimes insoluble problem. Indeed, as is seen from Fig. 3, which shows the results of the study of a film shielded only by a layer of lead 2 mm thick, no appreciable increase above background could be observed for the number of tracks of electrons with energies above 200 kev. Longer tracks could be observed by the irradiation of a fresh electron-sensitive emulsion placed in a container with lead walls 20 mm thick. In this case the total length of the experiment came to some tens of hours, and the total number of discharges was about 250. Longer irradiation was found to be impracticable because of the increase of the cosmic-ray background. The results of a study of the experimental material are shown in Figure 4, which shows a distinct increase of the effect above background right up to electron energies of 250 kev. If the tracks are produced by recoil electrons, then the energy of the primary quanta must be at least 350 kev. In this range of energies the probability of Compton scattering of the quanta is about seven times as large as that of the photoelectric effect in the emulsion.

We did not succeed in observing the nuclear photoelectric effect in beryllium. From the negative result of this experiment it follows that quanta with energies above 1.66 Mev are not present to the number of more than $1\text{-}2 \cdot 10^7$ per discharge.

The combination of these measurements enables us to make the following assertion: the limiting energy of the X-radiation observed under the conditions in question is not less than 350 kev, but in all probability does not exceed 800 kev. It must be emphasized once more that although the spectral distribution curve has not been studied in detail it evidently makes a very flat approach to the axis of abscissas. Thus the concept of limiting energy is to some extent a question of definition.

We now give our attention to the results concerning the intensity of the radiation. As the experiments with the scintillation detector showed, under identical initial conditions the amplitude of the X-ray pulses varies from discharge to discharge by factors of some thousands, so that it is resonable to speak only of the intensity averaged over a large number of discharges. The measurement of the intensity of the radiation was obtained from the blackening of an X-ray film placed at some distance from the discharge chamber. The "effective" energy of the X-ray quanta was already known, so that there was no difficulty in choosing the conditions under which calibrating measurements were to be made. Unfortunately we cannot enter here into a detailed description of the experiments in question. In the determination of the total number of quanta use was made of the data on the spatial distribution of the radiation (cf. following section). The analysis of the experimental data showed that the average number of X-ray quanta obtained by the exposure of the film to the radiation from 150 discharges is about $5 \cdot 10^{10}$ quanta per discharge. Individual pulses were recorded with intensities up to 10^{12} quanta per discharge. The stated figures are obtained by conversion to quanta with average energy 200 kev. Additional confirmation of the correctness of these estimates is provided by the measurement of the intensity of the radiation from the number of tracks in emulsions.

The data considered above refer to discharges which were produced with the initial pressure of hydrogen corresponding to the maximum production of X-ray quanta. The dependence of the intensity of the X-radiation on the initial pressure, as determined by the scintillation method, is shown in Figure 5. The analogous dependence for the pulse of radiation at the start of the discharge has the form of a monotonically decreasing curve over the whole range of occurrence of the effect. It is interesting to note that the curve giving the dependence of the neutron radiation from a discharge in deuterium [4] on the initial pressure of the gas (see the dotted curve in the same diagram) does not differ significantly from the curve of the intensity of the X-rays.

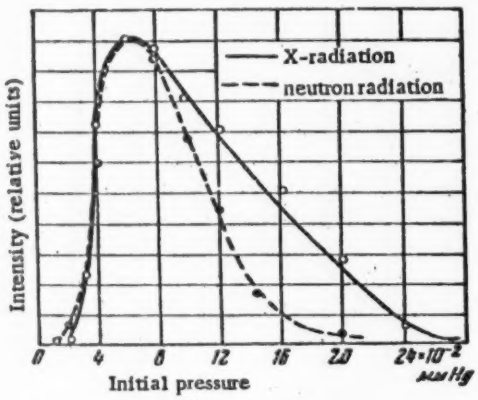

Fig. 5. Dependence on the initial pressure of the intensities of the X-ray and neutron radiations from a discharge in deuterium.

Hard X-radiation not connected with the start of the discharge is observed not only with discharges in hydrogen and deuterium, but also with discharges in helium.

The instant of appearance of the X-radiation from deuterium agrees with great precision with the instant of appearance of the neutron radiation. In the registration of the X-ray quanta accompanying discharges in deuterium by the scintillation method, the detector was placed at such a distance from the discharge chamber that the time interval between the instants of registration of X-rays and neutrons, caused by the time of flight of the neutrons, was greater than the width of the pulses. An oscillogram with X-ray and neutron pulses separated in time is shown in Figure 2f. In this case the second beam of the oscillograph indicates the pulse from the gas-filled counter. In Figure 6 the points show the measured dependence of the time of flight on the distance between the discharge chamber and the detector. The straight line in the diagram represents the dependence of the time of flight on the distance for the neutrons produced by the reaction (d, d).

X-rays were also observed from the discharge in such a heavy gas as xenon, but the energy of the quanta in this case did not exceed 10 kev. The addition of a small amount of xenon to hydrogen that was at such low pressure that the effect was not observed led to the appearance of radiation at a mass of the mixture that corresponds to the appearance of the effect from the discharge in hydrogen. Hard X-radiation was not observed from mixtures of light and heavy gases, even in cases in which as little as 0.1% of xenon was added to hydrogen at its optimum pressure. At the present time the dependence of the energy of the radiation on the properties of the gas in the chamber has not been thoroughly studied, but the authors propose to return to this question later.

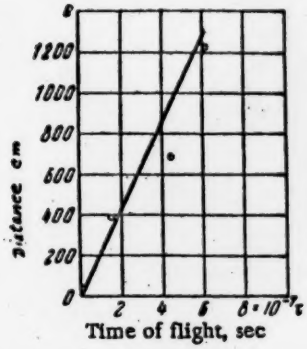

Fig. 6. Time of flight of neutrons emitted from the discharge in deuterium. The straight line shows the calculated time of flight.

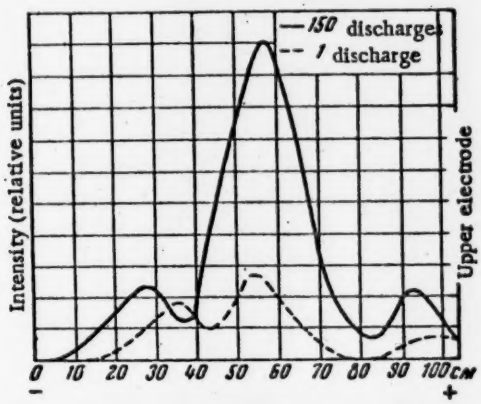

Fig. 7. Longitudinal distribution of intensity of the X-radiation for unsymmetrical flow of current on the feeders.

Spatial Distribution of the Radiation

The location of the sources of X-ray quanta along the axis of the discharge chamber has been studied by various methods.

In the first method the experiments were made with two scintillation detectors. One of the photomultipliers monitored the intensity of the X-ray pulse in the discharge in question; the second, provided with a collimator, registered the quanta originating in a certain limited part of the discharge chamber. The results of the experiment showed that the radiation originates both at the electrode that is at positive potential at the initial instant and in the middle portion of the discharge chamber.

In the second method the distribution function of the radiation along the axis was found directly by photometric measurements on an X-ray photograph of the discharge, which was obtained by means of a camera obscura made of lead. The distribution function shown in Figure 7 does not, however, enable us to judge the character of the distribution of the centers of emission of the X-rays in each individual discharge, since about 100 discharges were required for sufficient blackening of the film.

To test the possibility of producing a picture with each individual discharge we used an X-ray film between intensifying screens, which was placed beside the discharge chamber along one of its generators. In those cases when the intensity of the given X-ray pulse considerably exceeded the average value, one discharge was enough to produce the blackening required for photometric study of the film. The intensity of radiation along a generator of the chamber, $\Phi(z)$, is connected with the longitudinal distribution function by the relation

$$\Phi(z) = \int_0^l \frac{f(z')\,dz'}{r^2 + (z-z')^2},$$

where f(z) is the distribution function along the axis, r is the radius, and l is the length of the chamber. If $r \ll 1$, then the experimental values of $\Phi(z)$, obtained by photometering the film, will be fairly close to the desired function f(z).

Figure 7 shows together curves representing the results of photometric measurement of X-ray pictures obtained with a camera obscura and of photometering an X-ray film which had been placed along a generator of the chamber. As has been explained, the first curve gives the distribution function averaged over a large number of discharges. The second shows the function $\Phi(z)$ characterizing the longitudinal distribution for a single discharge. A comparison of the curves shows that the average longitudinal distribution function has just the same character as the distribution curve obtained in a single discharge.

Some of the experiments made to study the longitudinal distribution were carried out with an apparatus in which the copper cylinder surrounding the discharge chamber had openings for the introduction into the chamber of connecting sleeves and measuring cartridges. The openings in the cylinder disturb the uniform flow of

current, and it could be supposed that the complicated picture obtained under these conditions in the X-ray photograph is connected to a certain extent with departures from cylindrical symmetry. Indeed, experiments with a discharge chamber for which the distribution of current in the cylindrical feeder was more nearly uniform showed that the maximum at the center was considerably reduced in comparison with the maximum at the anode (compare Figures 7 and 8).

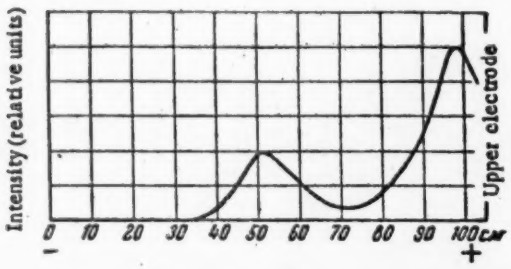

Fig. 8. Intensity distribution of the X-radiation along the axis of the discharge chamber (copper cylinder-feeder without openings).

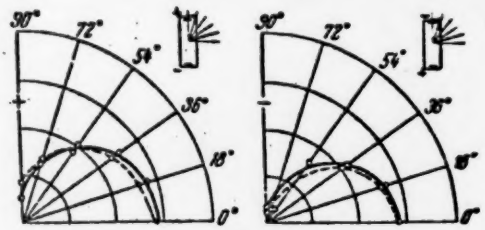

Fig. 9. Angular intensity distribution of the X-radiation, obtained by the scintillation method and the photographic method (dotted).

The angular distribution of the X-rays was also studied by two methods, scintillation and photographic. In the first case two scintillation detectors were used, shielded by a layer of lead 2 mm thick. During the whole experiment one of the photomultipliers remained in the same position, while the second registered the radiation emitted from the discharge chamber in various directions. Since the intensity of the radiation varies greatly from one discharge to another, at a fixed amplification in the registering apparatus there always occurred pulses whose sizes lay outside the range of registration. Therefore from the whole series of measurements there were selected for analysis only a limited number of classes. The distribution curve so obtained is shown in Figure 9. It could be suspected that this selective treatment of the results distorts the picture of the distribution. This objection does not apply to the photographic method, which averages the effect from a large number of discharges. Cassettes with X-ray films placed between intensifying screens were placed uniformly around a circumference whose center coincided with the center of the discharge chamber. The corresponding curves are shown in Figure 9 by dotted lines. The differences between the results obtained by the two methods are small and probably due to errors of measurement.

For the analysis of the results obtained we use the curves of the longitudinal distribution. Starting with the distribution function of the emission sources along the axis, f(z), the angular distribution was calculated on the assumption of isotropic emission of the quanta and with no account taken of absorption (cf. dotted curve in Figure 10). The complicated geometry, the uncertain localization of the emission centers, and the uncertainty of the energy spectrum of the radiation made it difficult to take the absorption into account quantitatively. We can, however, compare the relation of the calculated and experimental intensities at various angles of the two polarities (Figure 10). In this case the absorption takes place in roughly similar layers of matter and, in the case of isotropy of the radiation, the relations of the experimental and calculated intensities should be like one another. This is actually so for all points except that for the angle 72°, where the absorption depends very sharply on the position of the emission centers. The isotropy of the radiation gives one more evidence of the absence from the spectrum of any perceptible number of quanta with energy larger than 1 Mev.

A separate study was made of the question of the possability of the emission of radiation in the interior of the discharge chamber. The experiments were made with two scintillation counters. One of the devices, placed at cartridge No. 2 (cf. Figure 1), could detect radiation coming from part of the volume of the discharge chamber, and also those quanta that were produced at the flange of the porcelain sleeve located opposite cartridge No. 2. The second device, placed at cartridge No. 3, could detect quanta produced at the walls and the flange of the sleeve, but quanta coming from the interior could not reach it. Radiation coming from the interior volume could not be distinguished for the discharge in hydrogen, evidently because of the small stopping power of light

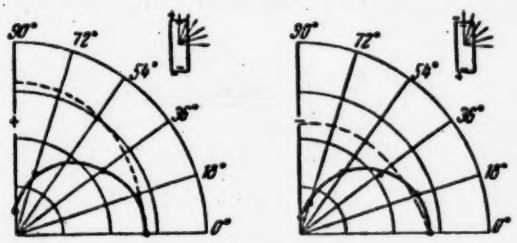

Fig. 10. Experimental angular intensity distribution of the radiation, and distribution calculated without taking account of absorption (dotted).

gases. The result was different for the discharge in xenon; here the pulses appeared only in the output of the multiplier placed at cartridge No. 2.

Discussion of the Results

We now give our attention to a possible explanation of the observed effect.

Specially arranged direct experiments, in which a 45 kev proton beam with current strength 10 milliamperes bombarded the wall of the discharge chamber, enable us to exclude a nuclear mechanism for the origin of the hard X-rays. Indeed, a gas-filled counter placed at the distance of 2.5 m from the target did not detect any increase of the count over the background without the beam. Thus, as was implicitly assumed in the preceding exposition, the radiation under investigation is the bremsstrahlung from electrons that have been accelerated in the electric field that occur in the discharge.

In principle the electrons can obtain the necessary energy either by cyclic acceleration in induced electric fields arising from the growth of the magnetic field, or by a single passage through large potential differences that occur for short times in the discharge.

Let us consider the first of these possibilities. Experimental investigation of pulsed gas discharges shows that in a number of cases the lines of current flow are curved. The longitudinal field produced by this induces an electric field, in which there can occur a gradual acceleration of electrons. Suppose that during the time τ the longitudinal magnetic field changes from the value $H = 0$ to H_{max}; then a simple calculation shows that an electron at a distance r_0 from the axis receives an energy

$$W = 7 \cdot 10^{-9} \frac{r_0^2 H_{max}^{3/2}}{\tau^{1/2}} \text{ ev}$$

Measurements have shown [5] that the maximum longitudinal magnetic field does not exceed 500 oersteds. We make the most generous estimate, taking $r_0 = 8$ cm and $\tau = 1$ microsecond, corresponding to the duration of the X-ray pulse; this gives $W = 5 \cdot 10^3$ ev*. The value obtained for W allows us to exclude this mechanism of acceleration. We note that in the calculation an asymptotic value for W was used, since $\tau \gg mc/eH$.

A considerable longitudinal potential difference can arise in the discharge chamber for a short time as a result of sufficiently rapid redistributions of the current density. The strong magnetic field of the current, however, will oppose the acceleration of electrons in the entire region of the discharge, with the exception of a small part of the space near the axis. The lines of the induced electric field are closed, and the corresponding potential differences cannot be registered in the measurement of the voltage across the electrodes of the chamber.

If one places inside the discharge chamber a wire circuit in a plane passing through the axis, then one can measure instantaneous values of $d\Phi/dt$, and consequently also instantaneous values of the electric field intensity near the axis. Experiments of this sort have recently been carried out [5] with a discharge of helium in an apparatus with a different geometry. Here in a number of cases an electric field of considerable magnitude was

* If we consider acceleration of the electrons during their motion in a spiral along the lines of force of the magnetic field, then we find larger values of the energy received, but these are still clearly insufficient for the explanation of the experimentally observed energy of the X-ray quanta.

observed; its direction coincides with that of the discharge current. Electrons accelerated by this field move to the anode, where, according to the data on the longitudinal distribution, the maximum of the radiation is indeed observed (cf. Fig. 9). At the instant of time corresponding to the appearance of the X-ray pulses the difference of potential determined from the experimental values of $d\Phi/dt$ reaches 80 kv. Of course, this value is markedly different from the estimate we have given for the limiting energy of the X-rays, and only further experimental investigations can confirm or disprove the hypothesis of the acceleration of electrons in strong electric fields arising because of the rapid redistribution of the discharge current density. But X-radiation was not observed.

The authors regard it as their pleasant duty to express their gratitude to L. A. Artsimovich for valuable discussions, and also to S. A. Chuvatin for aid in carrying out the experiments.

LITERATURE CITED

[1] K. H. Kingdon and H. E. Tanis, Phys. Rev., 53, 128 (1938).

[2] E. M. Reikhrudel, A. V. Kustova, and A. G. Zimlev, J. Tech. Phys. (USSR) XIV, 1779 (1955).

[3] I. M. Podgornyi, Doklady Akad. Nauk SSSR, 108, 5, (1956).

[4] L. A. Artsimovich, A. M. Andrianov, E. I. Dobrokhotov, S. Yu. Lukyanov, I. M. Podgornyi, V. I. Sinitsyn, and I. V. Filipov, Atomic Energy, 1956, No. 3, 375*.

[5] A. M. Andrianov, O. A. Bazilevskaya, and Yu. G. Prokhorov (to be published).

* Consultants Bureau Translation pagination.

SOLAR BATTERIES

(ON THE DIRECT TRANSFORMATION OF RADIANT ENERGY INTO ELECTRICAL ENERGY BY MEANS OF PHOTOELEMENTS)

V. S. Vavilov

Consideration is given to the possibilities of direct transformation of the energy of solar radiation into electrical energy by means of semiconducting photoelements. Brief descriptions are given of the main electrical and optical properties of germanium and silicon, and of methods for producing them and controlling their electrical properties by the introduction of small amounts of impurities. The principle of action of photoelements with electron-hole junctions is discussed, and the basic parameters determining their spectral sensitivity and efficiency are indicated. Data are presented on the action of experimental solar batteries as generators of current.

Introduction

In the course of the next ten or twenty years atomic electric stations will come to be the source of an important part of the electrical energy necessary for the people's economy of our country. Regions remote from the usual sources of energy will acquire the means of rapid development of industry and culture.

It must not be forgotten, however, that besides large power plants it is extremely important to have simple and long-lived sources of modest amounts of electrical energy that do not require technical servicing and can provide power for portable and stationary radio stations, intermediate amplifiers in telephone lines, and lighting for homes.

One of the ways to produce such generators is the use of semiconducting thermal batteries, proposed by Academician A. F. Ioffe and being successfully developed in the Soviet Union.

In the present paper we shall consider another means of direct transformation of radiant energy into electrical energy – the use of semiconducting photoelements. We note that in this case direct use is made of the energy developed by a natural "thermonuclear reactor" – the sun.

The fact that barrier-layer semiconducting photoelements can be used as "generators" of electric current has been known for almost 70 years, from the time of the discovery of the valve photoelement by W. A. Ulianin in 1888 [1]. But up to the most recent times the efficiency of conversion of solar energy by semiconducting photoelements (for example, the widely known selenium elements) did not exceed tenths of a percent, and the use of photoelements was confined to laboratory practice or, at best, to devices producing electrical power of the order of microwatts (for example, photoelectric exposure meters).

The investigation of the basic properties of semiconductors, such as the mechanism of electron and "hole" conductivity, the lifetimes of carriers of charge in crystals of a semiconductor, and the rectification of current at contacts between semiconductors, has made it possible to predict the properties of photoelements of germanium and silicon and in practice to achieve conversion efficiencies up to 11 percent, i. e., to obtain more than 100 watts of electrical power from 1 m^2 of surface directly illuminated by the sun's rays.

Some Properties of Semiconductors Used in Solar Batteries

The basic element of a solar battery is a crystal of a semiconductor, containing two regions with different mechanisms of electrical conductivity separated by a sharp boundary, which has received the not entirely fortunate name of "electron-hole (n-p) junction".

A crystal of silicon, as used in solar batteries, consists of a combination of atoms; each of them is surrounded by four neighboring atoms, with which it is connected by valence bonds; none of the valence electrons of a regularly periodic crystal is able to take part in the transfer of electric charge. Like their "relative", diamond, pure germanium and silicon, free from impurities and structural defects, would be insulators at and below room temperature. The introduction of trifling amounts (10^{-5}%) of impurity atoms of elements of groups III and V of the Mendeleev system makes it possible to control the mechanism of electrical conductivity and the specific resistance in various regions of the crystals.

As an example we consider a silicon crystal containining at one of its lattice points an atom of arsenic, which has five valence electrons. In this case four electrons are "bound" by the bonds holding the atom at the lattice point, and one remains "free" and, because of thermal agitation, wanders about in the crystal; its weak connection with the arsenic atom comes into play only when the temperature is greatly reduced. Thus if in a silicon crystal of volume 1 cm^3 there are 10^{15} atoms of arsenic among the $5 \cdot 10^{22}$ atoms of silicon, the concentration of free electrons (negative charge carriers) is also nearly 10^{15} cm^{-3}, and in a germanium crystal, where the fifth electron of arsenic is still more weakly bound, it is just 10^{15} cm^{-3}.

By using impurity atoms with three valence electrons, one can produce crystals of silicon or germanium in which the electric current will be carried, as it were, by positive charges. This sort of conductivity is called hole conductivity, according to the following conception of the transfer of charge.

A trivalent atom (for example, of boron) replacing a silicon atom at a lattice point, does not have a sufficient number of electrons to fill the valence bonds with the neighboring atoms. The missing bond is supplied by the capture of an electron from one of the neighbors, i. e., by the formation of a "hole" (absence of an electron in a neighboring atom). Successive transitions of electrons from atom to atom can be regarded as displacements of a positive carrier of charge in the opposite direction. The boron atom, remaining immovable at the lattice point, is charged negatively. The simplified scheme considered above of course does not explain many peculiarities of the mechanism of electrical conductivity in semiconductors, in particular the large mobility of "holes" in their motion in an electric field or their diffusion inside the crystal. One must not lose sight of the fact that although the conception of "hole" conductivity provides a correct interpretation of experimental results, in the final analysis it is only a convenient way of describing the behavior of an "incomplete set" of electrons in the crystal. The assignment to the "hole" of a positive charge, electronic mass, and mean free path between collisions of the order of 10^{-5} cm makes it possible to calculate the average distances that this disturbance of the crystal structure travels in diffusion or in its drift motion in an electric field. Since the processes of diffusion and drift are the main phenomena considered in the theory of semiconducting devices, the conception of "holes" is here an entirely suitable one.

The main types of admixtures and the values of the mobilities of electrons and "holes" in "doped" semiconductors – silicon and germanium – are given in Tables 1 and 2.

The phenomena considered above, connected with the presence of impurity atoms in the crystal, explain the electrical conductivity of a semiconductor under equilibrium conditions. The action of solar batteries is connected with departures from equilibrium, consisting in the appearance of excess electrons and "holes" through the absorption of radiation by the semiconductor. Photons with energies exceeding 1.12 ev (i. e., infrared rays of wavelength shorter than 1.1 microns, and visible light) transfer their energy to the silicon crystal, freeing bound

TABLE 1

Properties of "Doped" Semiconductors, Si and Ge

Chemical admixtures	Carriers of charge	Type of conductivity
Donors (+) (elements of the fifth group)	Excess (free) electrons (-)	Electron
Acceptors (-) (elements of the third group)	"Holes" (+) .	"Hole"

TABLE 2

Mobilities in cm/sec per volt/cm in Single Crystals Containing Not More Than 10^{-5}% Admixture

	Electrons	"Holes"
Silicon	1250	250
Germanium	3600	1700

(valence) electrons; the free electrons and "holes" that thus appear act as additional carriers of charge. These electrons diffuse in the crystal until the time when recombination takes place, i. e., the disappearance of an electron from the "conduction zone" and of a "hole" from the valence zone; the energy thus released usually goes into the thermal vibrations of the crystal. The presence of certain impurities that do not act as donors or acceptors can cause a considerable increase of the probability of recombination [8], which manifests itself in a decrease of the diffusion length traversed on the average by electrons or "holes", which is given by

$$L = \sqrt{D\tau} = \sqrt{\frac{\mu kT}{q}},$$

where τ is the average lifetime of the charge carriers before recombination, D is the diffusion coefficient of the carriers, μ is the mobility of the carriers, q is the charge of the electron, k is Boltzmann's constant, and T is the absolute temperature. The magnitude of L is the most important characteristic of the purity and perfection of structure of a crystal of a semiconductor, and to a considerable extent determines the efficiency of semiconducting converters of radiant energy.

Rather large diffusion lengths of the carriers, reaching several millimeters, are observed only in very perfect single crystals of semiconductors. Although the making of photoelements of high efficiency requires only that the diffusion lengths be not less than 0.2-0.5 mm, it is not feasible to use semiconductors in the form of layers deposited by chemical means or by sputtering. These layers always have a polycrystalline structure, and the boundaries between the grains are places of disturbance of the periodic structure and increase by a large factor the recombination of the excess electrons and "holes".

We now pass on to the properties of electron-hole "junctions" (boundaries), which are the basic elements of semiconducting electronic devices. Consider such a "junction", more accurately a boundary between regions inside one whole crystal of semiconductor. It can be produced in the following way. A large crystal is grown from molten material (germanium or silicon). Into the melt is lowered a small crystal (a seed or "primer"). If the temperature is then lowered a bit and at the same time the primer is raised, the material solidifies, beginning at the boundary of the partially melted primer. Successive layers or rows of atoms follow the original orientation of the primer crystal. Suppose at the beginning of the growth the melt consisted of the pure substance with an admixture of donor atoms. Then at a certain moment of the growth acceptors are added to the melt. After the whole crystal is grown and cooled, a piece is cut out, containing the boundary separating the region enriched with donors from that in which the concentration of acceptors exceeds that of donors. Figure 1 shows such a crystal. In the right-hand part of it there occurs the phenomenon of compensation, which is extremely important from the point of view of the technology of semiconducting devices. It might be supposed that this part would contain a number of carriers of charge – electrons and "holes" – corresponding to the sum of the concentrations of both admixtures. But because of recombination a dynamic equilibrium is established, and there remains only an excess concentration of "holes" sufficient to make this part of the crystal electrically neutral. Thus for the artificial preparation of crystals with an n-p junction it is not necessary to remove the admixture of one type in order to use the addition of the other admixture to give part of the crystal the desired type of conductivity. For this it is sufficient to introduce the quantity of the admixture required to neutralize the original admixture of the other type, plus a certain excess. Later, in connection with the description of the technical construction of solar batteries, we shall return to the methods used in practice for the introduction of admixtures.

The boundary between the regions with different conductivities is not visible to the eye and is not associated with a change of the mechanical properties of the silicon or germanium. The concentrations of the admixtures are so small that if we go from atom to atom along one of the crystal axes, in the extent of the whole crystal only a few hundred atoms will be donors or acceptors instead of atoms of the original substance. For one donor or acceptor there are 10-100 million atoms of the main substance.

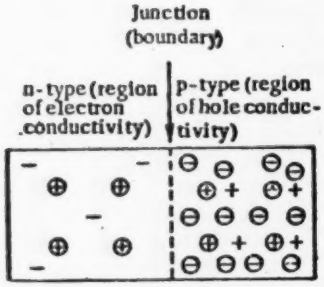

Fig. 1. A crystal of a semiconductor with an electron-hole junction, in which the p-region is formed by means of recombination.

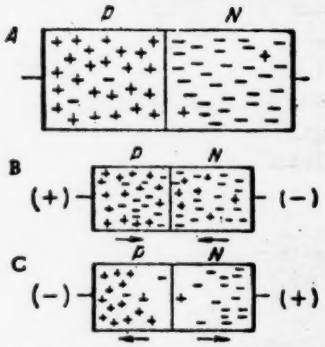

Fig. 2. Rectification of current in a crystal with an n-p junction.

It is very probable that the germanium and silicon used in present-day semiconducting devices are the purest chemical substances ever prepared in the solid state. The concentration of impurities in the purest specimens of such crystals does not exceed the concentration of a gas in a vessel at a pressure of the order of 10^{-9} mm Hg. The usual chemical methods for control of impurities are of course useless for the detection of such quantities. They are estimated from the conductivity of the crystal, the mobilities of the electrons and "holes", and the diffusion length of the carriers.

A basic property of n-p junctions is their ability to rectify an electric current. This property is due to the presence of a region of space charge forming a potential barrier for electrons and "holes," whose height can approach the "width of the forbidden zone", i. e., the minimum amount of energy necessary for the freeing of one of the electrons, i.e., the formation of a "hole"-electron pair. We shall give a qualitative picture of the phenomena that account for the rectification of current by a crystal of semiconductor with an n-p junction.

We consider Fig. 2, which shows the distribution of charge carriers near an n-p junction. In case A there is thermal equilibrium (the applied potential difference is zero). In case B the current flows in the "right" direction; case C corresponds to "reversed" current. The diagrams show only the carriers of charge and not the impurity atoms — donors and acceptors. In case A there are some "holes" in the region of electron conductivity, and in the hole region there are a few electrons. The number of these electrons and "holes" is determined by the conditions of thermal production, i.e., mainly by the energy required for the production of a "free" electron and by the temperature of the crystal.

If the negative pole of a battery is attached to the region of electron conductivity, this region becomes energetically a little less favorable for electrons and more favorable for "holes"; the height of the potential barrier is decreased. Some of the electrons penetrate into the region of hole conductivity, and some of the "holes" into the region of electron conductivity. For a sufficient potential difference in the external circuit the barrier disappears completely and the crystal transmits a considerable current density in the "right" direction.

Figure 2 B illustrates the case in which the crystal with an n-p junction "blocks" the current.

The electric field applied from outside tries to remove electrons and "holes" from the boundary region. Penetration of the charge carriers into a "foreign" region cannot occur. A very weak "reverse" current flows in the external circuit because of the few electrons and "holes" that are liberated by thermal agitation near the n-p junction. The number of liberated "holes", and consequently the reverse current, is the smaller, the lower the temperature and the larger the minimum energy E_g that is necessary for the freeing of an electron from the system of "valence bonds" in the crystal. For germanium this energy is 0.75 ev, and for silicon 1.12 ev; because of the exponential dependence on $\left(-\frac{E_g}{kT}\right)$ the reverse current of a silicon rectifier is smaller than for germanium one. The reverse currents of semiconducting rectifiers with n-p junctions in single crystals remain unchanged with changes of the external voltage over wide ranges (up to hundreds of volts).

Solar Batteries – Silicon Photoelements with Electron-"Hole" Junctions*.

If by electrical energy we mean the energy of electrons in the crystal, then a direct conversion of solar energy into such energy occurs in the act of absorption of photons and formation of electron-"hole" pairs. But if there is no n-p junction near the region of absorption of the light, the only result will be an increase of the concentration of carriers of charge (photoconductivity).

Let us consider the diagram of the energy states in a semiconductor near an n-p junction; it explains the working principle of a photoelement capable of transforming energy.

In Figure 3 are shown the conduction zone and the zone of valance binding, separated by the forbidden zone. It is seen from the diagram that in the region of the n-p junction there is a potential barrier, whose height V_k can be nearly E_g.

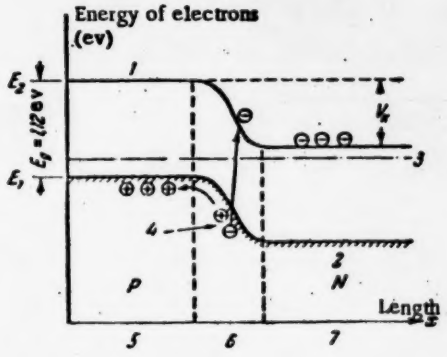

Fig. 3. Energy diagram of an n-p junction in silicon. 1) Conduction zone; 2) valence zone; 3) Fermi limit; 4) production of an electron-"hole" pair through absorption of a photon or ionization by a fast particle; 5) region of hole conductivity; 6) region of n-p junction; 7) region of electron conductivity.

The non-equilibrium electrons and "holes" (those produced by absorption of radiation) diffuse to the region of the n-p junction. We may say that the potential barrier of the n-p junction "separates" them, i. e., the electrons freely pass into the region of electron conductivity, charging it negatively, and the "holes", passing into the "hole" region, charge it positively. Owing to the changing concentration of change carriers the height of the potential barrier V_k is decreased. If the external circuit is open, a dynamic equilibrium is established between the primary diffusion current of excess carriers and the current in the opposite direction caused by the accumulation of a space charge of "holes" in the p-region and of electrons in the n-region. If the external circuit is shorted, the whole diffusion current passes through it, and in the intermediate case there is a division of the currents between the external circuit and the interior of the crystal. As before, the sum of these currents is equal to the diffusion current, which can in general be written:

$$I = q\alpha N,$$

where N is the total number of pairs of carriers generated by the radiation and α is a quantity smaller than unity, which may be called the coefficient of utilization of the carriers [6]. The quantity α is determined by the absorption coefficient of the radiation, the diffusion lengths L_n and L_p of electrons and "holes", the rate of surface recombination of carriers, and the geometry of the photoelement. In the simplest case, when the dimensions of the crystal exceed the diffusion lengths and the radiation is absorbed uniformly (the generation does not depend on the coordinates) and, moreover, only in the electron region, we have

$$I_d = qNL_p$$

(in this case I_d is the density of the diffusion current and N is the number of pairs generated per cm^3 per sec). Questions connected with the geometry and the coefficients of absorption and recombination are considered in more detail in references [5] and [7].

In Figure 4 is shown an approximate equivalent circuit of an element of a solar battery. The diffusion current I_d, equal to the current at short circuit, is caused by the absorption of radiation. Thus current divides: a

* The properties of germanium photoelements with n-p junctions are described in references [2-4]. The question of the conversion of the energy of nuclear radiations by means of semiconductors is considered in reference [5], and also in a survey article [6].

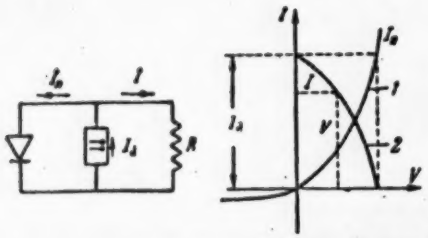

Fig. 4. Equivalent circuit, and voltage-current and load characteristics of a semiconducting converter of radiant energy.
1) Voltage-current characteristic of the n-p junction; 2) load characteristic:

$$I_n = I_0\left(e^{\frac{qV}{kT}} - 1\right),$$
$$I = I_d - I_0\left(e^{-\frac{qV}{kT}} - 1\right).$$

part of it equal to I passes through the circuit of the load R, and the other part, equal to I_n, is caused by the reverse passage of carriers through the junction; the corresponding part of the developed energy is lost.

The current I_n can be calculated by the usual formula for the voltage-current characteristic of an n-p junction:

$$I_n = I_0\left(e^{\frac{qV}{kT}} - 1\right),$$

where V is the difference of potential at the output of the element.

The internal resistance of such an element is thus a function of the current through the load, and consequently of the size of the load. The expression for the limiting value of the efficiency of the energy converter can be written in a simple form if we assume that $\alpha = 1$, i. e., that there is no recombination. In this case all the non-equilibrium carriers that are produced diffuse through the n-p junction. If in the original process (photoelectric effect, ionization) the energy W is expended in the formation of a pair of carriers, then, since the potential difference is equal to V and the fraction of the current going into the load R is equal to $\frac{I}{I_d}$, the efficiency η can be expressed in the following form:

$$\eta = \frac{qV}{W} \cdot \frac{I}{I_d} = \frac{qV^2}{RWI_d}.$$

In the conversion of the energy of monochromatic light

$$W = h\nu,$$

i. e., the whole originally absorbed energy is expended in the formation of an electron-"hole" pair, but the excess energy $h\nu - E_g$ is ordinarily lost, going into the thermal vibrations.

From the equivalent circuit and voltage-current characteristic of the n-p circuit as given above, it follows that the maximum potential difference V_0 depends on the temperature, the zero-voltage resistance R_0 and the diffusion current I_d in the following way:

$$V_0 = \frac{kT}{q} \ln\left(\frac{qI_dR_0}{kT} + 1\right),$$

where R_0 is related to the saturation current I_0 of the n-p junction:

$$I_0 = \frac{kT}{qR_0}.$$

From the expression given it is clear that the voltage V_0 is primarily determined by the current I_d (i. e., by the intensity of the incident radiation) and the resistance R_0. It is obvious that n-p junctions in silicon, where the saturation currents are very small (of the order of 10^{-7}-10^{-8} amp/cm^2) are decidedly preferable to those in

germanium, in which the saturation currents are usually [5] 10^2-10^3 times greater. This difference is mainly due to the greater width of the forbidden zone in Si (1.12 ev) as compared with Ge (0.75 ev).

It has been shown theoretically that the efficiency of silicon photoelements with n-p junctions for the conversion of solar radiation (for normal incidence of the sun's rays), for elements at the temperature 25°C, can reach 18%. A slight cooling, (for example, to 0°C) leads to an increase of the efficiency [5]. It would seem that a still greater increase of the efficiency could be achieved by increasing the intensity (for example, by means of lenses) and lowering the reflection coefficient, which for silicon comes to 28%. But it must be taken into account that at large concentrations of excess carriers of charge their lifetime decreases [8], which leads to a slowing of the growth of the efficiency with the intensity [6]. A lowering of the reflection coefficient by the known interference method (non-reflecting coatings) is possible only in a rather narrow wavelength interval and obviously can give only a small advantage in the conversion of solar energy.

Photoelements that have received the name "solar batteries" were constructed in 1954-1955. They consist of silicon crystals of large area (up to 4 or 5 cm^2 per element) with n-p junctions located very near the surface on which the radiation falls (Fig. 5). The part of the solar radiation that is most effectively converted is absorbed in a surface layer of depth of the order of 25 microns. The problem of obtaining single crystals of silicon with the necessary diffusion length of electrons and "holes", not less than 0.2-0.5 mm, presents great difficulties up to the present time, and has been successfully solved only on a small scale. For this purpose use is made of complicated chemical methods of purification and a final purification by melting by zones without a crucible, and also growing the single crystals in crucibles of specially prepared quartz in an atmosphere of hydrogen or inert gases.

Another technical difficulty is the application of a surface electrode that is transparent for visible and infrared radiation.

This problem , as well as the obtaining of the n-p junction itself at the required distance from the surface of the crystal, was solved by an application of a method of thermal diffusion of the impurity atoms. According to the data [10], the best results were obtained by the use of diffusion of boron, which is an acceptor, into n-silicon at a temperature near the melting point of silicon (1400°C). One of the possible methods consists of prolonged heating of plates of n-silicon (containing arsenic) in an atmosphere of a gas containing boron. The depth of the diffusive penetration of the boron is determined by the temperature and the duration of the heating. Near the surface the silicon is strongly saturated with boron atoms and becomes a hole semiconductor with very low resistance, so that the need for a special electrode is obviated. The concentration of boron falls with increasing distance from the surface, and at a depth of 2-3 microns it becomes equal to the initial concentration of arsenic. The boundary corresponding to compensation determines the position of the n-p junction. After the plate is cooled the distribution of the impurity atoms, and consequently the position and properties of the n-p junction, remain completely fixed, since the rate of diffusion of impurities at any working temperature of the element is negligible. In one of the surfaces of the plate a depression is made by honing, after which metal electrodes are applied by sintering or sputtering (Fig. 5). An important condition for obtaining high efficiency is the low rate of surface recombination, which is achieved by etching the surface of the silicon. So that the quantity α will not decrease during long subsequent operation, the complete photoelements are enclosed in flat protective cases of plastic, transparent for visible and infrared radiation (Fig. 6). In some varieties use is made of immersion in transparent liquids, or of filling the cases with gases, to preserve optimum conditions at the surface of the silicon [9].

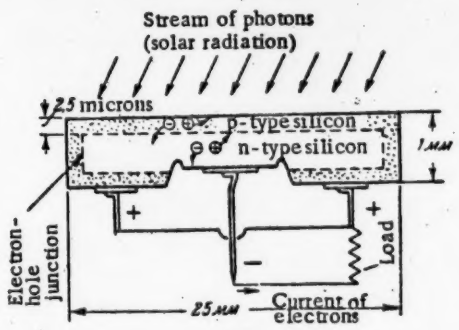

Fig. 5. Section of an element of a solar battery.

In order to show the characteristics of the silicon photoelement as a receiver of the solar radiation coming to the earth's surface, we consider Fig. 7, which shows three curves. Curve A shows the distribution of energy in the solar spectrum in relative units. This distribution is drawn from data taken in clear weather with the sun at the

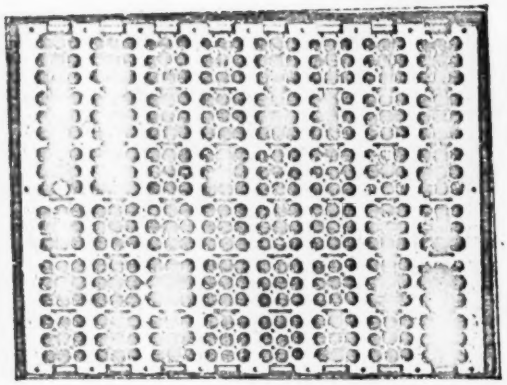

Fig. 6. Solar battery composed of 432 silicon photoelements. Useful output power, 10 watts. Limiting potential difference, about 200 volts.

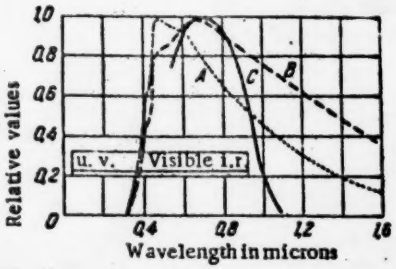

Fig. 7. Spectral characteristics of a silicon photoelement.
A) Distribution of energy in the solar spectrum; B) distribution of number of photons in the solar spectrum; C) sensitivity of a silicon solar battery operated at short circuit.

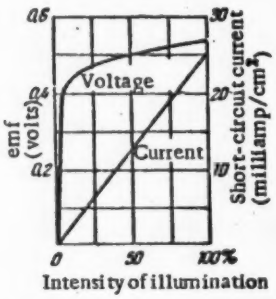

Fig. 8. Dependence of the emf and short-circuit current of a silicon photoelement on the conditions of illumination at 25°C. 100% means direct illumination by the sun's rays.

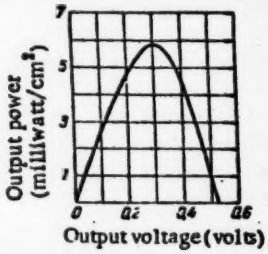

Fig. 9. Load characteristic of a silicon photoelement.

zenith. Curve B is obtained from A by multiplying the latter by the wavelength λ; it gives the relative numbers of photons present in various portions of the spectrum. Curve C shows the sensitivity of a silicon photoelement (for current at short circuit). This curve was obtained by means of a monochromator, from the exit slit of which equal amounts of energy were sent to the photoelement at various wavelengths. Then the values of the sensitivity (i. e., the values of the short-circuit current) were multiplied by the relative values of the energy flux in the solar spectrum for the same wavelengths.

We recall that at the left side of the diagram the energies of the photons are large, and the number corresponding to a given energy flux is smaller.

Photons with energy below 1.12 ev pass through the silicon crystal without producing any electron-"hole" pair. The excess energy of photons of higher frequencies is expended uselessly in heating the silicon. Besides this, part of the energy is lost because of the fact that the production of electrons and "holes" is particularly large near the very surface of the crystal, i. e., in the region of increased recombination rate, owing to structural defects and surface impurities. According to the data [9] the maximum conversion efficiency in silicon photoelements occurs at $\lambda = 0.75\ \mu$, at the boundary between the visible (red) and the infrared parts of the spectrum. It is interesting that this wavelength corresponds almost exactly to the maximum number of photons in the spectrum of solar radiation (cf. curve B of Fig. 7). Thus for a location of the n-p junction near the surface, a silicon photoelement is very close in its spectral sensitivity to a receiver that is ideal from the point of view of

the conversion of solar energy. Because clouds and fog are relatively transparent for infrared rays, solar batteries continue to work in cloudy weather, though indeed with somewhat lower efficiency.

In Figure 8 is shown the dependence of the emf and the short-circuit current of a silicon photoelement on the conditions of illumination at 25°C. The load characteristic of a similar photoelement is shown in Fig. 9; in this case the abscissas are potential differences across the load for various values of the load resistance. The

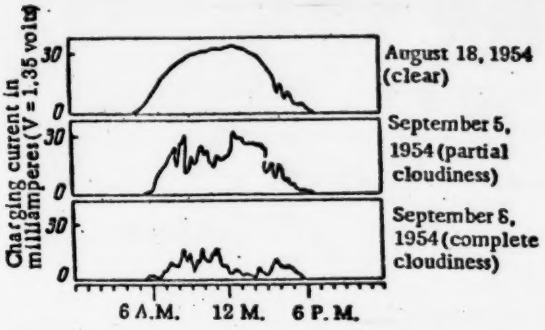

Fig. 10. Operation of an experimental solar battery with various conditions of illumination.

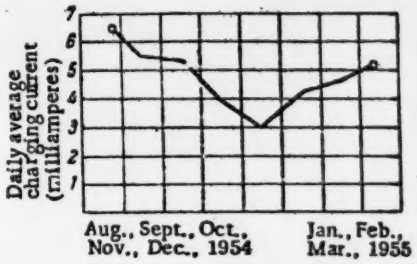

Fig. 11. Average charging current from an experimental battery of area 10 cm^2 over a long period of time.

load characteristics for smaller illuminations have their maxima at nearly the same values of the voltage – about 0.3 volts per element. This means that a receiver requiring constant input voltage, for example a storage battery, can be used in combination with a solar battery over a wide range of conditions of illumination.

From the point of view of practical use, great importance is attached to data on the operation of sources of electrical power, such as solar batteries, for long periods of time. Rather a short time has passed since the construction of the first experimental models, but nevertheless we can present the experimental results, from which some estimates can be made.

In Figure 10 are shown curves characterizing the action of a small experimental battery (area about 10 cm^2) under different conditions of illumination. The curve in Figure 11 gives daily averages of charging current from such a battery for nearly 7 months, and graphically shows the lowering of the daily average charging current with shortening of the days, and the growth of the current after the winter solstice.

There can be no doubt that in the course of the next few years there will be developed simple and sufficiently cheap methods for producing semiconducting photoelements with large areas and high efficiencies, after which the direct conversion of solar energy will take its proper place in "small-scale energetics".

LITERATURE CITED

[1] W. A. Ulianin, Wied. Ann., 34, 241 (1888).

[2] S. M. Ryvkin, J. Tech. Phys. (USSR) 25, 21 (1955).

[3] Zh. I. Alferov, B. M. Konovalenko, S. M. Ryvkin, V. M. Tychkevich, and A. I. Uvarov, J. Tech. Phys. (USSR) 25, 11 (1955).

[4] V. S. Vavilov and L. S. Smirov, Reports at the Eighth All-Union Conference on Semiconductors, 1955 (in the press).

[5] W. Pfann, and W. van Roosbroeck, J. Appl. Phys., 25, 1422 (1954).

[6] V. S. Vavilov, Prog. Phys. Sci., 56, 111 (1955).

[7] R. Cummerow, Phys. Rev., 95, 16 (1954); 95, 561 (1954).

[8] W. Shockley, and W. Read, Phys. Rev., 87, 835 (1952).

[9] D. Chapin, C. Fuller, and G. Pearson, Bell. Labs. Record, 33, 241 (1955).

[10] D. Chapin, C. Fuller, and G. Pearson, J. Appl. Phys., 25, 676 (1954).

DECOMPOSITION OF PLUTONIUM OXALATES BY INTRINSIC ALPHA RADIATION

V. V. Fomin, R. E. Kartushova and T. I. Rudenko

Decomposition of the oxalates of tri-, tetra- and hexavalent plutonium was studied in air and in a vacuum at room temperature and −80° both under illumination and in darkness. It was found that the decomposition is caused by alpha radiation from the plutonium, but in the oxalates of tetra- and hexavalent plutonium the carbon monoxide which is formed acts as a reducing agent which transforms the tetravalent plutonium to the trivalent form and the hexavalent to the tetravalent. The oxalates are then transformed into carbonates and, apparently, also partially into oxides or an oxyoxalate-carbonate mixture.

In the study of the properties of tetravalent plutonium oxalate it was discovered that protracted storage in air at room temperature is accompanied by a change of color and loss of weight. The decomposition products were analyzed by combustion in oxygen as described in reference [1].

The results of a few analyses are given in Table 1. These show that the oxalate disintegrates during storage, as the relative content of oxalate ions and of water decreases and the amount of plutonium increases. When the residues formed after storage of tetravalent plutonium oxalate for a few months are treated with acid a gas is liberated. The plutonium content of the resulting solutions is much larger than would follow from the solubility of $Pu(C_2O_4)_2 \cdot 6H_2O$. From these experiments it may be concluded that the oxalate is transformed into a carbonate during storage.

A more detailed investigation was begun of the transformation of stored plutonium oxalate not only for tetravalent plutonium but also for trivalent $Pu_2(C_2O_4)_3 \cdot 9H_2O$ and in part for $PuO_2(C_2O_4) \cdot 2H_2O$.

For the purpose of determining the cause of this transformation and the composition of the products a chemical analysis was made of the transformation products, the absorption spectra* of the compounds was studied both in the solid state and in solutions and observations were made of the pressure changes of the gases liberated from oxalates stored in a vacuum. Absorption spectra were taken for oxalates of tri-, tetra- and hexavalent plutonium and their decomposition products when stored in air and in a vacuum at room temperature for various periods of time. The measurements were made at the temperature of liquid nitrogen with a triple prism glass spectrograph (ISP-51). The microphotograms of the absorption spectra were taken with a recording microphotometer.

In the case of the solid salts a thin layer of the preparation was placed between two watch glasses. A comparison of the absorption spectra (Fig. 1) of freshly prepared trivalent plutonium oxalate with the products of its transformation shows that the latter retained the absorption bands which are characteristic of the initial compound. Some changes of band structure, in particular the disappearance of individual sharp components,

* The spectrophotometric studies were made by L. V. Lipis.

Table 1

Change of Composition of Tetravalent Plutonium Oxalate as a Function of Time of Storage

Storage period (months)	Weight (g)	Content (%)		
		Pu	CO_2	H_2O
2	0.0131	58.8	29.0	12.2
2	0.0212	57.0	28.0	14.8
3	0.0088	61.96	27.0	12.0
3	0.0108	62.31	26.5	13.2
4	0.0084	64.0	24.0	–
6	0.0166	68.3	17.1	8.8
6	0.0158	69.5	17.4	8.2
17	0.0261	73.5	10.7	5.8

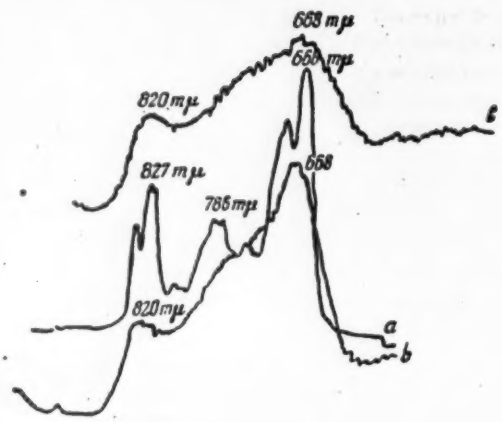

Fig. 1. Microphotograms of a portion of the absorption spectrum of trivalent plutonium oxalate and of its decomposition products.

a) For a freshly prepared oxalate of trivalent plutonium; b) for an oxalate stored in air for 2 months; c) for an oxalate stored in a vacuum for 17 months.

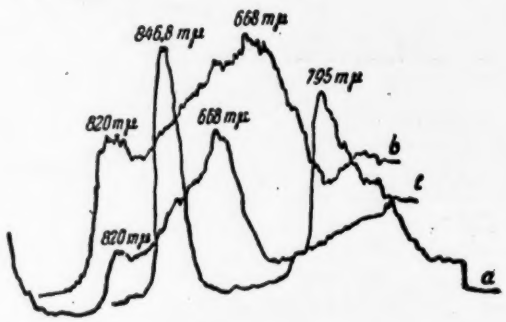

Fig. 2. Microphotograms of a portion of the absorption spectrum of tetravalent plutonium oxalate and of its decomposition products.

a) For a freshly prepared oxalate of tetravalent plutonium; b) for an oxalate stored in air for 2 months; c) for an oxalate stored in a vacuum for 17 months.

evidently result from the loss of water of crystallization and from the transformation of the oxalate into a new compound. The valence of the plutonium in the resulting compounds does not change.

For tetravalent plutonium oxalate (Fig. 2) the absorption spectra of the decomposition products no longer agree with the spectra of the freshly prepared specimen.

After limited storage in air and prolonged storage in a vacuum there is a clear reduction of tetravalent plutonium to the trivalent form. However, a visual study of the absorption spectrum of a specimen which was kept in air for 17 months showed that the plutonium was mainly in the tetravalent state. This can be explained by subsequent oxidation of the previously formed trivalent plutonium.

The microphotograms (Fig. 3) show that when the hexavalent plutonium oxalate is stored a change of valence also takes place.

This can be determined from the disappearance of the band which is characteristic of hexavalent pluto-

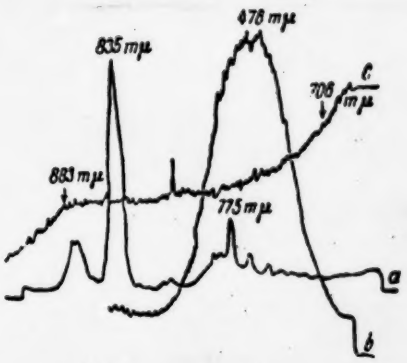

Fig. 3. Microphotograms of a portion of the absorption spectrum of hexavalent plutonium oxalate and of its decomposition products.

a) For a freshly prepared oxalate of hexavalent plutonium; b) for an oxalate stored in air for 2 months; c) for a solution of the decomposition products of hexavalent plutonium oxalate stored in a vacuum for 17 months.

nium. In the sulfuric acid solution of a specimen which had remained in a vacuum for 17 months the absorption spectrum revealed the characteristic band of tetravalent plutonium near 480 mμ.

The decomposition of the oxalates of tri- and tetravalent plutonium may be due to photochemical reduction, but this explanation can hardly apply to trivalent plutonium oxalate. Another cause may be the action of alpha radiation from the plutonium.

The effect of light was first studied. For this purpose tetravalent plutonium oxalate was put into ampoules which were kept in darkness for a year. Analysis showed that the change of composition was similar to the change observed following storage under light. Consequently, light is not important for the decomposition of tetravalent plutonium oxalate.

It is easily calculated that if all the energy of alpha radiation from plutonium is absorbed by the oxalate and that the decomposition of a molecule requires 100 ev, the rate of decomposition should be about 0.4% of the oxalate per day. Therefore it is entirely possible that the observed decomposition is caused by alpha radiation. In order to verify this, experiments were performed in which tetravalent plutonium oxalate was kept in evacuated vessels at room temperature and at −80°C. Samples (containing 50 mg of plutonium) of freshly prepared oxalate were placed in suspended quartz test tubes which were then put into a glass vessel connected with a mercury manometer. The air pressure was reduced to 10^{-3} mm Hg and the vessel was sealed. The initial position of the mercury was recorded and the pressure was measured periodically. During two weeks at −80°C no liberation of gases was observed. After two weeks the vessel containing the oxalate was heated to room temperature at which it was maintained for two hours. The pressure then rose to 107 mm; following this the vessel was again cooled to −80°C. The pressure fell to 75 mm, which is in satisfactory accord with the lowered temperature.

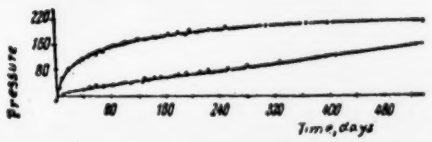

Fig. 4. Changes of pressure during decomposition of plutonium oxalates over a period of 17 months.

I) Tetravalent plutonium oxalate; II) trivalent plutonium oxalate.

After a week at −80°C the pressure had not changed. The cooling was then discontinued and the pressure rose to 132 mm at room temperature. The pressures of 107 and 132 mm correspond to pressures obtained in a parallel experiment at room temperature, although in the latter case the pressure rose gradually. Therefore we conclude that the decomposition of an oxalate at −80°C proceeds at the same rate as at room temperature but that the liberated gases are not separated from the crystals because of a slow diffusion rate.

In our opinion, this experiment shows that the decomposition of tetravalent plutonium oxalate results from alpha radiation. As a confirmation we performed experiments with sodium oxalate. This latter compound was carefully mixed with finely pulverized plutonium dioxide. The powder was stored for two months. Analysis showed that a portion of the sodium oxalate had been converted into the carbonate.

These results for the decomposition of the oxalates by alpha rays are confirmed by the experiments of Bertold Stech [2]. The latter used x-rays to examine sodium oxalate which had been subjected to alpha radiation and concluded also that it had been converted into the carbonate.

In order to obtain an idea of the rate of spontaneous decomposition of the plutonium oxalates, experiments

Table 2

Quantity of CO_2 and CO Formed by the Decomposition of Trivalent and Tetravalent Plutonium Oxalates (the samples of oxalates contained 50 mg of plutonium and were stored for 17 months)

Substance	Quantity of gas (g)	
	CO_2	CO
Trivalent plutonium oxalate	0.0030	0.0010
Tetravalent plutonium oxalate	0.0090	0.0013

Table 3

Decomposition Products of Tri- and Tetravalent Plutonium Oxalates

Initial Compound	Content (%)			
	Pu^{+3}	C_2O_4	CO_3	H_2O
Trivalent plutonium oxalate	61.6	17.35	7.5	11.2
Tetravalent plutonium oxalate	66.7	15.7	10.8	6.25

were performed in which the trivalent and tetravalent plutonium oxalates were kept in evacuated vessels, as described above, but at room temperature. The decomposition was observed for 17 months. The observed pressure changes are shown in Fig. 4, where the measurements made at various temperatures are reduced to 0°C. The volumes of the vessels were 30 and 27.6 ml; the specimens of the oxalates contained approximately 50 mg of plutonium.

The curves show the possibility of making a qualitative comparison of the decomposition rate of plutonium oxalates of different valences. It is seen from a comparison of the curves that the pressure in the case of the tetravalent plutonium oxalate increased more rapidly during 2 months than for the trivalent plutonium oxalate. After 17 months a constant pressure had not been reached but the rate of pressure changed as compared with the first few days had been considerably slowed down (0.1 mm per day instead of 4 mm). It is difficult to obtain a numerical value for the rate of decomposition from the data since the pressure is caused not only by the carbon monoxide and carbon dioxide formed through decomposition but also by water vapor formed through the efflorescence of crystal hydrates and by the products of their decomposition.

The conversion of an oxalate into a carbonate should lead to the formation of carbon monoxide in an excited state, which can reduce hexavalent plutonium into the trivalent and tetravalent forms. To verify this assumption we determined the quantity of carbon dioxide and carbon monoxide accumulated in the sealed ampoules when the oxalate was kept for 17 months. The results are shown in Table 2.

From Table 2 it can be seen that the relative amount of carbon monoxide in the experiments with trivalent plutonium oxalate is considerably larger than for the tetravalent form.

A number of analyses of the decomposition products were performed; the content of plutonium, C_2O_4 and water were determined by Penfield's combustion method [3] using Berg's buret [4] and potentiometric titrimetry with potassium permanganate. To measure the carbon dioxide the specimen was dissolved in sulfuric acid through which oxygen was blown after being purified of organic impurities, carbon dioxide and moisture. The oxygen and carbon dioxide formed as a decomposition product entered a flask for titration which was filled with $Ba(OH)_2$ titrant, where the carbon dioxide combined with the barium carbonate, which was then separated by filtering. The remainder of baryta water was back-titrated in a 0.1 N solution of HCl.

For the titrimetry it was assumed that all of the plutonium had the same valence; the oxalate content was determined from the difference between the quantity of permanganate used in titrating the hot solution and the quantity required to oxidize the plutonium. The average decomposition products obtained after 17 months storage of the oxalates at room temperature are shown in Table 3.

It follows from Table 3 that the composition of these products can be expressed by the formulas

$$Pu(C_2O_4)_{0.76}(CO_3)_{0.47}O_{0.27}H_2O$$

$$Pu(C_2O_4)_{0.64}(CO_3)_{0.65}O_{0.2}H_2O_{0.35}$$

for initial trivalent and tetravalent plutonium oxalates, respectively.

The oxygen content was determined from the condition of saturation of all plutonium valence bonds.

Thus, a chemical analysis shows that under irradiation the plutonium oxalates are gradually transformed into carbonates and later, apparently, into oxides. There is the possibility of formation of mixed oxyoxalates or oxycarbonates as well as oxalate-carbonates.

When the tetravalent plutonium oxalate is kept in air at room temperature for 17 months the decomposition is comparatively more complete. In this instance the specimen contained: PuO_2 - 83.6%; C_2O_4 or CO_3 - 10.7% (not separated) and H_2O - 5.8%.

The reducing activity of the carbon monoxide leads to the result that during the same time interval the number of decomposing C_2O_4 groups in the tetravalent plutonium oxalate is almost twice as large as in the trivalent form, per mole of plutonium.

LITERATURE CITED

[1] M. O. Korshun and N. E. Gelman, New Methods of Elementary Microanalysis, State Tech. Press, 1949.

[2] Bertold Stech, Z. Naturforsch. 2, 175 (1952).

[3] S. L. Penfield, Am. J. Sci. (3) 48, 30 (1894).

[4] A. G. Berg, Factory Lab. 10, 1171 (1948).

A STUDY OF THE IODIDE PROCESS OF REFINING ZIRCONIUM*

THE LOWER ZIRCONIUM IODIDES AND THE EFFECT OF TETRAIODIDE PRESSURE ON THE RATE OF METAL DEPOSITION

V. S. Emelyanov, P. D. Bystrov and A. I. Evstyukhin

It was shown in Part I that the rate of zirconium deposition is determined principally by the tetraiodide vapor pressure in the reaction tube and is only slightly dependent on the temperature of the raw metal. However, the experimental data was insufficient to explain the nature of the influence exercised by the tetraiodide vapor pressure on the rate of metal deposition. For the purpose of solving this problem we especially need more reliable information concerning the lower zirconium iodides since it is quite obvious that the latter play an important part in the refining process and under certain conditions may even determine the entire course of the process. We discuss below the principal experimental results obtained from an investigation of the conditions for formation of the lower iodides in the reaction tube and their roles in the preparation of zirconium iodides.

Formation of Lower Iodides on the Raw Metal Surface

According to Fast [1] zirconium iodide is formed on the surface of powdered zirconium at 400°C, while at 560°C the diiodide is formed.

Döring and Moliere [2] explain the observed dependence of the rate on the tube temperature by the formation of the lower iodides on the surface of the raw metal. On the other hand, Rainor [3] believes that this dependence can be explained by a change of pressure in the tube rather than by the formation of a lower iodide on the raw metal. These writers [2, 3] do not report any specific data on the characteristics and conditions for the formation of the lower zirconium iodides in the reaction tube, and their conclusions regarding the role of these iodides in the preparation of zirconium by the iodide method are apparently based on indirect observations.

In our experiments, after the refining process we almost always found on the surface of the raw zirconium rod a deposit of a lower iodide which was black, brown-black or sometimes blue-black in color.

Chemical analysis showed that the deposit on the zirconium rod which was formed at comparatively low reaction tube temperatures (300-500°C) was close in composition to the triiodide. The composition of samples of the lower iodide in different experiments fluctuated considerably. Experiments on the dissociation of the lower iodides, which will be described in another article, showed that these fluctuations are caused by the existence of a broad range of solid solutions on a triiodide lattice base. These experiments indicated that zirconium triiodide dissociates at a considerably lower temperature than the diiodide and that, consequently, at sufficiently high temperatures and low pressures of the tetraiodide not ZrI_3 but ZrI_2 should be formed on the surface of the raw zirconium. In fact, the lower iodide which was near ZrI_2 in composition was obtained at a zirconium rod temperature of 620°C and tetraiodide pressure of about 25 mm Hg.

* Part II. Part I was published in Atomic Energy 1956, No. 1, 43.

Lower Iodide Formation on the Surface of a Heated Zirconium Rod

The lower zirconium iodides are not only formed on the surface of the raw metal. We have also observed the formation of a lower iodide on the surface of an incandescent zirconium bar.

This phenomenon is similar to that observed by Runnols and Pidgeon [4] in a study of the iodide process for titanium.

The formation of a lower iodide on the surface of the rod can be explained as follows. When a reaction tube containing a large excess of the tetraiodide is heated, then at a sufficiently high tetraiodide pressure (which, as we shall see below, depends on the temperature of the rod) puffs of "smoke" appear around the zirconium rod which soon cloud up the entire tube. As the tetraiodide pressure is raised the rate of formation of this smoke increases. When this process continues for a long time the current through the rod begins to drop, thus indicating dissolution of the bar. When this process ends the tube contains a certain quantity of very fine black or brown-black powder which has settled on the bottom. Chemical analysis showed that the powder was close in composition to the triiodide. In this instance, just as in the case of the triiodide formed on the surface of the raw metal some deviations from the stoichiometric composition were observed. We performed a series of experiments for the purpose of determining the nature of this new phenomenon.

1. Effect of the material of the rod on the formation of the lower iodide.

When a tungsten wire was used instead of the zirconium rod no formation of a lower iodide was detected in the tube. From this one can conclude that the formation of a lower iodide is the result of some reactions on the surface of the heated zirconium rod. This is supported by the fact that the rod is dissolved in the formation of a lower iodide.

2. Role of the raw metal.

If the lower iodide is formed by a reaction on the surface of the rod it may be assumed that the presence of the raw metal is not required. An experiment performed in the absence of raw metal (the rod had been coated) confirmed this. Thereafter all experiments on the production of a lower iodide were performed without the presence of raw metal.

3. Effect of the tetraiodide vapor pressure in the tube and of the rod temperature on the formation of a lower iodide.

Preliminary experiments showed that the lower the tube temperature (and, consequently, the lower the tetraiodide vapor pressure), the lower was the rod temperature at which the first "smoke" puffs appear.

For a more exact determination of the mutual dependence of the rod temperature and tube pressure an ordinary reaction tube was used with an auxiliary tubular section for providing tetraiodide vapor pressure. After coating of the rod the raw metal was removed, the tube was washed with water and again evacuated and then filled with the tetraiodide in sufficient quantity to provide a saturated vapor at the temperature of the experiment. Following this the tube was placed in a furnace and heated to 450°C. The end of the auxiliary tube was maintained at a lower temperature (from 300 to 430°C), which determined the tetraiodide vapor pressure in the tube. Each temperature was maintained for 1 to 1.5 hours in order to establish equilibrium in the tube. During this time the rod was maintained at a somewhat higher temperature.than the temperature at which the lower iodide appeared.

When stability had been achieved the bar temperature was gradually dropped until the first puffs of smoke appeared; this temperature was registered. The temperature of the bar was then again raised by 20-30° and maintained until the smoke disappeared from the tube. The rod temperature was again lowered and we determined the time of appearance of the lower iodide. In this way a few temperatures were obtained for the same tetraiodide vapor pressure. The average temperature was taken as the temperature of appearance of the lower iodide. This temperature will be designated briefly hereafter as the "critical temperature" (t_{cr}) and the corresponding pressure will be called the "critical pressure" (P_{cr}).

The data obtained from these experiments is presented in Fig. 1. From the preceding discussion it follows that the region above the curve corresponds to the operating conditions for the normal process (the rod is coated); the region below the curve corresponds to operating conditions for the formation of the lower iodide (the bar dissolves).

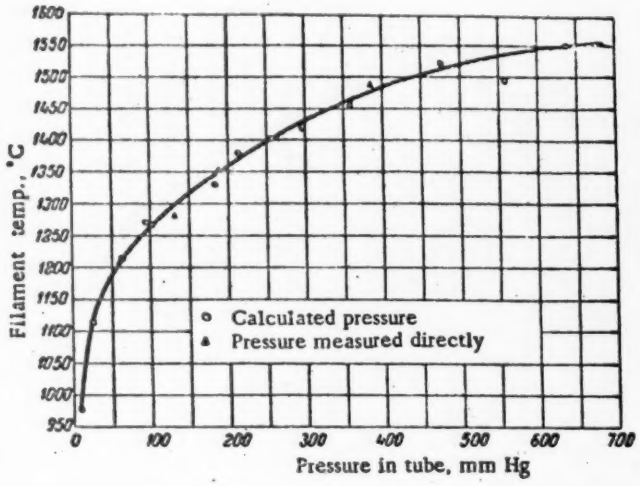

Fig. 1. Temperature of rod at which lower iodide appears as a function of the tetraiodide vapor pressure in tube.

It should be noted that at low tetraiodide pressures and, consequently, at comparatively low rod temperatures the formation of the lower iodide proceeds very sluggishly and it is very difficult to determine the critical temperature by the method described above. Therefore the onset of the formation of the lower iodide at small tetraiodide pressures was fixed not by the appearance of the first smoke puffs but by the darkening of the thin quartz tube fastened over the bar. Upon the appearance of the lower iodide the bright quartz tube was darkened by the deposition of particles of the lower iodide.

In most experiments the tetraiodide pressure has been determined by a calculation [5]. Some experiments involved direct measurements of the pressure in the tube. For this purpose a quartz manometer in the form of a flat thin-walled spiral was sealed into the tube in which the lower iodide was formed. The corresponding experimental values are represented by triangles in Fig. 1.

Formation of Crystalline Deposits of the Lower Zirconium Iodide on the Rod

When the formation of the lower iodide has proceeded for a long time another interesting phenomenon is observed: the lower iodide is formed not only as a very fine powder which settles to the bottom of the tube but also begins to accumulate around the rod itself forming a sort of sheath after a time, through which the bar can hardly be seen. This covering is retained when the tube is cooled. Its shape varies — at times it is cylindrical, at other times it is flat. Fig. 2 shows a tube with two such flat "flags". In external appearance this lower iodide differs from the powdered form by the fact that in this instance the iodide has a pronounced crystalline form. However, x-ray analysis shows that both products are identical and their external difference apparently results from the difference in the conditions under which they are formed.

Nature of the Processes on the Rod

The phenomenon described above can be explained very simply if it is assumed that the formation of the lower iodides takes place not only on the surface of the raw metal but also around the surface of the hot zirconium rod.

As a result the gas phase on the surface of the hot zirconium rod will consist of ZrI_4, I, I_2, ZrI_3 and ZrI_2 vapors close to thermodynamic equilibrium (since the temperature of the rod is high and the reactions apparently take place very rapidly).

Because of the different concentrations of the gaseous components continuous diffusion occurs at the surface of the rod and at the surface of the raw metal: the molecules of the lower iodides and of iodine diffuse to the raw metal. With increased distance from the rod the temperature of the gaseous mixture drops so that its molecular composition undergoes change: the lower iodides react with the iodine in the reaction

$$ZrI_3 + [I] \rightleftharpoons ZrI_4 \qquad (1)$$

$$ZrI_2 + 2[I] \rightleftharpoons ZrI_4. \qquad (2)$$

There are three possible cases:

1. Small tetraiodide vapor pressure in the tube. There is a correspondingly small concentration of lower

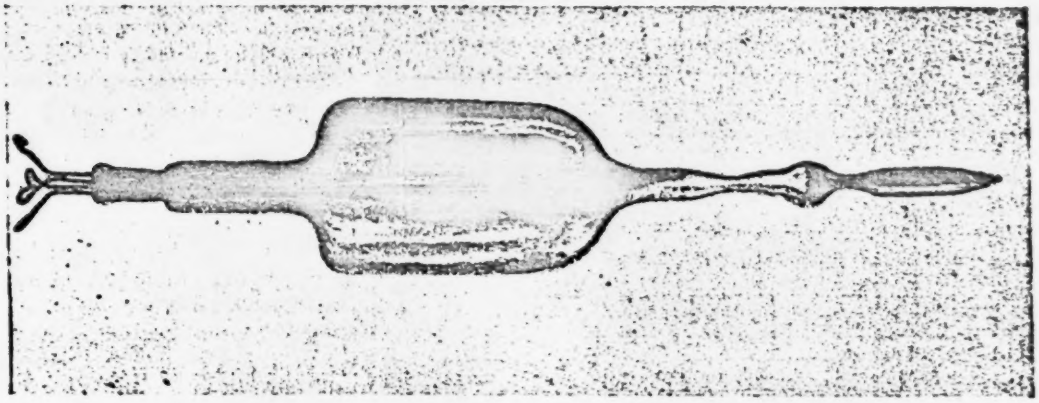

Fig. 2a. Reaction tube which shows a lower zirconium iodide forming flat hollow "flags" on zirconium wires.

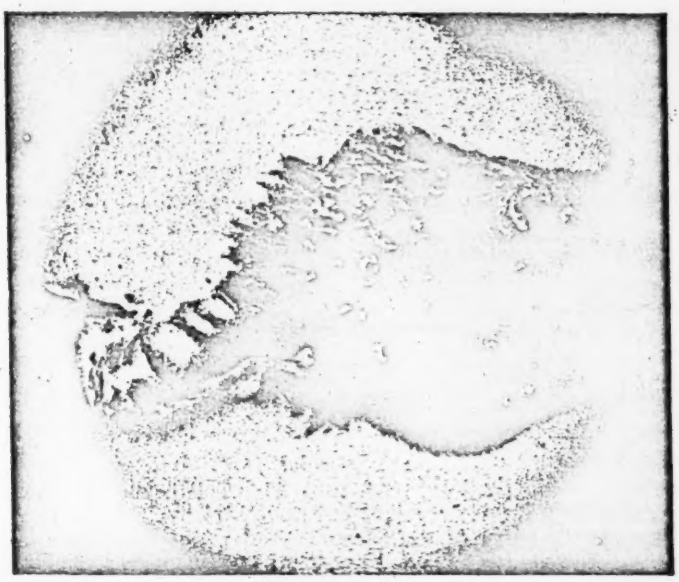

Fig. 2b. Accumulation of lower iodide at end of rod.

iodide vapor on the surface of the heated rod. In this case with increasing distance from the rod the lower iodides practically disappear by reacting with the iodine, while some portion of the free iodine remains. This "residual" iodine reaches the surface of the raw metal and accomplishes its transfer to the rod.

2. With a rise of tetraiodide vapor pressure the partial pressures of the iodine and lower iodides around the surface of the rod will be increased. As can be seen from the graphs given below, at comparatively high tetraiodide pressures the iodine pressure increases much more slowly than the diiodide pressure*. At a certain tetra-

* This also holds true for the triiodide.

iodide pressure the equilibrium pressures of the iodine and lower iodides will be such that at a distance from the rod these substances will practically disappear and only the tetraiodide will remain in the gas phase. The number of iodine molecules which will reach the raw metal will drop to zero and the transfer of the metal will be completely halted. The tetraiodide vapor will then be at the critical pressure.

3. With further increase of tetraiodide vapor pressure the zirconium rod begins to dissolve and the lower iodides are formed in such quantity that in the flow from the rod there will not be sufficient iodine for their complete binding and the excess of lower iodide vapor will be borne from the rod by convection currents, forming the smoke which we observed.

According to the experiments, the greater the difference between the actual pressure in the tube and the critical pressure, the greater the excess of lower iodides formed and the more rapid the formation of the smoke should be. The experimental relationship $P_{cr} = f(t_{cr})$ can be explained by the fact that increased rod temperature increases the equilibrium iodine concentration around the rod, in connection with which, as follows from the above discussion, the critical pressure should rise.

Although the final product of the processes taking place at the surface of the zirconium rod is the triiodide, this does not mean that the triiodide is formed immediately around the surface of the rod. It is possible (and also, as we shall see below, more probable) that zirconium diiodide is formed at the surface of the rod and that the triiodide is a secondary product formed at some distance from the rod by the reaction

$$ZrI_2 + ZrI_4 \rightleftharpoons 2ZrI_3 \qquad (3)$$

The formation of a macrocrystalline mass of lower iodide on the rod takes place, we believe, as follows. At the onset the surface of the heated rod is smooth. The lower iodide vapor formed at a small distance from the rod condenses in extremely fine particles which are borne from the rod by convection currents. As the dissolution of the rod proceeds its surface becomes more and more "dirty" -- small scales of an oxide film and, possibly, other impurities appear on it. The ends of such scales can stand out from the rod to such a distance that their temperature is lower than the condensation temperature of the lower iodide vapor. These "cold" scales can become condensation centers of the lower iodide. Consequently, in this case the condensed lower iodide is not removed from the rod but begins to accumulate at some distance therefrom. Growing gradually, such condensation nuclei finally cover the entire rod. This process usually begins at the ends of the rod but cases have been observed in which the black lump of lower iodide was formed in the middle of the rod.

The accumulation of lower iodide on the rod gradually sinks lower under the influence of gravity and as a result of evaporation of the lower iodide around the surface of the rod. As a result the lower iodide forms a flat hollow flag. The crystalline form of this flag can be explained by the higher temperature (and consequent greater molecular mobility) at which this form of the lower iodide is produced.

In our opinion, this is the nature of the processes which occur on the surface of the zirconium rod.

In conclusion we consider it necessary to point out the following fact. Since in the work by Rainor to which we have referred he does not report dissolving of the rod we can conclude that in his experiments the tetraiodide pressure never exceeded its critical value. This confirms, in particular, our earlier hypothesis based on other data, that Rainor's optimum quantity of iodine is many times greater than the amount actually present in the gas phase in his experiments.

We recall that according to Rainor the optimum quantity of iodine is about 82.5 g per liter of volume of the tube when the temperature of the latter is 460°C. This should correspond to a tetraiodide pressure of about 3 atmospheres, which is about 40 times greater than the critical pressure at a rod temperature of 1200°C.

Effect of Tetraiodide Vapor Pressure on Rate of Deposition

1. Role of the lower iodides on the raw metal surface

If the lower iodides actually passivate the raw metal surface, this effect can have two different causes:

1) The reaction of the lower iodide with iodine proceeds rapidly, but the equilibrium iodine pressure near the raw metal surface covered with the lower iodide is high, being commensurable with the iodine pressure around the rod.

2) The iodine equilibrium pressure is low but iodization proceeds slowly. The iodine diffusing from the rod

cannot react with the raw metal and its pressure on the surface of the latter again becomes commensurable with the iodine pressure around the rod.

In both instances the increased iodine pressure around the raw material results in a decreased concentration gradient of the diffusing substances and, consequently, to a decreased rate of transfer of zirconium to the rod.

We performed experiments which showed that the cause does not lie in the iodization rate of the triiodide. In these experiments the original material was zirconium triiodide. The process occurred in a tube containing two tungsten wires on one of which zirconium had been deposited to a diameter of about 1.5 mm. The other tungsten wire was left uncoated. In this tube, just as in the experiments on the preparation of the lower iodide, we introduced a large quantity of zirconium tetraiodide.

At a tube temperature of 450°C the coated wire was heated up and a layer of triiodide appeared on the bottom of the tube; the tube temperature was then lowered to 150-350°C and the usual deposition of zirconium took place on the second wire.

The dependence of deposition rate on tube temperature* found in this way agrees with the usual curve obtained by using a zirconium rod as raw material.

This shows that the triiodide interacts with the iodine just as easily as does metallic zirconium. Thus the possibility of passivating the raw material with the triiodide only amounts to shifting the equilibrium in reaction (1) strongly to the left.

We performed an experimental estimate of the order of magnitude of the free iodine pressure around the surface of the heated rod and at the surface of the raw material. For this purpose we inserted into the usual reaction tube a capillary whose length and diameter were such as to ensure a sufficient flow of vapor from the tube into an ampoule cooled by liquid nitrogen, without greatly disturbing equilibrium in the tube.

The end of the capillary in some of the experiments touched the surface of the zirconium rod and drew off the gas from the surface of the heated rod and from its immediate vicinity. In other experiments the capillary was lowered to the raw metal.

Before the beginning of an experiment the collecting ampoule was separated from the tube by a thin diaphragm which was fractured after the required conditions had been established in the reaction tube.

The condensate in the collecting ampoule consisted of the tetraiodide and iodine. From its weight and from the tetraiodide pressure in the tube, which was given by the temperature of the end of the auxiliary tube, we were able to calculate the iodine pressure.

The removal of gas from the surface of the raw metal proceeded at a tetraiodide pressure of 13 mm; the rod temperature was 1300°C. The rate at which the process took place was very low - about 4 a/hr. According to the passivation hypothesis this would mean that the iodine pressure near the raw metal was high and comparable with the iodine pressure near the rod.

However, the quantity of iodine which flowed into the collecting ampoule in this case was negligibly small, so that the iodine pressure at the raw metal surface was calculated to only about $4 \cdot 10^{-3}$ mm. At lower tetraiodide pressures the iodine pressure should be still lower.

The removal of gas from the surface of a rod at 1300°C rod temperature showed that at a tetraiodide pressure of $3.5 \cdot 10^{-1}$ mm the free iodine pressure is only $4 \cdot 10^{-4}$ mm, i.e., two orders higher than at the raw metal surface.

This set of data is a basis for assuming that under normal refining conditions the formation of lower iodides on the raw metal surface does not result in its passivation and does not directly affect the rate of metal deposition on the rod. The lower iodides have an indirect effect: the binding of the tetraiodide in a lower iodide leads in the end to the disappearance of the excess of solid tetraiodide and to lowered pressure in the tube; this in turn results in a changed rate of zirconium deposition.

* Triangles in Fig. 5, see Part I (Atomic Energy 1956, No. 1, 43).

2. Role of the lower iodide formed at the surface of a heated zirconium rod

The formation of a lower iodide near the surface of a heated zirconium rod can be considered in the last analysis to be the result of the fact that a portion of the molecules of the tetraiodide dissociate only to a lower iodide rather than to the free metal. The number of molecules which dissociate to the free metal is correspondingly reduced with consequent reduction of the rate of metal deposition on the rod.

The slower rate of deposition can also be treated as a result of the fact that when formation of the lower iodides occurs not all of the iodine liberated at the rod surface can reach the raw metal, since a portion is bound in the lower iodides upon entering colder regions of the tube. These are essentially two aspects of a single phenomenon.

In order to determine how great a role is played by the lower iodides formed on the rod under normal refining conditions (low tetraiodide pressures), it is necessary to obtain quite precise thermodynamic data concerning the lower zirconium iodides. At the present time such data are not available. We have performed an approximate calculation which permitted only a rough estimate of the effect of the processes at the rod on the rate of zirconium deposition. The following assumptions served as a basis for the calculation:

1. The gas phase in the immediate vicinity of the rod surface is in thermodynamic equilibrium with the metal.

2. The published thermodynamic data [6] for zirconium tetraiodide are correct. This assumption is based on the fact that our experimentally derived partial iodine pressures near a heated zirconium rod are very close to the values obtained by calculation from such data.

3. The partial triiodide pressure is so small that it can be neglected; it is then assumed that the gas phase at the surface of the heated zirconium rod consists of ZrI_4, ZrI_2 and [I][the partial pressure of the molecular iodine is also negligibly small, as shown by a calculation). This assumption is also based on the fact that, as indicated in [6], zirconium triiodide is unstable in the gas phase.

The pressure of atomic iodine was found from the data of [6] by the condition $P_I = \sqrt[4]{kP_{ZrI_4}}$, where k is the equilibrium constant of tetraiodide dissociation:

$$ZrI_4 \rightleftharpoons Zr + 4[I].$$

In order to determine the partial diiodide pressure we made use of the fact that for all experimental points of the curve $P_{cr} = f(t_{cr})$ (see Fig. 1) the following condition must be satisfied approximately*:

$$P_{ZrI_2} = \frac{P_I}{2}.$$

On the basis of these assumptions we calculated the equilibrium composition of the gas phase at the rod when heated to 1500° K for different tetraiodide pressures. The results are shown in Fig. 3.

It follows from the discussion above that the section of a vertical line between the two curves corresponds to the pressure of the "residual" iodine. In Fig. 4 the dependence of the residual iodine pressure on the tetraiodide pressure near the rod is shown separately (constructed from the data of Fig. 3). As we see, the residual iodine pressure increases sharply at low tetraiodide pressures and attains a maximum at about 4 mm Hg, after which it drops slowly to zero at the critical tetraiodide pressure.

The question arises as to whether the decreased rate of zirconium deposition with increased tetraiodide pressure is due to the formation of lower iodides at the surface of the heated zirconium rod. We advanced this hypothesis previously [7].

To what extent this is the case can be determined only after a more detailed investigation of the processes occurring at the surface of the rod. Our thermodynamic calculation is based on considerable simplifications and it is reasonable to assume that the results cannot serve as a sufficient basis for any definite quantitative conclusions.

* The approximate nature of this condition follows, in particular, from the fact that it assumes identical flow rates from the rod for both iodine and the lower iodide.

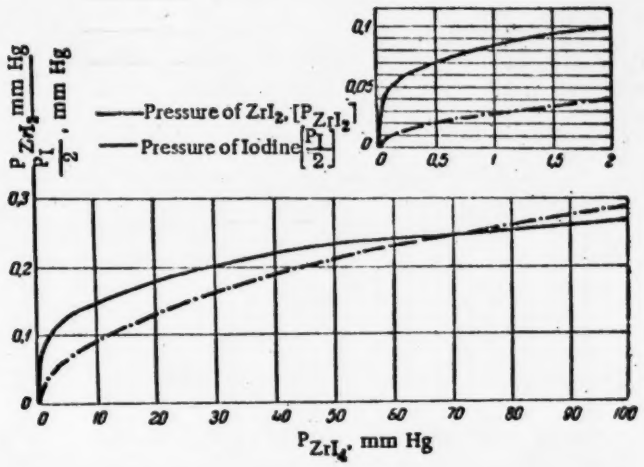

Fig. 3. Diiodide pressure and iodine pressure at the surface of a zirconium rod as a function of the tetraiodide pressure (at 1500° K). The upper figure shows the curves on an enlarged scale at low pressures.

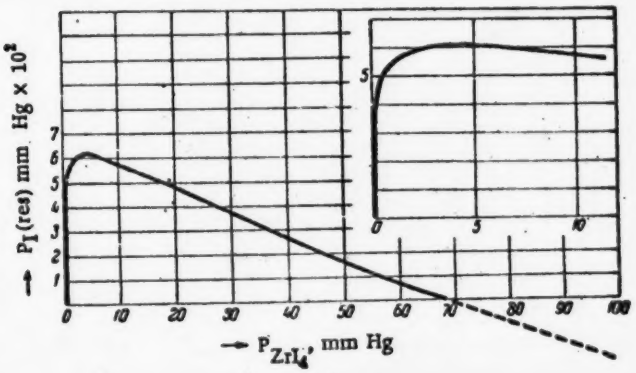

Fig. 4. The pressure of free (residual) iodine as a function of the tetraiodide pressure. Negative ordinates correspond to an excess of diiodide ("smoke" formed in the reaction tube). The upper figure shows the curves on an enlarged scale at low pressures.

We consider it necessary, however, to call attention to the following circumstance: the maximum of the curve for the quantity of residual iodine is located at about 4 mm tetraiodide pressure, whereas the rate of zirconium deposition has a maximum at a much lower tetraiodide pressure, 0.2-0.3 mm Hg.

In addition, the decrease of the deposition rate immediately after the maximum takes place considerably faster than the decrease of residual iodine pressure. A calculation shows that the situation changes very little if it is assumed that there is formed at the surface of the rod not the diiodide but the triiodide or both iodides at the same time.

These facts lead us to suppose that the formation of the lower iodides at the surface of the heated rod is not the only factor which determines the dependence of the zirconium deposition rate on the tetraiodide pressure. We believe that another important factor must be the pressure dependence of metal transfer processes.

The principal mechanism for the transfer of matter in a reaction tube under ordinary conditions is diffusion. Since the diffusion coefficients are inversely proportional to the pressure the rate of diffusive transfer of zirconium must depend strongly on the pressure in the tube. In this connection it is entirely logical to assume that the observed experimental dependence of the process rate on the tetraiodide pressure in the tube results to a considerable extent from this very pressure dependence of the transfer processes. This view has been expressed, in particular, by Gimmelman [8] and Busol [9]. Support for the decisive role of the diffusion has been expressed also by Moravits (in a discussion of the article by Döring and Moliere [2]) and by Shapiro [10]. The latter showed experimentally the significance of the transfer processes for the rate of zirconium deposition: by introducing a small quantity of argon into the reaction tube he found that the deposition rate is strongly slowed down by increased pressure of the gas.

In this connection it should be noted that the increase of tetraiodide vapor pressure is somewhat similar in its effect on the transfer rate to the increase of inert gas pressure. In both cases the principal result of increased pressure is the decrease of the diffusion coefficients and, consequently, of the rate of transfer. A change of the free iodine pressure near the rod when the tetraiodide pressure is changed takes place comparatively slowly and has no decisive effect on the pressure dependence of the transfer rate.

For tetraiodide pressures below 0.2 mm the situation changes considerably. The vapor pressure of the lower iodides near the rod and their effect on the zirconium deposition rate are not important. There must also be a change in the nature of the pressure dependence of the transfer rate since the pressure range which we observed is intermediate between the high pressures at which the transfer is determined by the ordinary laws of diffusion and the very low pressure region in which, as we know, the transfer rate is proportional to the pressure. It can be assumed that at pressures of the order of 0.2 mm and lower the principal factor affecting the rate is the number of molecular carriers, as a result of which the rate of zirconium deposition in this case increases with higher pressures.

PRINCIPAL CONCLUSIONS

1. The lower iodides which are formed on the surface of the raw metal do not directly influence the rate of zirconium deposition. Their effect is indirect: the formation of a lower iodide during a protracted refining process results in the complete disappearance of the solid tetraiodide and to changes of its vapor pressure inside the reaction vessel, and this, in turn, leads to a change of the rate of metal deposition.

2. The principal causes of a diminished rate of zirconium deposition at tetraiodide pressures above 0.2-0.3 mm are the slowing down of diffusion (smaller diffusion coefficients with increased pressure) and the formation of the lower iodides on the surface of the heated zirconium rod.

The role of the latter factor is considerably strengthened at very high tetraiodide pressures, when the reverse process - that of dissolution of the rod - can also begin.

LITERATURE CITED

[1] J. D. Fast, Z. anorg. allgem. Chem. 239, 145 (1938).

[2] J. H. Döring and K. Moliere, Z. Electrochem.; Ber. Buzenges. Phys. Chem. 56, 4, 403 (1952).

[3] W. M. Rainor, Some Problems of the Iodide Process of Refining Zirconium, Symp. "Zirconium", Ch. I, For. Lit. Press, 1954 (translation).

[4] O. Runnols and L. Pidgeon, A Study of the Iodide Method of Refining Titanium, Symp. "Titanium", Ch. III, For. Lit. Press, 1954 (translation).

[5] O. Rahlfs and W. Fischer, Z. anorg. allgem. Chem. 211, 349 (1933).

[6] L. Quill, (ed.), The Chemistry and Metallurgy of Miscellaneous Materials, Thermodynamics, NNES, Div. IV, Vol. 19 B, McGraw-Hill Book Company, N. Y., 1950.

[7] A. I. Evstyukhin and P. D. Bystrov, A Study of the Iodide Process of Refining Zirconium, Research Re-

port of MIFI, 1955 (unpublished).

[8] G. A. Gimmelman, Private Communications, 1954.

[9] F. L. Busol, Private Communications, 1954.

[10] Lusmen (ed.), The Metallurgy of Zirconium, McGraw-Hill Book Company, N.Y., 1955, p. 135.

NENADKEVITE – A NEW URANIUM SILICATE

V.A. Polikarpov

A description is given of the properties of the new uranium mineral – nenadkevite, which was discovered in the USSR in 1952. This mineral is a member of the silicate group and is in reality a continuous isomorphic series. The author postulates that it is, in addition, the last member of the thorite group and the richest in uranium.

Nenadkevite, which is named after K.A. Nenadkevich, was first found in 1952. Its formula is $(U^{+4}Y, Ce, Th)\,U^{+6}(Ca, Mg, Pb)\,[SiO_4]_2[OH]_4 \cdot nH_2O$. It is in reality not a single mineral but a continuous isomorphic series whose last members are, on the one hand, a silicate of tetravalent uranium, rare-earths, calcium and magnesium and, on the other hand, a silicate of essentially the same composition but with a strong predominance of hexavalent uranium.

The continuous change of chemical composition causes a gradual change of all physical properties of the mineral.

Nenadkevite was discovered in the sodium metasomatic zones of a uranium-iron deposit in paragenesis with brannerite, yttrosphene, uranite, uraniferous malacon and apatite.

It is developed in the interstices of the grains and along the contact surfaces of aggregates of albite, alkali amphiboles and aegirite, and cements fragments of magnetite. In time of formation it precedes uraninite.

Nenadkevite is usually found in the form of very fine crystals (0.05-0.001 mm), their concretions and solid masses. Nenadkevite crystals are characterized by an elongated prismatic habit. It does not show cleavage but is roughly separable along one direction. In color it is black, green-black, brown (the dark varieties) to reddish brown, orange and yellow (the light varieties). There is frequently a change of coloring in a single piece of ore. Colored streaks: in the dark varieties dark with brownish shading; in the light varieties yellow. Luster: vitreous to greasy. Specific gravity: 4.16-4.81 for the black variety; 3.80-3.91 for the brownish variety; 3.56-3.70 for the yellow-orange variety. Flat-conchoidal fracture. Very brittle. Nonfluorescent.

It dissolves in acids (1:10) with a white gelatinous and husklike precipitate. It is nonelectromagnetic.

The mineral is transparent, usually isotropic, infrequently shows spotty anisotropy. In transmitted light the dark varieties are bottle-green: Nm 1.716-1.781; light varieties are yellow: Nm 1.618-1.635. In reflected light nenadkevite is gray; its reflecting power $R \ll R$ of uraninite.

In an x-ray analysis the light-colored varieties of nenadkevite in their natural state give the diffraction picture of a crystalline substance (Table 1) while the dark varieties are amorphous; only after heating to 600° does a crystal lattice appear in the latter, which is similar to the lattice of the light varieties in the natural state. Consequently, the revealed lattice is stable and characteristic of the mineral. No analogs have been found. The mineral evidently possesses an individual crystal lattice which is characteristic of all its varieties.

Table 2 presents the results of six of the most typical assays of nenadkevite.

The heating-up curves of all varieties are identical. Two endothermic and one exothermic effect have

TABLE 1

Intensities and Interplanar Spacings of Nenadkevite.

I/I_1	d/n	I/I_1	d/n	I/I_1	d/n
1	5.26	0.5	2.39	1	1.534
4	4.65	1	2.08	0.5	1.482
0.5	4.16	1	1.96	1	1.456
1	3.79	4	2.18	1	1.400
4	3.50	6	1.883	1	1.360
1	3.29	1	1.810	1	1.320
2	3.20	4	1.746	1	1.283
3	3.06	0.5	1.689	1	1.229
10	2.90	0.5	1.655	1	1.178
1	2.47	1	1.597	1	1.152

TABLE 2

Color \ Oxides, %	MgO	CaO	PbO	Fe_2O_3	TR_2O_3*)	ThO_2	SiO_2	UO_2	UO_3	H_2O 115–140°	H_2O 140–1000°	Insoluble residue	Total	Assayer
Black	0,7	4,04	7,42	2,85	0,70	0,34	12,55		66,10	2,64	3,1		100,44	M.K. Klimova
Black	7,46	4,31	6,37	8,64	0,66	0,03	11,97	21,72	30,94	7,80			99,99	Yu.N. Knipovich
Reddish-brown	3,2	7,2	11,7	traces	1,10	0,01	11,97		55,0	2,06	7,80		100,04	R.P. Khodzhaeva
Brownish-orange	5,5	5,27	10,2	6,64	0,31	0,05	16,61		50,10	5,59			100,27	R.P. Khodzhaeva
Yellowish-orange	11,08	8,30	7,00	5,74	0,63	сл.	20,25		38,50	2,33	6,38		100,21	K.I. Orekhova
Yellowish-orange	3,71	4,71	9,59	1,76	1,29		10,60	0,60	58,10	6,95		3,09	100,31	K.I. Orekhova

*) The rare earths according to a semiquantitative x-ray analysis are represented by the yttrium and cerium groups. The amount of these increases in the lighter varieties.

TABLE 3

	Coffinite	Nenadkevite
Formula	$(USiO_4)_{1-x}(OH)_{4x}$	$(U^{+4}Y, Ce, Th)U^{+6}(CaMgPb)[SiO_4]_2[OH]_4 \cdot nH_2O$
Color	Black	Black, brown, orange, yellow
Transparency	Opaque	All varieties transparent
Specific gravity	3.3	3.56–4.81
Debye powder pattern	Similar to thorianite pattern	Rhombic (?); possesses inherent crystalline structure

been observed. The first endothermic effect at 100-200° is associated with the release of "dissolved" water, and the second at 680° with the liberation of water of crystallization; the exothermic effect at 760° results from the transition of nenadkevite to the crystalline state.

A study of the isotopic composition of the lead in nenadkevite showed the presence principally of uranium isotopes of lead: Pb^{204} - 0,082; Pb^{206} - 87.7; Pb^{207} - 10.1; Pb^{208} - 2.1..

In 1954 data was published concerning another new silicate of tetravalent uranium, coffinite, which was discovered in endogenic ores together with uraninite, vanadium oxides and pyrites in mines of the states of Colorado, Utah and New Mexico [1].

Table 3 gives a comparison of the two minerals.

Unlike coffinite, nenadkevite possesses a complicated composition of the cation group, a considerably higher specific gravity and total transparency.

In a number of its properties (specific gravity, color, etc.) and in its paragenetic associations, nenadkevite is close to minerals of the uranothorite-thorite series.

Nenadkevite is evidently the last (richest in uranium and with an insignificant amount of thorium) term of the following series:

thorite (content: uranium 1%; thorium 46-64%)
uranothorite (" 17%; " 46%)
nenadkevite (" 66%; " less than 1%).

This hypothesis is supported by the similarity of physical properties, the presence of rare-earths and thorium, and by the similarity of the conditions of formation (judging by the analogy of the paragenetic associations).

A similar hypothesis has been advanced with regard to coffinite by Stiff and Stern (see reference [1]).

LITERATURE CITED

[1] A.D. Weeks, and M.E. Thompson, Geol. Surv. Bull., 1009-B (1954).

HYDROPITCHBLENDE AND URGITE – NEW HYDROUS URANIUM OXIDES

R.V. Getseva

A description is given of two new uranium minerals discovered in the USSR in 1947 – hydropitchblende and urgite. These minerals are hydrous uranium oxides and are members of a single series in the successive oxidation and hydration of pitchblende. They are compounds of varying composition.

Hydropitchblende and urgite were discovered in 1947 in the oxidized zone of a hydrothermal deposit of uranium ores. They are members of a single series of successively oxidized and hydrated pitchblende and show varying composition. Hydropitchblende, which develops in the initial stages of the process, retains a different amount of tetravalent uranium, while urgite is a product of total pitchblende oxidation. In 1952 two varieties of hydropitchblende and two varieties of urgite were studied.

Hydropitchblende – $UO_2 \cdot kUO_3 \cdot nH_2O$; $k = 2.3\text{-}5$; $n = 3.9\text{-}9$

This mineral is widely developed in the deep portion of the oxidation zone (incomplete oxidation subzone) where it almost completely replaces pitchblende in carbonate-quartz veins. Higher in the profile of the deposit the hydropitchblende is preserved in the form of relicts – "eyes" within a mass of urgite and uranyl silicates which had replaced it.

The mineral is found in dense masses in nodular sinter precipitates inherited from pitchblende. There is an absence of cleavage. Its color is black; thin fragments are translucent, assuming a bottle-green color; as the relative amount of hexavalent uranium increases it becomes transparent. The color of the powder varies from greenish brown to ash-gray. The mineral possesses a conchoidal fracture, strong vitreous luster and is very fragile. Its hardness diminishes with increase of the amount of UO_3 and H_2O from 165 kg/mm^2 to 87 kg/mm^2, or on the Mohs scale from 3.8 to 3.1. The specific gravity of a strongly hydrated variety is 4.3. It dissolves in HCl, leaving an insoluble precipitate.

Under the microscope in transmitted light the color of hydropitchblende is bottle-green. It is isotropic. The refractive index is diminished with hydration and oxidation from 1.738 to 1.715. In reflected light its color is gray and is characterized by brownish-yellow internal reflections. Its reflecting power, like the refraction, is reduced from 11.40 to 7-7.5%.

X-ray patterns do not, as a rule, show a diffraction picture; the strong diffusion lines of the uraninite lattice (inherited from pitchblende) are seldom located.

Its chemical composition on the basis of two incomplete microchemical analyses is:

UO_2	UO_3	PbO	H_2O^-	H_2O^+
22.2	54.07	5.64	5.71	
11.90	63.00	5.78	3.77	3.44

At 100° and 300° water is liberated leaving the mineral in an amorphous state; at 500° it acquires a rhombic structure resembling that of the synthetic oxide U_3O_8.

Urgite – $UO_3 \cdot nH_2O$; n = 2.3-3.1

The name is taken from the words uranium and hydrate* which represent the composition of the mineral. Urgite develops at the expense of hydropitchblende principally in the middle of the oxidation zone; close to the surface of the earth it is replaced by uranyl silicates. In pieces of ore all varieties of urgite are frequently observed with a transition from the comparatively dark varieties which directly replaced the hydropitchblende, to the lighter-colored varieties which are rich in water. It is less widely distributed and less important industrially than hydropitchblende.

Urgite forms dense amorphous deposits. Cleavage is absent. Its color varies from reddish-yellow to amber-yellow and is transparent with a strong vitreous luster. It possesses a conchoidal fracture, is very fragile and has hardness 2-3. The specific gravity of the water-impoverished variety is 4.17. It shows practically no fluorescence. Urgite is partly soluble in cold dilute HCl with the liberation of chlorine bubbles; the remaining white crystalline precipitate dissolves completely upon heating.

The color of urgite is yellow in transmitted light. It shows a characteristic metacolloidal structure with slight undulatory and cluster polarization. The crystalline compounds are biaxial, Ng = 1.669-1.680; Np = = 1.647-1.657. In separate portions urgite remains completely isotropic. The refractive index in isotropic and slightly polarized portions oscillates inversely to the quantity of water from 1.681 to 1.705.

X-ray powder patterns of urgite do not reveal diffraction lines.

The chemical composition of urgite from incomplete microchemical analysis is as follows:

	UO_3	PbO	$Al_2O_3+Fe_2O_3$	SiO_2	H_2O^-	H_2O^+
Reddish-yellow variety	70.83	2.67	4.23	3.92	10.42	
Amber-yellow variety	71.09	2.90	1.89	3.80	7.95	6.14

A spectral analysis revealed admixtures of Mg, Co, Bi, V, Cu, I, Be (?).

As can be seen from the data given below, in its $UO_3 : H_2O$ ratio and correspondingly in its refractive index amorphous urgite differs from crystalline (rhombic) hydrates of hexavalent uranium previously described in the literature.

TABLE

Comparative data for hydrous hexavalent uranium oxides

Mineral	$UO_3 : H_2O$	Nm
Becquerelite	1 : 1.66	1.825
Mineral "X"	1 : 1.8	1.810
Parascupite	1 : 1.9	1.760
Product of ianthinite alteration	1 : 2	1.730
Scupite	1 : 2.2	1.714
Urgite	1 : 2.3 - 1 : 3.1	1.705 - 1.681 (traces)

* Russian word for hydrate = "gidrat". – Publisher.

SOME CHARACTERISTICS OF RADIATION VULCANIZATION

A. S. Kuzminsky, T. S. Nikitina and V. L. Karpov

We have investigated the radiation vulcanization of the following rubbers: natural rubber (NK), butadiene-styrene (SKS-30), butadiene (SKB-40) and nitrile (SKN-26). We established the dependence of the relative rate of formation of the spatial structure and of the tensile strength on the integral radiation dosage. We examined the question of the effect of certain ingredients of the rubber mixtures on the process of radiation vulcanization. We showed the peculiar role of carbon blacks and of the degree of their surface oxidation in the process.

It is well-known that the vulcanization of rubber, terminating in the formation of a single tridimensional system of its molecules, requires special vulcanizing agents (sulfur vulcanization) or high temperatures (hot vulcanization of synthetic rubber).

Recently reports have appeared in the literature concerning the behavior of high weight molecular compounds (in particular, rubbers and plastics) when subjected to ionizing radiation [1-7]. The profound structural changes which then take place in polymers are due to processes of structuralization (radiation "vulcanization"), disordering, and also certain phase transitions [3, 5-7].

We have investigated radiation vulcanization under intense x-irradiation. The source was a sectional x-ray tube operating at 200 ma and 80 kv.

The rubbers were subjected to irradiation in the form of pressed sheets 0.3-0.4 mm thick in cellophane wrapping, which served as a certain amount of protection of the specimen from the action of atmospheric oxygen during irradiation.

Ordinary commercial products were used in the investigation.

Irradiation continued for 10-20 hours, corresponding to a total energy absorption of $3 \cdot 10^8$-$6 \cdot 10^8$ rep.

Radiation vulcanization was applied both to pure rubbers: natural (NK), butadiene-styrene (SKS-30), butadiene (SKB-40) and nitrile (SKN-26), and to mixtures of these rubbers with carbon black. In addition, we investigated the problem of the effect on the rate of formation of the space lattice of the principal ingredients of the rubber mixtures (sulfur, accelerants, activators, fillers).

The rate of vulcanization was estimated from the rate of formation of the spatial structure, for which purpose we employed the method of measuring the equilibrium modulus [8]. As is seen from Figure 1, the rubbers which we investigated can be arranged in the following order with regard to vulcanization speed (by numerical values): NK, SKS-30, SKB-40 and SKN-26.

The tensile strengths (breaking load and relative stretch) for NK, SKS-30, SKB-40 and SKN-26 were very different. Thus the decrease of relative stretch for identical integral dosages was greatest for SKB-40 and least for NK.

The curve of breaking load as a function of integral dosage shows a sharp maximum corresponding to energy absorption $2 \cdot 10^8$ rep for NK and $1.5 \cdot 10^8$ for SKN-26.

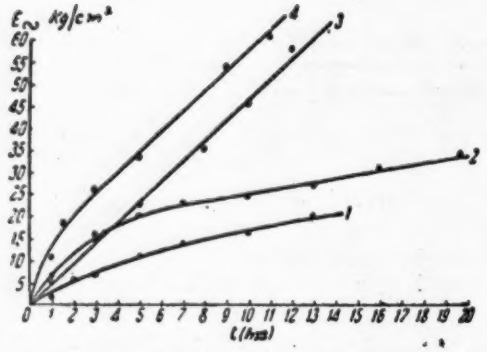

Fig. 1. Relationship between rate of formation of spatial structure and radiation dosage for pure rubbers (1 hour on the graph corresponds to $3 \cdot 10^7$ rep): 1) NK; 2) SKS-30; 3) SKB-40; 4) SKN-26.

The breaking-load curve of SKS-30 also passes through a maximum after which it changes little with further irradiation. For SKB-40 after a dosage of $\sim 0.6 \cdot 10^8$ rep we observed (up to our limit of $2 \cdot 10^9$ rep) a slow and linear rise of the breaking load.

It is an interesting fact that through radiation vulcanization NK loses its ability to crystallize. (The maximum breaking loads obtained did not exceed 30 kg/cm² at 500-600% relative stretch). This may possibly be caused by a considerable amount of branching during irradiation.

SKS-30 was used as an example for the study of the effect of different components of the rubber mixtures on the rate of radiation vulcanization*. Figure 2 shows the dependence of the equilibrium modulus on the integral dosage, which is proportional to the time of irradiation, for the original SKS-30 and a number of two-component systems.

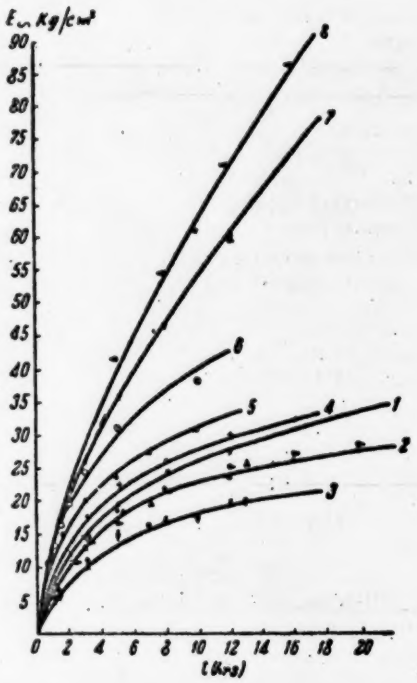

Fig. 2. Effect of different ingredients on speed of radiation vulcanization of SKS-30. 1) Pure SKS-30; ×) SKS-30 + mercaptobenzothiazole 2.0 parts by weight (p.w.); 2) SKS-30 + sulfur: ●) 5.0 p.w.; ▲) 1.0 p.w.; ●) 1.5 p.w.; 3) SKS-30 + + tetramethylthiuram disulfide: ○) 1.5 p.w.; ×) 3.0 p.w.; 4) SKS-40 + DFG 1.5 p.w. (diphenylguanidine); 5) SKS-30 + ZnO 5.0 p.w.; 6) SKS-30 + ZnO 10.0 p.w.; 7) SKS-30 + chalk 50.0 p.w.; 8) SKS-30 + + kaolin 50.0 p.w.

On the basis of the experimental results all of the components that were introduced can be divided into three groups:

1. Compounds which in small quantities (0.5-1%) considerably lower the vulcanization rate of SKS-30; these include sulfur and tetramethylthiuram disulfide (Figure 2, curves 2, 3). This effect of sulfur and thiuram is a basis for assuming that they have an inhibitive effect on radiation vulcanization. It is well known that under specific conditions both of these compounds act as inhibitors of polymerization and thermal disordering of hydrocarbons [11, 12].

2. Compounds which do not affect, or accelerate vulcanization only insignificantly; mercaptobenzothiazole and diphenylguanidine (Figure 2, curves 1, 4).

* This part of the work was conducted by M. A. Akimova.

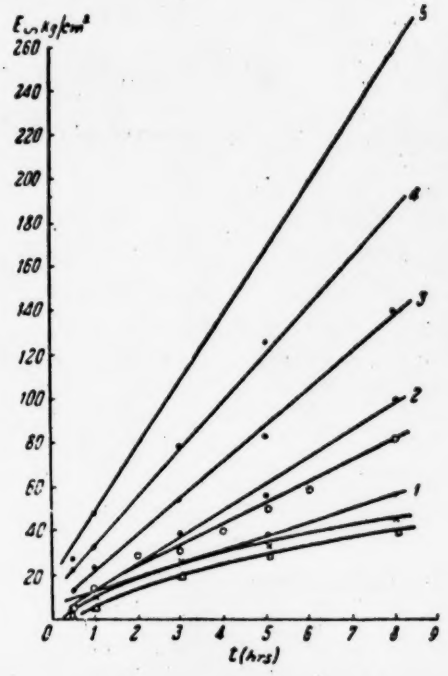

Fig. 3. Effect of carbon black on speed of radiation vulcanization of SKB-40 (1 hour on the graph represents $3 \cdot 10^7$ rep).
1) SKB-40 + 20 p.w. lampblack; 2) SKB-40 + 40 p.w. lampblack; 3) SKB-40 + 75 p.w. lampblack; 4) SKB-40 + 100 p.w. lampblack; 5) SKB-40 + 120 p.w. lampblack; Δ) SKB-40 + channel black; x) SKB-40 + chimney black; O) SKB-40 + bone black.

3. A number of compounds which considerably accelerate vulcanization (Fig. 2, curves 5, 6, 7 and 8). Among the substances which we investigated this effect was manifested by compounds containing metal ions — ZnO, chalk and kaolin. The first of these showed that the accelerating effect increases with increased amounts of the material (ZnO) in the rubber.

It can be assumed that this effect results from increased absorption of radiation energy, since the absorption coefficient, as we know, depends on the effective atomic number as the fourth power [10]. This is a sort of increased efficiency of the energy.

From the above we can conclude that almost all of the ingredients of the rubber mixtures behave quite differently in radiation vulcanization as compared with ordinary sulfur vulcanization [9] and exhibit a specific radiation-chemical effect on the formation of the spatial structure in rubber.

The effect of carbon black on vulcanization speed was studied using two forms, channel and lampblack, in all the rubbers studied, in the amount of 50 parts by weight for 100 parts of the polymer.

In all instances it was observed that both blacks very strongly affect the formation of the lattice during radiation vulcanization. It must be noted that there is comparatively little difference in the action of the two blacks, and that lampblack, which ordinarily only slightly affects the rate of lattice formation in hot vulcanization, was in our case very active. The unique behavior of these two blacks in radiation and hot vulcanization can be understood if it is assumed that as a result of ionizing radiation a considerable number of bridges are formed by chemical bonds between the rubber and carbon black particles. It is possible that active centers may appear not only on the surface of the carbon black particles but also within them before migration to the surface. With identical weight of filler the maximum difference in the size of the equilibrium molecule was of the order of 1.2-1.4 times, whereas channel black has a specific surface of 90-100 m^2/g, and lampblack has about 20 m^2/g.

In a study of the effect of the degree of oxidation of the carbon blacks (with equivalent surfaces) on the speed of radiation vulcanization it was found that the greater the oxidized surface of carbon black, the smaller the effect it had on the speed of formation of the lattice.

Figure 3 shows the increase of vulcanization speed for channel, chimney, lamp- and bone black.

It should be noted that the above forms of carbon black in their effect on the rate of formation of the lattice in hot vulcanization are in reverse order, as was observed by Lezhnev and one of the authors of this article.

For lampblack we established the proportionality between the quantity of carbon black used (up to 100 parts by weight) and the rate of formation of the lattice (Fig. 3, curves 1-5).

LITERATURE CITED

[1] A. Charlesby, Atomics 5, 12 (1954).

[2] A. Charlesby, Proc. Roy. Soc. (London) 215-A, 187 (1952).

[3] I. H. Messenger, India-Rubber J. 125, 41 (1953).

[4] J. W. Ryan, Nucleonics 11, 13 (1953).

[5] A. Charlesby, Plastics. 18, 142 (1953).

[6] A. Shapiro, J. chim. phys.. 52, 246 (1955).

[7] V. L. Karpov, Report at Conference of Academy of Sciences USSR on the Peaceful Uses of Atomic Energy, Acad. Sci. USSR Press, 1955.

[8] G. M. Bartenev, J. Tech. Phys. (USSR) 22, 1154 (1952).

[9] B. A. Dogadkin, Chemistry and Physics of Rubber, State Chem. Press, 1947.

[10] R. G. Fluharty, Nucleonics 3, 46 (1948); Chemical Effects of High Energy Radiation, For. Lit. Press, 1952, p. 34.

[11] A. L. Klebansky and L. I. Fomina , Problems of Chemical Kinetics, Catalysis and Reactivity, Acad. Sci. USSR, Press, 1955, p. 845.

[12] J. W. Breitenbach, H. Schneider, Monatsh.. 78, 1 (1948).

NEWS OF FOREIGN SCIENCE AND TECHNOLOGY

CONSTRUCTION OF RESEARCH REACTORS IN ENGLAND

The atomic energy administration of the United Kingdom is building at Harwell two reactors, "Dido" and "Pluto", intended for broad investigations in physics and technology. Furthermore it is planned to construct a reactor of the "Pluto" type in Douneray. In addition, England is providing aid to Australia in the building of a "Dido" type reactor.

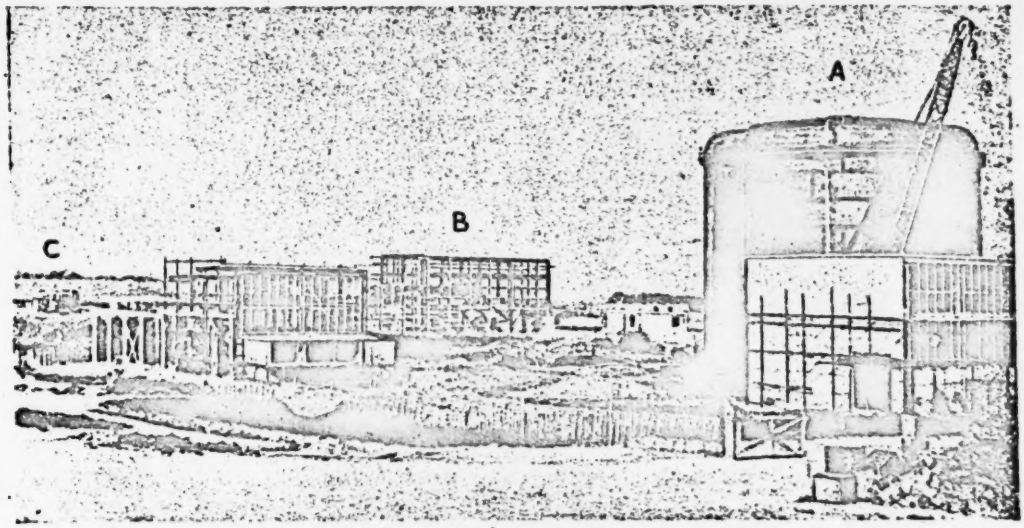

Fig. 1. Construction of new reactors for physical investigations at Harwell. A) Reactor "Dido", designed for general physical investigations; B) construction of a reactor of the "basin" type, of 100 kw power and with neutron flux 10^{12} neutrons per cm^2/sec; C) reactor "Pluto", similar to the reactor "Dido", but designed for testing fuel elements.

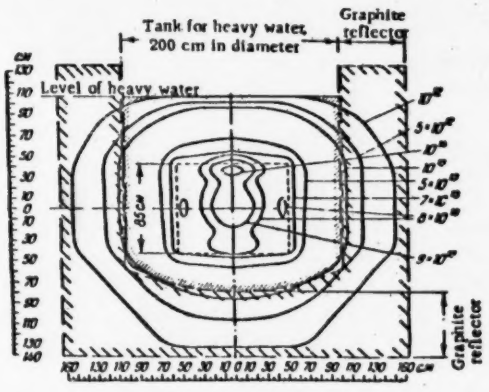

Fig. 2. Undisturbed distribution of thermal neutrons in the reactor "Dido" (all values in neutrons per cm^2/ sec.).

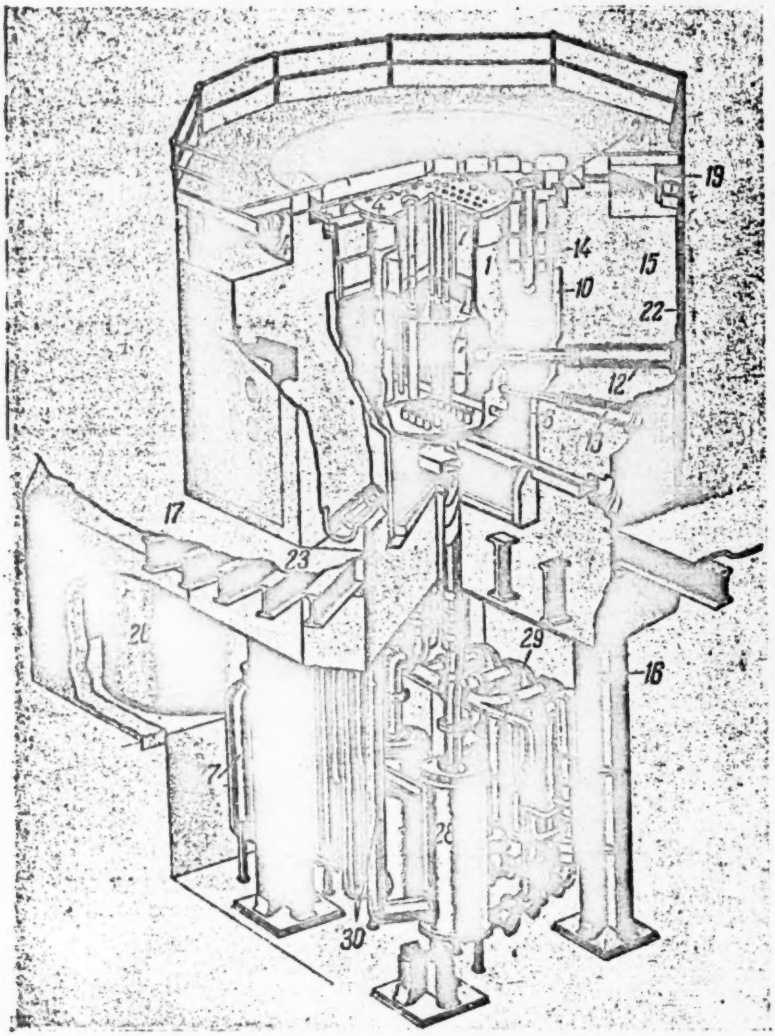

Fig. 3. 1) Aluminum tank for heavy water; 2) level of heavy water; 3) fuel element; 4) vertical experimental channel; 5) guides of six emergency rods; 6) experimental channel 10.16 x 5.08 cm; 7) biological shield; 8) graphite reflector; 9) experimental channels 30.48 x 20.32 cm; 10) lead heat shield (water cooled); 11) steel reactor vessel with boron covering; 12) experimental channel for taking neutrons from the active zone; 13) experimental channel for taking neutrons from the graphite reflector; 14) vertical channel from the graphite zone; 15) concrete shield; 16) supports of reactor; 17) first floor; 18) thermal column; 19) bracing of reactor foundation; 20) steel upper lid of thickness 25.4 cm; 21) experimental channel.

The "Dido" reactor is intended for use in physical experiments, for example the measurement of neutron cross sections, and the study of the parameters of various types of reactor lattices; besides this, the irradiation of small specimens of materials can be carried out in the reactor. The moderator and heat transfer agent of the reactor is heavy water, and the fuel is enriched uranium (about 6 kg, of which 2.5 kg is U^{235}).

The active zone of the reactor, with a volume of about 0.3 m^3, has the form of a cylinder of height 60 cm and diameter 86 cm. It is composed of lamellar fuel elements, whose filler is a mixture of uranium with

aluminum. The active zone is located in the center of an aluminum tank of height 2 m and diameter 2 m. The reflector of the reactor is of graphite, 60 cm thick. The reactor and reflector are inclosed in a steel jacket filled with helium.

The nominal power of the reactor is 10 megawatts, with neutron flux 10^{14} neutrons per cm^2/sec. The maximum possible flux is $5 \cdot 10^{14}$ neutrons per cm^2/sec. The starting of the reactor is set for autumn, 1956.

At the end of 1957 the two reactors of the "Pluto" type are to go into operation. The construction and physical characteristics of these reactors are similar to those of the reactor "Dido", but their purpose is somewhat different; they are designed for the long-time testing of fuel elements. For this purpose it is planned to install six or eight testing loops in the reactor "Pluto".

I. S.

LITERATURE CITED

[1] The Journal of the British Nuclear Energy Conference 1, 1, 3 and 35 (1956).

[2] Engineering 180, 4673, 235 (1955).

A REACTOR WITH AN ORGANIC MODERATOR

According to reports there will be set in operation at the end of this year a reactor with an organic moderator (OMRE) with power 5 to 15 megawatts. The moderator used in the reactor is diphenyl, and the fuel is highly enriched uranium.

Preliminary experiments have shown the good stability of the organic moderator in the neutron field and insignificant deposition of precipitates (which had been feared earlier) in the form of a film on the surface of the fuel elements.

The reactor will probably be built by the Atomic Energy Commission, together with the "North American Aviation" Company in Arco, Idaho, U.S.A.

I. S.

LITERATURE CITED

[1] Nucleonics 14, 1, 14 (1956).

[2] Atomic Energy News Letter 15, 2 (1956).

ECONOMIC INDICES OF ATOMIC STATIONS

Quite recently there have appeared in the American literature communications on the economic indices of certain reactors.

Admiral Rickover announced that upon the third loading of an active zone* of the reactor PWR at the Shippingport atomic station the cost of electrical energy will be lowered from 5.2 to 1.5 cents/kw-hr.

* In the reactor PWR it is planned to load successively the assemblies of different active zones.

At the first loading of an active zone the cost of energy is composed of fixed expenditures (1.5 cents/kw-hr.) the cost of preparing fuel elements, the cost of zirconium and other construction materials (3.9 cents/kw-hr.) and operating costs (0.3 cent/kw-hr). From these 5.7 cents/kw-hr is subtracted the value of the processed fuel, equal to 0.5 cent per kw-hr.

At the second loading of an active zone the total cost of the energy will be reduced to 3.2 cents per kw-hr through the lower cost of fuel, a decrease of operating cost, and the increase of the power from 60 to 90 megawatts. At the third loading of an active zone the cost will be lowered to 1.5 cents/kw-hr. For the loading of the first active zone the working time of the reactor will be equivalent to 8000 hours of operation at full power, which means, including idle time of the reactor, more than one and one-half years. The exact working time with the first active zone is not known, since at first the reactor will be mainly used for experimental purposes. Its power will be increased gradually: 1st year, 10%; 2nd year, 20%; 3rd year, 40%; 4th year, 60%; 5th year, either 80% or full power.

The third loading of an active zone in the reactor will be accomplished not earlier than 1965.

The firm "Alco" has released formerly secret data on the cost of electric energy from the portable army reactor APPR, which is being constructed in Fort Belvoir (Virginia).

The fuel component of the cost of electrical energy will not exceed 0.95 cent/kw-hr. This sum includes 0.6 cent/kw-hr cost of fuel calculated at 25 dollars per gram of U^{235}, 0.25 cent/kw-hr for preparation of fuel elements, and 0.1 cent/kw-hr for reprocessing. Operating expenses for an installation of power 2000 kw will amount to approximately 0.15 cent/kw-hr. Fixed costs will be 0.58 cent/kw-hr at load factor 80%.

Thus the cost of electrical energy will come to about 1.68 cents/kw-hr. The cost of energy from an analogous coal-burning station is 1.4 cents/kw-hr.

I. S.

LITERATURE CITED

[1] Nucleonics 14, 1, 14 (1956).

A PERFECTED METHOD OF FILM DOSIMETRY

The Oak Ridge Laboratory has developed a film dosimeter with which the following measurements can be carried out:

a) determination of dose and radiation energy of x-rays;
b) measurement of dose of γ-rays;
c) approximate determination of dose of β-rays acting alone;
d) approximate determination of dose of mixed β- and γ-rays.

For this purpose a system of filters is used to simplify the measurements and make them more exact.

An ideal filter for the measurement of a broad spectrum of x-rays is one with which the degree of blackening of the film depends only on the dose of radiation and not on the energy of the protons. Three types of filter are described in the report:

1. The filter consisting of the material of the cassette body, conventionally designed "OW" - "open window".

2. The "OW" filter plus 1.56 mm of cellulose acetate, called the "plastic" filter.

3. The filter of "OW" + 0.25 mm tungsten + 0.5 mm cadmium + 0.5 mm cellulose acetate, called the "shielding" filter.

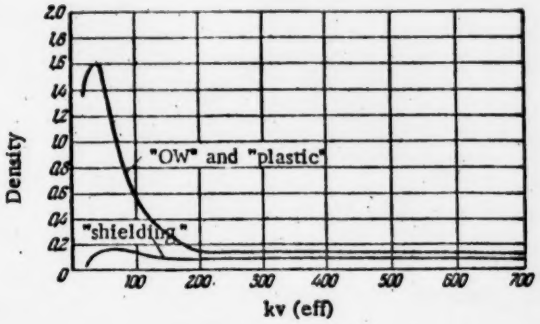

Fig. 1. Dependence of blackening density of film on energy of radiation (dose 200 mr). Upper curve with "OW" and "plastic" filters; lower curve with "shielding" filter.

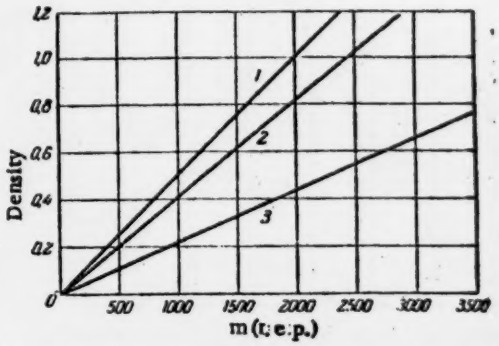

Fig. 2. Typical calibration curve for β- and γ-radiations with the different filters.
1) γ-Rays of radium, "plastic" filter; 2) γ-rays of radium, "shielding" filter; 3) β-rays of uranium, "OW" filter.

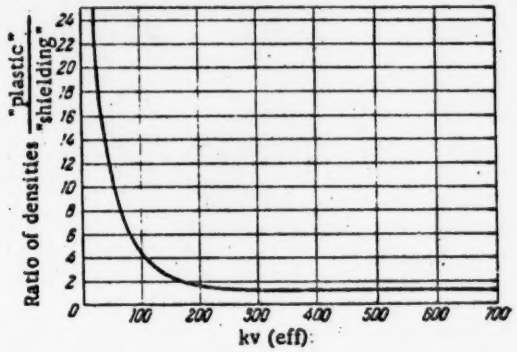

Fig. 3. Dependence of the ratio of the blackening densities for "plastic" and "shielding" filters on the energy of the radiation.

All three filters are placed side by side in one cassette so that each of them acts separately.

Fig. 1 shows a comparison of the blackening densities of the film with the "OW" and "shielding" filters for a 200 mr dose of radiation at various energies. The curves show that the blackening densities with the "OW" and "plastic" filters are equal. But for the action of β-particles the blackening under the "OW" filter is greater than under the "plastic" filter, and on this basis one can determine the dose of β-radiation in cases of mixed action of β- and γ-rays from the difference of the degrees of blackening.

The "OW" filter together with the film wrapper has thickness 80 mg/cm². β-rays of penetrating power 7 mg/cm² and over are considered harmful to human beings.

Figure 2 shows a typical calibrating curve for various radiations with the different filters. To determine the dose of β-radiation one needs only to multiply the difference of the readings with the "OW" and "plastic" filters by 1.5.

The dose of photons is determined in the following way:

1) from the calibration curve one finds the dose for γ-rays with the shielding filter;

2) by subtracting the density of blackening for β-rays from that for γ-rays with the "plastic" filter one finds a "correction" density, and then the dose corresponds to 1/10 of the "correction" density. The greater of the two doses found is taken as the dose of x- or γ-rays.

Although the determination of the dose of photons by the method described does not depend on the energy of the radiation, the filters make possible the determination of the energy of the radiation in effective kilovolts. This may be needed in case a knowledge of the relative "depth" of the dose is required. The determination of the energy of the radiation is made from the curve shown in Fig. 3, which gives the ratio of the degrees of blackening under the "OW" or the "plastic" filter to that under the "shielding" filter as a function of the energy of the photons.

S. L.

LITERATURE CITED

[1] E. D. Gupton, Radiology 66, 2, 253 (1956).

DOSIMETRY BY MEANS OF GLASS

The majority of existing methods of dosimetry, based on ionization measurements or on the calorimetric principle, do not provide speed, accuracy, and constancy of readings in the measurement of large doses. The changes of absorption for the visible spectrum of most sorts of glass when irradiated with doses of the order of 10^6-10^7 r.e.p. make it possible to use glass for the measurement of large doses of radiation. As a dosimeter glass has a number of advantages that make its use in this field very attractive. These are: chemical inertness, insolubility, small size, and durability. But there are a number of factors limiting the use of glass. The most important are low sensitivity, linearity of readings, and the rapid fading of glass at room temperature.

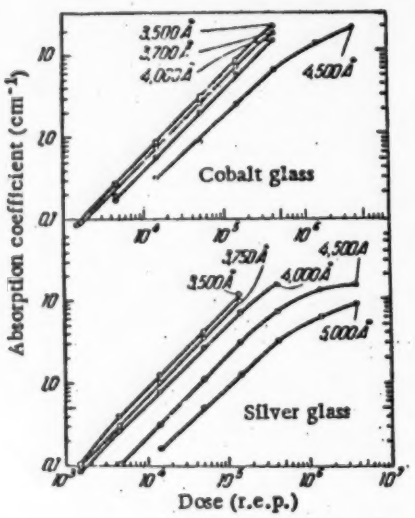

Fig. 1. Change of absorption of cobalt (upper curves) and silver (lower curves) glasses as functions of the dose of radiation.

In an investigation of these phenomena it was found that the addition to glass of elements such as cobalt and silver considerably increases the sensitivity of the glass to radiation and reduces the speed of its fading after irradiation. These types of glass have an absorption band for visible light in the part of the spectrum near the ultra-violet, and thus the investigation of their optical density was conducted with rays of wavelength from 3500 to 5000 A with a "Spectronic 20" colorimeter.

The paper gives data from tests of glass of the following chemical compositions: a phosphate glass, activated with silver: 50% $Al(PO_3)_3$, 25% $Ba(PO_3)_2$, 25% KPO_3, with 8% $AgPO_3$ added to this base; and a lime-silicate glass consisting of 70% SiO_2, 18% Na_2O, 10% CaO, 1% MgO, and 1% B_2O_3, activated by addition of 0.5% cobaltic oxide. For these types of glass, irradiated from a powerful source of Co^{60}, the calibration curves shown in Fig. 1 were constructed. From the curves it is seen that it is expedient to measure small doses in the short-wave part of the spectrum, and large doses with the longer waves. As is seen from the diagram, the cobalt glass has a change of its absorption coefficient after irradiation with a dose of $1.5 \cdot 10^4$ r.e.p. amounting to 0.54 for λ - 4000 A and 0.30 for λ = 4500 A. For doses from $5 \cdot 10^3$ to $4 \cdot 10^5$ r.e.p. the readings vary linearly. Above this limit the changes are smaller and nonlinear. But in the whole nonlinear part of the curve the changes of optical density with respect to the dose are well marked. The same dependence is also presented for the glass activated with silver.

It is known that the radiophotoluminescent reaction of silver glass does not depend on the energy of the radiation, if the energy exceeds 200 keV, but below this limit the reaction is stronger, reaching a maximum of 18:1 at 65 keV. Since the measurement of large doses is based on the very same process of absorption, it is very probable that the dependence of the absorption on the energy of the radiation is maintained. The authors calculated the absorption coefficients of the silver and cobalt glasses for three energies.

The paper of Davidson, Goldblith, and Proctor presents the data of an investigation of a phosphate glass activated with silver, which was subjected to the action of various physical agencies.

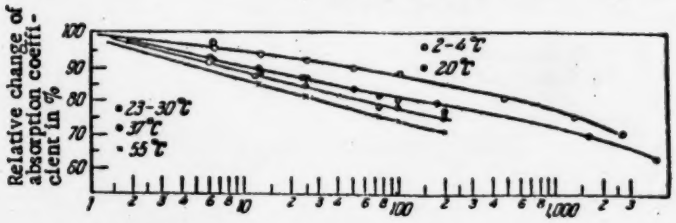

Fig. 2. Influence of storage temperature on irradiated glass that has not had heat treatment.

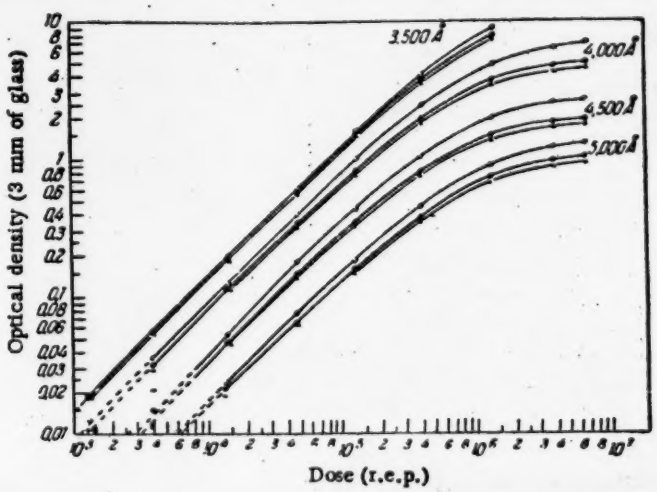

Fig. 3. Calibration curves for phosphate glass activated with silver. ○ An hour after irradiation; ◌ after heating for 10 minutes at 130°C; X after 8 days of storage at room temperature.

The source of radiation in the experiments described was a highly active preparation of Co^{60} with dosage power 1400 r.e.p./min. In some experiments a van de Graaf generator was used as a source of electrons with energy 3 Mev.

The optical density was measured by a Beckman spectrophotometer with a photomultiplier. The absorption coefficient was calculated by dividing the measured optical density by the thickness of the glass. The absorption in each glass was measured at four wavelengths: 3500, 4000, 4500, and 5000 A. The absorption coefficient referred to in this work is equal to the absorption coefficient of the irradiated glass minus that of the unirradiated glass.

For purposes of practical application of the method studies were made of some physical agencies influencing the readings given by the glass. Six pieces of glass, irradiated with a dose of $1.30 \cdot 10^5$ r.e.p. were kept under five different temperature conditions: room temperature (23-30°), refrigerator temperature (2-4°), and temperatures of 20, 37, and 55°. The pieces kept at 20 and 37° and at room temperature gave similar results in regard to fading. The low temperatures slowed down, and the high ones accelerated, the fading process in glasses that had not been subjected to the stabilizing action of heat (Fig. 2).

To determine the influence of high temperature on the optical readings of irradiated glass, pieces of glass were heated to temperatures of 130 and 150°C an hour after irradiation. The testing of pieces so treated

was conducted at different intervals after irradiation, from 5 minutes to 8 days. The data from the tests showed that :

1) the absorption coefficient changes in inverse proportion to the elapsed time and to the temperature of the heating after irradiation;

2) the degree of fading during storage at room temperature is markedly decreased after the heat treatment;

3) the readings from pieces of glass that have had heat treatment are practically unaffected by the storage temperatures within the range from 2 to 43°C.

Fig. 3 shows calibration curves obtained by irradiation of glass with doses from $1.3 \cdot 10^3$ to $7 \cdot 10^6$ r.e.p., with subsequent heat treatment at 130° for 10 minutes. It is seen from the diagram that the slope of the curves is markedly reduced for doses exceeding $3 \cdot 10^5$ r.e.p., which indicates a decrease of sensitivity of the glass at such doses.

In the experiments described above the heat treatment was applied 1 to 1.5 hours after irradiation. In practice it is not always convenient to perform the heating at such an early time. Therefore a group of pieces of glass was heated at different time intervals after irradiation, and was then tested with the spectrophotometer. The tests showed that the absorption coefficient decreases almost linearly with the logarithm of the time for all intervals tried between irradiation and heat treatment, from 1 hour to 8 days.

In some cases irradiation at a low temperature can serve as a measure to decrease certain undesirable physical and chemical changes produced by irradiation. To study this matter, one group of pieces of glass was irradiated at room temperature, and another in ice water. The dose of radiation was $3.66 \cdot 10^5$ r.e.p. The chilled pieces of glass showed considerably less change of their optical readings. Thus the phosphate glass activated with silver can be used as a dosimeter at low temperatures, if the corresponding correction is made in constructing the calibration curves.

Preliminary tests have shown that irradiated glass can be bleached at temperatures of 400-500°. Further experiments will be conducted to determine how the sensitivity of the glass varies with repeated bleachings and how many bleachings can be used without damage to the accuracy of the readings. It was found that 15 minutes heating at a temperature of 450° is enough for complete bleaching of pieces of glass irradiated with doses up to $5 \cdot 10^6$ r.e.p. The sensitivity of pieces subjected to tens of repeated irradiations with bleaching after each irradiation was essentially unchanged. It follows that pieces of glass that have been irradiated once can be repeatedly used as dosimeters, which considerably increases their practical value.

The fact that the optical density of a large number of pieces of glass was measured under identical conditions made possible a statistical study of the results. The statistical study showed that the variations of optical density for pieces of glass from the same batch (melt) are inappreciable, so that the average values from measurements on several unirradiated pieces from a given batch suffice to give an idea of the optical density of all the pieces.

The study of pieces of glass irradiated with electrons of energy 3 MeV from a van de Graaf generator showed the possibility of using silver-activated phosphate glass for dosimetry of electron beams.

S. L.

LITERATURE CITED

[1] N. J. Kreidl, G. E. Blair, Nucleonics 14, 1, 34 (1956).

[2] S. Davidson, S. A. Goldblith, B. E. Proctor, Nucleonics 14, 1, 56 (1956).

PRODUCTION OF GRAM QUANTITIES OF METALLIC PLUTONIUM

Buttons of plutonium weighing about 1 g have been produced by reducing plutonium trifluoride with calcium in an induction furnace with an atmosphere of argon (see diagram). The method for obtaining plutonium was previously developed with uranium; gram quantities of which were produced by reducing UF_4 with calcium. The starting material for the production of the PuF_3 was oxalate of plutonium (III). It was decomposed

in a stream of air by the procedure: heating for 2.5 hours to 400°C and holding at this temperature for 0.5 hour. The plutonium dioxide so formed was fluoridized in a tube of monel metal by a (1:1) mixture of pure dry HF and H_2, by the reaction:

$$PuO_2+3HF+\frac{1}{2}H_2\xrightarrow[5\ hr]{450^\circ C}PuF_3+2H_2O.$$

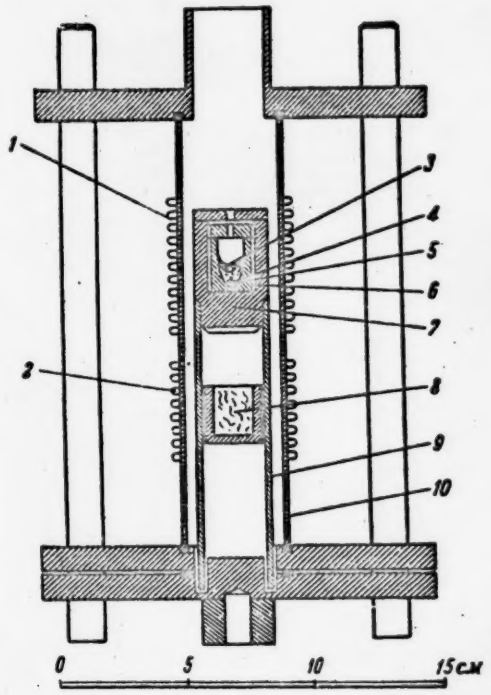

Induction furnace for smelting plutonium. 1) Circuit for heating crucible; 2) circuit for heating getter; 3) fluoride slag; 4) corrosion zone; 5) button of metal; 6) reaction crucible; 7) protective crucible; 8) getter (Ti−Zr chips); 9) quartz support; 10) quartz tube.

There was obtained a blue-violet trifluoride with composition: F−19.3%; Pu−80.1% (theoretical composition F−19.25%, Pu−80.7%).

Because of the great radioactive poisonousness of plutonium all of these operations were carried out in protective chambers filled with dry argon, in which were placed the furnaces and other apparatus.

The trifluoride was carefully mixed with fine chips of calcium (in 100% excess over stoichiometric quantity) and was placed in a calcium fluoride crucible, shaped parabolically in the used part to facilitate separation of the metal. The crucible was covered with a lid having a hole for observation of the flash at the start of the reaction, and was placed in the furnace, inside an outer protective crucible of calcium fluoride. The furnace was closed, evacuated, and washed out and filled with argon. Then for complete purification of the argon the getter was heated by the lower high-frequency circuit. The other circuit heated the crucible with its charge. The reaction began after several seconds, when the melting temperature of calcium was reached. After being continued for about a minute to allow reduction and separation of the metal, the heating was stopped. The excess calcium, mixing with the mass of fluoride slag, helped to heat it. If the heating were continued, there would be a fast reaction with the calcium fluoride crucible and it would melt. After cooling, the crucible was broken and the button of metal was removed from under the slag.

Despite the fact that the heat of reaction was considerably less than in the reduction of PuF_4, the reaction went through quite satisfactorily; the yield of metal was 85-90%.

Ya. P.

LITERATURE CITED

[1] F. Anselm, P. Faugeras, S. Erison, Compt. rend. Acad. Sci. USSR 242, 16, 1996 (1956).

BIBLIOGRAPHY

NEW LITERATURE ON QUESTIONS OF THE PEACEFUL USE OF ATOMIC ENERGY.

BOOKS AND COLLECTIONS

Application of Marked Atoms in Biology, Action of Radiation and Use of Isotopes in Biology, Collections of Translations, Surveys, and Reviews of Foreign Periodical Literature, No. 1, 1956, 126 pp., 8 rubles 40 kopecks.

Dorfman, Ya. G., Magnetic Properties and Structure of Substances, State Chem. Press, 1955, 376 pp., 14 rubles 15 kopecks.

Dynamics of Plasma, Problems of Contemporary Physics, Collections of Translations and Surveys of Foreign Periodical Literature, 1956, No. 2, 199 pp., 10 rubles 50 kopecks.

Essays on Radiobiology, Edited by A. M. Kuzin, Acad. Sci. USSR Press, 1956, 312 pp., 18 rubles 45 kopecks.

Heavy Unstable Particles, Problems of Contemporary Physics, Collections of Translations and Surveys of Foreign Periodical Literature, No. 4, 1955, 214 pp., 10 rubles 50 kopecks.

Kikoin, A. K., Atomic Energy and the Achievements of Contemporary Physics, Sverdlovsk, Book Press, 1955, 62 pp., 1 ruble 15 kopecks.

The Tamm-Dancoff Method, Problems of Contemporary Physics, Collections of Translations and Surveys of Foreign Periodical Literature, 1955, No. 10, 231 pp., 10 rubles 50 kopecks.

Pi Mesons, Problems of Contemporary Physics, Collections of Translations and Surveys of Foreign Periodical Literature, No. 3, 183 pp., 10 rubles 50 kopecks.

Quantum Theory of Fields, Problems of Contemporary Physics, Collections of Translations and Surveys of Foreign Periodical Literature, 1955, No. 3, 198 pp., 10 rubles 50 kopecks.

Veksler, V. I., Accelerators of Atomic Particles, Acad. Sci. USSR Press (Popular-Science Series), 1956, 48 pp., 70 kopecks.

Zhukovitsky, A. A., Marked Atoms, "Knowledge" Press, Series III, 1955, No. 15, 40 pp. 60 kopecks.

ARTICLES IN JOURNALS

Akhiezer, A. I. and Pomeranchuk, I. Ya., "On the Radiation of Quanta Accompanying the Absorption of Fast Protons by Nuclei," J. Exptl.-Theoret. Phys. (USSR) 30, 1 (1956).

Akhiezer, A. I. and Sitenko, A. G., "On the Diffraction Scattering of Fast Deuterons by Nuclei," Doklody Akad. Nauk SSSR 107, Doklady.

Balakhovsky, S. D. and Kuznetsov, I. B., "On the Influence of Garotenoids on the Rate of Penetration of Methionine (S^{35}) Into Liver Sections," Doklady Acad. Nauk. SSSR 107, 4 (1956).

Barannik, V. P., "New Chemical Elements—Einsteinium (99), Fermium (100), and Mendelevium (101)," Chemistry in the School 2 (1956).

Baranov, S. A. and Shlyagin, K. N., "Electronic Spectrum of U^{237}, J. Exptl.-Theoret. Phys. (USSR) 30, 2 (1956).

Baranova, V. A., "On Ways of Using Radioactive Indicators and Radiations in Non-ferrous Metallurgy (review)," Non-Ferrous Metals, 3 (1956).

Barinsky, R. L., "X-Ray Spectra and Electronic Structure of Th in the Compounds $Th(NO_3)_4$ and ThO_2", Bull. Acad. Sci. USSR, Phys. Ser. XX, 1 (1956).

Bibergal, A. V. and Margulis, V. Ya., "Shielding from X- and γ-Radiation," Biophysics 1, 1, (1956).

Bogdanov, G. F. and others, "Spectra of Neutrons from the Bombardment of Tritium and Deuterium by 14 Mev Deuterons" (Letter to the Editor) J. Exptl. Theoret. Phys. (USSR) 30, 1 (1956).

Dulkova, L. S. and others, "Interaction of 300 Mev π-Mesons With Protons, Deuterons, and Nuclei of Photographic Emulsion," Doklady Akad. Nauk. SSSR 107, 1 (1956).

Eliseev, G. P., and others, "Primary Ionization Spectrum of Fast π-Mesons," Doklady Akad. Nauk. SSSR 107, 2 (1956).

Elovich, S. Yu. and Matorina, N. N., "Study of Complex-Formation Chromatography by the Use of Marked Atoms," J. Phys. Chem. (USSR) XXX, 1 and 2 (1956).

Evropin, V. A. and others, "Kinetics of Interaction of Carbon Dioxide with Coal and Isotope Exchange," J. Phys. Chem. (USSR) XXX, 2 (1956).

Fomin, V. V. and Maslova, R. N., "Valence States of P^{32} Formed in the Reaction S(n, p)P," J. Inorg. Chem. (USSR) 1, 2 (1956).

Fomichev, M. S., "Atomic Energy in Technology," Nature (USSR) 3 (1956).

Fridlender, E. and Bercha, S., "An Unusual V^0-Disintegration," Doklady Akad. Nauk. SSSR 107, 1 (1956).

Gerling, E. K., "Occurrence of Inert Gases in Meteorites and Their Isotopic Composition," Doklady Akad. Nauk. SSSR 107, 4 (1956).

Gusev, N. G., "On the Problem of Measurement of Gamma-Radiation," Meas. Technol. 2 (1956)

Ilyin, G. S., "Synthesis of Nicotine C^{14} in Tobacco Stalks," Biokhimiya 21, 1 (1956).

Inopin, E. V., "Scattering of Neutrons by Semitransparent Nonspherical Nuclei" (Letter to the Editor), J. Exptl. Theoret. Phys. (USSR) 30, 1 (1956).

"International Values for Thermal Cross Sections of Separated Isotopes" (Reference), Progr. Phys. Sci. 58, 2 (1956).

Kalinin, I. A. and Vertebnyi, P. Ya., "Calculation of Physical Doses of γ-Radiation," J. Phys. Chem. (USSR) XXX, 2 (1956).

Kelman, V. M. and others, "Determination of the Ratios of the Internal Conversion Coefficients for the Isomeric Transition In^{114}," Doklady Akad. Nauk SSSR 107, 3 (1956).

Klechkovsky, B. M., "On the First Appearance of Atomic Electrons With Given l, n, n_r, and n + l" (Letter to the Editor). J. Exptl. Theoret. Phys. (USSR) 30, 1 (1956).

Kolbanovsky, Yu. A. and Lavrovsky, K. P., "Ways of Using Atomic Energy in the Chemical Technology of Petroleum," Chem. and Tech. of Fuel, 1 (1956).

Koperzhinsky, V. V., and Shcheberstov, V. V., "Entrance and Distribution of Marked Phosphorus in Leaf Fertilization of the Opium Poppy," Doklady Akad. Nauk. SSSR 106, 6 (1956).

Korenman, I. M. and Baryshnikova, M. N., "Measurement of the Radioactivity of Weak β-Emitters," Factory Lab., 3 (1956).

Korotkova, V. A. and others, "Effective Cross-Sections of Photofission of Nuclei of Uranium and Thorium," Doklady Akad. Nauk. SSSR 106, 4 (1956).

Korotkova, V. A. and others, "Energy Distribution of Fragments From Fission of Uranium and Thorium Nuclei by γ-rays," Doklady Akad. Nauk. SSSR 106, 5 (1956).

Kozodaev, M. and others, "Study of the Scattering of Negative π-Mesons in Water by Use of a Diffusion Chamber," Doklady Akad. Nauk. SSSR 107, 2 (1956).

Krat, V., "Inhomogeneity of the Solar Chromosphere and the Problem of the Excitation of Helium," Doklady Akad. Nauk SSSR 106, 4 (1956).

Kryanin, I. R. and others, "Study of the Liquefactionof Copper and Steel by Means of Radioactive Isotopes," Metal Sci. and Working 3 (1956).

Kryzhanovsky, V. V. and others, "Radioactive Method of Sampling Rolled Steel," Factory Lab. 3 (1956).

Kurdinovsky, Yu., "Rays Produced by the Atom," Science and Life 3 (1956).

Kursanov, D. N., "Hydrogen Exchange of Carbonyl Ions With Acids and Hydrogen Exchange of Carbonyl Compounds With Deuterium Oxide in an Alkaline Medium," Report at the Conference on the Mechanism of Hydrogen Exchange, May, 1955), Ukrain. Chem. J. 22, 1 (1956).

Kutyurin, V. M., "On the Rate of Penetration of Deuterium into Vegetable Tissue," Biokhimiya 21, 1 (1956).

Kuzin, A. M. and Budilova, E. V., "Sensitization of Radiolytic Depolymerization of Desoxyribonucleic Acid," Biophysics 1, 1 (1956);

Levintov, I. L., "On the Question of the Applicability of the Fermi Formula Describing the Polarization of Fast Nucleons to Scattering from Nuclei," Doklady Akad. Nauk. SSSR 107, 2 (1956).

Leporsky, V. V. and others, "Study of the Reduction of Phosphorous Irons With a Radioactive Indicator," Steel 1 (1956).

Mandelshtam, S. L. and others, "The Evaporation Method and Its Application for the Determination of Boron and Other Impurities in Uranium," J. Anal. Chem. (USSR) II, 1 (1956).

Markov, M., "Note on the Systematics of Hyperons and Heavy Mesons," Doklady Akad. Nauk. SSSR 106, 5, (1956).

"Measurer of Radiations" (About the Discoveries of the Hungarian Physicist Zh. Narai), Science and Life 3 (1956).

Meisel, M. N., "Radioactive Isotopes in Microbiology," Science and Life 4 (1956).

Okun, L. B., "Charge Exchange of K-Mesons in Hydrogen and Deuterium," J. Exptl.-Theoret. Phys. (USSR) 30, 1 (1956).

Ormont, B. F., "On the Question of the Possibility of Formation of the Structures of Deuterides (Hydrides) of Metals With Preservation of Molecules or Pairs of Atoms of Hydrogen in the Lattice," Crystallography 1, 1 (1956)

Palladin, A., "Radioactive Isotopes in the Biochemistry of the Brain," Science and Life 3 (1956).

Perelman, R. G., "An Atomic Icebreaker," Science and Life 4 (1956).

Perumova, N. D., Technique of Measuring the Activity of Histological Sections Containing Radioactive Isotopes by Contact Radiograms," Doklady Akad. Nauk. SSSR 107, 1 (1956).

Pisarzhevsky, O., "The Energy of Atomic Nuclei" (On the Problem of the Economic Use of Atomic Energy), Knowledge is Power 2, (1956).

Pushkarev, V. V., "Absorption of Radioactive Isotopes by Iron Hydroxide," J. Inorg. Chem. (USSR) 1, 1 (1956).

"Radioactive Methods in Investigations in the Physics of Metals," Academician N. T. Gudtsov and others, Herald Acad. Sci. USSR 3 (1956).

Rempel, S. I. and Popov, R. B., "Determination of Continuous Output of Industrial Electrolyzers for Aluminum Production by the Method of Radioactive Indicators," Non-Ferrous Metals 3 (1956).

Rodnyansky, B. B. and Malinsky, D. M., "The Significance of Determination of the Functional Activity of the Thyroid Gland by Means of Radioactive Iodine (I^{131}) in the Diagnosis of Incipient and Latent Forms of Thyrotoxicosis," Problems of Endocrinology and Hormone Therapy 2, 1 (1956).

Samsonov, G. V. and Grodshtein, "Some Properties of Hexaborides of Alkali and Rare-Earth Metals," J. Phys. Chem. (USSR) XXX, 2 (1956).

Segalin, V. G., "Experience in the Use of Radioactive Radiations in the Coal Industry," Coal 4 (1956).

Sheka, Z. A., "Conference on the Use of the Method of Marked Atoms in the Chemistry of Complex Compounds" (Review), J. Inorg. Chem. (USSR) 1, 2, (1956).

Shinel, V. S. and Kuznetsova, G. A., "Investigation of Chains of Radioactive Transformations," J. Exptl.-Theoret. Phys. (USSR) 30, 2 (1956).

Shumilovsky, N. N. and Melttser, L. V., "Use of Radioactive Isotopes for Measuring Rates of Gas Flow and For the Automatic Control of Gas Consumption by the Method of "Marked Molecules," Doklady Akad. Nauk. SSSR 106, 4 (1956).

Shushunov, V. A. and Zateev, V. G., "Isotope Exchange of Carbon Between the Solid Carbonates of Lithium, Sodium, Potassium, and Barium and Gaseous Carbon Dioxide," J. Phys. Chem. (USSR) XXX, 2 (1956).

Sokolov, V. S., "Use of Atomic Energy for the Control, Investigation, and Regulation of Processes in Power Plants," Electric Stations, 4 (1956)

Striganov, A. R., "Isotopic Spectral Analysis," Progr. Phys. Chem. LVIII, 3 (1956).

Talroze, V. L. and Frankevich, E. L., "On the Temperature of the Gas in the Ion Source of a Mass Spectrometer," J. Tech. Phys. (USSR) XXVI, 3 (1956).

Terentyev, A. P. and others, "Synthesis of 2-Ethylanthraquinone Marked With Carbon C^{14} in the Nucleus," Doklady Akad. Nauk.SSSR 107, 3 (1956).

Tumulkan, A. D., and Yanushkovsky, V. A., "Radioactive Method of Sampling Rolled Steel," Bull. Acad. Sci. Latvian SSR 1 (1956).

Turpaev, T. M. and Usypina, M. G., "The Role of Sulfohydryl Groups in the Contraction of Heart Muscle, According to Experiments With Radioactive Silver," Biophysics 1, 1 (1956).

Vinogradov, A. P. and others, "Isotopic Composition of Sulfur in Connection With the Question of the Age of Pyrites of Alluvial Origin," Geochemistry 1 (1956).

Vlasyuk, P. A. and Grodzinsky, D. M., "On the Problem of the Action of Nuclear Radiations on Plants," Doklady Akad. Nauk. SSSR 106, 3 (1956).

Vlasyuk, P. A. and others, "Action of Small Doses of Ionizing Radiation on Oxidation-Reduction Processes in Plants," Doklady Akad. Nauk. SSSR 106, 4 (1956).

Voevodsky, V. V., "On the Exchange of Free Alkyl Radicals With Molecular Deuterium"(Report at the Conference on the Mechanism of Hydrogen Exchange, May, 1955), Ukrain. Chem. J. 22, 1 (1956).

Zbarsky, I. B. and Perevoshchikova, K. A., "Embodiment of Marked Amino Acids in Proteins of Whole Tissue, Cell Nuclei, and Nuclear Fractions of Artificial Tumors and Normal Organs," Doklady Akad.Nauk SSSR 107, 2 (1956).

Zakutinsky, D. I., "Some Particulars of the Action of Radioactive Substances on the Organism," Medical Radiology, 1 (1956).

Zaslavskyi, Yu. S. and others, Radiochemical Method of Investigation of the Stability of Solutions of Additives in Lubricating Oils," Factory Lab. 4 (1956).

CONTENTS (continued)

		Page	Russ. Page
21.	A Study of the Iodide Process of Refining Zirconium. The Lower Zirconium Iodides and the Effect of Tetraiodide Pressure on the Rate of Metal Deposition. V.S. Emelyanov, N.D. Bystrov and A.I. Evstyukhin	415	122
22.	Nenadkevite – A New Uranium Silicate. V.A. Polikarpov	425	132
23.	Hydropitchblende and Urgite – New Hydrous Uranium Oxides. R.V. Getseva	429	135
24.	Some Characteristics of Radiation Vulcanization. A.S. Kuzminsky, T.S. Nikitina and V.L. Karpov	431	137
	News of Foreign Science and Technology	435	141
	Construction of Research Reactors in England (435). A Reactor with an Organic Moderator (437). Economic Indices of Atomic Stations (437). A Perfected Method of Film Dosimetry (438). Dosimetry by Means of Glass (440). Production of Gram Quantities of Metallic Plutonium (442).		
	Bibliography		
	New Literature on Questions of the Peaceful Use of Atomic Energy	445	149

SOVIET JOURNAL OF ATOMIC ENERGY NUMBER 3, 1956

CONTENTS

		Page	Russ. Page
1.	Some Problems of Atomic Power Development in the USSR. I.V. Kurchatov.	283	5
2.	On the Number of Neutrons Emitted by Pu^{239} on Fission by Thermal and Super-thermal Neutrons. V.I. Kalashnikova, V.I. Lebedev, L.A. Mikaelian and M.I. Pevzner.	291	11
3.	Determination of the Average Number of Neutrons ν_{eff} Emitted in a Single Capture Event by the Isotopes U^{233}, U^{235} and Pu^{239} in the Superthermal Region of Neutron Energies. P.E. Spivak, B.G. Erozolimsky, G.A. Dorofeev, V.N. Lavrenchik, I.E. Kutikov and Yu.P. Dobrynin.	295	13
4.	The Average Number of Neutrons ν_{eff} Emitted by the Isotopes U^{233}, U^{235} and Pu^{239} on Capture of Neutrons with Energies From 30 to 900 Kev. P.E. Spivak, B.G. Erozolimsky, G.A. Dorofeev, V.N. Lavrenchik, I.E. Kutikov and Yu.P. Dobrynin.	303	21
5.	Measurement of the Average Number ν_{eff} of Neutrons Emitted Per Single Capture Event for Samples of Pu^{239} with Impurities of the Isotope Pu^{240} and the Effective Resonance Capture Integral of Pu^{240}. B.G. Erozolimsky, I.E. Kutikov, Yu.P. Dobrynin, M.I. Pevzner, L.S. Danelian and S.S. Moskalev.	311	27
6.	Slowing Down of Fission Neutrons by Water. L.M. Barkov and K.N. Mukhin.	317	31
7.	Measurement of Slowing Down of Neutrons by Water in the Energy Interval From 1.46 to 0.025 ev. L.M. Barkov, V.K. Makaryin and K.N. Mukhin.	321	33
8.	Slowing Down of Fission Neutrons by Uranium – Water Media. L.M. Barkov, A.P. Venediktov and K.N. Mukhin.	329	40
9.	Scattering of Slow Neutrons by Water Molecules. A.F. Gorlunov.	335	45
10.	Scattering of Neutrons by Para- and Ortho-Hydrogen. S.I. Drozdov.	341	50
11.	Relative Pu^{239} Breeding Ratio in Natural Uranium-Ordinary Water Lattices. L.V. Komissarov and V.A. Tarabanko.	349	56
12.	The Ratio of the Average Fission Cross Sections of Pu^{239} and U^{235} in Uranium-Water Lattices. V.P. Katkov, Yu.V. Nikolsky and G.A. Stoliarov.	355	61
13.	The Possibility of Producing Thermonuclear Reactions in a Gaseous Discharge. I.V. Kurchatov.	359	65
14.	Investigations of Pulse Discharges at High Currents. L.A. Artsimovich, A.M. Andrianov, O.A. Bazilevskaya, Yu.G. Prokhorov and N.V. Filippov.	367	76
15.	On the Mechanism by Which the Current Contracts in Fast and Intense Gas Discharge. M.A. Leontovich and S.M. Osovets.	371	81
16.	Penetrating Radiation From Pulse Discharges. L.A. Artsimovich, A.M. Andrianov, E.I. Dobrokhotov, S.Yu. Lukyanov, I.M. Podgornyi, V.I. Sinitsyn and N.V. Filippov.	375	84
17.	Spectroscopic Studies of Intense Pulse Discharge in Hydrogen. S.Yu. Lukyanov and V.I. Sinitsyn.	379	88
18.	Hard X-Radiation Accompanying a Discharge in a Gas. S.Yu. Lukyanov and I.M. Podgornyi.	389	97
19.	Solar Batteries (On the Direct Transformation of Radiant Energy into Electrical Energy by Means of Photoelements). V.S. Vavilov.	399	107
20.	Decomposition of Plutonium Oxalates by Intrinsic Alpha Radiation. V.V. Fomin, R.E. Kartushova and T.I. Rudenko.	409	117

(Continued on inside back cover)